

Glycidyl Ether-Based Coatings on Polystyrene Culture Substrates for Temperature-Triggered Cell Sheet Fabrication

Dissertation zur Erlangung des akademischen Grades des
Doktors der Naturwissenschaften (Dr. rer. nat.)

im Fachbereich Biologie, Chemie, Pharmazie
der Freien Universität Berlin eingereichte Dissertation

vorgelegt von

M.Sc. Daniel David Stöbener

aus Landau in der Pfalz

August 2018

Diese Arbeit wurde unter Anleitung von Dr. Marie Weinhart und Prof. Dr. Rainer Haag im Zeitraum von September 2013 bis August 2018 am Institut für Chemie und Biochemie an der Freien Universität Berlin angefertigt.

1. Gutachter: Prof. Dr. Rainer Haag

2. Gutachter: Dr. Marie Weinhart

Disputation am 12.12.2018

Acknowledgements

First and foremost, I want to thank Prof. Rainer Haag for providing me with the opportunity to conduct this thesis under his supervision, for welcoming me into his group and for introducing me to Dr. Marie Weinhart and her research project. In that regard, Dr. Marie Weinhart deserves special gratitude for her excellent guidance through the past years.

I want to thank Dr. Florian Paulus, Dr. Tobias Becherer, Dr. Jonathan Vonnemann, Dr. Qiang Wei, Dr. Dirk Steinhilber and Dr. Mathias Dimde for guiding me through my first encounters with synthetic polymer chemistry during my master's studies and for always making me feel welcome at FU Berlin.

I also want to thank all of my current and former undergraduate students for their active as well as indirect contribution to this thesis, including M.Sc. Marius Gaedke, M.Sc. Kevin Li, M.Sc. Maikel Kulka, B.Sc. Mikołaj Kozłowski, M.Sc. Scott Kilbride, B.Sc. Arush Agrawal, M.Sc. Ghazala Nadeem, Karl Pfaff, Leon Lehmann, and especially B.Sc. Dorian Donath, B.Sc. Mohammed Raia and B.Sc. Marcel Neuert.

All the current and former members of the Weinhart group deserve special thanks for their steady and unequivocal support, motivating and engaging scientific discussions as well as their continuous comradery. I especially want to thank Dr. Anke Hoppensack, B.Sc. Melanie Uckert and Johanna Scholz for their dedication towards numerous and often times tedious cell culture experiments, without which this thesis wouldn't have been possible in its final state. My gratitude further goes to Dr. Silke Heinen, whose scientific and worldly opinions, openness for worthwhile discussions as well as exemplary work attitude were highly appreciated. I also want to thank my former colleague M.Sc. Dennis Müller for his excellent lab companion- and friendship and his persistent patience with me during the final period of the making of the presented thesis.

I am very grateful for my friends, who were always encouraging to bring out the best in me, never shied away from criticism and sometimes reminded me of the positive in case I forgot.

Finally, I want to thank my family for supporting the entirety of my studies as well as for their unconditional affection, patience, humor and guidance, which I was fortunate to experience throughout my life.

Contents

1	Introduction	1
1.1	Thermoresponsive Polymers	1
1.1.1	Temperature-Triggered Phase Transition.....	1
1.1.2	Thermoresponsive Polymers for Tissue Culture Applications	5
1.1.3	Synthetic Strategies for thermoresponsive Poly(glycidyl ether)s	12
1.2	Thermoresponsive Coatings for Cell Sheet Engineering	15
1.2.1	Design Guidelines for Thermoresponsive Surfaces for Cell Sheet Fabrication.	15
1.2.2	Coating Approaches for Plastic Cell Culture Substrates.....	21
1.2.2.1	The Photochemistry of Benzophenone.....	21
1.2.2.2	UV-induced Grafting as a “Grafting From” Approach	26
1.2.2.3	Adsorption of Block Copolymers as a “Grafting To” Approach	35
2	Objectives.....	43
3	Publications and Manuscripts	45
3.1	Ultrathin Poly(glycidyl ether) Coatings on Polystyrene for Temperature-Triggered Human Dermal Fibroblast Sheet Detachment	49
3.2	Cell Sheet Fabrication from Self-assembled Thermoresponsive Poly(glycidyl ether) Brushes - Approaching Vascular Tissue Engineering.....	83
3.3	Fast and Solvent-Free Microwave-Assisted Synthesis of Thermoresponsive Oligo(glycidyl ether)s.....	127
3.4	Switchable Oligo(glycidyl ether) Acrylate Bottlebrushes “Grafted-from” Polystyrene Surfaces - A Versatile Strategy towards Functional Cell Culture Substrates.....	165
4	Summary and Conclusions	211
5	Outlook.....	217
6	Kurzzusammenfassung / Short Summary	219
6.1	Kurzzusammenfassung	219
6.2	Short Summary	220
7	References	221
8	Patent Applications, Publications and Conference Contributions.....	249
9	Curriculum Vitae.....	251

1 Introduction

Responsive polymers constitute a class of “smart” materials which can undergo a structural, conformational, physical or chemical property changes upon physical, chemical or biological stimuli.¹⁻⁶ As such, these polymers bear a significant potential for implementation in various fields ranging from textile design, food packaging and optical data storage to a great diversity of biomedical devices and coatings. There are numerous biomedical applications for which polymers responding to physical triggers, such as temperature, light or electricity, chemical triggers, such as ionic strength or pH, as well as biological triggers, such as supramolecular binding to enzymes and receptors, as external stimuli have been thoroughly investigated. For example, responsive polymeric materials have been used in the form of dendrimers, micelles, vesicles, nano-, micro- as well as macroscopic gels for therapeutic use in drug delivery, gene delivery, and molecular recognition⁷⁻¹¹ and in the form of various surface coatings, such as monolayers, films and gels, for diagnostic sensor and imaging applications, in tissue engineering and regenerative medicine as well as for bioseparation.¹⁰⁻¹⁷

1.1 Thermoresponsive Polymers

Especially polymers which react to temperature changes have been in the focus of research in the past years and are currently on the brink of becoming state-of-the-art high-tech materials. This is due to convenient adjustability of temperature as a physical quantity, its importance in biological processes and the great diversity of polymers which are known to exhibit thermoresponsive behaviour in aqueous environments.¹⁸ Hence, thermoresponsive polymers have laid the foundation for the development of multi-responsive, truly “smart” materials, which are able to approximately mimic naturally occurring processes.

1.1.1 Temperature-Triggered Phase Transition

Most of the known polymers reacting to temperature as an external stimulus exhibit a lower critical solution temperature (LCST) in aqueous media. This means that such polymers dissolve in water at low temperatures and undergo phase separation via a so-called “coil-to-globule” transition upon heating, which is schematically illustrated in Figure 1A.¹⁸⁻¹⁹ In most cases, this temperature-triggered transition is reversible, and the critical temperature at which phase

1 Introduction

separation occurs is mainly governed by the hydrophilicity, the molecular weight, the architecture and the concentration of the thermoresponsive polymer as well as by solutes in the aqueous medium, such as salts or various biomolecules.⁶ By definition, the LCST is the lowest point of the coexistence curve (binodal) in the phase diagram corresponding to a specific polymer concentration, which is defined as the lower critical solution concentration (LCSC). All the other points along the binodal at which phase separation occurs are accurately referred to as cloud point temperatures (CPTs) and are always directly associated to a specific polymer concentration.¹⁹ A schematic phase diagram of a polymer exhibiting LCST behaviour is shown in Figure 1B.

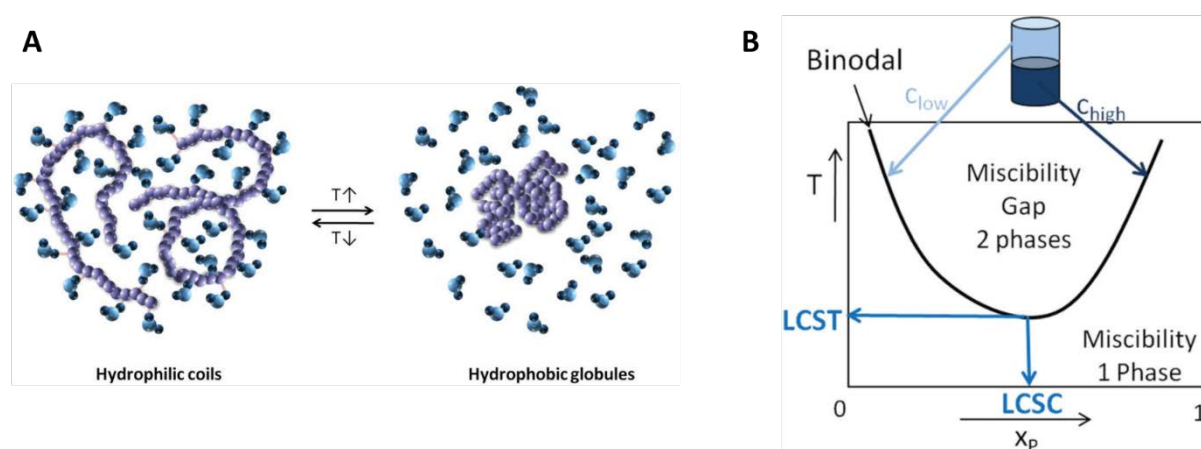


Figure 1. (A) Schematic illustration of the “coil-to-globule” transition of a thermoresponsive polymer in water.²⁰ (B) Schematic phase diagram of a binary mixture exhibiting an LCST.²⁰

Generally, the phenomenon of LCST-type behavior is governed by inter- and intramolecular H-bonds between the polymer and water. In fact, the ability of water to restructure and bind to various polar molecules via H-bonding is also one of the main driving forces in biological processes.⁶ In addition, the relatively low enthalpic gain and the unfavorable entropy accompanied by the dissolution of high molecular weight polymers in water makes such mixtures sensitive to changes in temperature as it can be illustrated by means of the Gibbs free energy (1).

$$\Delta G_{mix} = \Delta H_{mix} - T\Delta S_{mix} \quad (1)$$

When the temperature reaches the critical value (LCST or CPT), the negative enthalpy term ($\Delta H_{mix} < 0$) is overruled by the positive entropy term ($\Delta S_{mix} < 0$), which in turn leads to an unfavorable positive free energy ($\Delta G_{mix} > 0$). Consequently, the system becomes unstable and phase separation occurs. This drives the increase in entropy of the system via the dehydration of the polymer, which comprises the cleavage of H-bonds between the polymer and water, the

formation of intra- and intermolecular H-bonds or dipole-dipole interactions within the polymer chains and the aggregation of the hydrophobic polymer segments, leading to a favorable negative free energy ($\Delta G_{mix} < 0$). Hence, the LCST-type phase transition is an entropy-driven phenomenon. Therefore, it is important to note that every polymer with an appropriate hydrophilic/hydrophobic balance exhibits LCST-type behaviour in aqueous solution at temperatures within the potentially and practically applicable range (~ 0 °C to 100 °C).¹⁹ In contrast to LCST-type polymer, thermoresponsive polymers which exhibit an upper critical solution temperature (UCST) show an inverse solution behaviour in water and undergo phase separation upon cooling. The solubility of UCST-type polymers in water is mainly governed by rather strong supramolecular interactions, such as H-bonds or zwitterionic interactions, between the polymer side chains. Compared to LCST-type polymers, the enthalpy of mixing for UCST polymers is positive (endothermic), since strong intra- and intermolecular bonds need to be cleaved in order to solubilize the polymers via polymer-water dipole-dipole or H-bond interactions. The rather low entropy of mixing makes UCST-type polymers extremely sensitive to small temperature changes (equation (1)). In analogy to LCST-type polymers, CPTs of polymers which undergo a UCST-type phase transition are influenced by polymer molecular weight and concentration. However, especially cosolutes like salts and pH strongly affect supramolecular polymer-polymer interactions by weakening H-bonds and zwitterionic bonds and can therefore be used to induce a phase transition under isothermal conditions.²¹

The most common techniques to determine the CPTs of thermoresponsive polymers in solution are turbidimetry, dynamic light scattering (DLS), NMR spectroscopy and calorimetric methods, such as differential scanning calorimetry (DSC). Although the determination of CPTs via these techniques is straight-forward, the results are prone to experimental variations, which is due to kinetic effects during the measurements. Hence, experimentally determined phase diagrams and CPTs do not coincide with the coexistence curve, since the binodal is of thermodynamic nature. In addition, depending on the heating and cooling rates applied during measurement, thermoresponsive LCST-type polymers often exhibit hysteresis.²² This kinetic effect leads to discrepancies between CPTs determined from heating and cooling cycles and is often observed when the polymers contain groups which exhibit strong hydrophobic-, dipole-dipole-, π - π - or Coulombic interactions.⁶ Turbidimetry, which is the most widespread technique used to determine CPTs and is usually conducted via UV-Vis transmittance measurements, is rather limited, since results depend on the wavelength of the used light and small polymer particles and aggregates formed during the coil-to-globule transition do not yet scatter light and are therefore not detected. Hence, in order to attain a more detailed insight into the nature of the

phase transition and to determine more realistic CPTs, additional measurement techniques are required. In that regard, DLS offers a way to determine the conformation of single polymer chains as well as the size of polymer aggregates via assessment of their hydrodynamic radii and is therefore a valuable method to determine temperature-induced changes in particle size as well as intermolecular aggregation on a broad nanometer-scale ($\sim 1 - 1000$ nm). In addition, high sensitivity DSC allows the quantification of the state of polymer hydration on the molecular level. Since the cleavage of hydrogen bonds between water and the thermoresponsive polymer constitutes an endothermic process, the enthalpy which can be measured during heating of a solution via DSC experiments allows an estimate of the degree of polymer dehydration. Figure 2A illustrates the characteristic endothermic peak of the dehydration of poly(*N*-isopropyl acrylamide) (PNIPAm) chains in water measured by DSC as well as a comparative cloud point curve measured by UV-Vis turbidimetry plotted in optical density vs. temperature.²³ A typical phase transition curve of a statistical, thermoresponsive copolymer based on the two monomers oligo(ethylene glycol) methacrylate (OEGMA, $M_n = 475$ g mol⁻¹) and 2-(2-methoxyethoxy)ethyl methacrylate (MEO₂MA) determined by DLS is shown in Figure 2B, which illustrates the abrupt change in particle size induced by the formation of multimolecular aggregates above the copolymer's CPT (~ 52 °C).²⁴

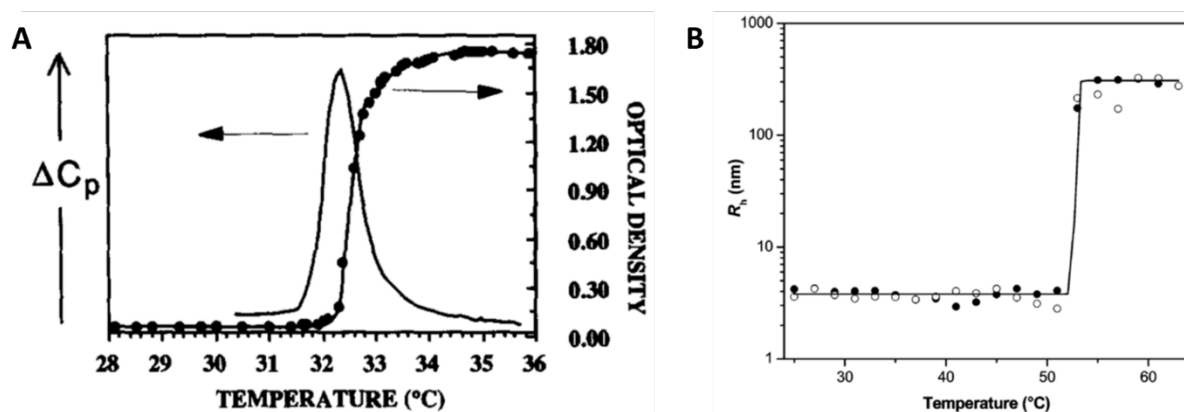


Figure 2. (A) CPT of PNIPAm (~ 32 °C) measured via UV-Vis transmittance (phase transition curve is plotted as optical density vs. temperature, black dots) and by DSC measurements (endothermic peak illustrates the required heat flow ΔC_p for the cleavage of H-bonds between water and PNIPAm, black curve).²³ (B) CPT of a statistical poly(MEO₂MA-*co*-OEGMA) copolymer determined from the hydrodynamic radius R_h via DLS measurements (black and white dots represent particle sizes determined during heating and cooling cycles, respectively).²⁴

Additional information on the changes in polymer chain mobility during an LCST-type phase transitions can be assessed using NMR spectroscopy, by which the hydration of the

hydrophobic and hydrophilic domains of the respective polymer chains can be estimated through the broadening or vanishing of the polymer's characteristic NMR signals. Among others²⁵⁻²⁷, a further technique that has been introduced recently in order to investigate the effect of cosolutes on the phase transition of thermoresponsive polymers is isothermal titration calorimetry (ITC). Compared to DSC, this method is suitable for the determination of critical cosolute concentrations at very low temperatures and potentially offers the determination of binding enthalpies and entropies as well as binding constants between cosolutes and thermoresponsive polymers in aqueous solutions.²⁸

1.1.2 Thermoresponsive Polymers for Tissue Culture Applications

As a result of their temperature-dependent behaviour in water, thermoresponsive polymers are frequently used for the functionalization of various biomedical substrate materials in order to obtain “smart” surface coatings, which can switch from a protein and cell adhesive state into a protein and cell repellent state upon temperature reduction.¹²⁻¹⁵ Whereas thermoresponsive polymers in aqueous solution usually undergo intramolecular collapse as well as intermolecular aggregation triggered by a temperature-induced coil-to-globule transition, thermoresponsive coatings change their state of hydration upon heating above and cooling below their volume phase transition temperature (VPTT).^{23, 29} Depending on the coating structure and composition, the VPTT might differ from the polymer's CPT in solution and generally exhibits a more gradual transition. This transition is either characterized by changes in the state of hydration of the coating on the nanoscale, as it is often observed for surface-tethered polymer brushes, or by macroscopic swelling and deswelling of, e.g., surface immobilized thermoresponsive hydrogels.²⁹ Similar to the characterization of thermoresponsive polymers in water, the VPTT of thermoresponsive coatings can be investigated by various complementary techniques. For example, non-destructive methods, such as ellipsometry³⁰⁻³³ and water contact angle (CA) measurements³⁴, can be used to probe the temperature-dependent swelling and wettability, respectively, of surface coatings on the macroscopic scale. The temperature-dependent swelling ratio of surface immobilized hydrogels based on statistical poly(MEO₂MA-*co*-OEGMA-*co*-BPEM) terpolymers with comprising different MEO₂MA/OEGMA comonomer ratios and a photo-reactive 2-(4-benzoylphenoxy)ethyl methacrylate (BPEM) crosslinker is illustrated in Figure 3A.³⁵ Compared to the copolymer's phase transition curves measured by UV-Vis turbidimetry which are shown for comparison in Figure 3A, swelling curves display a gradual change over a large temperature range (~ 20-50 °C), which clearly indicates the broad VPTT

range of surface immobilized, thermoresponsive gel coatings. To assess temperature-dependent changes in surface wettability, CA measurements may provide an estimate of the VPTT of thermoresponsive coatings.³⁶⁻³⁸ Changes in CA thus indicate the de- and rehydration of a coating upon heating and cooling, respectively, and are useful to assess and estimate, e.g., the cell adhesive properties of the surface. For example, Figure 3B illustrates the temperature-dependent equilibrium water CAs of poly(MEO₂MA-*co*-OEGMA) brush coatings with different MEO₂MA/OEGMA comonomer ratios measured in decane.³⁹ The broad temperature range of the wettability transition again exemplifies the gradual change in coating hydration upon temperature variation.

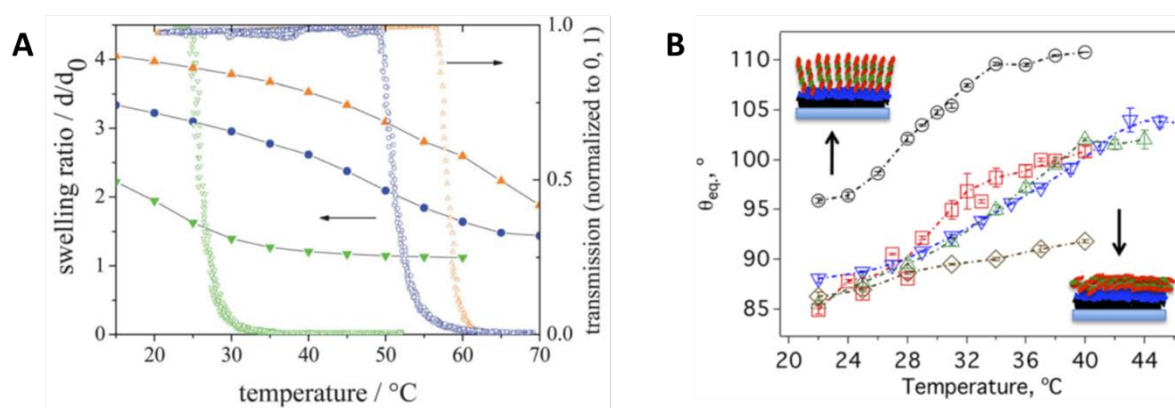


Figure 3. (A) Temperature-dependent collapse of poly(MEO₂MA-*co*-OEGMA-*co*-BPEM) terpolymer-based gels plotted as swelling ratio (d/d_0) and comparative normalized cloud point curves of the terpolymers measured by UV-Vis transmittance in aqueous solution.³⁵ (B) Temperature-dependent equilibrium water CAs (θ_{eq}) of poly(MEO₂MA-*co*-OEGMA) brush coatings measured in decane.³⁹

In addition to ellipsometry and CA measurements, characterization via quartz crystal microbalance with dissipation (QCM-D) constitutes a sensitive technique to investigate VPTTs.^{37, 40} By utilizing temperature dependent QCM-D measurements, the water content and degree of swelling of a thermoresponsive coating can be deduced from changes in quartz crystal frequency as well as from changes in coating dissipation, which is a measure for the viscoelastic properties of the polymer layer. Further, the determination of protein adsorption from biological media, such as blood serum or cell culture medium, by QCM-D can be used as indirect evidence for the VPTT of coatings and as an indicator for protein mediated cell adhesion of thermoresponsive substrates at 37 °C and 20 °C.⁴¹ In addition, atomic force microscopy (AFM) has shown to be a powerful method to assess temperature-dependent changes in coating morphology and thickness. Moreover, AFM allows to probe the physical material properties of thermoresponsive coatings. In that respect, not only changes in the elastic modulus and

1 Introduction

deformation can be determined, but also adhesive forces between the thermoresponsive coating and AFM tips or even cells can be assessed in order to investigate the mechanism of temperature-modulated cell detachment.⁴²⁻⁴⁵

The vast majority of thermoresponsive coatings are based on PNIPAm, since it has been the most thoroughly investigated polymer due to its sharp phase transition in aqueous solution and an LCST around ~ 32 °C.^{23, 29} This is ideal for biomedical applications as it allows protein and cell adhesion under physiological conditions (37 °C) and exhibits protein and cell repellent properties at ambient temperatures (~ 20 °C). Hence, PNIPAm has been used for various purposes, such as therapeutic delivery⁴⁶⁻⁴⁸, biosensing⁴⁹⁻⁵⁰, bioseparation^{17, 51-52} and as “smart” tissue culture substrates for the temperature-triggered detachment of single cells as well as confluent 2D cell monolayers (sheets).⁵³⁻⁵⁵ A myriad of different cell culture substrates based on PNIPAm, including crosslinked gels, polymer brushes and physically adsorbed polymer layers, have been utilized for the fabrication of various cell sheet types of both mammalian and human origin.⁵⁶⁻⁶⁰ As such, thermoresponsive PNIPAm surfaces constitute a functional basis for cell sheet engineering, which is a bottom-up tissue engineering approach that allows the fabrication of 3D artificial tissues as well as facilitates the efficient transplantation of cell mono- or multilayers in regenerative therapy.⁶¹⁻⁶⁸ Regarding the latter, commercial, thermoresponsive UpCell™ substrates based on PNIPAm have been successfully used as functional tissue culture substrates to detach cell sheets comprising tissues of various origins.^{55, 69} For example, oral mucosal epithelial cell sheets have been used for cornea reconstruction⁷⁰, the treatment of esophageal stricture⁷¹ and the prevention of intrauterine adhesion.⁷² In addition, primary hepatocyte, periodontal ligament and nasal mucosal epithelial cell sheets have been applied for *in vivo* 2D and 3D liver models⁷³, periodontal reconstruction⁷⁴ as well as the regeneration of middle ear mucus⁷⁵, respectively. Further, Ebihara, Sato *et al.* used layered chondrocyte sheets for cartilage regeneration⁷⁶⁻⁷⁷ and sheets of lung and skin fibroblast were utilized by Kanzaki *et al.* for lung sealing.⁷⁸ In another striking example, Okano and co-workers transplanted myoblast sheets detached from PNIPAm culture substrates during open heart surgery to treat dilated cardiomyopathy and showed that the cell sheet technology is a promising alternative to heart transplantation.⁷⁹

Besides PNIPAm, thermoresponsive coatings based on poly[oligo(ethylene glycol) methacrylate]s (POEGMAs), polyoxazolines (POx), poly(glycidyl ether)s (PGEs), poly(methyl vinyl ether) (PMVE)⁸⁰⁻⁸² and poly(*N*-vinylcaprolactam) (PVCL)⁸³⁻⁸⁴ are among the most promising with regards to cell sheet fabrication applications. As depicted in Figure 4, the main structural difference between those polymers and PNIPAm is the absence of strong

1 Introduction

H-donors, such as the amide groups in PNIPAm. Hence, the often-observed thermal hysteresis of PNIPAm, which arises from rather strong intra- and intermolecular H-bonds in its collapsed, dehydrated state^{22, 29}, is usually rather negligible for POEGMAs, POx and PGEs, depending on the experimental conditions as well as the applied measurement technique.¹⁹ Comparative cloud point curves of a POEGMA copolymer and PNIPAm, which were synthesized with comparable molecular weights by atom transfer radical polymerization (ATRP) (Figure 5A), measured by UV-Vis turbidimetry are illustrated in Figure 5B.⁸⁵

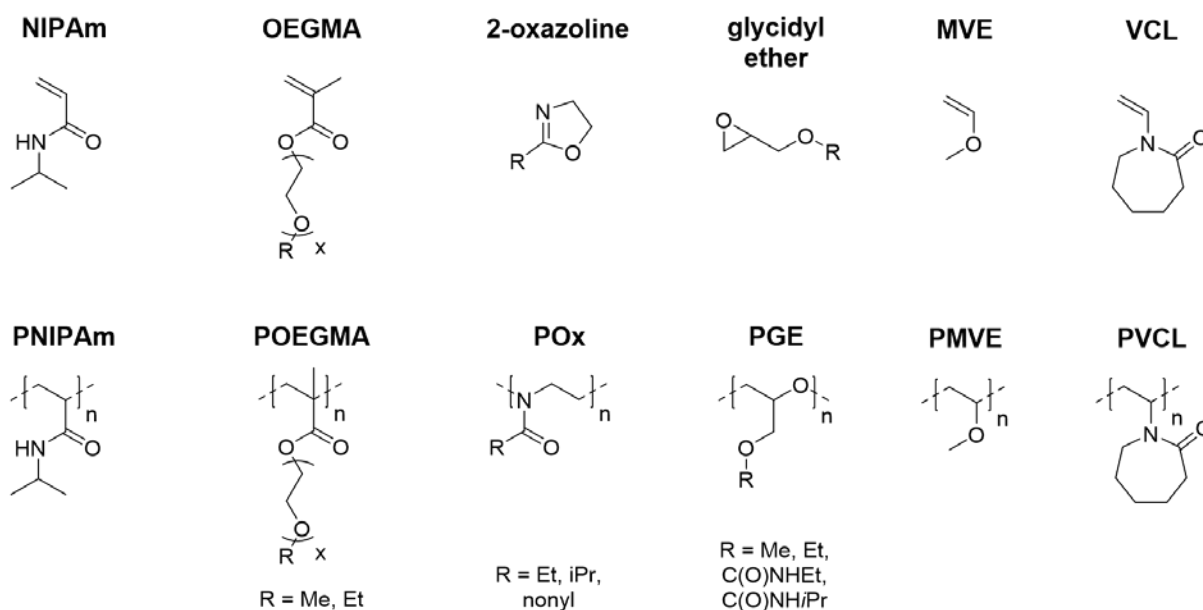


Figure 4. General chemical structures of thermoresponsive polymers applied for tissue culture applications and their respective monomeric building blocks.

To provide an alternative for PNIPAm, Lutz *et al.* introduced thermoresponsive POEGMA copolymers based on the two monomers MEO₂MA and OEGMA ($M_n = 475 \text{ g mol}^{-1}$).⁸⁵ They showed that the phase transition of such copolymers can be adjusted within a range of 28 to 90 °C via comonomer composition and that crosslinked POEGMA gels exhibited VPTTs close to the CPTs of the respective linear polymers in solution.^{24, 86-87} Although exhibiting a tunable phase transition in the physiological range^{35, 37, 42, 88}, thermoresponsive brush coatings comprising POEGMA copolymers demonstrated rather cell repellent properties and did not allow the efficient adhesion of cells without prior treatment of the culture substrates nor cell proliferation to confluent monolayers.⁸⁹⁻⁹²

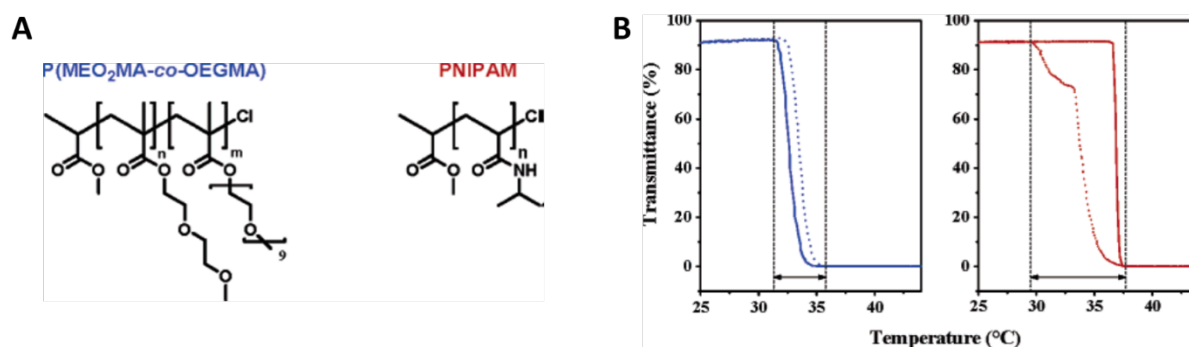


Figure 5. (A) Chemical structure of well-defined POEGMA and PNIPAm synthesized by ATRP.⁸⁵ (B) Comparative cloud point curves of POEGMA and PNIPAm measured by UV-Vis turbidimetry. Whereas PNIPAm exhibits a characteristic hysteresis behaviour, POEGMA does not exhibit marked hysteresis.⁸⁵

However, the accessibility of a multitude of thermoresponsive methacrylate polymers as well as PEG-substituted acrylates with side chains of different hydrophilicities still potentially provides an extensive library for the design and optimization of thermoresponsive PEG-based surface coatings for tissue culture applications.⁹³⁻⁹⁴ For example, Dworak and co-workers used tri(ethylene glycol) monoethyl ether methacrylate (TEGMA-EE) as a monomer to prepare polymer brushes on glass culture substrates. They obtained thermoresponsive coatings on which human dermal fibroblasts (HDF) showed good adhesion and detached as confluent sheets in a temperature-modulated manner after lowering the temperature to 17.5 °C.⁹⁵⁻⁹⁶

Due to their “pseudopeptide” structure, POx are non-toxic and known to be highly biocompatible.⁹⁷ Further, the polymerization of 2-oxazoline monomers via the “living” cationic ring-opening polymerization (ROP)⁹⁸⁻⁹⁹ has shown to be very robust, allows excellent control over polymer molecular weight and architecture¹⁰⁰⁻¹⁰³, and enables the synthesis of POx with various properties, depending on the nature of the pendant side groups.¹⁰⁴⁻¹⁰⁵ As the two most hydrophilic POx, poly(2-methyl-2-oxazoline) and poly(2-ethyl-2-oxazoline) have been utilized as, e.g., bioinert coatings¹⁰⁶ and are currently investigated and proposed as alternatives to poly(ethylene glycol) (PEG) for biomedical applications. This is mostly owed to their stability against oxidative degradation as compared to PEG and other polyethers, such as PGEs.¹⁰⁶⁻¹⁰⁷ It has been shown that thermoresponsive POx homo- and copolymers show a sharp phase transition in aqueous solution, that their CPTs are dependent on molecular weight and concentration and can be tuned via comonomer composition. Further, poly(2-n-propyl-2-oxazoline) and poly(2-isopropyl-2-oxazoline) exhibit CPTs in the physiological range as well as tend to crystallize upon temperature-induced aggregation.¹⁰⁸⁻¹¹¹ Dworak and co-workers were

the first to introduce thermoresponsive coatings based on poly(2-isopropyl-2-oxazoline) as well as poly[(2-ethyl-2-oxazoline)-*co*-(2-nonyl-2-oxazoline)] brushes. They immobilized their POx on Si substrates via surface-termination of the cationic ROP and used the brush coatings for the fabrication of HDF sheets, which they detached within 40-60 min after cooling to 20 °C.¹¹¹⁻¹¹²

A relatively new class of thermoresponsive polymers which have a considerable potential for tissue culture applications are PGEs. In general, PGEs can be regarded as biocompatible PEG analogs with low toxicity and high functionality due to their pendant side groups.¹¹³⁻¹¹⁵ Depending on the hydrophilicity of these side groups, many PGE homo- and copolymers have shown to exhibit thermoresponsive behaviour in aqueous solution. In 2002, Aoki *et al.* were the first to report the thermoresponsive nature of low molecular weight homopolymers (~ 3 kDa) based on the monomers glycidyl methyl ether (GME), ethyl glycidyl ether (EGE) and ethoxy ethyl glycidyl ether (EEGE) which all displayed CPTs with a sharp phase transition in the vicinity of the physiological temperature range.¹¹⁶ In the following, Watanabe and co-workers further investigated the temperature-dependent aggregation behaviour and self-assembly of poly(EGE) homopolymers and amphiphilic poly(EGE-*block*-EG) block copolymers in water¹¹⁷⁻¹¹⁹ as well as in ionic liquids.¹¹⁸⁻¹²⁰ They further showed for the first time, that self-assembled poly(EEGE) monolayers on gold exhibit a temperature-dependent change in wettability indicating a VPTT at ~ 36 °C¹²¹, which was close to the previously reported CPT of poly(EEGE) in aqueous solution (~ 40 °C).¹¹⁶ Labbé *et al.* were the first to synthesize high molecular weight (~ 3-90 kDa) poly(GME) using the monomer-activated anionic ROP and showed that the CPT slightly decreased with increasing polymer molecular weight from ~ 61 °C for 10 kDa to ~ 57 °C for 40-90 kDa polymers.¹²² Most surprisingly, although exhibiting a phase transition temperature of ~ 63 °C, low molecular weight poly(GME) (~ 3 kDa) were not fully soluble even at low temperatures (20 °C) and yielded opaque solutions over the entire temperature range studied.¹²² Labbé *et al.* further reported the statistical copolymerization of GME with glycidyl methacrylate (GMA) to obtain crosslinkable polymers as a basis for thermoresponsive hydrogels.¹²³ Schmalz and co-workers prepared double-responsive hydrogels based on triblock copolymers comprising a pH-responsive poly(2-vinylpyridine) and a statistical, thermoresponsive poly(GME-*stat.*-EGE) block. They showed that the CPT was tunable via the GME/EGE comonomer ratio and that the copolymer blocks exhibit a sharp phase transition with negligible hysteresis.¹²⁴⁻¹²⁵ Based on the reports of Schmalz and co-workers, Weinhart *et al.* synthesized low molecular weight copolymers (~ 2-3 kDa) with a GME:EGE ratio of 1:3, which exhibited CPTs in the physiological range in both, aqueous buffer solutions as well as in the presence of the protein bovine serum albumin (BSA).¹²⁶ They further synthesized

copolymers based on GME with additional *N*-isopropyl carbamate side groups via copolymerization of GME with EEGE and subsequent post-functionalization. As a first proof of principle, Weinhart *et al.* utilized self-assembled monolayers (SAM) on gold model substrates to culture NIH-3T3 mouse fibroblasts and successfully detach confluent cell monolayers by reducing the temperature. In addition, cell sheet detachment was correlated with the temperature-dependent adsorption of the cell adhesion promoting protein fibrinogen measured via surface plasmon resonance, which verified the temperature-modulated switchability of the PGE coatings.¹²⁶⁻¹²⁷ Weinhart and co-workers further used both the thermal- and the monomer-activated anionic ROP to synthesize thermoresponsive PGEs based on GME and EGE and demonstrated that their CPT can be adjusted via the comonomer ratio, that the CPTs are dependent on molecular weight and polymer concentration, and that GME and EGE copolymerize in a random manner utilizing the monomer-activated synthesis.¹²⁷⁻¹²⁸ In addition, they investigated the optimal conditions for the manufacture of functional PGE SAMs on gold substrates with respect to the fabrication of NIH-3T3 fibroblast cell sheets in order to define general design guidelines for PGE-based thermoresponsive brushes¹²⁹⁻¹³⁰ as well as successfully transferred those guidelines order to establish PGE coatings based on block copolymers comprising adhesive, cationic amine anchor blocks to applied glass substrates, from which they detached HDF sheets in a temperature-triggered manner.¹³¹ In an approach similar to the one reported by Weinhart *et al.*¹²⁶, Dworak and co-workers synthesized high molecular weight poly(glycidol-*co*-ethyl glycidyl carbamate) copolymers to functionalize glass culture substrates. Utilizing those thermoresponsive substrates, they successfully cultured and detached skin-derived fibroblasts as well as keratinocytes as singularized cells.¹³² Recently, Isono *et al.* extended the existing library of thermoresponsive PGEs to homo- and copolymers based on the monomers 2-methoxyethyl glycidyl ether (MeEOGE), 2-ethoxyethyl glycidyl ether (EtEOGE) and 2-(2-ethoxyethyl)ethyl glycidyl ether (EtEO₂GE). These can be regarded as analogs to the OEGMA and OEGA systems discussed above. They showed that the side chain structure had a significant effect on the polymer's CPT, that the CPTs of statistical copolymers could be tuned via comonomer composition and that block copolymers exhibited a complex thermoresponsive behaviour governed by micelle formation.¹³³

1.1.3 Synthetic Strategies for thermoresponsive Poly(glycidyl ether)s

PGEs are traditionally synthesized via the “classical” oxy-anionic ROP in which alcoholates, but sometimes also hydrides or amines, are used as initiators for the S_N2 -type ring-opening reaction of epoxide groups in a thermal manner.^{114, 134-135} This polymerization method has a “living” character and tolerates the presence of many functional groups which are not prone to nucleophilic attack through the initiator or the reactive alkoxide chain end and has therefore been utilized for the ROP of various protected and functional glycidyl ether monomers, such as EEGE¹³⁶, allyl glycidyl ether (AGE)¹³⁷ and *tert.*-butyl glycidyl ether (*t*-BuGE).^{113, 138-139} However, in contrast to the oxy-anionic ROP of ethylene oxide (EO), substituted oxiranes like alkylene oxides and glycidyl ethers are prone to chain transfer reactions via proton abstraction in α -position of the epoxide ring, which leads to ring-opening of the oxirane and the formation of a new allyloxy initiator species (Figure 6).^{114, 140} This commonly observed side reaction occurs more frequently as the basicity of the used initiator increases and has shown to limit the attainable molecular weight of PGEs synthesized via this approach and good control over the chain length is usually only given for polymers with molecular weights of up to ~ 6-30 kDa, depending on the used monomers.¹⁴⁰

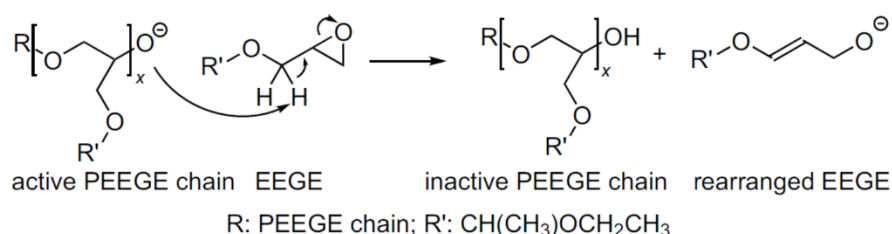


Figure 6. Mechanism of the molecular weight-limiting chain transfer reaction to the monomer and the formation of an allyloxy initiator species during the oxy-anionic ROP of EEGE.¹⁴⁰

In general, the reactivity of PGEs towards thermal ROP depends on the size of the counterion of the alkoxide initiator, the applied polymerization temperature, as well as on the electronic and steric influence of the glycidyl substituents.¹³⁴⁻¹³⁵ For example, increasing counterion sizes ($\text{Na}^+ < \text{K}^+ < \text{Cs}^+$) increase the dissociation of the reactive alkoxide species and usually lead to higher reaction rates, which are commonly in the time frame of at least several hours up to days. Utilizing the thermal oxy-anionic ROP, thermoresponsive PGE copolymers based on GME and EGE with molecular weights ranging from ~ 2 to 5 kDa have been synthesized using alcoholate initiators, such as PhOK, *t*-BuOK or MeOK, as well as functional, protected initiators, such as benzylthioundecanol, in order to further couple the PGEs to gold model substrates after thiol deprotection.^{116, 124, 126-128} Reinicke *et al.* determined the copolymerization parameters of GME

and EGE in THF at 50 °C and *t*-BuOK as initiator to be $r_{\text{GME}} = 1.31$ and $r_{\text{EGE}} = 0.55$ (Fineman-Ross), which indicates the slightly preferential incorporation of GME into the statistical copolymers.¹²⁴ Heinen *et al.* suggested that this slight compositional gradient could have an effect on the thermoresponsive properties of the PGEs and showed that the gradient PGE structure broadened the phase transition regime around the CPT of 2 kDa copolymers as compared to random copolymers synthesized via the monomer-activated anionic ROP.¹²⁸

On that note, in order to obtain PGEs with higher molecular weights, the monomer-activated anionic ROP has demonstrated to be an efficient and versatile method.^{122, 141-142} In particular, the use of quaternary ammonium salt initiators, such as tetraoctylammonium bromide ($\text{N}(\text{Oct})_4\text{Br}$)^{122, 142} or tetrabutylammonium azide ($\text{N}(\text{Bu})_4\text{N}_3$)¹⁴³⁻¹⁴⁴, in combination with Lewis acid activators, such as triisobutyl aluminum ($\text{Al}(i\text{-Bu})_3$), have shown to facilitate the synthesis of PGEs with molecular weights of up to 100 kDa in a controlled, “living” manner. This method further allows the polymerization of monomers, such as epichlorohydrin (ECH)¹⁴¹, epicyanohydrin (EPICH)¹⁴⁵ or GMA¹²³, which are generally not accessible via the “classical” approach due to side reactions with reactive alcoholate groups. The reason that high molecular weights are attainable is mainly due to the bulky tetraalkylammonium counterions, which suppress alkoxide-driven chain transfer reactions. Although bromide and azide are weak nucleophiles and therefore constitute rather poor initiators as compared to alkoxides, the reaction rates during the monomer-activated method are much faster than those of the “classical” oxy-anionic ROP and the polymerization usually proceeds to completion within a few hours at low temperatures ≤ 0 °C. This is due to the presence of a trialkyl aluminum compound, which activates both the initiator and the monomer via coordination to the weakly nucleophilic tetraalkylammonium counterion (Br^- or N_3^-) as well as via coordination to the epoxide oxygen, respectively. The mechanism of the monomer-activated anionic ROP is illustrated in Figure 7.

1 Introduction

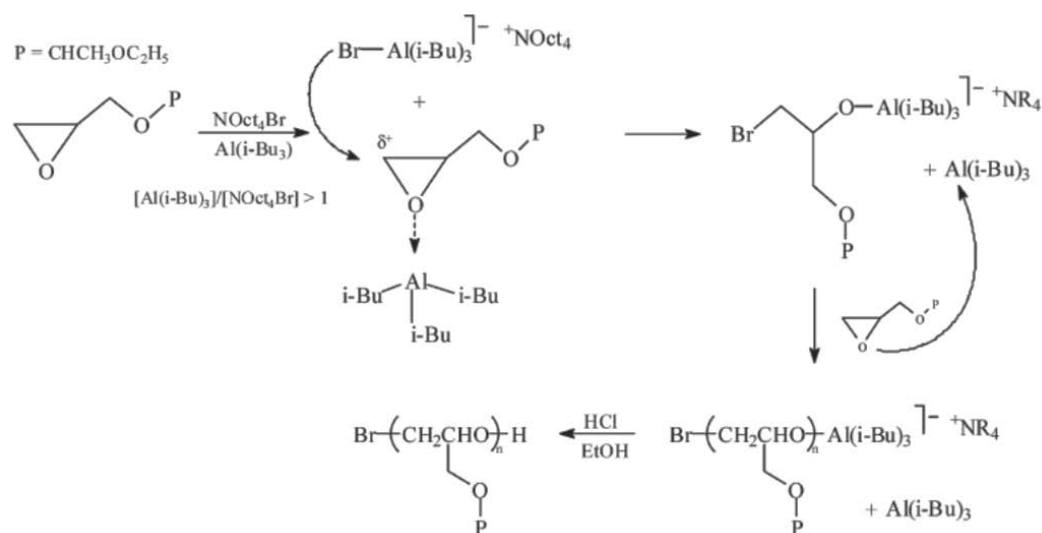


Figure 7. Mechanism of the monomer-activated anionic ROP of EEGE using tetraoctylammonium bromide ($\text{N}(\text{Oct})_4\text{Br}$) as initiator and triisobutyl aluminum ($\text{Al}(\text{i-Bu})_3$) as activator.¹⁴²

Since the activator forms a quantitative complex with the initiator, an excess of the Lewis acid is necessary for the reaction to occur in order to sufficiently activate the monomer. In addition, the synthesis of high molecular weight PGEs ($\sim 30\text{-}100$ kDa) generally requires activator/initiator ratios in the realm of about 3:1 to 7:1, which is due to the loss of activator via its coordination to the oxygen atoms of the formed polyether chains.^{122, 142} Heinen *et al.* have synthesized thermoresponsive copolymers of molecular weight between 9 and 24 kDa using GME and EGE as monomers. Using activator/initiator ratios of 4:1, they determined the copolymerization parameters to be $r_{\text{GME}} = 0.95$ and $r_{\text{EGE}} = 0.92$ (Fineman-Ross), which indicates a close to random incorporation of the two comonomers.¹²⁸ The monomer-activated anionic ROP has further shown to be a viable method for the synthesis of multifunctional block copolymers.¹⁴⁶ For instance, Heinen *et al.* performed a sequential polymerization of thermoresponsive block copolymers comprising a random GME/EGE and a homo-AGE block (Figure 8) suitable for post-modification via thiol-ene chemistry.¹³¹

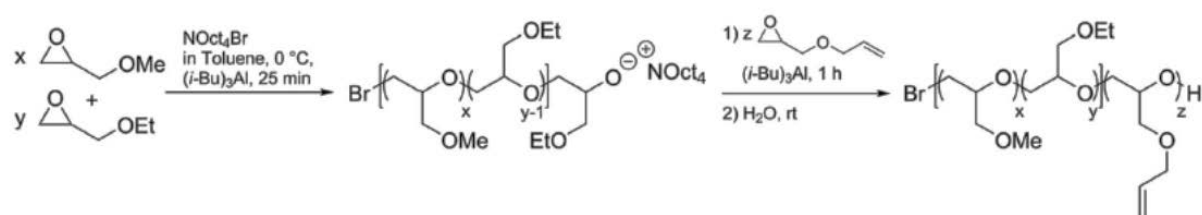


Figure 8. Sequential monomer-activated anionic ROP of a block copolymer comprising a random GME/EGE block and an AGE anchor block.¹³¹

1.2 Thermoresponsive Coatings for Cell Sheet Engineering

The practicality of using thermoresponsive surfaces for cell culture applications and especially for the detachment of cell monolayers with further use in cell sheet engineering and as artificial tissues for regenerative medicine has sparked the development of thermoresponsive coatings over the past two decades.¹⁴⁷⁻¹⁴⁹ While a myriad of coating approaches and different polymer systems have been utilized for the manufacture of such coatings, most studies are still conducted using PNIPAm as well as PNIPAm-based copolymers.⁵⁵⁻⁵⁶ Nevertheless, depending on the coating technique, structure and the chemical nature of the used polymers and copolymers, the formulation of some general guidelines for the design of thermoresponsive surfaces can be inferred when studying the available literature, although the underlying mechanisms of cell sheet detachment are not fully understood in many cases and are still in demand of thorough investigation.^{54, 150-154}

1.2.1 Design Guidelines for Thermoresponsive Surfaces for Cell Sheet Fabrication

The main factor governing the functionality of thermoresponsive coatings is their hydrophilicity¹⁵⁵, which usually correlates with protein adsorption¹⁵⁶ and therefore cell adhesion and proliferation at 37 °C. Equally important are the layer thickness and architecture of the coating including homogeneity as well as grafting density, which mainly depend on the applied coating method and govern the material properties often resulting in a profound effect on cellular behaviour. It cannot be overstated at this point, that the material properties of the used culture substrate, its chemical nature, hydrophilic/hydrophobic balance, physical interaction with the thermoresponsive coating, intrinsic adhesiveness towards cells as well as its geometry, morphology and roughness may influence cell behaviour and thermal response of the coating. Therefore, the performance of the thermoresponsive coatings with regards to cell sheet fabrication is governed by several factors. However, systematic investigations on the influence of the culture substrate on its thermoresponsive coating are yet rare, although effects of the substrate nature on cell adhesion and detachment have been reported.^{44, 157-159}

The most prominent thermoresponsive surfaces, which were developed in the group of Okano and finally got commercialized under the brand name UpCell™, have been used for the fabrication of numerous cell sheet types as well as transplantable 3D tissue constructs so far. The latter surfaces are manufactured by electron beam polymerization (EBP) of NIPAm on

standard tissue culture polystyrene (TCPS) substrates.^{53-54, 160-162} Due to the relatively poor control over the polymerization process, PNIPAm coatings manufactured by EBP resemble branched and crosslinked brush- to gel-like structures with highly layer thickness-dependent properties. Akiyama *et al.* showed, that PNIPAm coatings on TCPS substrates promote cell adhesion of bovine carotid artery endothelial cells (BAECs) and temperature-triggered cell sheet detachment only when the PNIPAm layer thicknesses were in the range between 15 and 30 nm and that cell adhesion was poor on layers with thicknesses exceeding 30 nm, which was attributed to the increased hydrophilicity, polymer chain mobility and higher water content and was further correlated with the decreased adsorption of fibronectin. In contrast, coatings thinner than 15 nm promoted cell adhesion of the investigated cell types, but did not allow the detachment of confluent cell sheets (Figure 9).¹⁵⁷ They further found, that the coatings resembled the characteristic elemental composition of PNIPAm, were evenly spread on the rough TCPS substrates as thin layers with PNIPAm particle-like domains and that the coatings exhibit a temperature-dependent change in hydrophilicity between 37 and 20 °C, although not accompanied by a significant macroscopic swelling.⁴⁴

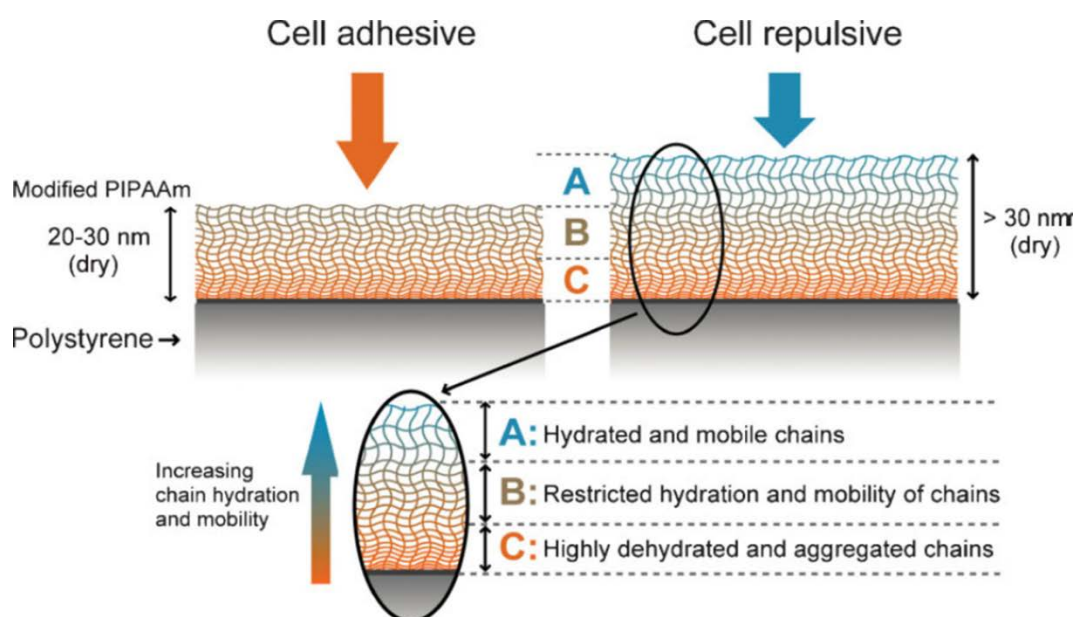


Figure 9. Schematic illustration of thickness-dependent cell-adhesive properties of PNIPAm gels grafted to TCPS by EBP.¹⁶³

In comparative studies of electron beam-grafted PNIPAm gels on more hydrophilic glass substrates, Fukumori *et al.* found that the dependence on layer thickness with regards to the functionality of the coating in cell culture was shifted to lower values with coatings exceeding 7 nm being cell repellent for BAECs.¹⁵⁸⁻¹⁵⁹ This behaviour was attributed to the more hydrophilic nature of glass culture substrates, which enables the more efficient swelling of the

PNIPAm coatings, whereas swelling is hampered and dehydration of the polymer layer is promoted on more hydrophobic TCPS substrates (Figure 10).

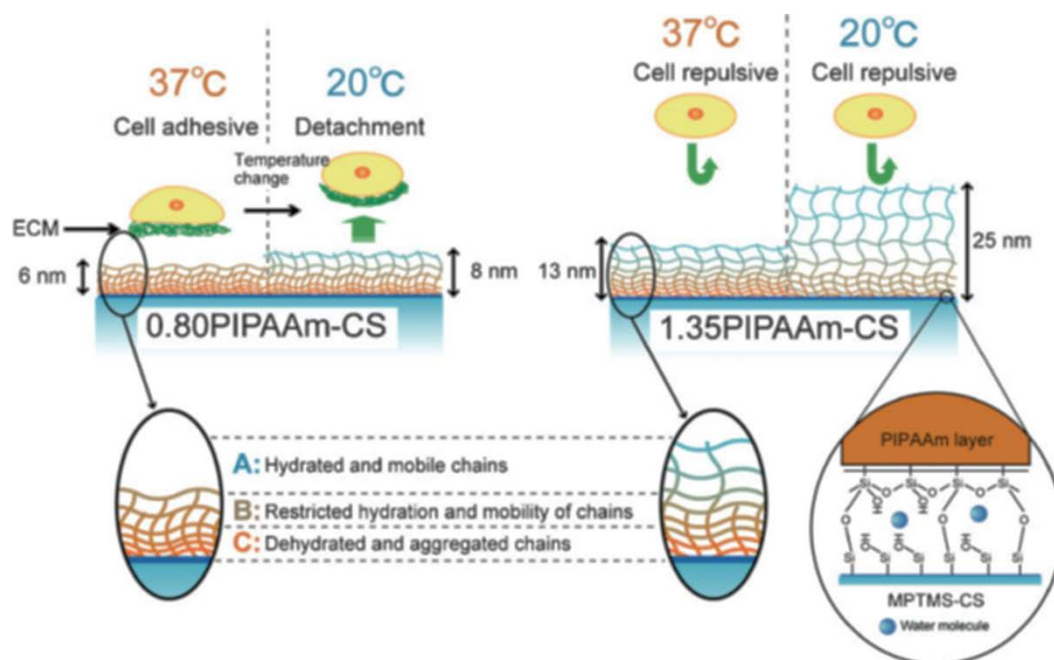


Figure 10. Schematic illustration of thickness-dependent cell-adhesive properties of PNIPAm gels grafted to glass cover slips (CS) by EBP.¹⁶³

However, morphological differences between the rather rough TCPS and the smoother glass substrates might also be a factor which needs to be considered. As shown in Figure 11, morphological AFM images of PNIPAm coatings on TCPS (Figure 11A) and glass (Figure 11B) exhibit markedly different topologies, presumably due to the different surface roughness of the two culture substrates.

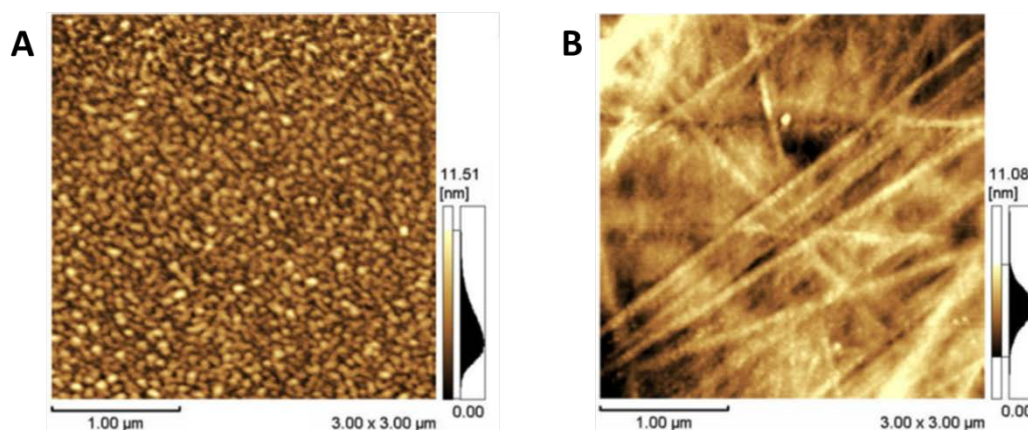


Figure 11. Representative morphology images of PNIPAm coatings prepared by EBP on TCPS (A) glass CS (B) measured by AFM at air under ambient conditions.¹⁵⁸

A similar relation between coating thickness and cell response using mouse 3T3 fibroblasts was found by Nash *et al.* using thermoresponsive hydrogels, which they manufactured by crosslinking PNIPAm chains onto TCPS substrates via covalently incorporated benzophenone (BP) units using UV light.¹⁶⁴ This approach was first introduced by Recum *et al.*, who copolymerized 4-(*N*-cinnamoyl carbamide) methyl styrene with NIPAm in order to crosslink and immobilize PNIPAm gels onto TCPS and to detach confluent BAEC and retinal pigmented epithelial cell sheets.¹⁶⁵⁻¹⁶⁶ In contrast to these findings, polymerization of vaporous NIPAm on TCPS substrates using the plasma glow discharge process, which was first reported by Pan *et al.*¹⁶⁷, did not show a dependence of cell adhesion applying BAECs and cell sheet detachment on the deposited layer thickness in the 50 to 80 nm range. This was attributed to the formation of an adhesion-promoting layer within the PNIPAm coatings, which is created by destructive side reactions of the NIPAm monomer or the formed polymer during the high energy plasma process.^{45, 151-153}

To overcome the inherent cell repellent properties of PNIPAm, which are typically observed for macroscopic layers¹⁶⁸, and to maximize the temperature triggered response, numerous hydrophobic and hydrophilic comonomers as well as cell adhesive ligands, such as peptide-based RGDs, or cell adhesion promoting proteins (CAPs), such as fibronectin, have been incorporated into PNIPAm coatings.¹⁶⁹ Utilizing spin coating and solvent casting techniques, Rochev and co-workers have made an extensive effort to render physically immobilized PNIPAm layers adhesive and suitable for cell sheet detachment. In this context, the tuning of the PNIPAm layer thickness, treatment with CAPs or the incorporation of hydrophobic comonomers did not only improve cell adhesion and detachment of mouse 3T3 fibroblast, mouse (MS-5) stromal cell and human umbilical vein endothelial cell (HUVEC) sheets, but was also beneficial for the physical adhesion as well as the intermolecular cohesion between the spin coated copolymers on hydrophobic TCPS and poly(ethylene terephthalate) (PET) as well as on hydrophilic glass culture substrates.¹⁷⁰⁻¹⁷⁶ Comprehensive studies regarding the adjustment of PNIPAm coating properties have been conducted by Okano and co-workers using EBP. By incorporating hydrophilic¹⁷⁷⁻¹⁸¹ or ionic comonomers comprising carboxylic acid or tertiary amine groups into their layers¹⁸²⁻¹⁸⁶, they were able to amplify the rehydration of their coatings and therewith, decrease BAEC sheet detachment times.¹⁸⁷⁻¹⁸⁸ In addition, the use of membranes improved BAEC sheet detachments via the enhanced rehydration of the PNIPAm coatings through the porous culture substrates.^{180, 189-190} They were further able to improve cell adhesion and enhance cell proliferation while retaining control over BAEC and rat primary hepatocyte sheet detachment by incorporation of hydrophobic comonomers¹⁹¹⁻¹⁹² as well as cell

adhesive peptides and/or growth factors¹⁹³⁻²⁰², which, at times, even allowed the serum free culture and detachment of neonatal HDF sheets and singularized HUVECs.

In addition to gel-like coatings, thermoresponsive polymer brushes have been successfully utilized as coatings for cell sheet fabrication. Brushes which are “grafted from” culture substrates via surface-initiated controlled radical polymerization (SI-CRP), such as ATRP and reversible addition-fragmentation chain-transfer (RAFT) polymerization, usually comprise densely grafted, highly elongated polymer chains due to the high concentrations of surface-immobilized initiators used. Hence, the main factors influencing the adhesion and detachment of confluent cell sheets are the hydrophilicity of the polymer and the thickness of the respective grafted brush layers. For example, Mizutani, Li *et al.* synthesized PNIPAm brushes on TCPS and Si substrates using ATRP and found that an increase in polymer chain length (layer thickness) decreased the adhesion of BAECs and HepG2 cells. They also found that the optimal layer thicknesses were 10 and 20-45 nm for TCPS and Si surfaces, respectively, and that the detachment of sheets was hampered at thicknesses below these values.²⁰³⁻²⁰⁴ Further studies also showed that cell sheet detachment became slower when the PNIPAm grafting density and/or the layer thickness were decreased, indicating a lower rate of rehydration for less dense and thinner polymer brushes, which also correlated with higher amounts of adsorbed proteins.²⁰⁵⁻²⁰⁶ CRP techniques further allow the fabrication of block copolymer brushes²⁰⁷⁻²⁰⁸ as well as post-functionalization of the brush-terminal group²⁰⁹, which are both useful tools to tune the phase transition as well as the cell adhesive properties of the coatings. For example, end-group modification by functionalization of PNIPAm brushes prepared by surface-initiated RAFT (SI-RAFT) polymerization with terminal carboxylic acid groups (Figure 12) facilitated the fabrication of confluent monolayers comprising smooth muscle cells (SMCs), which usually poorly adhere to PNIPAm layers as well as other thermoresponsive coatings.²⁰⁹

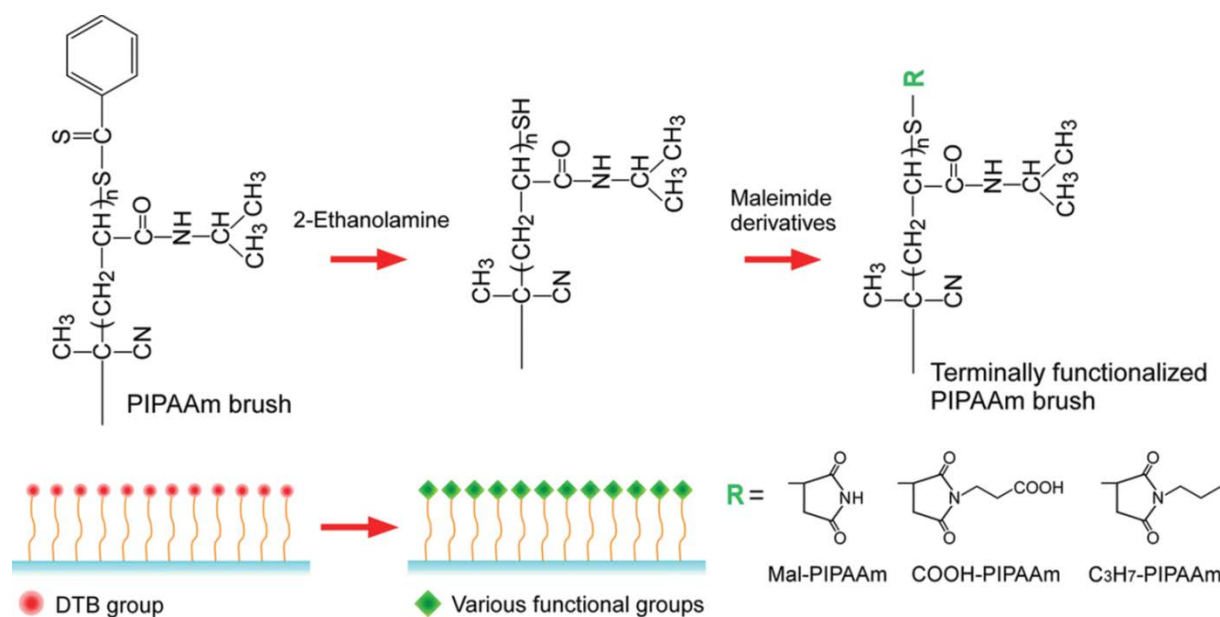


Figure 12. Schematic illustration of the terminal group functionalization of PNIPAm brushes grafted to glass by SI-RAFT via dithiobenzoate (DTB) cleavage and thiol-ene coupling with maleimide derivatives.²⁰⁹

In contrast to PNIPAm brushes, thermoresponsive POEGMA brushes prepared by SI-ATRP have not shown to support cell adhesion without additional modification, which is likely due to their comparably high inherent hydrophilicity. Consequently, the successful fabrication of cell sheets from such substrates has not been reported.^{39, 210-211} However, using an optimized, slightly more hydrophobic system based on the monomer TEGMA-EE, Dworak and co-workers prepared ATRP brushes with thicknesses ranging from 3 to 18 nm on glass substrates from which they successfully detached confluent HDF sheets.⁹⁵⁻⁹⁶

Compared to thermoresponsive brushes prepared by “grafting from” techniques, the grafting densities attainable via the “grafting to” method are usually much lower, which is due to the steric repulsion between the polymer chains, which have to diffuse and assemble onto the substrate surface. Nevertheless, there are some examples of thermoresponsive coatings prepared by this approach which yield highly functional thermoresponsive coatings. Dworak and co-workers used the surface-terminated cationic ROP to immobilize poly(2-isopropyl-2-oxazoline) and poly[(2-ethyl-2-oxazoline)-*co*-(2-nonyl-2-oxazoline)] onto glass substrates. The coating thicknesses were in the range of 4 to 11 nm and allowed the culture and detachment of HDF sheets.¹¹¹⁻¹¹² The same group also reported the surface-immobilization of high molecular weight ($R_g \sim 100$ nm) poly(glycidol-*co*-ethyl glycidyl carbamate) copolymer onto glass culture substrates via the coupling of residual glycidol hydroxyl groups with surface bound anhydrides. They obtained brush-like coatings with thicknesses between 20 and 60 nm

supposedly comprising polymer loops and tails with which they could culture and detach singularized skin derived fibroblast as well as keratinocyte sheets.¹³²

1.2.2 Coating Approaches for Plastic Cell Culture Substrates

From a technical point of view, strategies for the fabrication of polymer coatings can be classified into “grafting from” and “grafting to” approaches. Whereas the latter relies on the immobilization of pre-formed polymers to plastic substrates, the former utilizes surface-initiated polymerization of reactive monomers from substrate surfaces.

1.2.2.1 The Photochemistry of Benzophenone

Utilizing photochemistry for the functionalization of surfaces and curing of coatings or adhesive layers has many advantages over thermal as well as chemically more sophisticated techniques (e.g. “click” chemistry). First, the use of UV- or visible light, which is more efficient than thermal energy in terms of energy density, allows for the precise temporal and spatial control over the curing/functionalization process and thus allows surface patterning and an exact adjustment of the desired material properties. Moreover, the availability of light sources with various geometries, wavelengths and intensities, allow for the accurate adjustment of the required reaction conditions with respect to the specific photochemical reaction or photophore used and further facilitate the scalability towards a high throughput production as well as the adaptation to different surface geometries.

BP is arguably the most widely used and versatile photophore used for industrial coatings as well as in (bio)organic chemistry and material science.²¹²⁻²¹³ Due to its outstanding photochemical properties, such as the long lifetime stability towards ambient light and convenient excitation wavelength of 365 nm²¹⁴⁻²¹⁵, as well as due to its decent chemical stability, low reactivity towards water, and a variety of accessible diaryl ketone building blocks, BP and its derivatives have had a sweeping impact on the development of organic surface coatings via different photografting and photoimmobilization techniques. In addition, BP has found widespread application in biochemistry and is frequently used for mapping of ligand-protein or protein-protein interactions and their respective binding sites, identification of molecular targets and mapping of interactome processes²¹⁶, bioconjugation and site-specific modification of biopolymers as well as for proteomic analyses.

Among other diaryl ketones, such as anthraquinones, xanthenes and thioxanthenes, BP belongs to the class of Norrish type II radical photoinitiators, which can undergo photoreduction in presence of hydrogen donor molecules and, unlike Norrish type I photoinitiators, do not dissociate into two separate radicals via α -cleavage.²¹⁷ Upon photon absorption, BP can be reversibly excited into biradicaloid triplet states by undergoing either $n \rightarrow \pi^*$ or $\pi \rightarrow \pi^*$ transitions. During $\pi \rightarrow \pi^*$ transition ($\lambda < 350$ nm) an electron of the carbonyl π bond is excited into a higher energy singlet state S_2 of the carbonyl p^* orbital, which rapidly (150 fs^{218}) undergoes internal conversion (IC) to the lower energy singlet state S_1 . In contrast, during $n \rightarrow \pi^*$ transition ($\lambda > 350$ nm), a non-binding electron from the carbonyl oxygen is directly excited into the lower energy singlet state S_1 of p^* . Through a rapid ($6\text{-}10 \text{ ps}^{218}$) intersystem crossing (ISC) process, BP can transfer into its first triplet state T_1 . This usually occurs via passing through the higher energy triplet state T_2 ($\pi\text{-}\pi^*$), which is isoenergetic to S_1 , or via a higher energy vibrational level of T_1 followed by the fast vibrational decay to T_1 .²¹⁹⁻²²¹ It has been shown recently that T_1 has a mixed $n\text{-}\pi^*/\pi\text{-}\pi^*$ character and that BP might directly react from its higher energy triplet state T_2 ($\pi\text{-}\pi^*$).²²² In Figure 13, the Jablonski diagram including all of the prevalent BP excitation and relaxation processes as well as both $n \rightarrow \pi^*$ and $\pi \rightarrow \pi^*$ transitions occurring on the molecular level of BP are illustrated.

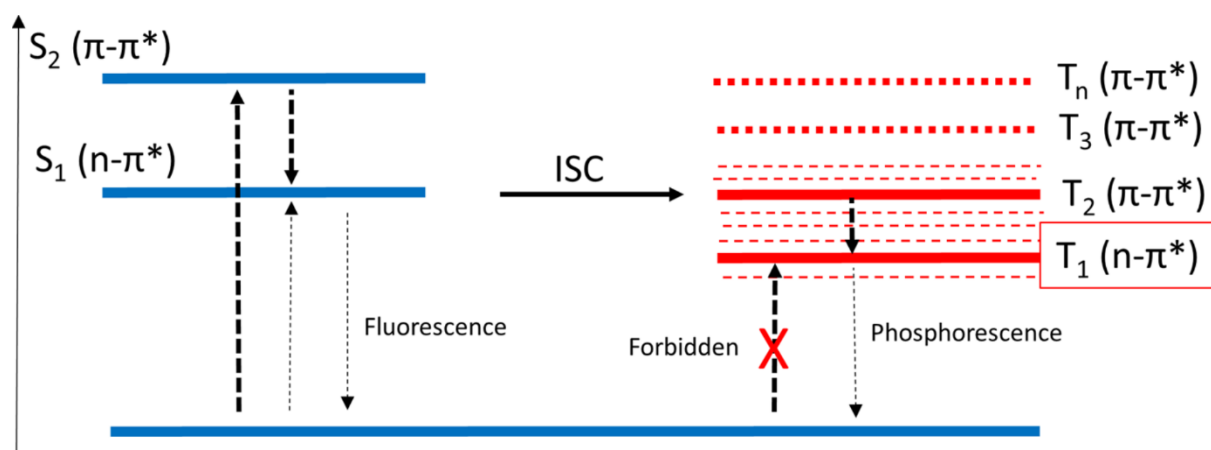


Figure 13. Excited states of BP illustrated by the Jablonski diagram.²¹²

In both excited S_1 and T_1 states, the C-O carbonyl bond becomes weaker and lengthens from 1.21 (S_0) to 1.35 (T_3) Å.²²¹ Further, due to the disruption of the electronic symmetry and the resulting electron-electron repulsion between the C and O lobes, the carbonyl C atom switches from a sp^2 -like to a pyramidal sp^3 hybridization as it is shown in Figure 14A. Among the three possible triplet states of BP, which are depicted in Figure 14B, the $n\text{-}\pi^*$ diradical is the most reactive, has the longest lifetime and decays within 5 ns to 3 μs , depending on the reaction medium as well as on the nature of the BP substituents. Especially due to the favorable

stereoelectronic orientation of the singly occupied n_p orbital, which allows the perpendicular access to the diradicaloid species, the $n-\pi^*$ state is more reactive than the higher energy delocalized $\pi-\pi^*$ state.

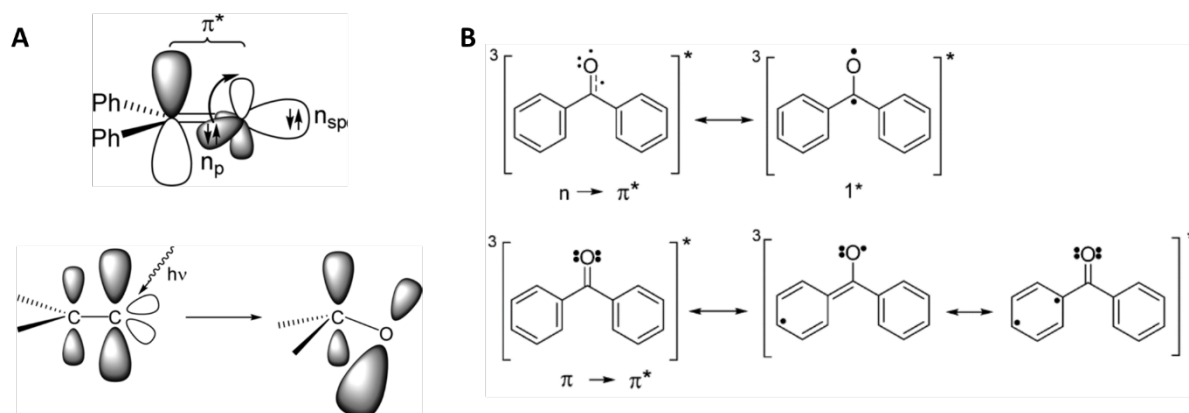


Figure 14. (A) $n \rightarrow \pi^*$ transition and symmetry change in electron density of the BP carbonyl group upon irradiation.²¹² (B) Possible triplet states and respective resonance structures of BP.²¹²

This allows a good overlap of the carbonyl n_p orbital with, e.g., s-orbitals of aliphatic C-H or hydroxylic O-H bonds. Hence, the most prominent reaction BP undergoes from T_1 ($n-\pi^*$) is the insertion into C-H or O-H bonds via hydrogen abstraction and subsequent radical recombination (Figure 15). Furthermore, well-known reactions of the excited BP triplet state are the [2+2] cycloaddition to C-C double bonds (Paterno-Büchi oxetane formation) and the sensitization of reactive, energy absorbing compounds. Additionally, the high bond strength of the carbonyl adjacent C-C bonds ($D_{C-CO} = 397 \text{ kJ mol}^{-1}$) in BP do not promote decarbonylation nor type I or type II cleavage reactions. Due to the biradicaloid character of T_1 ($n-\pi^*$), which is owed to the presence of unpaired electrons in the nonbinding carbonyl orbitals n_p , BP can either directly abstract hydrogen atoms from aliphatic or hydroxyl groups or, in case of amines providing α -hydrogens, facilitate hydrogen abstraction via intermediate charge-transfer complexes (Figure 15).

1 Introduction

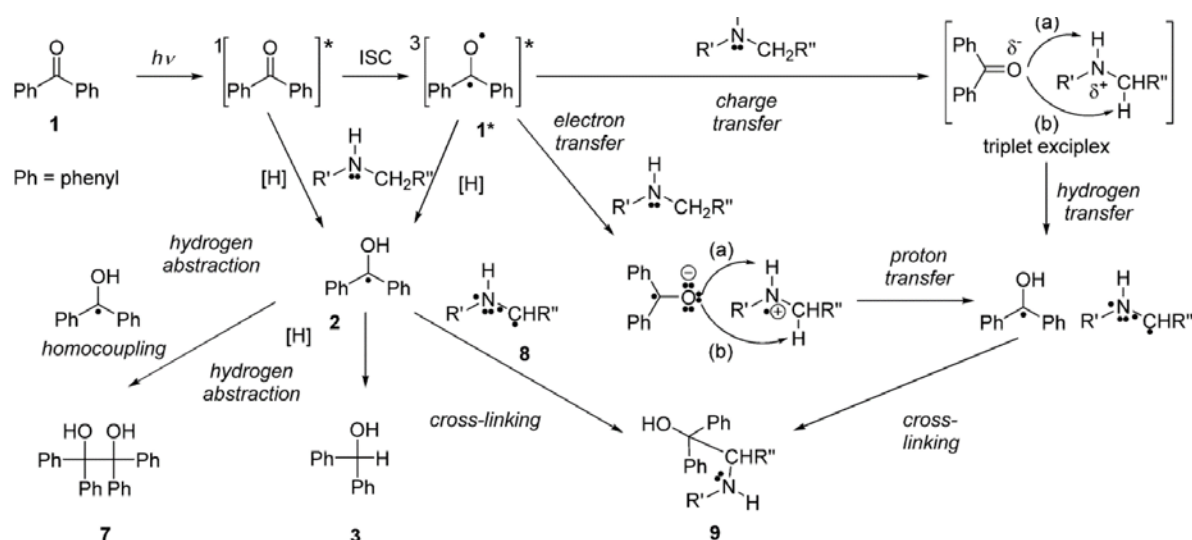


Figure 15. Possible pathways for crosslink formation via BP photochemistry.²¹²

In general, the BP ketyl radical is formed rapidly via H-abstraction within 10-100 ns, whereas radical recombination is the rate-limiting step ($> 1 \mu s$) since recombination from T_1 is forbidden and can only occur through S_1 after reverse ISC. Additionally, self-recombination to benzpinacol, which has recently shown to undergo thermally triggered reversible C-C bond formation²²³, is generally about one order of magnitude slower than cross-recombination reactions, which result in benzhydrol compounds comprising a newly formed, stable C-C bond (Figure 15). The reactivity of the ketyl radical is also highly dependent on the nature of BP substituents. Electron donors, such as alkoxy and alkylamino groups as well as phenyl substituents lower the energy of the n_p orbital, which is only susceptible to inductive effects, whereas the π^* orbital is influenced by both inductive and mesomeric effects and its energy level is increased. Due to the lower energy level and the electrophilic nature of the diradical in the $n-\pi^*$ state, hydrogen abstraction is therefore inhibited, especially in polar media. Electron withdrawing BP substituents have the opposite effect and increase the reactivity of the $n-\pi^*$ state. Compared to hydrogen abstraction from O-H bonds, the reaction of BP with aliphatic C-H bonds, which is commonly known as C, H-insertion, is much faster, which offers a myriad of possible pathways for various coupling, crosslinking and immobilization reactions between small organic molecules, biological macromolecules as well as many polymeric materials. C-H bonds which are especially prone to C, H-insertion reactions are methylene groups in α -position next to heteroatoms (N, O and S) and in tertiary benzylic position as well as methylene groups in α -position of amino acids. The reactivity of further aliphatic methylene groups is generally lower and increases in the direction of primary aliphatic $<$ secondary aliphatic $<$ tertiary aliphatic $<$ primary benzylic/allylic $<$ secondary benzylic/allylic $<$ double benzylic/allylic.

With respect to the manufacture of surface coatings on organic/plastic substrates, BP can be applied as a photoinitiator utilizing two essentially different approaches. The first approach relies on the formation of reactive radicals, which are generated on the substrate surface via H-abstraction by a BP diradical in a triplet state. Subsequently, the surface radicals can serve as reactive centers for the initiation of the free radical chain growth polymerization of monomers with reactive double bonds, such as acrylates or various vinyl compounds. Hence, the formation of polymer layers via this approach classifies as a “grafting from” method and can either be accomplished using monomer solutions, under bulk conditions or even from the gas phase. In the second strategy, already preformed polymers are immobilized and/or crosslinked onto a substrate surface via a “grafting to” approach, which mainly relies on the C, H-insertion of active BP diradicals into a myriad of C-H bonds presented on the surface and/or the coating material but might also occur through [2+2] cycloaddition or the recombination of secondary radicals. As a result, efficient immobilization/crosslinking is only achieved when the BP moiety is already covalently attached either to the substrate surface or to the coating material. With regards to plastic cell culture substrates, most of the applied materials fulfill the requirements for the utilization of BP chemistry as a basis for the fabrication of functional coatings, which can be used for tissue culture applications. For example, the tertiary benzylic position in PS as well as the ester α -position in PET provide excellent reactivity towards BP-induced H-abstraction and enable both “grafting from” and “grafting to” approaches. In addition, due to the relative non-specificity of H-abstraction as well as radical recombination reactions, many different plastic substrates, except aromatic materials without appropriate H-donor groups (e.g. polyether sulfone (PES)), have been successfully coated utilizing BP chemistry. Besides PS and PET, application-relevant substrates, such as polycarbonate (PC), cycloolefin copolymers (COC), polypropylene (PP), polyethylene (PE), polyvinyl chloride (PVC), polyvinylidene fluoride (PVDF) and nitrocellulose (NC), are frequently used as tissue culture substrates, which makes coating strategies based on BP a very versatile and powerful tool for the fabrication of coatings used as functional tissue culture substrates. Similarly, thermoresponsive polymers such as PGEs, are themselves prone to react with BP, since they almost exclusively comprise hydrogen atoms in α -position, which allows intermolecular crosslinking and, hence, the formation of thermoresponsive hydrogels. However, it is important to keep in mind, that polymers like PS and PGE, which bear their most reactive methylene groups in the polymer backbone, are especially prone to chain scission through radical non-oxidative or oxidative side reactions.²²⁴⁻²²⁸ Such side reactions can occur

particularly at high BP concentration and may in principle impair efficient surface functionalization via immobilization, crosslinking or grafting polymerization.

1.2.2.2 UV-induced Grafting as a “Grafting From” Approach

Surface-initiated polymerizations of reactive monomers, such as vinyl compounds, (meth)acrylates or (meth)acrylamides, are commonly classified as “grafting from” techniques. To efficiently manufacture coatings via this approach, reactive centers, which are mostly radicals, but in some cases may also be nucleophiles or ions, must be generated on the top surface layer of a substrate. This can either be achieved by subjecting the substrate to high-energy treatment, such as exposure to electron beams^{53, 162}, plasmas^{167, 229} or hard radiation (gamma rays)²³⁰ or by chemical modification of the substrate with initiators for UV- or thermally initiated CRP.²³¹⁻²³³ Alternatively, surface radicals can also be created via the irradiation with UV- and/or visible light using a variety of free radical-type photoinitiators, which are either soaked into, adsorbed to or covalently bound to the substrate surface, or simply dispersed in the reactive monomer phase deposited on the substrate.

The first report on a “grafting from” approach for the fabrication of thermoresponsive cell culture substrates utilized EBP and was published by the group of Okano in 1990.⁵³ This was followed by the elucidation of the underlying mechanism of cell sheet detachment^{54, 160-162} and eventually lead to the commercialization of UpCell™ surfaces based on PNIPAm on standard TCPS substrates. In principle, a NIPAm solution in isopropanol (20-80 wt.-%) is homogeneously spread over a TCPS surface and grafted from the substrate by subjecting the solution to an electron beam (0.25-0.30 MGy). The resulting coatings have a branched to crosslinked, gel-like structure and have been used consistently to harvest various types of cell sheets for regenerative medicine (chapter 1.2.3). Similar strategies were employed using the plasma polymerization of NIPAm vapor as well as the gamma ray-induced polymerization of NIPAm from solution to functionalize PS culture substrates.^{167, 230} Furthermore, there are numerous reports on the CRP of thermoresponsive polymer brushes on gold and Si-based model surfaces, which include systematic studies on the influence of polymer brush characteristics, such as comonomer composition, chain length and grafting density, on cell adhesion and detachment. However, well defined coatings fabricated by CRP on more applied glass and plastic culture substrates are rather scarce and often involve extensive modification of the substrate surface with either physically adsorbed adhesive interlayers, such as ionic multilayers

containing CRP initiators^{39, 210-211, 234}, or covalent immobilization of CRP initiators, such as alkyl halides (e.g. for ATRP)²³³ or dithiocarbamates (e.g. for RAFT polymerization).²³¹⁻²³²

In one of the first reports which utilized UV irradiation in a “grafting from” approach, NIPAm was polymerized on PS substrates from isopropanol solution (5-40 wt.-%) containing BP (0.1%) as photoinitiator. The resulting thermoresponsive substrates prove to be suitable for the culture and detachment of L-929 mouse fibroblasts.²³⁵ Since then, a number of thermoresponsive coatings on various substrate materials have been fabricated using the “grafting from” approach, including PNIPAm and poly[2-(dimethylamino)ethyl methacrylate] (PDMAEMA) on oxygen plasma treated PTFE²³⁶, PNIPAm on PET membranes²³⁷, PNIPAm on oxidized PET and PS films²³⁸, poly(*N,N*-diethyl acrylamide) (PDEAAm) on Nylon membranes²³⁹ and PNIPAm on PS Petri dishes²⁴⁰ as well as on poly(dimethyl siloxane) (PDMS) culture substrates.²⁴¹⁻²⁴³ In general, the technique relies on the formation of radicals on the substrate surface, which can be either generated by cleavage or excitation of surface functional groups, such as double bonds, peroxides or ketones^{236, 238, 244}, respectively, or by H-abstraction through radical photoinitiators, such as BPs^{237, 239, 245}, acetophenones²⁴⁴⁻²⁴⁵ or anthraquinones.²⁴⁰ From the methodological viewpoint, which mainly depends on the grafting efficiency of the used substrate-monomer system, UV-induced grafting can be performed from a monomer solution, which is either spread over the substrate macroscopically²⁴⁵⁻²⁵⁴ or applied as a thin film between the substrate and, e.g., a quartz glass plate²⁵⁵⁻²⁵⁷, from a gaseous monomer/initiator phase^{253, 258-259} or directly from a thin bulk monomer/initiator film.²⁶⁰⁻²⁶³ In cases where a free, non-covalently bound photoinitiator is used, it is either dispersed in the respective gaseous, dissolved or bulk monomer phase^{245, 249, 251-254, 256, 261-263} or pre-adsorbed on the substrate before monomer deposition.^{246-248, 250, 255, 259} The general scheme of the photopolymerization of reactive vinyl monomers is illustrated in Figure 16.

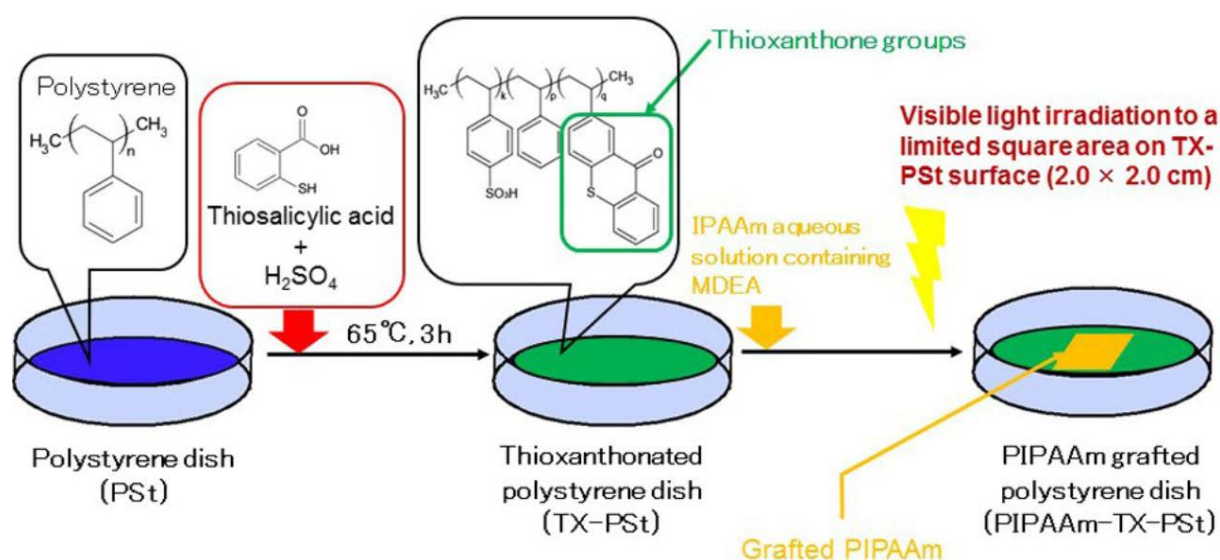


Figure 17. Preparation of a thermoresponsive PS culture dish by chemical modification with thioxanthone and photografting of PNIPAm using visible light.²⁶⁸

UV-induced Grafting from the Bulk Monomer Phase

Bulk surface photografting was originally developed for the lamination of polymer films^{264, 269} and, in terms of reaction rate and grafting efficiency, it is much faster than photografting from the gas phase and from solution, as layers of up to 5 μm can be obtained in time frame of about 30 s.²⁷⁰ It is further advantageous for the grafting of monomers with limited water solubility, since many organic solvents have adverse effects on grafting efficiency due to radical side reactions. In addition, the diffusion of rather hydrophobic monomers and photoinitiators to the commonly hydrophobic polymer substrates may further be limited by organic solvents, which subsequently lowers grafting efficiencies and increases the probability of polymerization in solution. Incidentally, the use of organic solvents or cosolvents is restricted with respect to the polymer substrate, since its dissolution is undesirable. Rånby and co-workers were one of the first to systematically investigate the bulk photografting in depth using various different monomers for the lamination of several different polymer film materials.²⁷⁰⁻²⁷¹ They found that in the first stage the bulk photografting comprises an induction period, which is much more pronounced for type II photoinitiators than for cleavable type I initiators and originates from the inhibition of radical formation on the surface by oxygen, which acts as a radical scavenger and is mainly responsible for the initial retardation of the polymerization. The second stage of the reaction is the surface initiation. Rånby showed, that the initiation of the polymerization is most probable on the surface of the polymer substrate rather than in the bulk monomer phase.

This is due to the relatively low energy of aliphatic C-H bonds, which are present on most polymer films and are easily cleaved by photoinitiators such as BP, as compared to many monomers which only comprise higher energy vinyl C-H bonds (e.g. acrylic acid). In such cases, it is only of minor impact if the photoinitiator is mixed into the monomer phase, since the predominant reaction is the initiation of the polymerization from the substrate surface. However, when monomers with aliphatic side chains are used, side reactions between BP and the monomers may occur more frequently and initiate uncontrolled polymerization or crosslinking within the bulk phase, which can interfere with the grafting from the surface and reduce its efficiency. In such cases, pre-adsorption or covalent coupling of the photoinitiator onto the substrate surface may offer better control over the photografting process. The successive polymerization stage is then followed by a solid-state photoreduction of BP, which leads to coupling of remaining BP moieties to the grafted chains ends as well as to further crosslinking of the formed polymer chains. The group of Rånby further found, that among other vinyl monomers acrylates have the highest reactivity towards photopolymerization and -grafting and that the reactivity of the polymeric substrates decreases in the order of Nylon (Polyamide) > PET > PP > PE > PC, which is in accordance to the reactivity of their respective C-H bonds towards H-abstraction by BP (chapter 1.2.2.1).²⁷¹ In addition, they showed that due to the self-screening effect, an increase in BP concentration as well as in the layer thickness of the liquid monomer mixture have a negative effect on bulk photografting, whereas an increase in reaction temperature or the addition of multifunctional crosslinkers influence the photopolymerization in a positive manner and lead to much higher grafting efficiencies.²⁷¹

Thermoresponsive Bottlebrushes and their Potential as Surface Coatings

As outlined in chapter 1.1.3, thermoresponsive, low molecular weight PGEs, which are referred to here as oligo(glycidyl ether)s (OGEs), are conveniently synthesized via the “classical” oxy-anionic ROP. Successive post-functionalization of the hydroxy end-group by, e.g., acrylation or methacrylation converts OGEs into macromonomers with reactivity towards free- and CRP and, hence, renders them applicable for surface functionalization via “grafting from” approaches. Serving as a general proof of concept, Gunkel *et al.* synthesized oligoGME methacrylates, which they grafted from gold model surfaces via SI-ATRP. They investigated the protein resistance of the oligoGME bottlebrush coatings and compared their anti-fouling properties to linear and dendritic glycerol based bottlebrush architectures with respect to molecular weight and bulkiness of the side chains (Figure 18).²⁷²

1 Introduction

In general, the characteristic feature of bottlebrushes, which are also commonly referred to as molecular brushes, cylindrical polymer brushes or brush-like macromolecules, is their high density of grafted oligomeric or polymeric side chains, which have significant effects on their conformation and physical properties, predominantly due to steric repulsion between the backbone-grafted side chains.²⁷³⁻²⁷⁷ Depending on the grafting density, molecular weight and chemical nature of the side chains, the flexibility, conformation and aggregation in solution as well as the adsorption and ordering of bottlebrushes on surfaces can be finely tuned, making them excellent model systems for experimental studies of polymer properties and the self-assembly to form hierarchical supramolecular architectures.²⁷⁴⁻²⁷⁹ Unsurprisingly, bottlebrushes are frequently used to modify the properties of polymeric bulk materials by blending and biomacromolecules with a brush-like structure²⁷⁷, such as proteoglycans and glycoproteins, are responsible for a myriad of biological functions in the human body.²⁷³

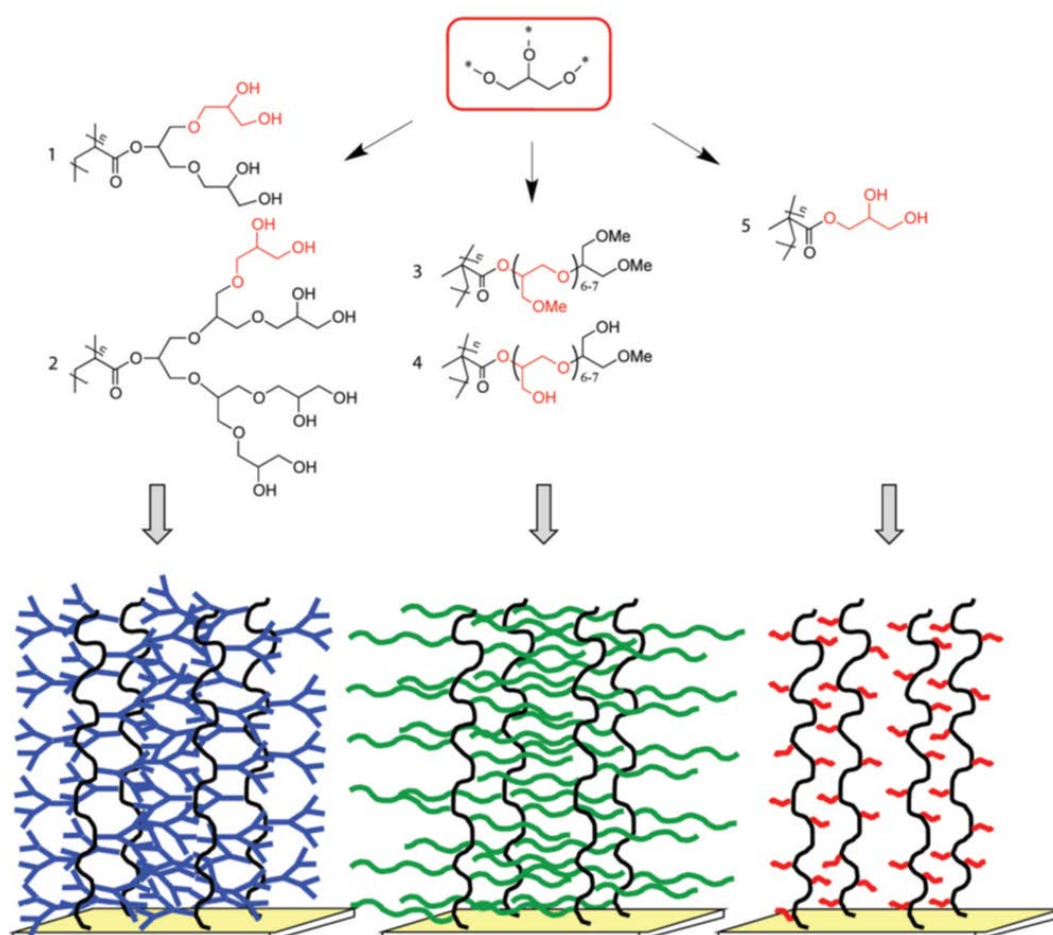


Figure 18. Structure of glycerol-based dendritic bottlebrushes (blue), linear bottlebrushes (green) and brushes with short side chains (red) grafted from gold substrates via SI-ATRP.²⁷²

From the synthetic point of view, bottlebrushes can be synthesized by “grafting through” of macromonomers, which automatically results in very high side-chain grafting densities.

However, the bulkiness of macromonomers often limits the attainable degree of polymerization and lowers control over the polymerization process, which usually results in low yields and broadened molecular weight distributions. Alternative strategies for the synthesis of bottlebrushes are the “grafting to” of preformed side chains to a polymer backbone and the “grafting from” of side chains from a backbone macroinitiator. While especially the former approach often suffers from a limited attainable grafting density due to the steric repulsion of side chains coupling to the backbone via functional group chemistry, the latter approach most notably requires extensive post-functionalization of the preformed backbone into a macroinitiator and offers limited control over side chain length, especially at high grafting densities. However, both “grafting to” and “grafting from” approaches potentially allow for the adjustment of the grafting density, at least in the lower realm, and introduce synthetic pathways for high molecular weight architectures, as compared to “grafting through” strategies, which are rather limited in this respect.^{273-275, 278} Altogether, the large variety of available polymerization techniques, coupling chemistries and polymer properties offer seemingly infinite possibilities to engineer macromolecules with specifically designed properties. The different approaches for the synthesis of macromolecular brushes are shown in Figure 19.

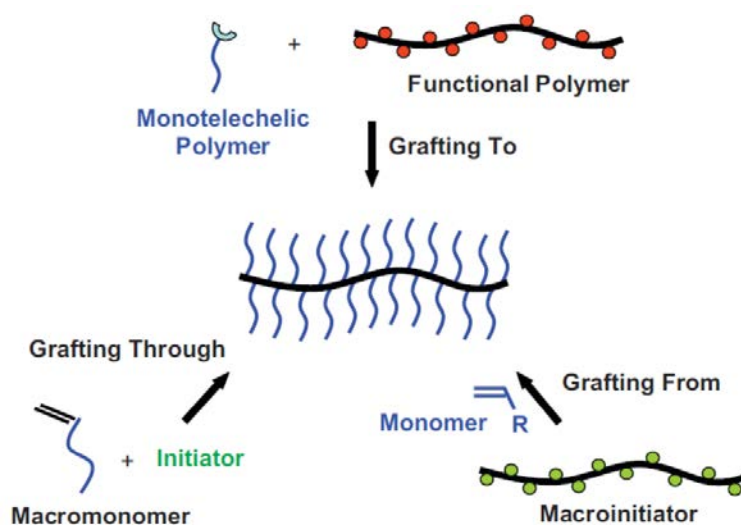


Figure 19. “Grafting through”, “grafting to” and “grafting from” as synthetic strategies to macromolecular bottlebrushes.²⁷³

Due to their extended conformation, bottlebrushes exhibit a rod-like structure in solution. Depending on the solvent and the respective solubility of the backbone and side chains, bottlebrushes can still undergo considerable conformational changes. This is especially the case for thermoresponsive bottlebrushes, which can undergo a transition from a rod-like to a globular conformation.^{273, 278} Li *et al.* showed that bottlebrushes with a polymethacrylate backbone

comprising grafted PNIPAm side chains exhibit a phase transition in aqueous solution and collapse from a rod-like to a globular structure upon increasing the temperature.²⁸⁰ Most importantly, they found that the conformational change only led to monomolecular particles which did not aggregate intermolecularly, as it would be typical for linear, thermoresponsive polymers. Further, the transition temperature of 32 °C perfectly matched the CPT of linear PNIPAm, which indicated a backbone-independent thermal response of the PNIPAm side chains.²⁸⁰ In another example, Pietrasik *et al.* grafted statistical copolymer side chains comprising *N,N*-dimethylacrylamide (DMA) and butyl acrylate (BA) or 2-(dimethylamino)ethyl methacrylate (DMAEMA) and methyl methacrylate (MMA) from polymethacrylate backbones.²⁸¹ Utilizing DLS measurements, they showed that the polymers collapsed intramolecularly at low concentrations when the average distance between the polymer chains was much larger than their hydrodynamic dimensions. Further, they showed that the thermal response of the polymers could be extenuated or even fully obliterated by increasing the incorporated amount of the hydrophobic comonomers BA and MMA. At high concentration, when the average distance between polymer chains was comparable to their hydrodynamic dimensions, intermolecular aggregation occurred, which concurs with the typical behaviour of linear PNIPAm chains.²⁸¹ Yet again, another unique temperature-triggered aggregation behaviour was observed by Yamamoto *et al.* who grafted statistical copolymer side chains comprising di(ethylene glycol) methyl ether methacrylate (MEO₂MA) and tri(ethylene glycol) methyl ether methacrylate (MEO₃MA) from a polymethacrylate macroinitiator backbone.²⁸² Upon heating in aqueous solution, both intra- and intermolecular aggregation of the bottlebrushes occurred and the phase transition as well as the hysteresis behaviour could be tuned via the comonomer ratio. In contrast, when PMEO₃MA-*block*-PMEO₂MA copolymer side chains were used, two separate aggregation stages were observed, and the bottlebrushes formed vesicles with aggregated PMEO₂MA shells and soluble PMEO₃MA cores.²⁸² These examples distinctly illustrate the accessibility of a large variety of properties attainable by combination of thermoresponsive polymers and bottlebrush architectures.

Although a variety of bottlebrushes have been synthesized in solution using CRP or ring-opening metathesis polymerization (ROMP)²⁸³, reports on the “grafting through” of bottlebrushes from substrate surfaces are rather scarce, mostly rely on SI-ATRP and involve sterically rather undemanding OEGMAs.^{39, 210-211, 234, 272, 284-287} In addition, while “grafting through” by FRP has been used to prepare bottlebrushes in solution to some extent and with mixed results with respect to attainable molecular weight²⁸⁸⁻²⁹³, the UV-induced grafting of macromonomers for surface functionalization has hardly been explored. In one example, Gao

1 Introduction

et al. synthesized methacrylated block copolymers comprising a bioinert PEG as well as an antimicrobial peptide block.²⁹⁴ They grafted the macromonomers from aqueous solution using argon plasma activated PDMS substrates by UV irradiation and obtained bottlebrush coatings with thicknesses between 1 and 2 μm and antimicrobial, antibiofilm as well as antifouling properties.²⁹⁴ Similar antimicrobial, antifouling coatings based on dual-functional bottlebrush coatings were fabricated by Zhi *et al.*²⁹⁵ They conjugated polyhexamethylene biguanide (PHMB) to allyl-terminated PEG (APEG) and also grafted the macromonomers from argon plasma activated PDMS using a dilute aqueous solution and either autoclaving-derived conditions or by UV irradiation to obtain bottlebrush coatings with an average thickness of 25 nm (Figure 20).²⁹⁵⁻²⁹⁶

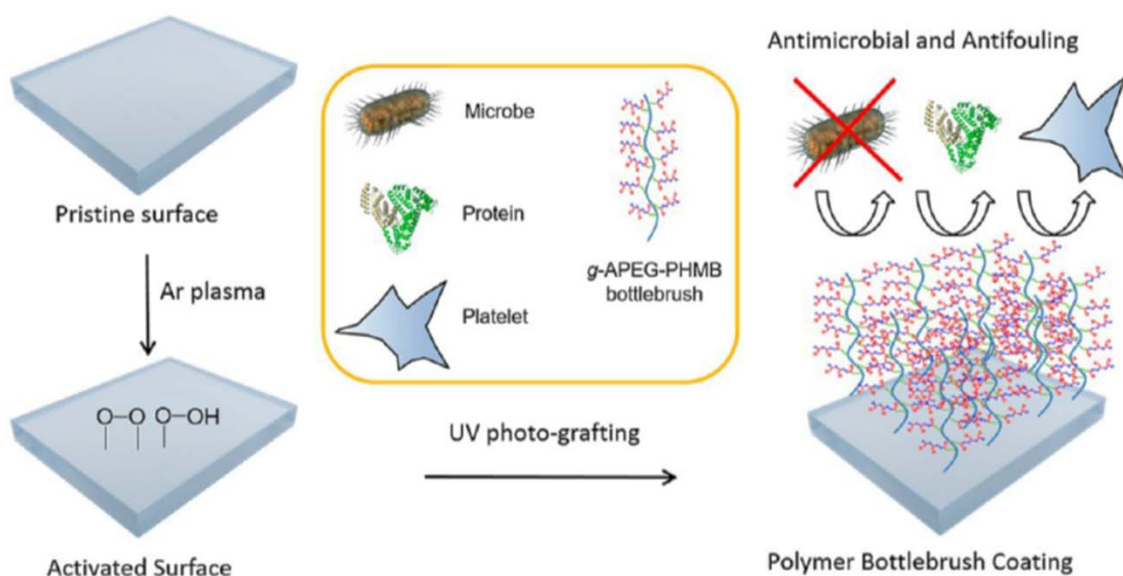


Figure 20. Grafting of antimicrobial, antibiofilm and antifouling APEG-PHMB bottlebrush coatings from argon plasma activated PDMS substrate.²⁹⁵

1.2.2.3 Adsorption of Block Copolymers as a “Grafting To” Approach

In “grafting to” approaches, presynthesized polymers are applied to a substrate material by either spin-, spray- or dip coating, solvent casting and physical adsorption or self-assembly from solution. Subsequently, the polymer coating is stably bound to the substrate surface via physical interactions or via covalent immobilization and/or crosslinking using various chemical coupling approaches. A big advantage over “grafting from” techniques is that the thermoresponsive polymers used are synthesized in advance and that their properties can be thoroughly investigated prior to coating. Furthermore, structural control over the coating architecture can be achieved by adjusting the molecular weight, composition and architecture of used macromolecules as well as by applying different coating techniques.

Nash, Gorelov, Rochev and co-workers used spin coating and solvent casting as facile techniques to deposit films of commercially available PNIPAm on TCPS and PET culture substrates. Although their coatings were solely annealed by drying under reduced pressure and not covalently bound to the substrate surfaces, they were able to fabricate cell sheets comprising mouse 3T3 fibroblasts¹⁷²⁻¹⁷³, human mesenchymal stem cells (hMSCs)¹⁷⁴ as well as mouse (MS-5) stromal cells.¹⁷⁵ To decrease the hydrophilicity and to increase the stability of their coatings via physical interactions, they further synthesized PNIPAm copolymers using *N-tert.*-butyl acrylamide (NtBAm)^{170-171, 176, 297-298} and octadecyl methacrylate (ODMA)²⁹⁷ as hydrophobic comonomers. This allowed the temperature-modulated fabrication of human pulmonary microvascular endothelial cell (HPMEC) sheets.²⁹⁸ By further applying CAPs to their poly(NIPAm-*co*-ODMA) and poly(NIPAm-*co*-NtBAm) coatings (Figure 21), they also cultured and detached confluent mouse 3T3²⁹⁷ as well as HUVEC sheets¹⁷¹, respectively. Building on this, Nash, Healy *et al.* used acrylamide benzophenone (AcBzPh) as a hydrophobic, photo-reactive comonomer to covalently immobilize and crosslink spin coated and solvent cast NIPAm-based gels onto PS culture substrates, which allowed mouse 3T3¹⁶⁴ and HPMEC sheet²⁹⁹ detachment, respectively. A similar approach based on a photo-reactive CCMS crosslinker, which was copolymerized with NIPAm, was used by Recum *et al.* to detach BAEC as well as retinal pigmented epithelial cell sheets.¹⁶⁵⁻¹⁶⁶

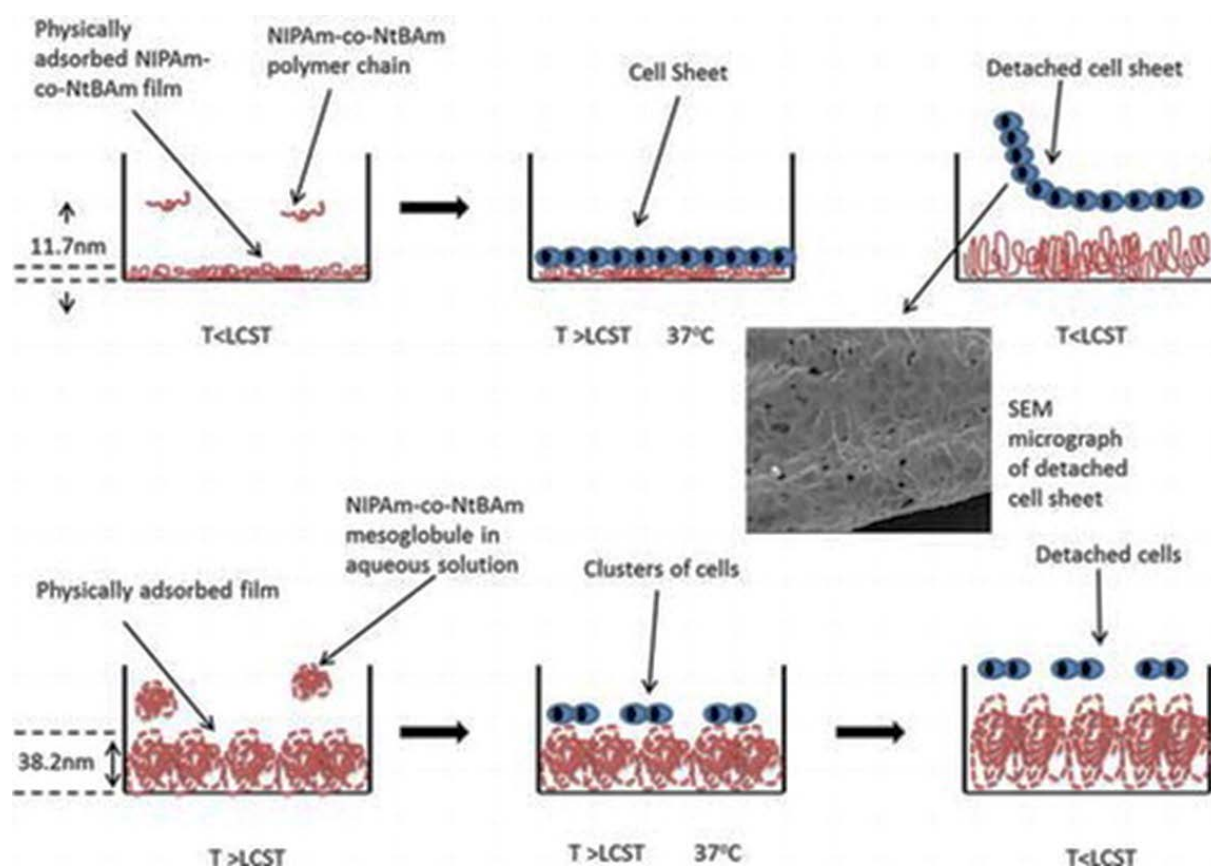


Figure 21. Physical adsorption of poly(NIPAm-co-NtBA) below and above its CPT yields cell adhesive coatings which allow cell sheet growth and proliferation and cell repellant coatings, respectively.²⁹⁸

The concept of physical adsorption of thermoresponsive NIPAm-based copolymers comprising hydrophobic comonomers onto plastic culture substrates has attracted some attention in recent years. As a simple and straightforward technique, which does not require expensive equipment and complicated polymerization procedures, it allows the controlled adsorption of thermoresponsive layers from, e.g., aqueous solution and is therefore independent on the geometry of the used culture substrate. Although thermoresponsive PNIPAm coatings have been immobilized onto glass culture substrates via physical adsorption through electrostatic interaction using polyelectrolyte primer layers³⁰⁰⁻³⁰¹, the adsorption of copolymers comprising hydrophobic blocks constitutes a more convenient and straightforward method. Hence, the functionalization of common hydrophobic cell culture materials, such as PS, PET or PC, does not require the introduction of ionic groups into the thermoresponsive polymer as well as no pretreatment of the culture substrates with, e.g., polyelectrolyte mono- or multilayers. However, due to the rather weak, short-range hydrophobic interactions between polymeric substrates and the hydrophobic segments of the thermoresponsive polymers, the block copolymer composition and architecture needs to be optimized. This is of particular relevance if physically adsorbed

coatings are used for cell culture experiments, since polymer depletion from the substrate surface may impair cell viability.

Physical Adsorption of Block Copolymers to Hydrophobic Substrates

To accurately understand and predict the adsorption behaviour of block copolymers to hydrophobic surfaces, it is important to consider some general phenomena regarding the adsorption and depletion of linear homopolymer chains at the interface between a liquid phase (e.g. a polymer solution) and a solid substrate. As it was laid out by Aubouy *et al.*, polymers reversibly adsorbing to an attractive substrate, which is mostly the case for physical adsorption via short-range hydrophobic interactions under good solvent conditions, generally form an interfacial layer with a well-defined structure, which is fundamentally governed by the thermodynamic balance between the entropy of the formed polymer loops, which constitute polymer segments in between two neighboring, adsorbed monomer units, and their steric repulsion.³⁰² As a result, under dilute conditions, the adsorption of higher molecular weight polymers is favored due to the higher entropy of the corresponding long-chain polymer loops. In contrast, under concentrated conditions, low molecular weight polymers preferentially adsorb to the surface, which is mainly driven by the steric repulsion between long molecular weight loops and the faster diffusion of shorter polymer chains to the substrate surface. In addition, as compared to thick polymer layers, ultrathin polymer films with thicknesses below the adsorbed polymer's radius of gyration R_g are more likely to dewet surfaces upon external stimuli, such as temperature changes, which is mainly due to their confined conformation.³⁰² These fundamental, theoretical considerations are a useful basis to describe the adsorption behaviour of block copolymers and imply the importance of the block copolymer architecture, namely the chain lengths of the respective blocks and their molecular weight ratio, on its adsorption behaviour as well as the structure and stability of the resulting polymer layer. However, with regards to the fabrication of functional surface coatings, the chemical composition and the resultant physical properties of the block copolymers further have a considerable effect on their adsorption behaviour. Hence, the adhesiveness of the substrate material towards the respective copolymer blocks, the physical interaction between the two blocks, as well as the solubility of both block copolymer segments in the used solvent are essential factors during the adsorption of polymer layers tethered to the surface via hydrophobic anchor blocks and comprising functional blocks directed away from the surface and adopting a brush-like conformation. In an extreme case, a block copolymer is adsorbed to a surface from

a selective solvent, which is a non-solvent for the anchor block and a good solvent for the “buoy” (brush) block.³⁰³ If the anchor block further has a high affinity towards the surface, while the brush block does not interact with the substrate material, the structure of the adsorbed film is governed by the chemical potential of the polymer solution at the solid-liquid interface and constitutes an equilibrium between a micellar, solvated copolymer phase and a lamellar, surface-bound copolymer film.³⁰⁴⁻³⁰⁵ For block copolymers with a high asymmetry comprising a low molecular weight anchor and a high molecular weight brush block, the thickness of the obtained layer depends on the balance between the van der Waals energy of the anchor block and the stretching energy of the brush, which often leads to densely grafted and highly extended polymer chains.^{303, 306-307} In case a non-selective solvent is used to adsorb a copolymer comprising two incompatible blocks of which only the anchor block is attracted to the substrate surface and the solvent is of good quality for both blocks, the structure of the adsorbed layer is almost entirely dependent on the copolymer’s asymmetry.³⁰⁸⁻³¹⁰ At a high asymmetry, the anchor block exhibits a pancake-like conformation on the substrate surface, while the buoy block forms a brush layer directed toward the solution and with a thickness proportional to its molecular weight.³⁰⁸ Concerning the practical implementation of adsorbed block copolymer coatings, most solvents can neither be regarded as entirely selective nor non-selective. Further, attractive interactions between the brush block and the substrate surface can usually not be excluded in practice. This is especially the case for thermoresponsive block copolymer coatings adsorbed to applied tissue culture substrates, since thermoresponsive polymers are potentially adhesive towards plastic culture substrates due to their partially hydrophobic character. Although PEG is itself not thermoresponsive and known to be highly water soluble, Pagac, de Vos *et al.* showed that PS-PEO block copolymers did not form well-defined polymer brushes when adsorbed to PS substrates from aqueous solution due to the competitive adsorption of both PS and PEG blocks to the surface.³¹¹⁻³¹² This illustrates that even under highly selective solvent conditions, the adhesive interaction between both copolymer blocks and the substrate plays a crucial role in the self-assembly of block copolymer brushes. It further implies the potential influence of the substrate material on the conformational structure and phase transition of thermoresponsive brush coatings, which was already shown to be an important factor concerning PNIPAm gels.¹⁵⁹

Thermoresponsive Block Copolymer Coatings for Cell Sheet Fabrication

In one of the first studies in which hydrophobic, physical adsorption was reported for the manufacture of thermoresponsive coatings for cell sheet fabrication, Ito and co-workers used PNIPAM-*block*-poly[(*R*)-3-hydroxybutyrate]-*block*-PNIPAM (PNIPAM-*block*-PHB-*block*-PNIPAM) triblock copolymers to coat PET culture substrates via the adsorption of PHB to the PET substrate surface. They performed the “grafting to” from dilute aqueous solution above the critical micelle concentration (CMC) of the copolymers and above their CPT at 37 °C and obtained stable coatings with thicknesses ranging from 4 to 8 nm. As compared to control surfaces comprising co-adsorbed gelatin, they were able to grow and detach single, sub-confluent mouse embryonic stem cells as well as hMSCs from triblock copolymer coatings in a temperature-triggered manner. Control experiments with PNIPAm homopolymers revealed that the driving force for the formation of functional, stable coatings was the adsorption of the PHB block to the PET substrates and that cell proliferation was improved due to the hydrophobic, cell adhesive nature of PHB.³¹³⁻³¹⁴ Nakayama *et al.* synthesized PNIPAm-*block*-poly(butyl methacrylate) (BMA) block copolymers using RAFT polymerization and spin coated them onto TCPS substrates from MeCN/DMF (5:1 v/v) solution. They obtained stable coatings comprising laterally phase-separated PNIPAm and PBMA domains (Figure 22).

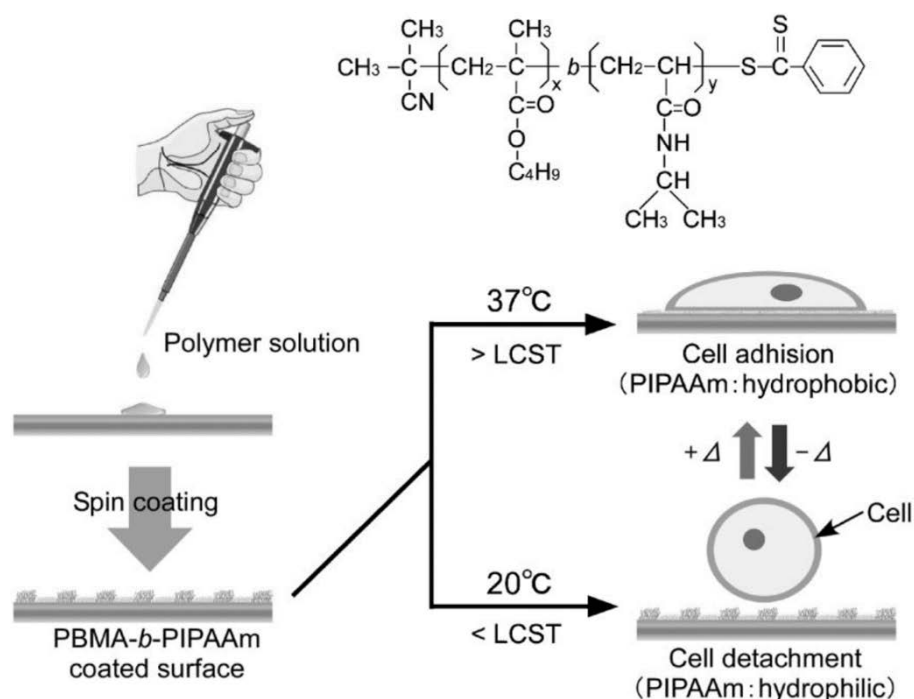


Figure 22. Chemical structure of a PNIPAM-*block*-PBMA block copolymer and fabrication of physically adsorbed, thermoresponsive coatings for cell sheet fabrication.³¹⁵

Via the adjustment of the layer thickness to 15 nm, the adhesion and proliferation of BAECs was mediated and the layers allowed the fabrication of confluent cell sheets.³¹⁵ To functionalize hydrophobically modified glass culture substrates, Sakuma *et al.* used RAFT polymerization to synthesize dodecyl terminated PNIPAm, adsorbed it to the substrates via the Langmuir-Schaefer method and successfully cultured and detached confluent BAEC sheets from their obtained films³¹⁶, which had thicknesses below 10 nm, hence, allowing cell adhesion as reported by Fukumori *et al.* on PNIPAm-coated glass substrates prepared by EBP.¹⁵⁸⁻¹⁵⁹ Using the same approach Sakuma *et al.* fabricated Langmuir-Schaefer films from PS-PNIPAm block copolymers. After transfer to hydrophobic glass substrates, they obtained adsorbed, particle-like aggregates as illustrated in Figure 23. They were able to control the size and grafting density of the coatings via adjusting the molecular weights of the copolymers as well as the relative lengths of the PS and PNIPAm blocks. At medium grafting densities of about 10 nm²/molecule and medium copolymer molecular weights of ~ 30 kDa as well as at low grafting densities of 40 nm²/molecule and high molecular weights of ~ 40-70 kDa, they were able to fabricate confluent BAEC sheets. In contrast, denser layer structures turned out to be non-adhesive towards cells and less dense layers did not allow cell sheet detachment³¹⁷, which emphasizes once more the importance of grafting density and layer thickness regarding the design of brush-like coatings based on PNIPAm (Figure 23).

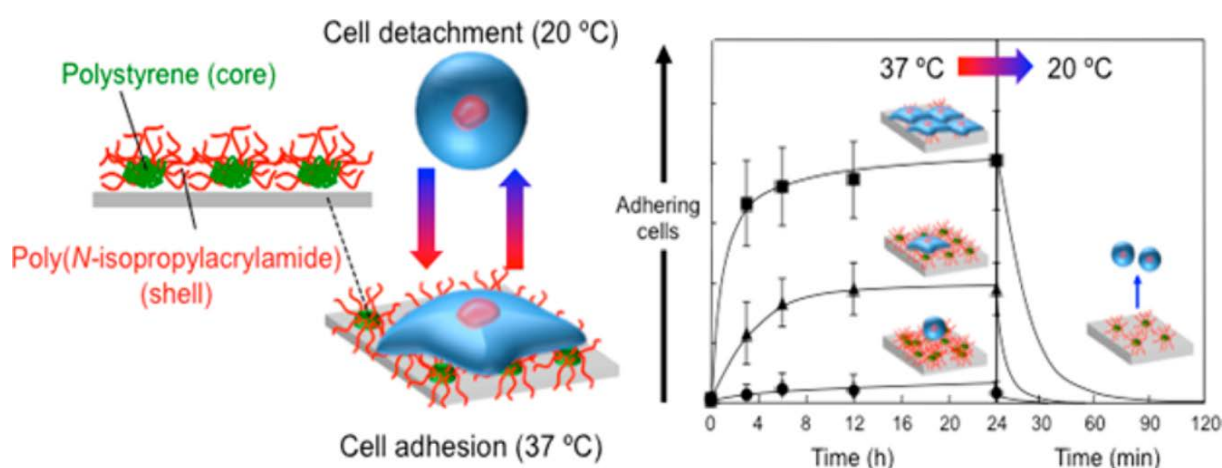


Figure 23. Schematic illustration of PS-PNIPAm block copolymers adsorbed to hydrophobized glass culture substrates and adhesion of BAECs on coatings with different block copolymer lengths and compositions.³¹⁷

Kakimoto and co-workers synthesized hyperbranched PS (HBPS) by ATRP and grafted PNIPAm from HBPS by RAFT polymerization to obtain core-shell-like block copolymers.³¹⁸⁻³¹⁹ They either adsorbed HBPS-*graft*-PNIPAm onto PS culture dishes by adsorption from solution³¹⁸ or via Langmuir-Blodgett films³¹⁹ and used the adsorbed layers to fabricate 3T3

1 Introduction

fibroblast sheets. Sudo *et al.* further prepared star-shaped PS-*graft*-PNIPAm copolymers to culture 3T3 fibroblast sheets and tuned cell adhesion and detachment properties via incorporation of comonomers, such as acrylic acid, *tert.*-BA and DMAEMA, into the grafted PNIPAm chains.³²⁰

2 Objectives

The central aim of this work was to develop thermoresponsive, glycidyl ether-based coatings for applied polystyrene (PS) tissue culture substrates. In that regard, strategies for the covalent immobilization of copolymers comprising GME and EGE via “grafting from” as well as “grafting to” methods were pursued to manufacture functional PGE coatings for the cultivation and the temperature-triggered detachment of cell monolayers/sheets. Moreover, a pivotal part of this thesis constituted the development of scalable and transferable coating procedures based on readily accessible raw materials with potential for technical application and possible industrial implementation. Since “grafting from” approaches based on reactive vinyl monomers are known to be suitable and efficient strategies for the preparation of a variety of functional coatings, the goal was to establish a convenient route for the synthesis of macromonomers based on thermoresponsive oligo(glycidyl ether) acrylates (OGEAs), which can be used for surface functionalization, for example via the UV-induced radical photografting approach. Thereupon, the feasibility of a “grafting from” processes involving OGEA macromonomers was ought to be explored in order to manufacture functional bottlebrush coatings applicable for cell sheet fabrication. A further aim of this work was to transfer the design parameters, which were established for the detachment of confluent fibroblast sheets on gold model surfaces as well as on glass substrates using coatings based on self-assembled thermoresponsive PGE monolayers, to applied PS substrates. In this context, the physical adsorption and self-assembly behaviour as well as the efficiency of covalent immobilization of photo-reactive PGE block copolymers onto PS culture substrates was investigated. A question of significance was directed to the influence of the nature of the culture substrate on the thermal response of the PGE coatings as well as on the effect of the PS substrates on cell sheet fabrication with respect to both cell adhesion and detachment. In this case, a comparison between the rather hydrophobic PS with the more hydrophilic gold and glass substrates constitutes an essential part for a better understanding of the structure-property relationship and the formulation of generalized design guidelines for thermoresponsive PGE coatings. In order to draw conclusions on the mechanism of cell sheet detachment from PGE-based coatings, another overarching aim was to compare the performance of different coating architectures, namely physically adsorbed or self-assembled PGE monolayers and photografted bottlebrushes, with regards to cell sheet detachment. To this end, comparative cell culture studies were exclusively performed on PS culture substrates using HDF as a common model cell line. The final objective of this work was to expand the range of applicability of glycidyl ether-based coatings with regards to the

2 Objectives

fabrication of different types of cell sheets. In this context, the adhesion and detachment of vascular cell sheet types on thermoresponsive PGE culture substrates was ought to be explored. Hence, the goal was to provide a functional, thermoresponsive platform as a prerequisite for the bottom-up engineering of 3D tissues, such as artificial blood vessels, based on the 2D cell sheet technology.

3 Publications and Manuscripts

In this work, thermoresponsive OGEA and PGE coatings based on the two monomers GME and EGE were developed for applied polystyrene (PS) tissue culture substrates. The coatings were evaluated regarding the adhesion and proliferation of HDF, human aortic smooth muscle (HAoSMC) and HUVEC monolayers and the intended temperature-triggered, nondestructive detachment of their respective cell sheets for potential use in cell sheet engineering. The functionality of self-assembled PGE monolayers for the fabrication of cell sheets was first reported on gold model substrates by Weinhart *et al.* in 2011.¹²⁶ In the following, Becherer, Heinen *et al.* investigated the structure-property relationship of thermoresponsive PGEs in solution and on gold model surfaces^{127-128, 130} and deduced general parameters for the design of self-assembled PGE brushes for fibroblast sheet fabrication¹²⁹, which were consequently transferred to applied glass substrates.¹³¹ Within the scope of this project, glycidyl ether-based coatings were transferred to the standard tissue culture plastic material PS. Both, “grafting from” and “grafting to” approaches were pursued utilizing BP as a photoinitiator for radical photografting of OGEA macromonomers or as an immobilizing/crosslinking agent of adsorbed PGE layers by coupling via C, H-insertion, respectively.

The first part of the presented work comprises the functionalization of PS culture substrates via the “grafting to” approach of PGE block copolymers. A novel, polymerizable epoxide monomer (EEBP) comprising a BP unit was synthesized and copolymerized as a short, hydrophobic, photo-reactive BP anchor block with a random, high molecular weight, thermoresponsive GME/EGE block using the sequential monomer-activated anionic ROP. The polymer was stably adsorbed from diluted ethanolic solution as an ultrathin, sub-nanometer layer and characterized via water CA, ellipsometry and QCM-D measurements. The coatings were immobilized by irradiation with UV light and were further verified and morphologically investigated by AFM force-distance measurements as well as quantitative nanomechanical mapping. Further, protein adsorption from cell culture medium was measured by QCM-D and compared to bare PS as well as standard TCPS surfaces. Successful fabrication of HDFs using ultrathin PGE coatings confirmed the adhesion promoting nature of PGE at 37 °C, which, as compared to bare PS, correlated with an increased protein adsorption, and indicated that HDF sheet detachment was mediated by both PGE rehydration and the rather cell repellent nature of the PS substrate. Polymer synthesis and characterization as well as surface preparation and characterization were performed by the author. AFM measurements were conducted by Dr. J. L. Cuellar-Camacho and the author. B.Sc. M. Uckert and Dr. A. Hoppensack performed cell

culture experiments. The research concept was conceived by Dr. M. Weinhart and the author. The corresponding article (chapter 3.3) was written by the author.

To attain self-assembled, brush-like PGE coatings, PGE block copolymers with a BP anchor block were adsorbed onto PS substrates from dilute aqueous solution at 10 °C. The thermoresponsive properties and aggregation behaviour of the polymers in water were characterized using concentration- and temperature-dependent DLS as well as UV-Vis turbidimetry to optimize the directed self-assembly and homogeneous arrangement of PGE chains on the PS surface from water, which can be regarded as a selective solvent at 10 °C below the CPT of the PGE block copolymer. The brush coatings were characterized by water CA, ellipsometry and AFM measurements and found to resemble self-assembled monolayers on gold and glass substrates. Fulfilling the previously defined design parameters of PGE brushes for use in cell sheet fabrication, the functionalized surfaces enabled the culture and detachment of confluent HDF, HAoSMC and HUVEC monolayers, which represent the three basic constituents of blood vessels. Polymer synthesis and characterization as well as surface characterization were performed by the author. Dr. A. Hoppensack conducted cell culture experiments with HAoSMCs. Cell culture experiments with HDFs and HUVECs were performed by J. Scholz. The research was conceptualized by Dr. M. Weinhart, Dr. A. Hoppensack and the author. The according manuscript (chapter 3.4) was written by the author.

The second part of the presented work comprises the synthesis and characterization of polymerizable OGEA macromonomers using the fast and solvent-free, microwave-assisted oxy-anionic ROP. OGEs with different chain lengths and monomer compositions were synthesized and thoroughly characterized via gel permeation chromatography (GPC) and matrix-assisted laser desorption/ionization time-of-flight (MALDI-ToF) mass spectrometry. Their thermoresponsive properties in aqueous solution were further investigated with respect to monomer composition, molecular weight and concentration in water using UV-Vis turbidimetry. To estimate the scalability of the microwave-assisted synthesis towards an applicable process on an industrial scale, OGEs were functionalized by *in-situ* acrylation to directly obtain OGEA macromonomers. In addition, the polymerization kinetics of the synthesis was investigated and compared to the “classical” oxy-anionic ROP using conventional heating. The results indicated that the fast reaction kinetics are predominantly governed by thermal, rather than microwave-specific effects and demonstrated that the bulk polymerization using microwave heating provides good conditions for the controlled polymerization of OGEAs. The polymers were synthesized by B.Sc. D. Donath and the author. Polymer characterization and kinetic studies were performed by the author. The concept of

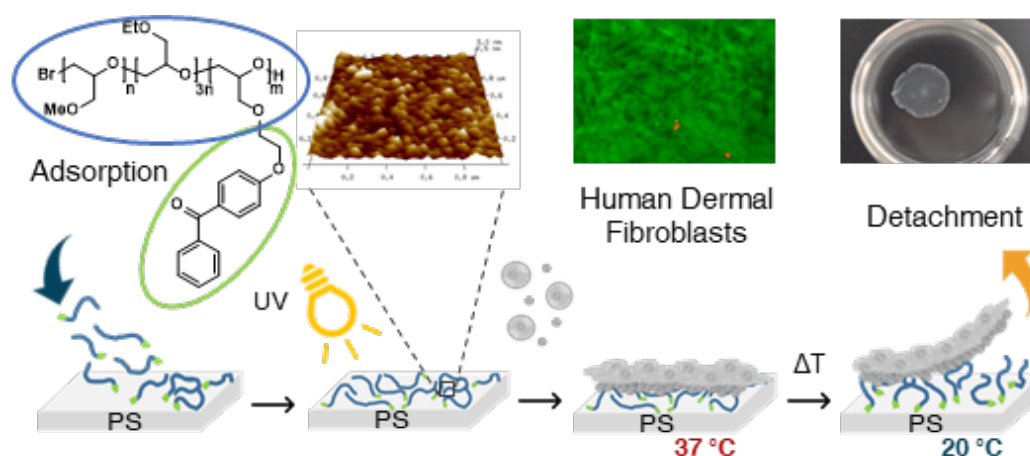
research was provided by Dr. M. Weinhart and the author. The following manuscript (chapter 3.1) was written by the author.

Based on the synthesized OGEA macromonomers, thermoresponsive bottlebrushes were “grafted from” PS culture substrates via a “grafting through” approach under bulk conditions by irradiation with UV light using BP as photoinitiator. The polymerization of OGE-based antifouling coatings on glass substrates via surface-initiated ATRP (SI-ATRP) was first reported by Gunkel *et al.* in 2011.²⁷² Within this project, the reaction conditions of the free radical polymerization of OGEAs and their grafting behaviour with respect to different monomer compositions and molecular weights were investigated. The resulting bottlebrush coatings were characterized by water CA, ellipsometry and AFM measurements. Proliferation and temperature-triggered detachment of HDF sheets was compared and correlated with the layer thickness, structure and hydrophilicity of the coatings as well as with the molecular weight and monomer composition of the grafted OGEA side chains. Synthesis and characterization of the polymers and thermoresponsive coatings were performed by the author. J. Scholz conducted cell culture experiments. The research concept was designed by Dr. M. Weinhart, Dr. U. Schedler and the author. The associated manuscript (chapter 3.2) was written by the author.

3.1 Ultrathin Poly(glycidyl ether) Coatings on Polystyrene for Temperature-Triggered Human Dermal Fibroblast Sheet Detachment

Daniel David Stöbener, Melanie Uckert, José Luis Cuéllar-Camacho, Anke Hoppensack,
Marie Weinhart*

The synthesis of a novel, photo-reactive BP monomer (EEBP) and its sequential copolymerization via the monomer-activated anionic ROP is described. The block copolymer stably attaches onto PS culture substrates via physical adsorption from ethanolic solution and can be covalently immobilized via UV irradiation. The ultrathin PGE layers are extensively characterized by CA, Ellipsometry, AFM and QCM-D measurements and used for the culture and detachment of HDF monolayers.



This chapter was published in the following journal:

"Reprinted with permission from

Daniel David Stöbener, Melanie Uckert, José Luis Cuéllar-Camacho, Anke Hoppensack,
Marie Weinhart, *ACS Biomaterials Science & Engineering*, **2017**, 3 (9), 2155-2165.

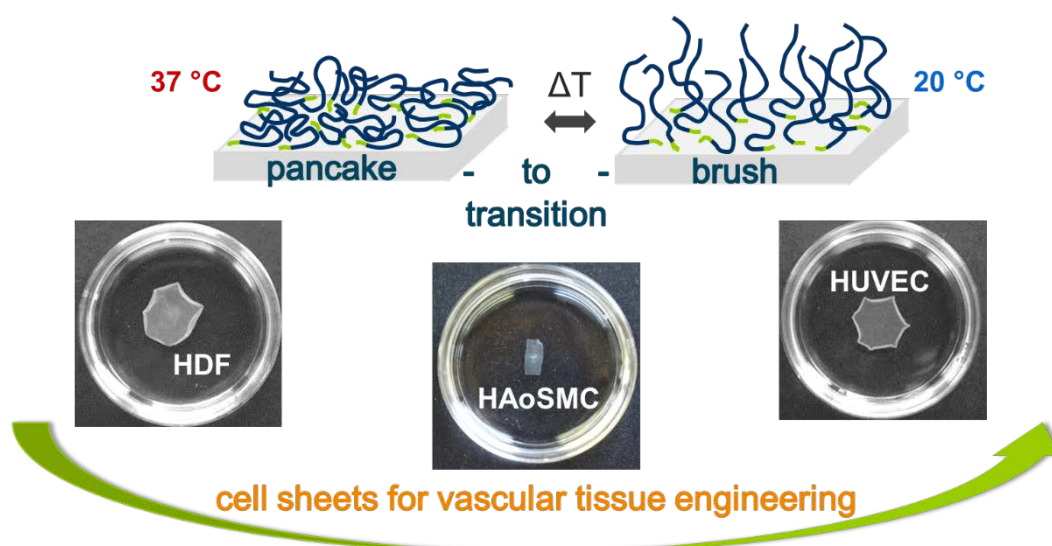
Copyright 2018 American Chemical Society"

DOI: <https://doi.org/10.1021/acsbmaterials.7b00270>

3.2 Endothelial, Smooth Muscle and Fibroblast Cell Sheet Fabrication from Self-assembled Thermoresponsive Poly(glycidyl ether) Brushes

Daniel David Stöbener, Anke Hoppensack, Johanna Scholz, Marie Weinhart*

The directed self-assembly of PGE block copolymers comprising a hydrophobic, photo-reactive BP anchor block to PS culture substrates from dilute aqueous solution below the polymer's CPT leads to physically adsorbed, thermoresponsive brush-like PGE coatings. The brush layers are immobilized by UV irradiation and used as a thermoresponsive platform for the fabrication of confluent HDF, HAoSMC as well as HUVEC sheets under optimized culture conditions.



This chapter was submitted to an appropriate scientific journal and is currently being revised.

Daniel David Stöbener, Anke Hoppensack, Johanna Scholz, Marie Weinhart, *Soft Matter*, **2018**, *14* (41), 8333-8343. - Reproduced by permission of The Royal Society of Chemistry.

Endothelial, Smooth Muscle and Fibroblast Cell Sheet Fabrication from Self-assembled Thermoresponsive Poly(glycidyl ether) Brushes

*Daniel David Stöbener, Anke Hoppensack, Johanna Scholz, Marie Weinhart**

Institute for Chemistry and Biochemistry, Freie Universität Berlin, Takustr. 3, D-14195 Berlin, Germany.

*Corresponding author: email marie.weinhart@fu-berlin.de, phone: +49 30 838 75050

Abstract

In this study, we introduce a platform to fabricate human dermal fibroblast (HDF), human aortic smooth muscle cell (HAoSMC) and human umbilical vein endothelial cell (HUVEC) sheets using thermoresponsive poly(glycidyl ether) coatings. Copolymer brushes based on glycidyl methyl ether (GME) and ethyl glycidyl ether (EGE) were self-assembled onto polystyrene (PS) culture substrates via the physical adsorption of a hydrophobic, photoreactive benzophenone anchor block based on the monomer 4-[2-(2,3-epoxypropoxy)ethoxy]benzophenone (EEBP). The directed self-assembly of well-defined, end-tethered poly(GME-*ran*-EGE)-*block*-poly(EEBP) (PGE) brushes was achieved via the selective, EEBP-driven adsorption of the asymmetric block copolymer from dilute aqueous solution below its cloud point temperature (CPT). Subsequently, the PGE brush layers were covalently immobilized onto the PS surfaces by irradiation with UV light and characterized by ellipsometry, static water contact angle (CA) measurements and atomic force microscopy (AFM). We found, that by decreasing the

temperature from 37 to 20 °C, the coatings undergo a pancake-to-brush transition, which triggers cell sheet detachment. In addition, cell culture parameters were optimized to allow proper adhesion and controlled detachment of confluent HDF, HAoSMC and HUVEC sheets, which can be applied in vascular tissue engineering.

Keywords

Cloud point temperature, benzophenone-driven aggregation, block-copolymer adsorption, UV-induced C, H-insertion, pancake-to-brush transition, switchable surface

Introduction

Vasculature constitutes a pivotal part in the engineering of three-dimensional (3D), artificial tissue and is essential for cell survival, since it provides the vital metabolic exchange of oxygen, carbon dioxide, nutrients and waste products in somatic systems.¹⁻⁴ In general, approaches for engineering vascular tissues can be divided into cell-based and scaffold-based techniques.⁵⁻⁷ A practical, bottom-up cell-based approach, which has not only increased the *in vivo* efficiency of cell implantation for therapeutic tissue reconstruction in general⁸⁻⁹, but also provides a straightforward strategy for *in vitro* engineering of different 3D tissues, relies on the use of cell sheets.¹⁰⁻¹⁵ Cell sheets constitute confluent, two-dimensional (2D) cell monolayers comprising an associated ECM, which can be harvested from thermoresponsive culture substrates. The sheets can be stacked to multilayered mammalian hepatic¹⁶ as well as human cardiac¹⁷ and pre-vascular¹⁸ tissue constructs either by simple pipetting, or by transfer via cell sheet manipulators, such as support membranes or plunger-like devices.¹⁹⁻²⁰ In principle, thermoresponsive coatings are based on polymers, which undergo a temperature-triggered phase transition in aqueous media within the physiologically relevant temperature range. Under standard cell culture conditions at 37 °C, such thermoresponsive coatings must be in a less hydrated, collapsed state and allow the adhesion of cells and their proliferation to confluent monolayers. Cooling below

the phase transition temperature of the polymer induces a rehydration and swelling of the polymer chains. This renders the coatings cell-repellant and allows for the non-invasive, enzyme-free detachment of cell sheets with their intact ECM and, in case of epithelial cells, retained polarization. Particularly thermoresponsive coatings based on poly(*N*-isopropyl acrylamide) (PNIPAm) have been developed into a platform for cell sheet engineering by Okano and co-workers starting in the early 1990s²¹⁻²². Nowadays commercially available under the brand name UpCell™, these PNIPAm-coated tissue culture polystyrene (TCPS) dishes prepared via electron beam polymerization (EBP)²³, have contributed to the rapid expansion of this field of research resulting in a variety of accessible tissues. It is important to mention here, that the successful translation of this technique to new cell types is not only predicated on the chemical nature of the thermoresponsive polymer and the specific thermal properties of the coating, but also on the fine-tuning of the applied cell culture conditions, such as seeding density, culture media and supplements. This is of special relevance if the goal is to provide a functional platform for engineering vascular constructs, which comprise multiple layers of connective tissue (fibroblasts) and smooth muscle cells as well as a tight monolayer of endothelial cells, which forms the lumen of blood vessels and constitutes the barrier to the blood stream.

Due to their limited adhesion and proliferation on hydrogel-like PNIPAm-based coatings prepared via EBP, the detachment of confluent human umbilical vein endothelial cells (HUVECs) from these commercial substrates has not been reported so far. However, sub-confluent HUVEC as well as endothelial colony-forming cell (ECFC) layers have been cultured on such PNIPAm surfaces and sandwiched between or co-cultured with human dermal fibroblast (HDF) and human skeletal muscle myoblast (HSMM) sheets in order to fabricate pre-vascularized 3D tissue constructs.^{18-20, 24-27} Additional post-functionalized with cell adhesive ligands, such as the RGD-motif bearing peptides, help to improve and control HUVEC adhesion on electron beam-grafted PNIPAm coatings.²⁸⁻³⁰ In contrast, under milder grafting conditions

structurally more defined PNIPAm brush coatings can be prepared on polystyrene (PS) substrates via a surface-initiated, UV-induced free radical polymerization, which allow HDF and HUVEC adhesion without further cell adhesive modification and sheet detachment within one hour at 20 °C. However, for initial cell seeding densities of 1.0×10^5 cells cm^{-2} culturing times reached up to seven days for the monolayers to grow confluent indicating hampered proliferation on the coated substrates.³¹

The fabrication of confluent human aortic smooth muscle cell (HAoSMC) sheets on PNIPAm-based culture substrates is often impeded by the weak adhesion on the substrates and the lack of control over HAoSMC detachment. Carboxylation of the PNIPAm end-groups is one strategy to increase HAoSMC cell-adhesion strength on PNIPAm-brushes on glass produced via the surface-initiated reversible addition-fragmentation chain-transfer (SI-RAFT) radical polymerization. The introduced negative charges within the coating allowed cell adhesion, proliferation and subsequent detachment of intact HAoSMC sheets.³² In order to generate isotropic as well as aligned SMC sheets, Wong and co-workers grafted PNIPAm onto flat as well as microtextured PS films using EBP. They found that under optimized grafting conditions (45-50% NIPAm in isopropanol), which slightly differed from the NIPAm EBP process on TCPS (UpCell™), confluent HAoSMC sheets detached within 45 min after cooling to 20 °C and could be harvested as intact isotropic or oriented monolayers.³³ Again, on the commercial PNIPAm-coated dishes, an additional physisorbed layer of cell-adhesive fibronectin (FN) was necessary to support HAoSMC adhesion. The FN was printed homogeneously or in stripes onto the coated surface to yield spontaneously detaching randomly oriented or aligned HAoSMC sheets within 120 min after temperature reduction.³⁴

In comparison to cell sheets composed of HUVECs and SMCs, HDF sheets are easily accessible with PNIPAm-coated substrates without additional cell adhesive modification.^{18, 20, 24, 35} In search of alternative, NIPAm-free thermoresponsive coatings, Dworak and co-workers prepared poly[tri(ethylene glycol) monoethyl ether methacrylate] brushes on glass culture

substrates and demonstrated successful HDF sheet detachment within 40 to 60 min when lowering the temperature to 17.5 °C.³⁶⁻³⁷ Furthermore, they also demonstrated thermoresponsive brush coatings based on 2-alkyl 2-oxazolines to detached confluent HDF sheets from covalently coated glass substrates within 30 min at 20 °C.³⁸⁻³⁹ Besides thermoresponsive ethylene glycol and oxazoline-based polymers, also glycidyl ether-based polymers have qualified as alternative coatings for cell sheet fabrication as demonstrated in a pilot study using self-assembled monolayers on gold and NIH-3T3 mouse fibroblasts.⁴⁰ Further developing such thermoresponsive coatings based on glycidyl methyl ether (GME) and ethyl glycidyl ether (EGE), we have recently shown that glycidyl ether based block copolymers (PGE, Figure 1a) adsorb to PS culture substrates from dilute ethanolic solution and form ultrathin layers (Figure 1b) with thicknesses in the sub-nanometer range (0.7 ± 0.1 nm).⁴¹ The applied block copolymer poly(GME-*ran*-EGE)-*block*-poly(EEBP) comprises, in addition to the thermoresponsive block, a hydrophobic, photoreactive anchor block based on the monomer 4-[2-(2,3-epoxypropoxy)ethoxy]benzophenone (EEBP). The generated ultrathin coatings support the adhesion of HDFs and allow the temperature-triggered detachments of confluent, viable HDF sheets.⁴¹ The aim of the present work was the generation of surface-tethered PGE brushes on PS in order to improve cell adhesion and the efficiency of cell sheet detachment. In this regard, we investigated the directed self-assembly of the asymmetric block copolymer from the selective solvent water to obtain PGE coatings with a brush-like conformation (Figure 1c). Our developed coating was applied for the fabrication of confluent HDF, HAoSMC and HUVEC sheets as the basic building blocks for artificial blood vessels.

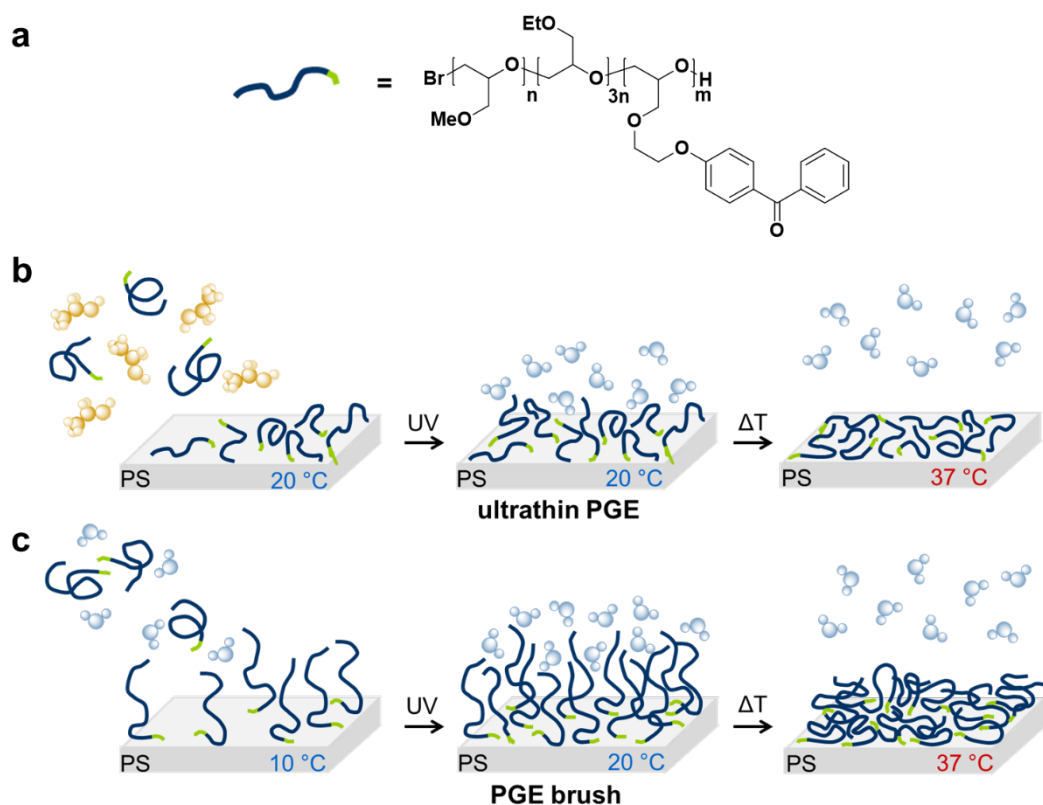


Figure 1. (a) Chemical structure of a poly(GME-*ran*-EGE)-*block*-poly(EEBP) block copolymer (PGE) synthesized via the sequential monomer-activated AROP; (b) Formation of ultrathin PGE monolayers via physical adsorption from diluted ethanolic solution at 20 °C and approximated chain conformation in aqueous solution at 20 and 37 °C; (c) Self-assembly of PGE brushes via directed, BP-driven adsorption from diluted aqueous solution at 10 °C and supposed chain conformation in aqueous solution at 20 and 37 °C.

Experimental methods

A detailed description of all materials and analytical methods used is given in the electronic supplementary information (ESI).

Polymer synthesis

The poly(GME-*ran*-EGE)-*block*-poly(EEBP) block copolymer was synthesized via the sequential monomer-activated anionic ring-opening polymerization as reported previously.⁴¹

Below, the thermoresponsive block copolymer is referred to as PGE.

Surface preparation

To characterize the thermoresponsive coatings, PS-coated silicon (Si) wafers were used as model substrates. Bare Si wafers (11 x 11 mm) were rinsed with ethanol and dried under a stream of N₂. The samples were spin-coated at 3000 rpm for 60 s on a WS-650-23 spin-coater from Laurell Technologies Corporation (North Wales, PA, USA) applying a PS solution (30 μL) in toluene (0.5% (w/w)). Spin-coated samples were dried at ambient conditions overnight. The thickness and the contact angles (CAs) of the PS layer were determined by ellipsometry and static water CA measurements, respectively. For PGE coating, the samples were kept in PS culture dishes (d = 35 mm) and immersed in a solution of PGE in Milli-Q water (10 μM, 2 mL) at 10 °C for 60 min. Subsequently, the PGE solution was removed, and the samples were immersed into Milli-Q water (2 mL) and incubated at 10 °C for another 30 min to wash off the excess of non-adsorbed PGE. The surfaces were dried under a stream of N₂, and irradiated by UV light using a UV-KUB 2 from KLOÉ (Montpellier, France) with a wavelength of 365 nm and a radiant exposure of 4.0 J cm⁻² for 160 s using an irradiance of 25 mW cm⁻² (100%) in order to covalently immobilize the PGE layer on PS. After rinsing with ethanol and Milli-Q water, the coatings immobilized on Si wafers were characterized by ellipsometry, static water CA, and atomic force microscopy (AFM) measurements. PS culture dishes (d = 35 mm) were coated with PGE as described above for PS-coated Si wafers. After rinsing with ethanol and

Milli-Q water, the substrates were used for culturing and detaching cell sheets of HDFs, HAoSMCs and HUVECs.

Cell isolation and culture

HDFs were isolated from human foreskin biopsies after ethical approval and informed parental consent as reported previously.⁴¹ HDFs were cultured in high glucose DMEM medium (10% FBS from PAN-Biotech), trypsinized, centrifuged (140 xg, 4 min) and used in passages 3 to 7. HAoSMCs were cultured in VascuLife Smooth Muscle Cell medium, detached by accutase, centrifuged (150 xg, 4 min) and used in passages 3 to 6. HUVECs were cultured in VascuLife VEGF medium, trypsinized, centrifuged (200 xg, 5 min) and used in passages 3 to 6. All cell types were cultured under standard culture conditions (37 °C and 5% CO₂)

Cell sheet fabrication

Experiments were performed with PGE-coated Falcon® PS culture dishes and bare TCPS dishes as controls. The dishes were sterilized with 70% ethanol for 10 minutes and washed twice with PBS before cell seeding. HDFs were seeded at a density of 1.6×10^5 cells cm⁻² in 2 mL DMEM (1 g/L Glucose) with 10% FBS (PAN-Biotech) per dish (d = 35 mm), followed by culture at 37 °C and 5% CO₂ for 24 h. Cells were analyzed after 4 and 24 h via phase contrast microscopy. For temperature-triggered detachment, confluent cell cultures were incubated in PBS at 20 °C for 10 min followed by incubation in fresh PBS (37 °C) for 5 min at 37 °C. Afterwards, cultures were kept at room temperature (20 °C) until the cell sheets detached from the surfaces.

HAoSMCs were seeded at a density of 1×10^5 cells cm⁻² in VascuLife SMC medium, supplemented with additional 5 % FBS (Biochrom, 10 % FBS in total) into a rectangular silicone frame (1 x 2 cm inner size, 5 mm height, Ospin GmbH, Berlin, Germany) on the PGE-coated PS dish followed by culture at 37 °C and 5% CO₂ for 16 h. For temperature-triggered detachment, confluent cell cultures were incubated in PBS at 20 °C. Cell sheet detachment was

observed visually. Additional samples were prepared for microscopic observation of proliferation and morphology 4 h after seeding.

HUVECs were seeded with a density of 8.5×10^4 cells cm^{-2} in Vasculife VEGF medium, which contains 2% FBS, per dish ($d = 35$ mm) followed by culture at 37°C and 5% CO_2 for 24 h. After 24 h, FBS concentration was increased to 10% (8 % FBS Biochrom) and HUVECs were cultured for further 48 h. Cells were analyzed after 4, 48 and 72 h via phase contrast microscopy. For temperature-triggered detachment, confluent cell cultures were incubated in PBS at 20°C until the cell sheets detached from the surfaces. Cell sheet detachment was observed and documented microscopically and visually.

Statistical evaluation

Graphical illustration of data and statistical analysis was performed with OriginPro[®]2018. Statistical comparison of water CAs (Figure 3b) was performed using the unpaired *t*-test for two independent sample sets following a normal distribution (*: $p < 0.05$, **: $p < 0.01$, ***: $p < 0.005$). The Shapiro-Wilk test was used to assess whether the raw data followed a normal distribution ($p < 0.05$). Cell detachment studies were performed in a minimum of three independent experiments with 2 to 3 replicates each. Detachment times were averaged over the total number *N* of investigated samples.

Results and discussion

Thermoresponsive properties of PGE in water

PGEs can be synthesized via sequential, monomer-activated anionic ring-opening polymerization (AROP) of a high molecular weight, thermoresponsive block consisting of glycidyl methyl ether (GME) and ethyl glycidyl ether (EGE), which copolymerize in a random fashion⁴², and a low molecular weight anchor block based on the photoreactive monomer 4-[2-(2,3-epoxypropoxy)ethoxy]benzophenone (EEBP).⁴¹ To predict the adsorption behaviour of PGE on PS substrates from aqueous solution and to establish optimal conditions for the directed self-assembly of PGE brushes, we conducted temperature- and concentration-dependent DLS measurements in order to investigate the CPT as well as the aggregation behaviour of the block copolymer in Milli-Q water. As illustrated in Figure 2a, at moderate concentration (2.5 mg mL^{-1}), PGE forms stable 30 to 50 nm aggregates at 10 and 20 °C and the particle size only slightly increases at 37 °C in both number and volume distributions (Figure S1a, b), which suggests a BP-driven aggregation of PGE. However, under dilute conditions (0.25 mg mL^{-1}), the PGE particle size shows a pronounced dependence on temperature and decreases to about 10 nm at 10 °C (Figure 2b, Figure S1c, d), which is in the same range as the hydrodynamic radii measured for poly(GME-*ran*-EGE) copolymers with similar molecular weight (24 kDa) and GME:EGE ratio (1:3).⁴² In contrast to PGE, poly(GME-*ran*-EGE) copolymers show a comparable temperature-dependent aggregation behaviour at low and high concentrations of up to 10 mg mL^{-1} . This further indicates that the aggregation of PGE is not only driven by the thermoresponsive GME/EGE block, but also largely influenced by the intermolecular association of the hydrophobic EEBP anchor blocks. Hence, there is reason to assume that PGE exhibits a micelle-like aggregation behaviour in water and might exhibit a critical micelle concentration (CMC) between 2.5 and 0.25 mg mL^{-1} . Similar micellar

aggregation has been reported for poly(styrene)-*block*-poly(ethylene glycol)⁴³⁻⁴⁴ and poly(styrene)-*block*-poly(glycidol)⁴⁵ copolymers.

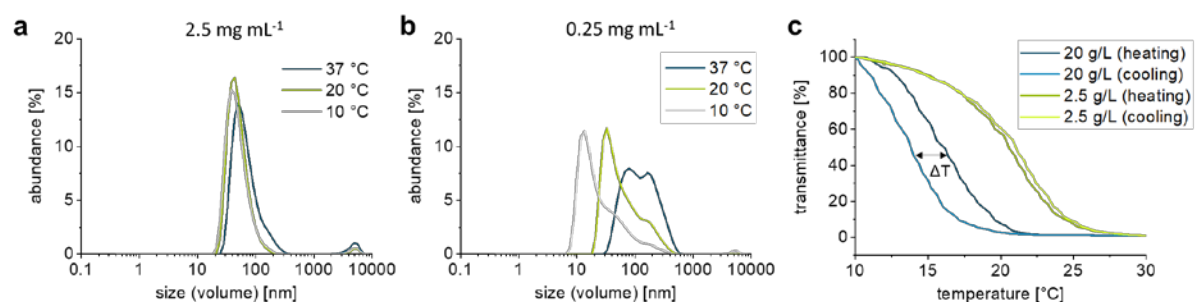


Figure 2. Temperature-dependent volume distributions of the hydrodynamic radii of PGE in Milli-Q water at a moderate concentration of 2.5 mg mL^{-1} (a) and under dilute concentration of $10 \text{ }\mu\text{M}$ (0.25 mg mL^{-1}) (b) measured by DLS and representative normalized transmittance curves (heating and cooling) at 500 nm of PGE solutions in Milli-Q water at high (20 mg mL^{-1}) and moderate (2.5 mg mL^{-1}) concentration (c).

Turbidimetry by UV-Vis transmittance measurements revealed a negligible concentration-dependence of the PGE CPT in a concentration range between 1 and 5 mg mL^{-1} with no detectable hysteresis (Figure 2c, Figure S2), which is in agreement with previous reports on poly(GME-*ran*-EGE).⁴² However, CPTs drop significantly at higher concentrations (10 - 20 mg mL^{-1}) and a marked hysteresis of up to $\Delta T = -3 \text{ }^\circ\text{C}$ between the heating and cooling curves is observed (Figure 2c, Figure S2). Moreover, the CPTs of PGE are slightly above $20 \text{ }^\circ\text{C}$ (Figure S3a) and the temperature transition regimes are broad and span ranges of more than $10 \text{ }^\circ\text{C}$ (Figure 2c, Figure S2b). In contrast poly(GME-*ran*-EGE) with a similar GME/EGE ratio (1:3) and molecular weight (24 kDa), which has noticeably lower CPTs ($\sim 17 \text{ }^\circ\text{C}$) and exhibits a much sharper phase transition regime (~ 2 - $3 \text{ }^\circ\text{C}$). This observation further underpins the assumption that over a large range of concentrations (2.5 - 20 mg mL^{-1}) PGE aggregation in aqueous solution is not only driven by the temperature-triggered coil-to-globule transition of the thermoresponsive GME/EGE block, but also strongly governed by the supramolecular

association of the hydrophobic, photoreactive EEBP block. Hence, the distortion and broadening of the phase transition might be the reason for the CPT discrepancy between PGE and poly(GME-*ran*-EGE) copolymers. Consequently, due to the results discussed above, coating of PS culture substrates with PGE was performed from dilute aqueous solution (0.25 mg mL^{-1}) at low temperature ($10 \text{ }^\circ\text{C}$) in order to provide optimal conditions for the directed self-assembly of the PGE block copolymer.

Self-assembly and characterization of PGE brushes

In order to self-assemble PGE brushes onto PS-coated Si model surfaces and to investigate the coating thickness and hydrophilicity by ellipsometry and static water CA measurements, respectively, the model substrates were incubated in a dilute, aqueous PGE solution (0.25 mg mL^{-1}) at $10 \text{ }^\circ\text{C}$ for 1 h. After further incubation of the substrates in cold water ($10 \text{ }^\circ\text{C}$) for 30 min, the samples were dried, and the PGE layers were covalently tethered to the PS substrate via UV irradiation. The thickness of the coatings was determined by ellipsometry after the self-assembly process as well as after additional UV irradiation and subsequent washing of the immobilized PGE layers with ethanol and Milli-Q water. As illustrated in Figure 3a, a thickness in the range slightly above 3 nm was obtained after the self-assembly process and the final layer thickness decreased only insignificantly to an average value of $3.0 \pm 0.4 \text{ nm}$ after photo-immobilization and washing. As shown in Figure 3b, water CAs on bare PS surfaces dropped from $88.8 \pm 1.1^\circ$ to $65.5 \pm 1.0^\circ$ after covalent coating with PGE and washing of the substrates. The slightly elevated CAs of $73.4 \pm 2.2^\circ$ after self-assembly indicates the presence of non-directed hydrophobic BP groups within the PGE brush layers. These non-assembled polymers are not covalently attached to the PS substrate by UV irradiation and consequently washed off. In addition, the final water CAs are slightly lower than reported for ultrathin PGE coatings ($70.1 \pm 2.7^\circ$)⁴¹, which indicates more uniform and thicker coatings and is in good agreement with self-assembled poly(GME-*ran*-EGE) monolayers on gold (Au).⁴⁶⁻⁴⁸

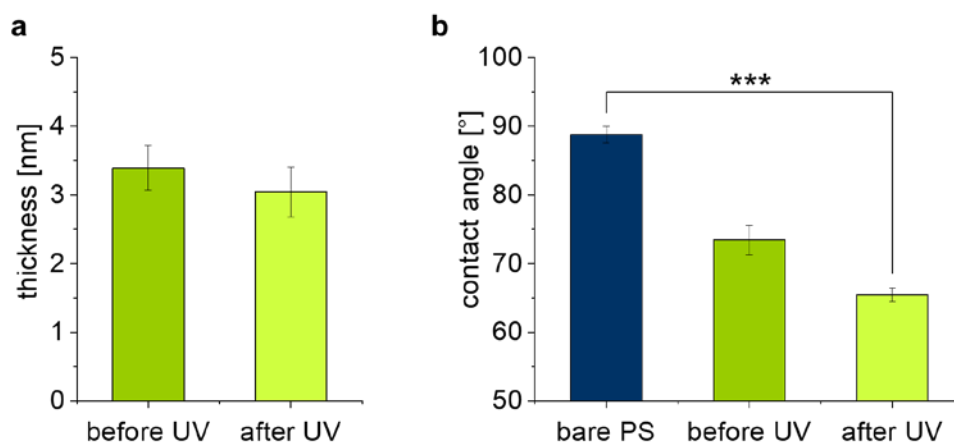


Figure 3. (a) Dry layer thickness of PGE coatings self-assembled from water on bare PS-coated Si wafers before and after and UV exposure measured by ellipsometry (N = 10, error bars indicate SEM); (b) Static water CA on bare and PGE-coated PS on Si wafers before and after UV exposure (N = 10, error bars indicate SEM, *t*-test: ***: $p < 0.005$).

These results indicate, that the hydrophobic asymmetry of the block copolymer and the affinity of the anchor block towards the hydrophobic PS substrate are large enough to allow an aligned self-assembly of brush-like PGE (PGE-3.0) coatings (Figure 1c), which can further be tethered to the PS substrates by immobilization via their photoreactive benzophenone anchor units. In addition, water acts as a selective solvent during PGE adsorption, since the thermoresponsive GME/EGE block is well hydrated below its CPT at 10 °C, whereas the hydrophobic EEBP block is virtually insoluble, which constitutes the main driving force for physical adsorption via PGE self-assembly.

Structural investigation of PGE brushes

To estimate the structure of the PGE-3.0 coatings under cell culture conditions at 37 °C and around the phase transition temperature at 20 °C, we used the layer thickness determined by ellipsometry (Figure 3a) and the molecular weight of PGE determined by GPC to calculate the surface grafting density and to infer the degree of chain overlap of the PGE-3.0 coatings. This approach has been used previously to assess the conformation of poly(ethylene oxide)⁴⁹,

PNIPAm⁵⁰⁻⁵¹ and poly(GME-*ran*-EGE)^{47-48, 52} monolayers on Si, Au and glass substrates under different solvent conditions and with various polymer molecular weights. Here, we estimated the degree of chain overlap using $2 R_f l^{-1}$, where R_f is the Flory radius and l is the average anchor distance between the immobilized polymer chains. We assumed water to be a bad solvent at 37 °C and a theta solvent at 20 °C and estimated the Flory radius according to $R_f = N^{1/3}a$ (bad solvent) and $R_f = N^{1/2}a$ (theta solvent), respectively, using $N = 266$ as the average number of repeating units (degree of polymerization P_n) and $a = 0.37$ nm as the approximate length of one repeating unit. The anchor distance l was calculated from the layer thickness via the chain density, which was determined to be 0.08 chains nm^{-2} . This corresponds to a chain area of $12 \text{ nm}^2 \text{ chain}^{-1}$ and is equivalent to an average anchor distance l of 4.0 ± 0.2 nm. Under bad solvent conditions, $2 R_f l^{-1}$ values are exclusively between 1.0 and 1.4 (Figure 4a). According to the applied model, surface bound spherical PGE coils are overlapping at 37 °C, however, the substrate surface is not entirely covered by the polymer coating (Figure 4b, c). In contrast, $2 R_f l^{-1}$ values are 3.1 ± 0.2 under theta solvent conditions (Figure 4a), which predicts that PGE coils are extensively overlapping and that the polymer chains adopt a brush-like, elongated conformation (Figure 4b, c). A comparison between the anchor distance and degrees of chain overlap of PGE-3.0 coatings after self-assembly and photo-immobilization of ultrathin PGE (PGE-0.7) coatings is presented in Figure S3.

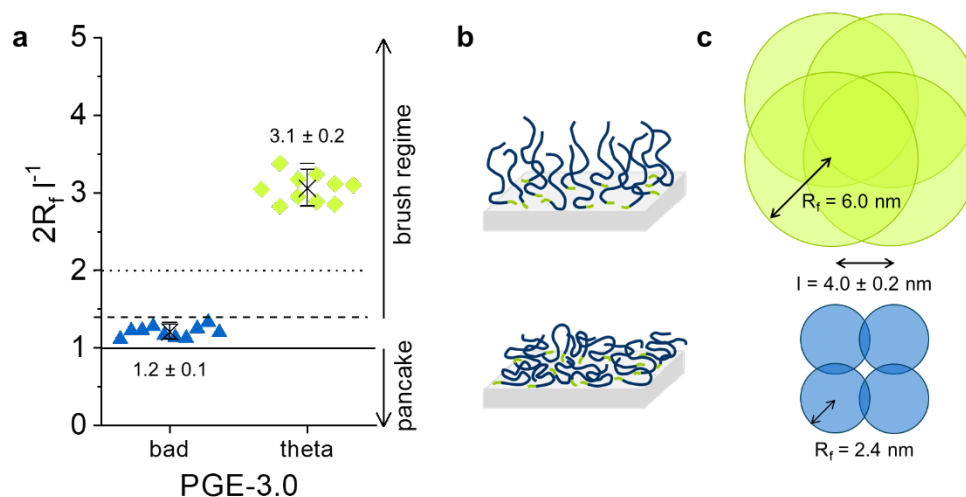


Figure 4. Theoretically estimated degree of chain overlap ($2R_f l^{-1}$) (a), schematic representation of polymer chain conformation (b) and visualized polymer coil overlap (c) of PGE on PS-coated Si wafers under bad (blue triangles and spheres) and theta (green diamonds and spheres) solvent conditions. $2R_f l^{-1}$ values are plotted for each replicate together with their mean value (black cross) and their 90% confidence interval (whiskers) (a).

Recent studies have shown that the adhesion and detachment of HDF sheets from thermoresponsive poly(glycidyl ether) coatings is noticeably influenced by the nature of the culture substrate. Regarding PGE-0.7 coatings on PS, cell sheet detachment is assisted by the relatively poor cell adhesion of the underlying, hydrophobic PS substrate, which is not entirely covered by the PGE monolayer (Figure S3b, c).⁴¹ A similar effect was observed for physically adsorbed poly(glycidyl ether) coatings on glass substrates. The rather poor HDF adhesion on bare glass resulted in a more reproducible and faster cell sheet detachment from coatings with incomplete surface coverage as compared to covalent coatings with a rather cell adhesive additional, intermediate polydopamine layer on the glass substrate.⁵² In order to deduce whether uncovered PS surface areas are accessible across PGE-3.0 coatings at 37 °C and to get an insight into the interaction between PS substrates and PGE chains, we investigated the adhesiveness of PS surfaces towards the adsorption of a poly(GME-*ran*-EGE) copolymer ($M_n = 43$ kDa, PDI = 1.45, GME:EGE = 1:3) without a hydrophobic EEBP anchor block. PS-coated Si wafers were incubated in a 10 μ M (0.25 mg mL⁻¹) polymer solution in ethanol for 30 min and rinsed excessively with ethanol and Milli-Q water. Ellipsometry and water CA measurements revealed, that a very thin layer with a thickness of 0.4 ± 0.1 nm remained on the PS substrates (Figure S4a, b). Further, the adsorption process was monitored via QCM-D measurements on PS-coated Au chips. A reproducible decrease in the frequency (Δf) of the quartz crystal as well as an increase in dissipation (ΔD) indicated the formation of a physically adsorbed layer of poly(GME-*ran*-EGE), which was stable against flushing with ethanol and did not significantly

change even after multiple incubation cycles (Figure S4c). The formation of a stable poly(GME-*ran*-EGE) layer on PS-coated model substrates demonstrates a rather strong adhesive interaction between the thermoresponsive poly(glycidyl ether)s and PS. Similar interactions with PS substrates have been reported previously for PEG as well as PEG-PS block copolymers.⁵³⁻⁵⁵ Due to this inherent affinity towards PS, we have reason to assume, that PGE-3.0 coatings completely cover the PS substrates even in their collapsed conformation at 37 °C. Hence, we conclude that PGE-3.0 layers undergo a pancake-to-brush transition when the temperature is decreased from 37 to 20 °C and that the cell-repellant nature of the underlying PS substrate is negligible with respect to cell adhesion as well as the temperature-triggered detachment of single cells or cell sheets.

To verify their brush-like structure and to detect their temperature-triggered phase transition, we investigated the thermoresponsive PGE-3.0 coatings in water at 37 and 20 °C by AFM quantitative nanomechanical mapping (QNM). Morphological pictures recorded in Milli-Q water at 37 °C revealed very flat and laterally homogenous layers with a roughness in the range of bare PS-coated Si wafers (Figure 5a, c, e), which indicates a homogeneously collapsed and dehydrated PGE-3.0 layer. In contrast, the surface roughness increases markedly when the temperature is reduced to 20 °C, indicating a phase transition of the PGE-3.0 coatings via a rehydration of PGE chains (Figure 5b, d, f). This morphological difference is further pronounced on the nanometer scale (Figure S5) and strongly suggests the rehydration of single polymer chains in a brush-like PGE assembly.

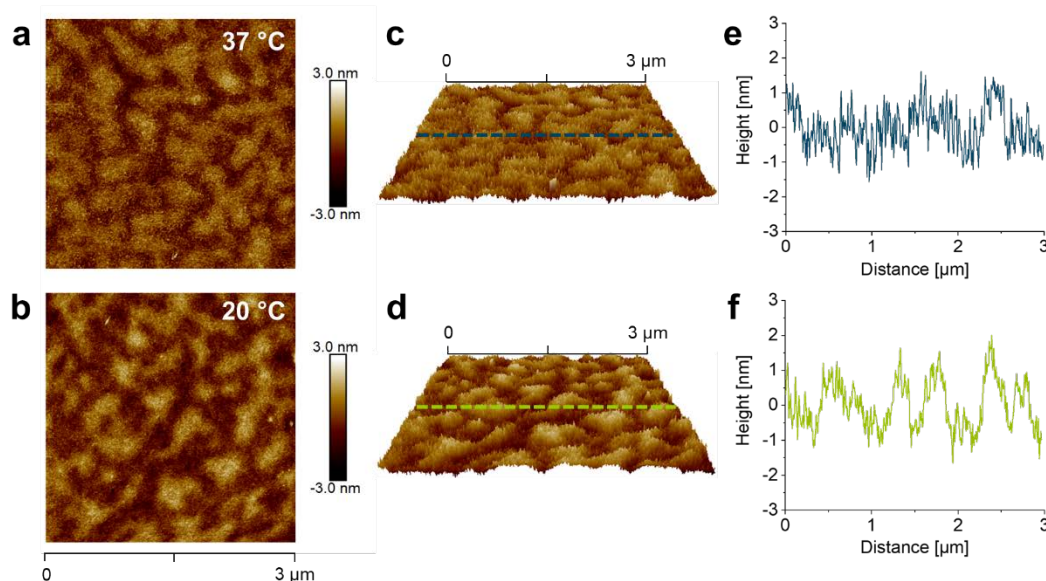


Figure 5. 2D and 3D surface topography and cross section profiles of 3 μm images of PGE-3.0 on PS-coated Si wafers in Milli-Q water at 37 $^{\circ}\text{C}$ (a, c, e) and 20 $^{\circ}\text{C}$ (b, d, f) measured by AFM in PeakForce QNM mode.

Although the surface roughness parameters, which are summarized in Table S1, are in the same realm as those of bare PS and ultrathin PGE-0.7 coatings, it is crucial to note, that the most significant differences in root-mean squared roughness R_q and mean roughness R_a are observed between PGE-3.0 coatings at 37 and 20 $^{\circ}\text{C}$ (Table S1, row 4-5). In contrast, the maximal roughness R_{max} of PGE-3.0 coatings is slightly lower than for PGE-0.7 coatings, which suggests a laterally more homogeneous coverage of the PS substrates by PGE-3.0 layers. These findings further illustrate that PGE-3.0 layers undergo a phase transition between 37 and 20 $^{\circ}\text{C}$ and that the directed self-assembly process of PGE from dilute aqueous solution at 10 $^{\circ}\text{C}$ results in homogeneous coatings with a brush-like conformation. Further, the materials properties of PGE-3.0 coatings were extracted from the AFM PeakForce images, which were recorded using a loading peak force of 500 pN. As illustrated in Figure S6, the Young's modulus and the deformation of the PGE-3.0 coating as well as the adhesion force between the AFM tip and PGE did not significantly differ between 37 and 20 $^{\circ}\text{C}$ as the respective depth histograms highly overlap (Figure S6g, h, i). Also, the deformation of the PGE-3.0 coatings is still below 1 nm

and hardly distinguishable from PS substrates due to the relatively low indentation force applied. However, Young's moduli indicate the presence of a soft PGE film and are in the range of about 10 MPa, which is about 3 orders of magnitude lower than it would be expected for bare PS surfaces.⁵⁶⁻⁵⁷ In addition, the relatively low adhesion force of about 50-100 pN clearly indicates the shielding of retractive hydrophobic interactions between the silicon nitride (Si_3N_4) AFM tip and the hydrophobic PS substrate by the presence of a more hydrophilic PGE coating. This effect was already reported for ultrathin PGE-0.7 coatings⁴¹ and is well documented in literature.⁵⁷⁻⁵⁸

Fabrication of cell sheets for vascular tissue engineering

Initial adhesion and proliferation studies with HUVECs revealed, that similarly to TCPS controls (Figure S7a, b), HUVECs grew to confluent cell monolayers on PGE-3.0 substrates within 3 d (Figure S7g, h). In contrast, cells did not adhere homogeneously on uncoated PS controls (Figure S7c, d), while cells did not grow to confluence on ultrathin PGE-0.7 substrates (Figure S7e, f), even after increasing the culture time up to a total of seven days. Due to these promising results, PGE-3.0 coatings were further investigated regarding the adhesion and temperature-triggered detachment of HDF, HAoSMC and HUVEC sheets. For cell culture experiments PS culture dishes ($d = 35 \text{ mm}$) were functionalized with PGE and culture conditions were optimized regarding the respective cell type. HDFs (passages 4-7) were seeded onto coated PS dishes with a density of $1.6 \times 10^5 \text{ cells cm}^{-2}$ and cultured for 24 h. As illustrated in Figure 6, HDFs adhered in a similar manner as on TCPS control surfaces. Cell sheets were detached according to our previously optimized detachment protocol.⁴⁸ Confluent cell sheets detached from the functionalized PS substrates within $33 \pm 10 \text{ min}$ ($N = 10$), whereas no detachment was observed on TCPS control surfaces. In our previous report we showed that HDF sheets detached from ultrathin PGE-0.7 coatings within $51 \pm 17 \text{ min}$ ($N = 10$).⁴¹ Since the layer thickness is significantly higher for PGE-3.0 coatings, the temperature-triggered

rehydration is more pronounced. However, the rather faint decrease in detachment time is presumably founded in the lacking cell-repellant effect of the underlying PS substrate as it was observed with ultrathin PGE-0.7 coatings. This implies that HDF sheet detachment from PGE-3.0 coatings is mainly caused by the temperature-triggered phase transition of the immobilized brushes rather than a cooperative effect of the partial PGE rehydration and the non-adhesive PS background. This further supports our hypothesis that PGE-3.0 coatings undergo a pancake-to-brush transition upon decreasing the temperature from 37 to 20 °C. In addition, detachment times are in the same realm as reported for HDF sheets harvested from poly(glycidyl ether) brushes on glass⁵² and poly(2-substituted-2-oxazoline) brushes on Si substrates developed by Dworak and co-workers.³⁸⁻³⁹

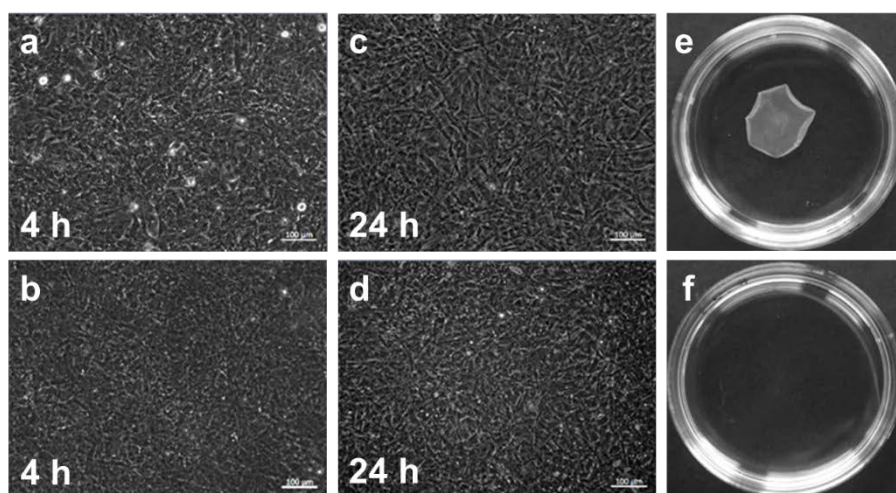


Figure 6. Representative phase contrast images of HDFs 4 and 24 h after seeding on PGE-3.0 (a + c) and TCPS (b + d) and respective macroscopic photographs of the culture dishes after temperature reduction to 20 °C (e + f). Only PGE-3.0 dishes released HDF sheets when triggered thermally.

Similarly, HAoSMCs (passages 4-6) were seeded at a density of 1×10^5 cells cm^{-2} on PGE-3.0. Because of occasional spontaneous cell sheet detachment during culture at 37 °C, which has also been reported by Takahashi *et al.*³², additional 5 % FBS were added to the cell culture medium. An increase of the amount of extracellular matrix proteins, such as fibronectin and

vitronectin, that adsorb from FBS-containing culture medium to the culture surface⁵⁹ can mediate and strengthen cell adhesion.⁶⁰ Likewise, Rayatpisheh *et al.*⁶¹ and Backman *et al.*⁶² pretreated PNIPAm-grafted polydimethylsiloxane surfaces with FBS and FBS-containing culture medium, respectively, before smooth muscle cell seeding.

For tissue engineering of vascular grafts via rolling of cell sheets into tubular structures, cell sheets of rectangular rather than round shapes are preferred.¹⁴ In order to demonstrate that cell sheets with a rectangular shape can also be generated on round Petri dishes, we seeded HAoSMCs into a rectangular silicone frame onto PGE-3.0 dishes. In addition to shape control, the use of the seeding frame further contributed to prevent premature detachment of the smooth muscle cell sheets. This might be a result of the more homogenous cell distribution on the surface observed when applying the seeding frames. Cell adhesion was comparable on PGE-3.0 coatings and the TCPS control (Figure 7), while HAoSMC adhesion on commercial PNIPAm-coated plates (UpCell™) was strongly impaired (Figure S8). Thus, cells on the PNIPAm surface yielded only cell clusters. The differential cell behavior on the two thermoresponsive substrates can be explained by the grafting density and related hydrophilicity of the surface. It has been shown previously for PNIPAm coatings that with increasing grafting density also the surface hydrophilicity is increased which leads to decreased adhesion of some cell types.^{32, 63-64} Takahashi *et al.*³² observed impaired HAoSMC adhesion on PNIPAm brush surfaces with a grafting density of 0.41 $\mu\text{g}/\text{cm}^2$ whereas a decrease of the grafted amount allowed for cell adhesion. Commercial UpCell™ plates possess an even higher PNIPAm grafting density of approximately 1.9 $\mu\text{g}/\text{cm}^2$ which most likely is the reason for the observed retarded SMC adhesion preventing successful HAoSMC sheet fabrication.⁶⁵

Under the described conditions, cell sheets of HAoSMCs detached reproducibly within 23 ± 12 min (N = 10) from PGE-3.0 coatings after replacement of cell culture medium by PBS (20 °C) whereas no cell sheet detachment was observable on the TCPS control (Figure 7).

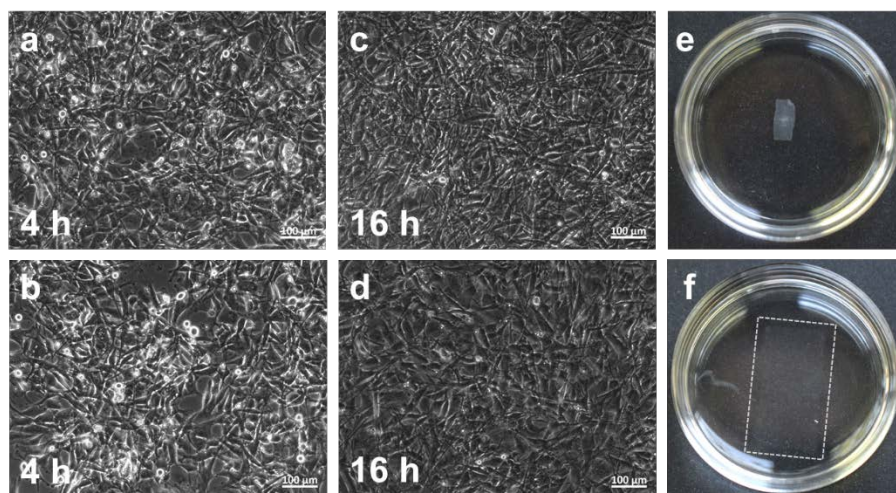


Figure 7. Representative phase contrast images of HAOsMCs 4 and 16 h after seeding on PGE-3.0 (a, c) and TCPS (b, d) and respective macroscopic photographs of the culture dishes after temperature reduction to 20 °C (e, f). Only PGE-3.0 dishes released HAOsMC sheets when triggered thermally whereas cells on TCPS did not detach (grey frame).

For the fabrication of endothelial sheets, HUVECs (passages 4-7) were seeded onto coated PS dishes with a density of 8.5×10^4 cells cm^{-2} and cultured in Vasculife VEGF medium containing 2% FBS for 24 h. After 24 h the medium was exchanged against fresh medium supplemented with 10% FBS and HUVECs were cultured for further 48 h. As illustrated in Figure 8, cells adhered and grew to confluency in a similar manner than on TCPS control surfaces without the necessity of an additional cell adhesion promoters which was applied by Moran *et al.*⁶⁶ to enable HUVEC adhesion on a thermoresponsive copolymer of PNIPAm and *N-tert*-butyl acrylamide. After treatment with PBS at room temperature (20 °C), intact cell sheets detached from the functionalized PS substrates within 9 ± 1 min ($N = 9$), whereas no detachment was observed on TCPS control surfaces.

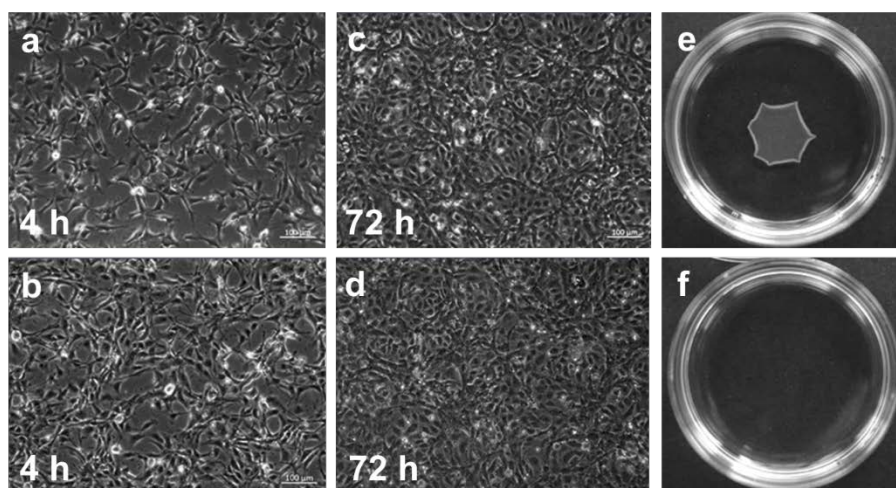


Figure 7. Representative phase contrast images of HUVECs 4 and 72 h after seeding on PGE-3.0 (a + c) and TCPS (b + d) and respective macroscopic photographs of the culture dishes after temperature reduction to 20 °C (e + f). Only PGE-3.0 dishes released HUVEC sheets when triggered thermally.

However, it should be noted that not only the coating properties but also the culture conditions of the individual cell types, in particular seeding density, culture time and serum concentration, influence the ability to generate cell sheets. For instance, HUVEC detached in cell sheet fragments when culturing them for 72 h in VasculoLife VEGF medium, which contains 2% FBS, whereas complete cell sheets were detached when serum concentration was increased to 10% after 24 hours (Figure S9).

Conclusions

A fast and geometry-independent directed self-assembly process for the generation of a functional, thermoresponsive PGE brush coating, which was covalently immobilized on untreated PS substrates via UV irradiation, was established. We demonstrated that thermoresponsive PGE brushes constitute versatile coatings for the fabrication of HDF, HAoSMC and HUVEC sheets for further vascular tissue engineering. Notably, this thermoresponsive surface does not require any additional cell-adhesive coating or cell-adhesive modification of the thermoresponsive polymer to allow adhesion of all investigated cell types. The theoretical estimation of the degree of chain overlap and the temperature-dependent change in coating morphology both indicate a temperature-triggered pancake-to-brush transition, which enables the detachment of intact cell sheets. In the future, the transfer of PGE brushes to other common cell culture materials, such as PET or PC, might offer a straightforward route to the functionalization of porous membrane substrates to further extend the range of application of thermoresponsive PGE brush coatings.

Conflicts of interest

There are no conflicts of interest to declare.

Acknowledgements

M.W. is grateful to financial support from the Federal Ministry of Education and Research through grant FKZ: 13N13523.

Supplementary material

Detailed description of materials and methods used, temperature- and concentration-dependent DLS measurements and UV-Vis turbidimetry, theoretically modelled surface structure of PGE-3.0 and PGE-0.7, investigation of PS substrate adhesiveness via QCM-D, temperature-dependent morphology and material properties of PGE-3.0 coatings measured by AFM in

PeakForce QNM mode, adhesion and proliferation study of HUVECs on TCPS, PS, PGE-0.7 and PGE-3.0 substrates, comparison of PGE-3.0 and UpCell™ plates for smooth muscle cell culture and impact of serum concentration on HUVEC sheet detachment.

References

- 1 O. O. Akintewe, E. G. Roberts, N.-G. Rim, M. A. H. Ferguson and J. Y. Wong, *Annu. Rev. Biomed. Eng.*, 2017, **19**, 389-414.
- 2 S. Pashneh-Tala, S. MacNeil and F. Claeysens, *Tissue Eng., Part B*, 2015, **22**, 68-100.
- 3 S. Li, D. Sengupta and S. Chien, *Wiley Interdiscip. Rev.: Syst. Biol. Med.*, 2014, **6**, 61-76.
- 4 M. B. Elliott and S. Gerecht, *J. Mater. Chem. B*, 2016, **4**, 3443-3453.
- 5 N. L'Heureux, S. Pâquet, R. Labbé, L. Germain and F. A. Auger, *The FASEB Journal*, 1998, **12**, 47-56.
- 6 A. H. Huang and L. E. Niklason, *Cell. Mol. Life Sci.*, 2014, **71**, 2103-2118.
- 7 M. Zhang, D. Methot, V. Poppa, Y. Fujio, K. Walsh and C. E. Murry, *J. Mol. Cell Cardiol.*, 2001, **33**, 907-921.
- 8 R. Takeuchi, Y. Kuruma, H. Sekine, I. Dobashi, M. Yamato, M. Umezumi, T. Shimizu and T. Okano, *J. Tissue Eng. Regener. Med.*, 2016, **10**, 700-710.
- 9 K. Tatsumi and T. Okano, *Current Transplantation Reports*, 2017, **4**, 184-192.
- 10 A. C. Yorukoglu, A. E. Kiter, S. Akkaya, N. L. Satiroglu-Tufan and A. C. Tufan, *Stem Cells Int.*, 2017, **2017**, 13.
- 11 N. Matsuda, T. Shimizu, M. Yamato and T. Okano, *Adv. Mater.*, 2007, **19**, 3089-3099.
- 12 I. Elloumi-Hannachi, M. Yamato and T. Okano, *J. Intern. Med.*, 2010, **267**, 54-70.
- 13 K. Matsuura, R. Utoh, K. Nagase and T. Okano, *J. Controlled Release*, 2014, **190**, 228-239.
- 14 T. Matsuda, T. Shirota and D. Kawahara, *J. Tissue Sci. Eng.*, 2014, **5**, 134.
- 15 K. Moschouris, N. Firoozi and Y. Kang, *Regener. Med.*, 2016, **11**, 559-570.
- 16 K. Kim, R. Utoh, K. Ohashi, T. Kikuchi and T. Okano, *J. Tissue Eng. Regener. Med.*, 2017, **11**, 2071-2080.
- 17 H. Komae, H. Sekine, I. Dobashi, K. Matsuura, M. Ono, T. Okano and T. Shimizu, *J. Tissue Eng. Regener. Med.*, 2017, **11**, 926-935.
- 18 T. Sasagawa, T. Shimizu, M. Yamato and T. Okano, *J. Tissue Eng. Regener. Med.*, 2016, **10**, 739-747.
- 19 Y. Haraguchi, T. Shimizu, T. Sasagawa, H. Sekine, K. Sakaguchi, T. Kikuchi, W. Sekine, S. Sekiya, M. Yamato, M. Umezumi and T. Okano, *Nat. Protoc.*, 2012, **7**, 850.
- 20 J. Akimoto, A. Arauchi, M. Nakayama, R. Kanaya, Y. Iwase, S. Takagi, M. Yamato and T. Okano, *J. Biomed. Mater. Res., Part B*, 2014, **102**, 1659-1668.
- 21 N. Yamada, T. Okano, H. Sakai, F. Karikusa, Y. Sawasaki and Y. Sakurai, *Macromol. Chem., Rapid Commun.*, 1990, **11**, 571-576.
- 22 T. Okano, N. Yamada, M. Okuhara, H. Sakai and Y. Sakurai, *Biomaterials*, 1995, **16**, 297-303.
- 23 Y. Akiyama, A. Kushida, M. Yamato, A. Kikuchi and T. Okano, *J. Nanosci. Nanotechnol.*, 2007, **7**, 796-802.
- 24 N. Asakawa, T. Shimizu, Y. Tsuda, S. Sekiya, T. Sasagawa, M. Yamato, F. Fukai and T. Okano, *Biomaterials*, 2010, **31**, 3903-3909.
- 25 T. Sasagawa, T. Shimizu, S. Sekiya, Y. Haraguchi, M. Yamato, Y. Sawa and T. Okano, *Biomaterials*, 2010, **31**, 1646-1654.

- 26 T. X. Ngo, E. Nagamori, T. Kikuchi, T. Shimizu, T. Okano, M. Taya and M. Kino-oka, *Biotechnol. Lett.*, 2013, **35**, 1001-1008.
- 27 H. Takahashi, T. Shimizu, M. Nakayama, M. Yamato and T. Okano, *Adv. Healthcare Mater.*, 2015, **4**, 356-360.
- 28 M. Ebara, M. Yamato, T. Aoyagi, A. Kikuchi, K. Sakai and T. Okano, *Biomacromolecules*, 2004, **5**, 505-510.
- 29 M. Ebara, M. Yamato, T. Aoyagi, A. Kikuchi, K. Sakai and T. Okano, *Adv. Mater.*, 2008, **20**, 3034-3038.
- 30 M. Nishi, J. Kobayashi, S. Pechmann, M. Yamato, Y. Akiyama, A. Kikuchi, K. Uchida, M. Textor, H. Yajima and T. Okano, *Biomaterials*, 2007, **28**, 5471-5476.
- 31 K. Fukumori, Y. Akiyama, M. Yamato and T. Okano, *ChemNanoMat*, 2016, **2**, 454-460.
- 32 H. Takahashi, N. Matsuzaka, M. Nakayama, A. Kikuchi, M. Yamato and T. Okano, *Biomacromolecules*, 2012, **13**, 253-260.
- 33 B. C. Isenberg, Y. Tsuda, C. Williams, T. Shimizu, M. Yamato, T. Okano and J. Y. Wong, *Biomaterials*, 2008, **29**, 2565-2572.
- 34 C. Williams, Y. Tsuda, B. C. Isenberg, M. Yamato, T. Shimizu, T. Okano and J. Y. Wong, *Adv. Mater.*, 2009, **21**, 2161-2164.
- 35 J. Kobayashi, M. Hayashi, T. Ohno, M. Nishi, Y. Arisaka, Y. Matsubara, H. Kakidachi, Y. Akiyama, M. Yamato, A. Horii and T. Okano, *J. Biomed. Mater. Res., Part A*, 2014, **102**, 3883-3893.
- 36 A. Dworak, A. Utrata-Wesołek, D. Szweda, A. Kowalczyk, B. Trzebicka, J. Anioł, A. L. Sieroń, A. Klama-Baryła and M. Kawecki, *ACS Appl. Mater. Interfaces*, 2013, **5**, 2197-2207.
- 37 M. Kawecki, M. Kraut, A. Klama-Baryła, W. Łabuś, D. Kitala, M. Nowak, J. Glik, A. L. Sieroń, A. Utrata-Wesołek, B. Trzebicka, A. Dworak and D. Szweda, *J. Mater. Sci.: Mater. Med.*, 2016, **27**, 111.
- 38 A. Dworak, A. Utrata-Wesołek, N. Oleszko, W. Wałach, B. Trzebicka, J. Anioł, A. L. Sieroń, A. Klama-Baryła and M. Kawecki, *J. Mater. Sci.: Mater. Med.*, 2014, **25**, 1149-1163.
- 39 N. Oleszko, W. Wałach, A. Utrata-Wesołek, A. Kowalczyk, B. Trzebicka, A. Klama-Baryła, D. Hoff-Lenczewska, M. Kawecki, M. Lesiak, A. L. Sieroń and A. Dworak, *Biomacromolecules*, 2015, **16**, 2805-2813.
- 40 M. Weinhart, T. Becherer and R. Haag, *Chem. Commun.*, 2011, **47**, 1553-1555.
- 41 D. D. Stöbener, M. Uckert, J. L. Cuellar Camacho, A. Hoppensack and M. Weinhart, *ACS Biomater. Sci. Eng.*, 2017, **3**, 2155-2165.
- 42 S. Heinen, S. Rackow, A. Schäfer and M. Weinhart, *Macromolecules*, 2017, **50**, 44-53.
- 43 T. Patel, L. Abezgauz, D. Danino, V. Aswal and P. Bahadur, *J. Dispersion Sci. Technol.*, 2011, **32**, 1083-1091.
- 44 M. Nawaz, M. K. Baloch, G. J. Price, I. Ud-Din and E.-S. E.-B. El-Mossalamy, *J. Polym. Res.*, 2013, **20**, 180.
- 45 Ł. Otulakowski, M. Gadzinowski, S. Slomkowski, T. Basinska, A. Forys, A. Dworak and B. Trzebicka, *Eur. Polym. J.*, 2018, **99**, 72-79.
- 46 T. Becherer, S. Heinen, Q. Wei, R. Haag and M. Weinhart, *Acta Biomater.*, 2015, **25**, 43-55.
- 47 S. Heinen and M. Weinhart, *Langmuir*, 2017, **33**, 2076-2086.
- 48 S. Heinen, J. L. Cuellar-Camacho and M. Weinhart, *Acta Biomater.*, 2017, **59**, 117-128.
- 49 S. J. Sofia, V. Premnath and E. W. Merrill, *Macromolecules*, 1998, **31**, 5059-5070.
- 50 E. Bittrich, S. Burkert, M. Müller, K.-J. Eichhorn, M. Stamm and P. Uhlmann, *Langmuir*, 2012, **28**, 3439-3448.
- 51 B. C. Choi, S. Choi and D. E. Leckband, *Langmuir*, 2013, **29**, 5841-5850.
- 52 S. Heinen, S. Rackow, J. L. Cuellar-Camacho, I. S. Donskyi, W. E. S. Unger and M. Weinhart, *J. Mater. Chem. B*, 2018, **6**, 1489-1500.

- 53 E. S. Pagac, D. C. Prieve, Y. Solomentsev and R. D. Tilton, *Langmuir*, 1997, **13**, 2993-3001.
- 54 W. M. de Vos, A. de Keizer, J. M. Kleijn and M. A. Cohen Stuart, *Langmuir*, 2009, **25**, 4490-4497.
- 55 B. Peng, X. Chu, Y. Li, D. Li, Y. Chen and J. Zhao, *Polymer*, 2013, **54**, 5779-5789.
- 56 B. Du, O. K. C. Tsui, Q. Zhang and T. He, *Langmuir*, 2001, **17**, 3286-3291.
- 57 A. Ghorbal and A. B. Brahim, *Polym. Test.*, 2013, **32**, 1174-1180.
- 58 Y. Zou, N. A. A. Rossi, J. N. Kizhakkedathu and D. E. Brooks, *Macromolecules*, 2009, **42**, 4817-4828.
- 59 S. J. G., D. B. Ann, J. Graham and U. P. Anne, *J. Biomed. Mater. Res.*, 1993, **27**, 927-940.
- 60 C. Wilson, R. Clegg, D. Leavesley and M. Percy, *Tissue Eng.*, 2005, **11**, 1-18.
- 61 S. Rayatpisheh, D. E. Heath, A. Shakouri, P.-O. Rujitanaroj, S. Y. Chew and M. B. Chan-Park, *Biomaterials*, 2014, **35**, 2713-2719.
- 62 D. E. Backman, B. L. LeSavage, S. B. Shah and J. Y. Wong, *Macromol. Biosci.*, 2017, **17**, 1600434.
- 63 N. A. Dzhoyashvili, K. Thompson, A. V. Gorelov and Y. A. Rochev, *ACS Appl. Mater. Interfaces*, 2016, **8**, 27564-27572.
- 64 H. Takahashi, M. Nakayama, M. Yamato and T. Okano, *Biomacromolecules*, 2010, **11**, 1991-1999.
- 65 K. Fukumori, Y. Akiyama, Y. Kumashiro, J. Kobayashi, M. Yamato, K. Sakai and T. Okano, *Macromol. Biosci.*, 2010, **10**, 1117-1129.
- 66 M. T. Moran, W. M. Carroll, A. Gorelov and Y. Rochev, *J. R. Soc., Interface*, 2007, **4**, 1151-1157.

Electronic Supplementary Information (ESI) for the following manuscript

Endothelial, Smooth Muscle and Fibroblast Cell Sheet Fabrication from Self-assembled Thermoresponsive Poly(glycidyl ether) Brushes

*Daniel David Stöbener, Anke Hoppensack, Johanna Scholz, Marie Weinhart**

Institute for Chemistry and Biochemistry, Freie Universitaet Berlin, Takustr. 3, D-14195
Berlin, Germany.

*Corresponding author: email marie.weinhart@fu-berlin.de, phone: +49 30 838 75050

Keywords

Cloud point temperature, benzophenone-driven aggregation, block-copolymer adsorption, UV-induced C, H-insertion, pancake-to-brush transition, switchable surfaces

Materials

Materials for surface modification. All chemicals and solvents were purchased from Sigma Aldrich (Steinheim, Germany) and used as received unless stated otherwise. Acetone and ethanol applied for surface modification and cleaning were distilled under reduced pressure before use to remove impurities. Bare Si wafers with a 2 nm SiO₂ layer were supplied by Silchem GmbH (Freiberg, Germany), cut into quadratic pieces (11 x 11 mm), washed with ethanol and dried under a stream of N₂. Gold-coated QCM-D sensor chips were obtained from Q-Sense LOT-QuantumDesign (Darmstadt, Germany).

Materials for cell culture. Falcon[®] PS culture dishes (d = 35 mm) were purchased from Th. Geyer GmbH & Co. KG (Berlin, Germany). Tissue culture PS dishes (d = 35 mm), 24-well TCPS plates and thermoresponsive 24-well culture plates with a hydrogel-like PNIPAM coating (UpCell[™]) were supplied by VWR International (Leuven, Belgium) and used as received. 24-well PS plates and Cellstar TCPS culture flasks were purchased from Greiner Bio-One GmbH (Frickenhausen, Germany). Dulbecco's modified Eagle medium (DMEM 4.5 g/L glucose #31966-021 and DMEM 1 g/L glucose #21885108), dispase II (#17105-041), Penicillin-Streptomycin (#15140122), and trypsin/EDTA solution (#15400054) were purchased from Thermo Fisher Scientific (Darmstadt, Germany). Accutase[®] solution (#A6964), propidium iodide (#P4170) and fluorescein diacetate (#F7378) were supplied by Sigma Aldrich (Steinheim, Germany). Fetal bovine serum was purchased from PAN-Biotech GmbH (#P30-3306, Aidenbach, Germany) and from Biochrom (#S 0615, Berlin, Germany). Collagenase NB4 (#17454) was supplied by Serva GmbH (Halle, Germany). HAoSMCs (#FC-0015), VascuLife SMC medium (#LL-0014), HUVECs (#FC-0003) and VascuLife VEGF medium (#LL-0003) were derived from CellSystems Biotechnologie Vertrieb GmbH (Troisdorf, Germany). All other expendable materials for cell culture were purchased from Sarstedt (Nümbrecht, Germany).

Methods

Characterization of thermal properties of PGE. Dynamic light scattering (DLS) was performed on a Zetasizer Nano-ZS analyzer (Malvern Instruments, Malvern, United Kingdom) equipped with a 50 mW frequency doubled DPSS Nd:YAG laser ($\lambda=532$ nm) at concentrations of 2.5 and 0.25 mg mL⁻¹ in Milli-Q water at 10, 20 and 37 °C. Measurements were performed at least in triplicate using Quartz cuvettes supplied by Hellma Analytics GmbH (Müllheim, Germany) and each sample was equilibrated for at least 120 s. Turbidity measurements were performed on a Lambda 950 UV-Vis spectrometer at $\lambda = 500$ nm with a PTP 6 Peltier Temperature Programmer from Perkin Elmer (Waltham, MA, USA). Cloud point temperatures (CPTs) were determined at concentrations between 1 and 20 mg mL⁻¹ in Milli-Q water employing heating/cooling rates of 0.5 °C min⁻¹ with a data point recording every 0.2 °C. The temperature-dependent transmittance of the aqueous polymer solutions was measured for at least three up- and down cycles and the CPT was defined as the temperature at the inflection point of the normalized transmittance versus temperature curve.

Surface Modification and Characterization. Spin-coating was performed using a WS-650-23 spin-coater from Laurell Technologies Corporation (North Wales, PA, USA). Si wafers (11 x 11 mm) were coated using a 0.5% (w/w) solution of PS (30 μ L) in toluene at 3000 rpm for 60 s. Solutions were prepared using PS ($M_n=132$ kg mol⁻¹, PDI=1.9) from Falcon® culture dishes supplied by Th. Geyer GmbH & Co. KG (Berlin, Germany). Static water contact angles (CAs) were measured with an OCA contact angle system from DataPhysics Instruments GmbH (Filderstadt, Germany) and fitted with the software package SCA202 (version 3.12.11) using the sessile drop method. CAs were determined before and after surface functionalization. A drop of MilliQ water (2 μ L) was placed onto the respective surface and CAs were determined with an elliptical fitting model. For each substrate, CAs were measured on at least three different spots to test for the homogeneity of the sample and ten independent substrates ($n = 10$) to test for reproducibility. The dry layer thickness of the polymer coatings was determined by multi-

angle spectroscopic ellipsometry at 70° with a SENpro spectroscopic ellipsometer from SENTECH Instruments GmbH (Berlin, Germany). The thickness of the SiO₂ layer before spin-coating and the additional thickness of the spin-coated PS layer were determined separately and respective average values of at least three different spots on the surface were taken as fixed values for the subsequent modeling of the adsorbed PGE layer. The PGE thickness was measured at wavelengths from 370 nm to 1050 nm and was fitted using a model consisting of the previously measured SiO₂ and PS layers with fixed parameters, a Cauchy layer with a fixed RI of $n=1.5$ and air as the surrounding medium. For photo-immobilization, samples with adsorbed PGE layers were irradiated with UV light using a UV-KUB 2 from KLOÉ (Montpellier, France) with a wavelength of 365 nm and a radiant exposure of 4.0 J cm⁻² for 160 s, which corresponds to an irradiance of 25 mW cm⁻² (100%). QCM-D measurements were performed on Q-Sense E1 system from LOT-QuantumDesign (Darmstadt, Germany) with a standard flow module and a Reglo Digital peristaltic pump from Ismatec (Wertheim, Germany). The software QSoft401 version 2.5.22 was used for data acquisition and QTools 3 version 3.1.25 from Biolin Scientific AB 2000-2014 (Stockholm, Sweden) was used for data analysis. AFM measurements were performed on an AFM Nanoscope MultiMode 8 equipped with a fluid cell and a thermal application (TA) controller from Bruker (Billerica, MA, USA). The morphology and material properties of the PGE-3.0 coatings was measured in PeakForce QNM (Quantitative NanoMechanics) mode. Coated Si wafers were mounted on the AFM head, degassed Milli-Q water was inserted into the liquid cell and the TA controller was set to the desired temperature (37 or 20 °C) and equilibrated for at least 10 min prior to each measurement. To obtain high resolution images with reduced sample damage, SNL-10 cantilevers from Bruker (Billerica, MA, USA) with a nominal spring constant of 0.35 N m⁻¹ and a tip radius of 2-12 nm were used, and images were recorded with a loading peak force of 500 pN, 512 points per line and scan rates of 0.7 Hz. Obtained images were analyzed with the Nanoscope analysis software (version 1.4) and processed using 1st order flattening. Roughness

and depth analysis tools were used to obtain the surface parameters. Microscopic images of HDFs, HAoSMCs and HUVECs were taken on a Zeiss Observer Z1 from Carl Zeiss Microscopy GmbH (Jena, Germany) and evaluated with the software Zen 2 Version 2.0.0.0 from Carl Zeiss Microscopy GmbH (Jena, Germany). Macroscopic photographs were taken with a Nikon D3100 from Nikon GmbH (Düsseldorf, Germany).

Dynamic light scattering (DLS) measurements

To investigate the temperature- and concentration-dependent hydrodynamic radius of PGE in Milli-Q water, DLS measurements were performed at 10, 20 and 37 °C and 2.5 as well as 0.25 mg mL⁻¹ (10 μM). At moderate concentration (2.5 mg mL⁻¹), PGE forms 30-50 nm sized aggregates at 10 and 20 °C and slightly bigger particles at 37 °C, as evident from both number and volume distributions (Figure S1a, c). It was previously reported that poly(GME-*ran*-EGE) copolymers with comparable molecular weight (24 kDa) and no benzophenone (BP) block form up to 1 μm sized aggregates at 20 and 37 °C, whereas their particle size decreases to about 10 nm upon cooling to 10 °C (measured at 10 mg mL⁻¹).¹ This rather uniform aggregation behaviour of the PGE block copolymer indicates the hydrophobically-driven association of the BP anchor-blocks in aqueous solution. At dilute concentration (0.25 mg mL⁻¹), however, the hydrodynamic radius of PGE decreases to about 10 nm at 10 °C (Figure S1b, d), which is in the same range as it was reported before for aqueous and ethanolic poly(GME-*ran*-EGE) solution (10 mg mL⁻¹) at 10 and 20 °C, respectively¹, as well as ethanolic PGE solutions (20 mg mL⁻¹) at 20 °C.² Due to the negligible aggregation of PGE under dilute conditions and lowered temperature, PS substrates were coated with PGE in Milli-Q water at 10 °C and 10 μM, in order to attain the homogeneous adsorption of PGE-3.0 as monolayers.

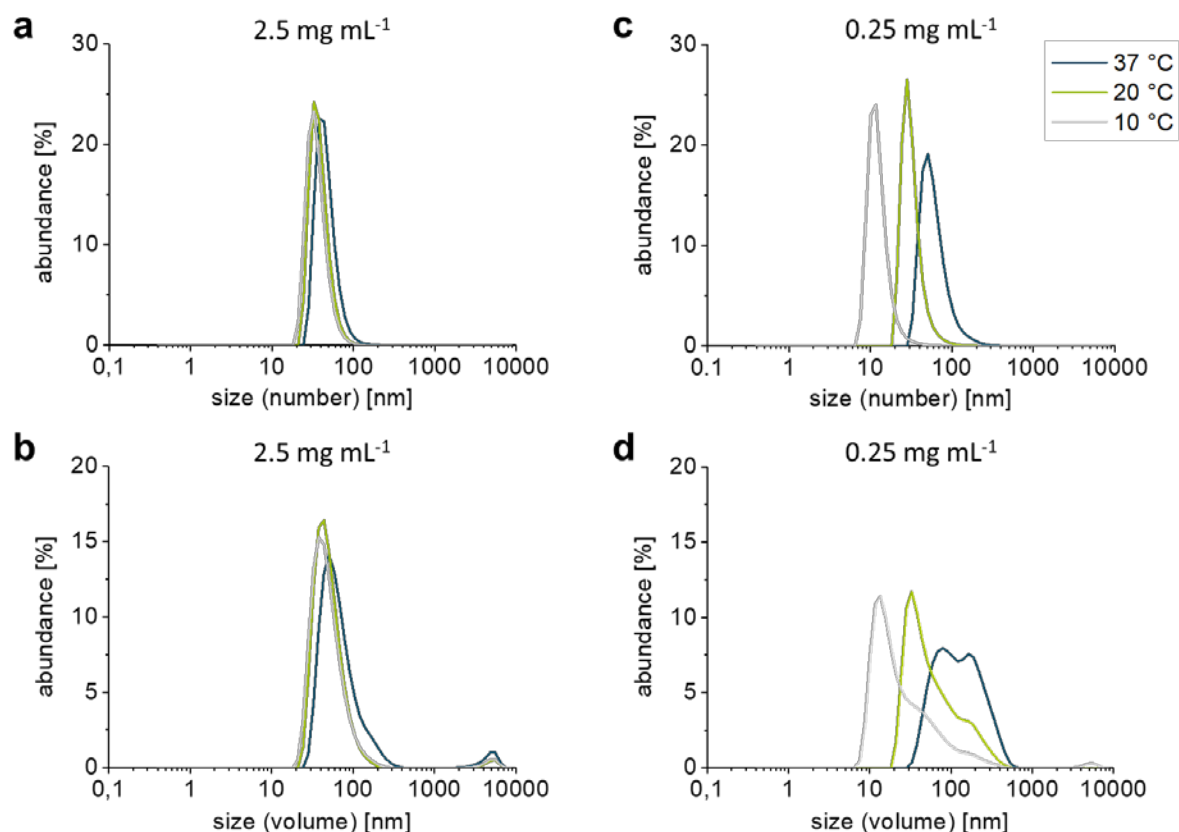


Figure S1. Temperature-dependent number and volume distributions of the hydrodynamic radii of PGE in Milli-Q water at moderate concentrations of 2.5 mg mL⁻¹ (a-b) and at dilute concentration of 10 μ M (0.25 mg mL⁻¹) (c-d) measured by DLS.

UV-Vis turbidimetry measurements

The concentration-dependent cloud point temperature (CPT) of PGE in Milli-Q water was determined by UV-Vis transmittance measurements in the range between 1 and 20 mg mL⁻¹. In accordance to previous reports of a poly(GME-*ran*-EGE) copolymer with comparable molecular weight (24 kDa) and without a BP block¹, the CPTs of PGE are only slightly dependent on the concentration between 1 and 5 mg mL⁻¹ and show only small hysteresis (Figure S2a). However, at higher concentration (10 - 20 mg mL⁻¹), CPTs decrease markedly and a significant hysteresis occurs (Figure S2b), which is presumably caused by the hydrophobic, supramolecular association of the BP anchor blocks. In addition, the CPTs of PGE in the concentration range between 1 and 5 mg mL⁻¹ is shifted to higher temperatures (20-22 °C)

and phase transition regimes are significantly broadened ($> 10\text{ }^{\circ}\text{C}$) as compared to poly(GME-*ran*-EGE) with a similar GME/EGE ratio of 1:3, which exhibits lower CPTs (16-18 $^{\circ}\text{C}$) and much sharper transition regimes ($\sim 2\text{-}3\text{ }^{\circ}\text{C}$).¹ This can be explained by the benzophenone-driven intermolecular aggregation of PGE, which is already prevalent at 10 $^{\circ}\text{C}$ below the temperature-triggered phase transition and hence, shifts the CPTs as well as broadens the phase transition.

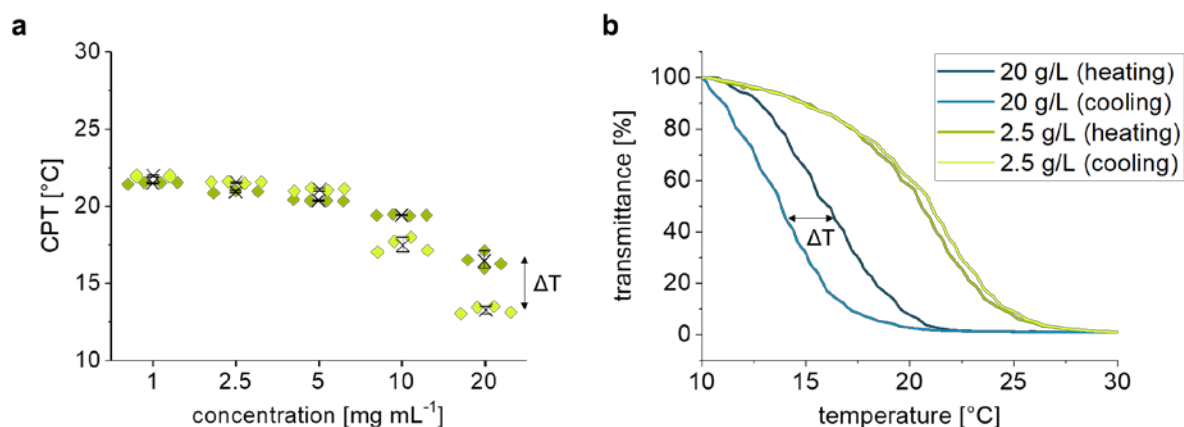


Figure S2. (a) Concentration-dependent CPTs of PGE measured by turbidimetry in Milli-Q water at concentrations between 1 and 20 mg mL^{-1} ; (b) Representative normalized transmittance curves (heating and cooling) of PGE in Milli-Q water at high (20 mg mL^{-1}) and moderate (2.5 mg mL^{-1}) concentration.

Theoretically modelled surface structure of PGE-3.0 in comparison to PGE-0.7

To compare PGE-3.0 brush conformation with ultrathin coatings, theoretical modelling was applied to PGE-0.7 layers. As illustrated in Figure S3, average anchor distances l is markedly higher and values for the packing parameter $2R_f l^{-1}$ are significantly lower for PGE-0.7 coatings under both bad as well as theta solvent conditions.

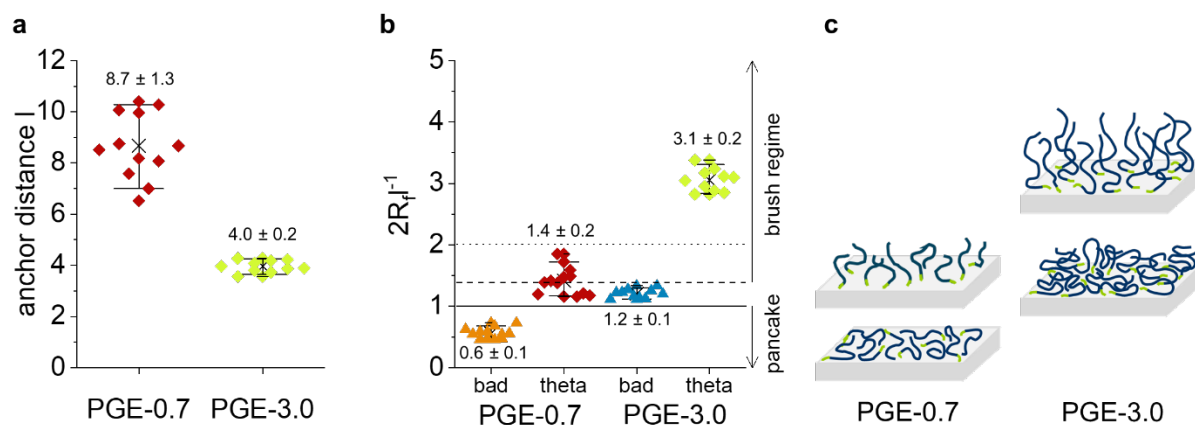


Figure S3. Theoretically estimated degree of chain overlap ($2R_f l^{-1}$) on PS-coated silicon wafers. (a) Anchor distance l calculated from the dry layer thickness of PGE-0.7 and PGE-3.0 coatings determined by ellipsometry. (b) Degree of chain overlap $2R_f l^{-1}$ calculated from the anchor distance l and the estimated Flory Radius R_f under bad (orange and blue triangles) and theta (red and green diamonds) solvent conditions. $2R_f l^{-1}$ values are shown for each replicate together with their mean value (black cross) and their 90% confidence interval (whiskers). (c) Schematic illustration of the temperature-dependent structure of the PGE-0.7 and PGE-3.0 coatings.

Investigation of the adhesive interaction between PS and poly(GME-*ran*-EGE)

To investigate the affinity of thermoresponsive GME/EGE copolymers towards PS and to therefore deduce their chain conformation on PS substrates, adsorption experiments of a poly(GME-*ran*-EGE) copolymer were conducted using quartz crystal microbalance with dissipation (QCM-D). Gold-coated QCM-D sensor chips were used as received and spin-coated as described above, applying a solution of PS in toluene (1.0% (w/w), 30 μ L). The PS-coated sensor chips were dried at ambient conditions overnight, rinsed with ethanol and dried under a stream of N_2 before use. Adsorption of a poly(GME-*ran*-EGE) ($M_n = 43$ kDa, PDI = 1.45, GME:EGE = 1:3) copolymer without a surface reactive anchor group was performed in a QCM-D to determine the adsorbed mass by online-monitoring of the change in resonance frequency (Δf) and dissipation (ΔD) of a piezoelectric quartz crystal over time. Changes in the

fundamental frequency (4.95 MHz) and in overtones 3 to 13 were measured. For calculation of the layer thickness, the Sauerbrey relation was chosen, as it sufficiently describes thin layers with negligible viscoelasticity. Calculations were conducted using the software package QTools[®] considering the 3rd overtone. Start and end of all measurements were performed in ethanol to generate a reliable and comparable baseline. Therefore, fluid density was set to 789 kg m^{-3} , fluid viscosity to $0.0012 \text{ kg m}^{-1} \text{ s}^{-1}$, and the layer density was estimated to be 1000 kg m^{-3} . Ethanol was distilled before use and degassed for 20 min in an ultrasonic bath. PS-coated sensor chips were inserted into the flow chamber and were equilibrated under ethanol flow (0.1 mL min^{-1}) until the baseline was constant. A solution of the polymer in ethanol (0.01 mM) was flown over the sensor chips for 8 min (0.1 mL min^{-1}), the flow was stopped to adsorb poly(GME-*ran*-EGE) under static conditions for 30 min, and the surfaces were flushed with ethanol to remove loosely adsorbed polymer. The dry thickness of the adsorbed films was measured by ellipsometry on PS-coated Si wafers and determined to be $0.4 \pm 0.1 \text{ nm}$ and the solvated thickness calculated from QCM-D measurements was $1.2 \pm 0.2 \text{ nm}$, indicating a degree of solvation of the adsorbed films of about 67% (Figure S4a). This is roughly in the range of what was determined for ultrathin PGE coatings.² In addition, the water CA significantly changes from $90.3 \pm 0.5^\circ$ to $69.8 \pm 0.3^\circ$ (Figure S4b), which was also reported for ultrathin PGE coatings. The reproducible formation of stable, ultrathin poly(GME-*ran*-EGE) layers with an average adsorbed areal mass of $124 \pm 18 \text{ ng cm}^{-2}$ ($n = 3$) reached saturation after one adsorption cycle and did not significantly change upon performing multiple cycles (Figure S4c). This indicates a rather strong interaction of the PS surface with the thermoresponsive polymer and suggests the formation of a pancake-like conformation of poly(glycidyl ether)s on PS substrates.

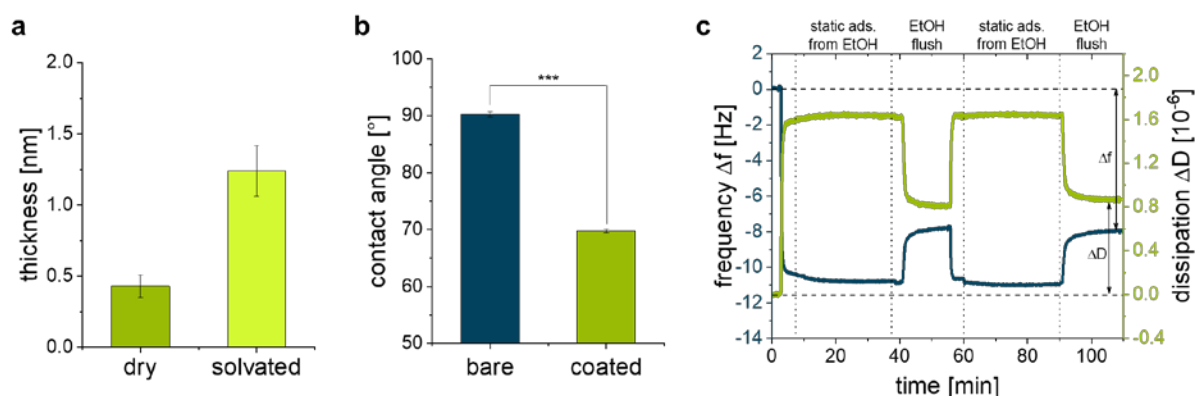


Figure S4. (a) Dry and solvated (EtOH) layer thickness of a poly(GME-*ran*-EGE) copolymer adsorbed onto PS from dilute ethanolic solution (10 μM) measured by ellipsometry and QCM-D, respectively ($n = 3$, error bars indicate SD) (b) Static water contact angle of bare PS and PS coated with poly(GME-*ran*-EGE) ($n = 3$, error bars indicate SD) (c) Representative frequency and dissipation curves of two consecutive online adsorption cycles of poly(GME-*ran*-EGE) measured by QCM-D.

Atomic force microscopy (AFM) quantitative nanomechanical mapping (QNM)

AFM measurements were performed to investigate the morphology and material properties of PGE-3.0 coatings. To obtain high resolution images with reduced sample damage, SNL-10 cantilevers from Bruker (Billerica, MA, USA) with a nominal spring constant of 0.35 N m^{-1} and a silicon nitride (Si_3N_4) tip radius of 2-12 nm were used, and images were recorded with a loading peak force of 500 pN. Prior to each measurement, calibration of the cantilevers was carried out on hard clean mica substrates and the spring constants of the cantilevers were extracted with the thermal noise method.³⁻⁴ The surface morphology was measured in Milli-Q water at 37 and 20 $^\circ\text{C}$. As shown in Figure S5, laterally homogeneous and smooth coatings were obtained. The increased roughness at 20 $^\circ\text{C}$ illustrates the temperature-triggered rehydration of the thermoresponsive PGE-3.0 coatings on the nanometer scale and shows characteristic island-like domains, which were previously reported for similar thermoresponsive brush coatings based on poly(N-isopropyl acrylamide) (PNIPAm).⁵

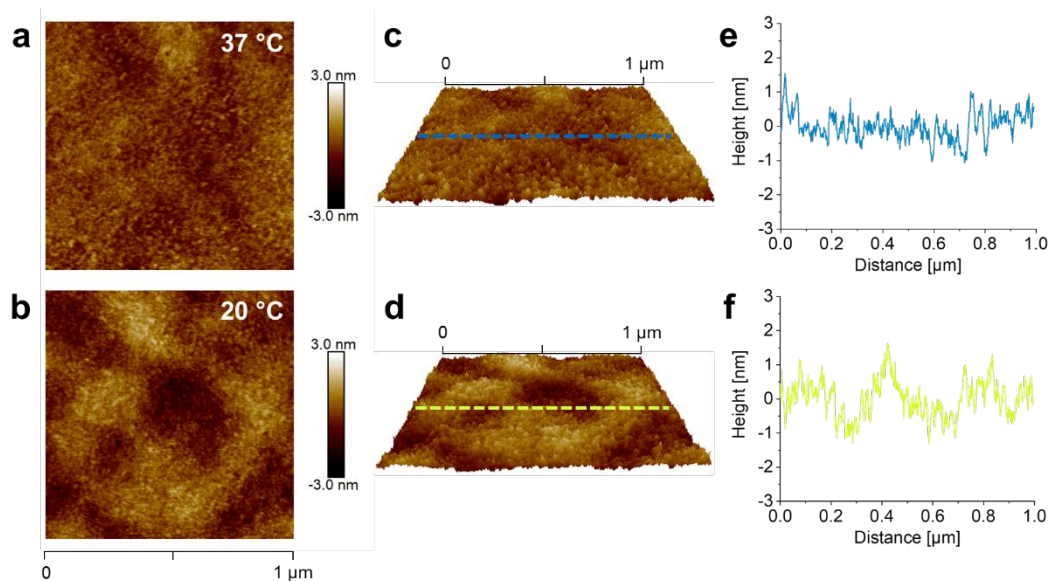


Figure S5. 2D and 3D surface topography and cross section profiles of 3 μm images of PGE-3.0 on PS-coated silicon wafers in Milli-Q water at 37 $^{\circ}\text{C}$ (a, c, e) and 20 $^{\circ}\text{C}$ (b, d, f) measured by AFM in PeakForce QNM mode.

The main roughness parameters of PGE-3.0 coatings were extracted from 3 different 1 μm pictures and are summarized in Table S1 and are compared to those of ultrathin PGE-0.7 coatings as well as to a bare PS substrate.

Table S1. Main roughness parameters obtained from 1 μm PeakForce QNM images measured by AFM. Values for the root-mean squared roughness R_q , mean roughness R_a , and maximal roughness R_{max} (peak to valley vertical variation) for bare PS, PGE-0.7 and PGE-3.0 measured in Milli-Q water at 37 and 20 $^{\circ}\text{C}$ ($n = 3$).

Sample	$R_q \pm \text{SD}$ [nm]	$R_a \pm \text{SD}$ [nm]	$R_{\text{max}} \pm \text{SD}$ [nm]
PS (20 $^{\circ}\text{C}$)	0.42 ± 0.02	0.33 ± 0.01	4.20 ± 0.85
PGE-0.7 (37 $^{\circ}\text{C}$)	0.55 ± 0.13	0.43 ± 0.10	5.44 ± 1.27
PGE-0.7 (20 $^{\circ}\text{C}$)	0.64 ± 0.12	0.50 ± 0.10	5.85 ± 0.87
PGE-3.0 (37 $^{\circ}\text{C}$)	0.49 ± 0.09	0.39 ± 0.08	4.67 ± 0.60
PGE-3.0 (20 $^{\circ}\text{C}$)	0.70 ± 0.11	0.57 ± 0.10	5.27 ± 0.67

The material properties of PGE-3.0 coatings on PS-coated Si wafers were determined by AFM in PeakForce QNM mode in Milli-Q water at 37 and 20 °C. Although temperature-dependent changes in surface morphology and roughness were evident (Figure 4, Figure S5, Table S1), the elasticity (Young's Modulus), deformation and adhesion of the PGE-3.0 coatings do not differ markedly between 37 and 20 °C (Figure S6). However, Young's moduli extracted from AFM retraction curves using the Derjaguin-Muller-Toporov (DMT) model revealed the presence of soft PGE films with moduli around 10 MPa, which is about 3 orders of magnitude lower than expected for bare PS.⁶⁻⁷

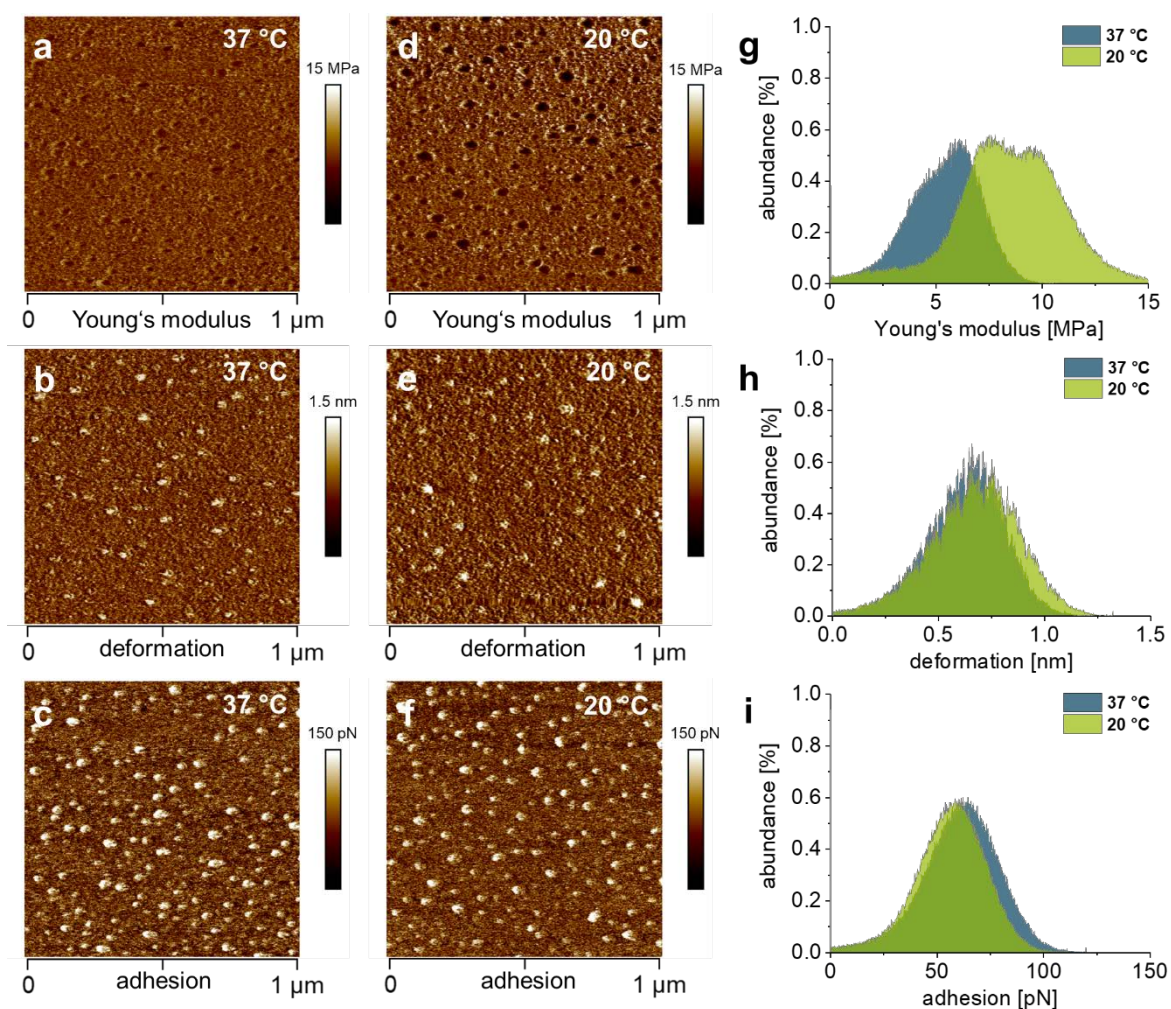


Figure S6. Comparison of PGE-3.0 material properties in Milli-Q water at 37 and 20 °C. Comparative 2D maps (a-f) and depth analyses (g-i) of the Young's modulus (a, d, g), deformation (b, e, h) and adhesion (c, f, i).

Adhesion and proliferation of human umbilical vein endothelial cells (HUVECs) on ultrathin PGE-0.7 and brush-like PGE-3.0 coatings

To compare the adhesion and proliferation of HUVECs on ultrathin (PGE-0.7) and brush-like PGE coatings (PGE-3.0), 5.0×10^4 cells cm^{-2} cells were seeded on coated 24-well PS plates in culture medium (Vasculife VEGF with 2 % FBS). The coated PS surfaces were sterilized with 70% ethanol for 10 min and washed twice with PBS before cell seeding. 24-well TCPS as well as bare PS plates were used as controls. Cells at the center of the plates were observed microscopically and pictures were taken after 48 and 72 h. The cell culture medium (Vasculife VEGF, 2% FBS) was exchanged after 48 h. HUVECs only proliferated to confluent monolayers on PGE-3.0 substrates (Figure S7g, h) and TCPS controls (Figure S7a, b), whereas cells did not attach well to bare PS substrates (Figure S7c, d) and did not proliferate to form confluent cell monolayers on PGE-0.7 substrates (Figure S7e, f).

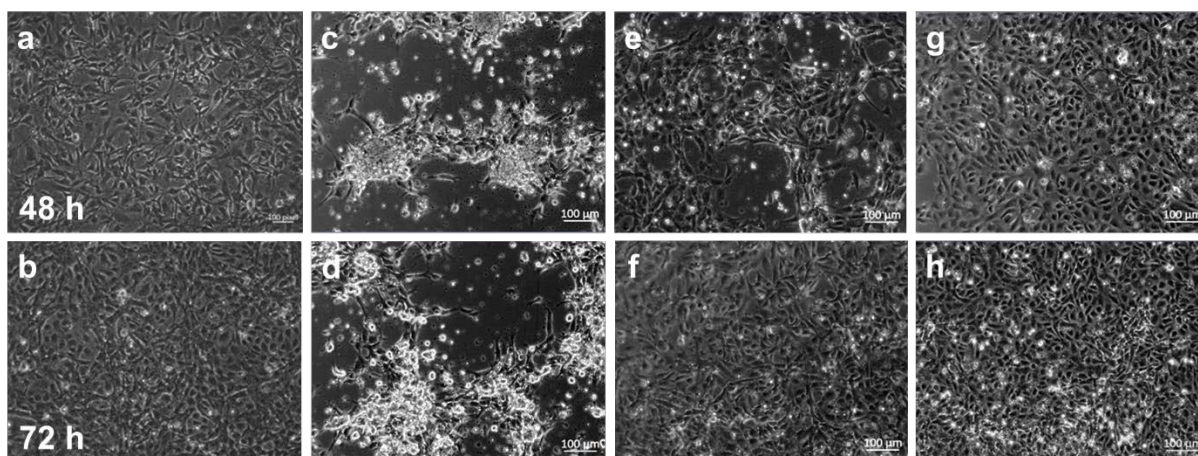


Figure S7. Representative microscopic pictures of HUVECs after 48 and 72 h on TCPS (a-b), PS (c-d), PGE-0.7 (e-f) and PGE-3.0 (g-h). HUVECs (passage 5) were seeded into 24-well plates (PS and TCPS, $A = 1.9 \text{ cm}^{-2}$) with a density of 5.0×10^4 cells cm^{-2} .

Comparison of PGE-3.0 and UpCell™ plates for smooth muscle cell culture

HAoSMCs were seeded on UpCell™ 24-well-plates at a density of 1×10^5 in Vasculife SMC medium with 10 % FBS and cultured for 16 h as on the PGE-3.0 dishes. For live/dead staining of adherent cultures 50 μ M propidium iodide and 10 μ M fluorescein diacetate were added to the cultures and incubated for 5 min. Samples were imaged on a Zeiss Observer Z1 microscope in fluorescent mode with appropriate filter sets.

HAoSMCs adhered homogeneously on PGE-3.0 and TCPS and stayed viable whereas on UpCell™ surface cell clusters containing several dead cells were observed.

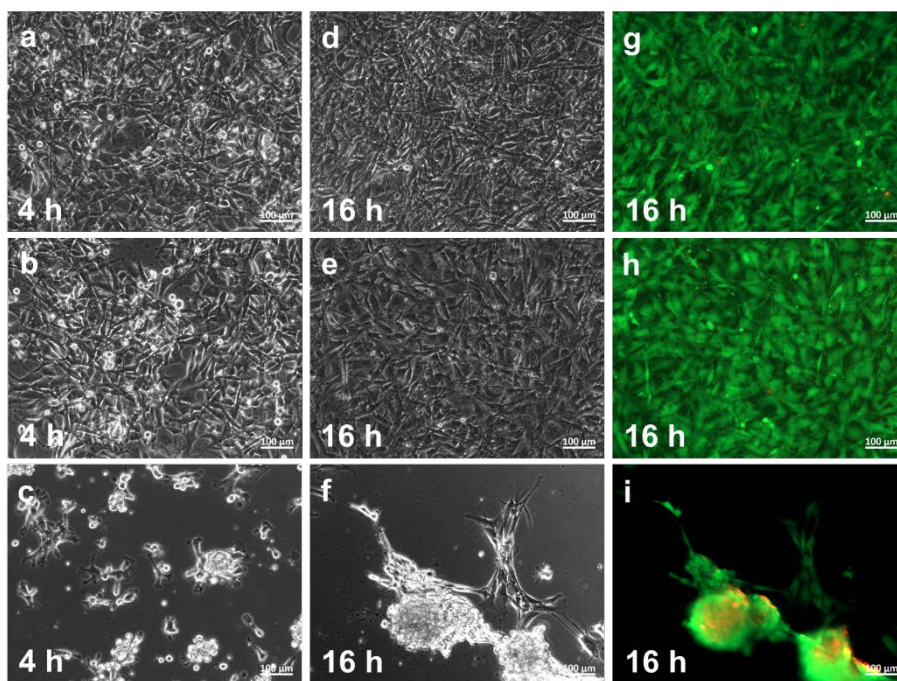


Figure S8. Representative phase contrast images of HAoSMCs 4 and 16 h after seeding on PGE-3.0 (a, d), TCPS (b, e) and UpCell™ (c, f) and respective images of live/dead staining (g, h, i) with fluorescein diacetate (green) and propidium iodide (red).

Impact of serum concentration on cell sheet detachment of HUVECs

Culture conditions of HUVECs on PGE-3.0 were initially optimized to achieve cell sheet detachment. Besides the described culture procedure (24 h in Vasculife VEGF with 2% FBS followed by 48 h in Vasculife with 10% FBS), the culture of HUVEC in Vasculife VEGF

medium, containing 2% FBS, for 72 h was tested. HUVECs were also seeded with a density of 8.5×10^4 cells cm^{-2} in VascuLife VEGF medium (2% FBS) per dish ($d = 35$ mm), followed by culture at 37 °C and 5% CO_2 for 72 h with a media exchange after 24 h. For temperature-triggered detachment, confluent cell cultures were incubated in PBS at 20 °C until the cell sheets detached from the surfaces. After the continuous culture in 2 % serum cell sheets could only be detached in fragments whereas complete cell sheets could be detached in the culture with elevated serum concentration after 24 h (Figure S9c, d). Microscopically it was observed that the latter samples exhibited a higher cell density (Fig. S9a, b) which can be explained by a higher proliferation rate with increased serum concentration.⁸ The higher cell density might have resulted in better cohesion of the cell sheet.

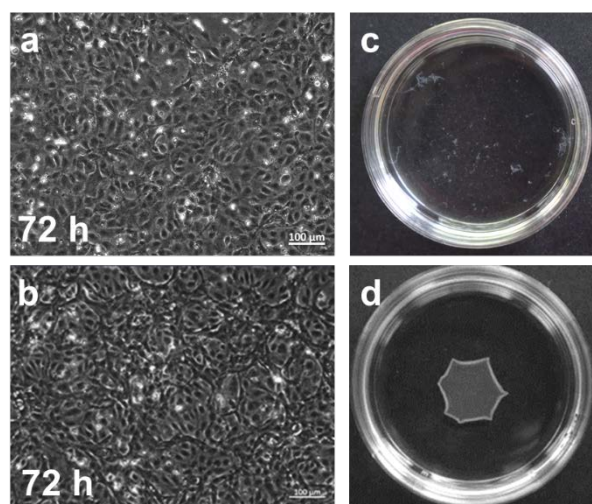


Figure S9. Representative phase contrast images of HUVECs on PGE-3.0 after (a) 72 h culture in VascuLife VEGF medium containing 2% FBS and (b) 24 h in VascuLife VEGF with 2% FBS followed by 48 h in VascuLife with 10% FBS and respective macroscopic images of cell sheet detachment in PBS at 20 °C (c, d).

References

- 1 S. Heinen, S. Rackow, A. Schäfer and M. Weinhart, *Macromolecules*, 2017, **50**, 44-53.
- 2 D. D. Stöbener, M. Uckert, J. L. Cuellar Camacho, A. Hoppensack and M. Weinhart, *ACS Biomater. Sci. Eng.*, 2017, **3**, 2155-2165.
- 3 J. L. Hutter and J. Bechhoefer, *Rev. Sci. Instrum.*, 1993, **64**, 1868-1873.
- 4 H.-J. Butt and M. Jaschke, *Nanotechnology*, 1995, **6**, 1-7.

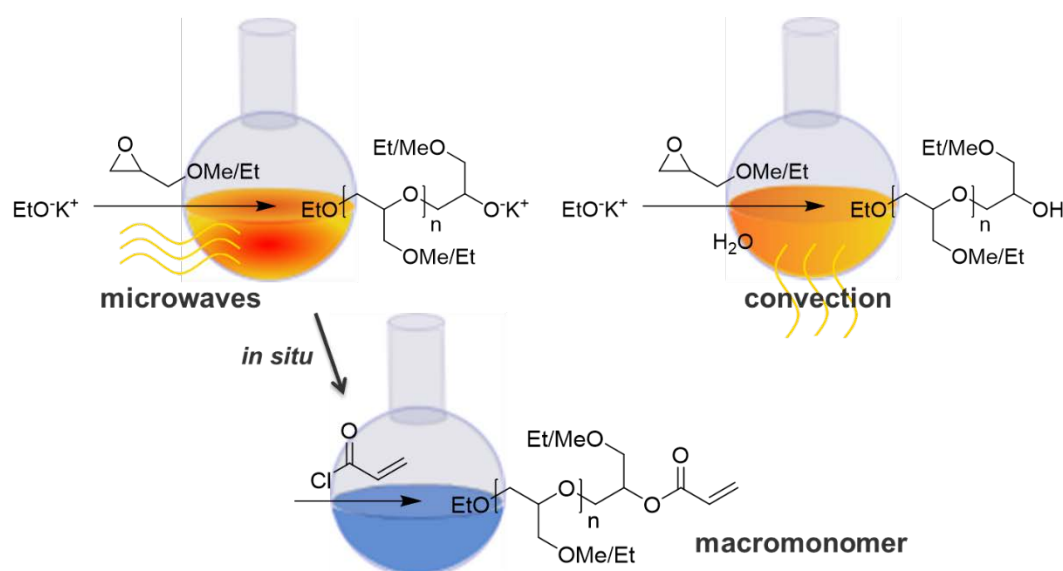
3 Publications and Manuscripts

- 5 Q. Yu, Y. Zhang, H. Chen, Z. Wu, H. Huang and C. Cheng, *Colloids Surf., B*, 2010, **76**, 468-474.
- 6 B. Du, O. K. C. Tsui, Q. Zhang and T. He, *Langmuir*, 2001, **17**, 3286-3291.
- 7 A. Ghorbal and A. B. Brahim, *Polym. Test.*, 2013, **32**, 1174-1180.
- 8 K. Bala, K. Ambwani and N. K. Gohil, *Tissue Cell*, 2011, **43**, 216-222.

3.3 Fast and Solvent-Free Microwave-Assisted Synthesis of Thermo-responsive Oligo(glycidyl ether)s

Daniel David Stöbener, Dorian Donath, Marie Weinhart*

The facile synthesis of OGEs in bulk using microwave heating is described. The reaction kinetics of the microwave-assisted oxy-anionic ROP are compared to the conventional oxy-anionic ROP and the thermo-responsive properties of OGEs in aqueous solution are investigated. Furthermore, *in situ* functionalization of OGEs to OGEA macromonomers, which have potential use as for surface functionalization via various “grafting from” methods, is presented.



This chapter was accepted for publication by the following journal:

"Reprinted with permission from

Daniel David Stöbener, Dorian Donath, Marie Weinhart, *Journal of Polymer Science, Part A: Polymer Chemistry*, **2018**, 56 (21), 2496-2504.

Copyright 2018 Wiley Periodicals, Inc."

Fast and Solvent-Free Microwave-Assisted Synthesis of Thermoresponsive Oligo(glycidyl ether)s

Daniel D. Stöbener¹, Dorian Donath¹, Marie Weinhart^{1}*

¹Institute of Chemistry and Biochemistry, Freie Universität Berlin, Takustr. 3, D-14195
Berlin, Germany.

*Corresponding author: e-mail marie.weinhart@fu-berlin.de, phone: +49 30 838 75050

ABSTRACT

Low molecular weight linear poly(glycidyl ether)s (PGEs) are typically synthesized via the “classical”, oxy-anionic ring-opening polymerization (ROP) of glycidyl ether monomers at elevated temperatures. To reduce reaction times, a fast process was developed to synthesize oligo(glycidyl ether)s (OGEs) in bulk at a gram scale utilizing microwave heating. Well-defined thermoresponsive copolymers comprising glycidyl methyl ether (GME) and ethyl glycidyl ether (EGE) with molecular weights of up to 3 kDa were synthesized via microwave-assisted ROP with reaction times of approximately 10 minutes. The fast reaction kinetics were attributed to the rapid and uniform heating and high temperatures reached during the reaction. Consequently, no significant microwave-specific acceleration of the oxy-anionic ROP was observed. The temperature-triggered phase transition of the OGEs in aqueous solution revealed cloud point temperatures (CPTs) that are highly dependent on the OGE molecular weight, concentration and comonomer composition, which extends previously reported data. Further, oligo(glycidyl ether) acrylates (OGEAs) with reactive, functional end-groups were directly accessible via *in situ* quenching of the anionic, microwave-assisted ROP with acrylic acid chloride (AAC). The obtained thermoresponsive OGEA macromonomers represent a promising material for the functionalization of surfaces via radical grafting methods to obtain functional, thermoresponsive coatings with potential application in cell culture.

KEYWORDS

Oxy-anionic ring-opening polymerization, cloud point temperature, lower critical solution temperature, thermoresponsive macromonomer

INTRODUCTION

Linear PGEs are typically synthesized via the oxy-anionic ROP of glycidyl ether monomers at elevated temperatures using alkali metal alcoholate initiators.¹⁻³ Via this method, several different protected and functional glycidyl ether monomers, such as *t*-butyl glycidyl ether⁴, ethoxy ethyl glycidyl ether^{2,4-6} or allyl glycidyl ether^{4,7,8}, have been successfully polymerized with molecular weights of up to 30 kDa⁵. The synthesis of thermoresponsive PGE homopolymers based on GME and EGE was first reported by Aoki et al. in 2002.⁹ The copolymerization of GME and EGE has recently been pursued in our group to prepare thermoresponsive monolayer coatings for cell culture applications.¹⁰⁻¹³ Side reactions during the classical oxy-anionic ROP of glycidyl ethers at elevated temperatures of 60 to 120 °C, however, limit the accessible molecular weight of PGEs.⁵ Over the past years, the monomer-activated anionic ROP applying triisobutyl aluminum as activator and tetraalkylammonium salts as initiator at lower temperature has rapidly gained in importance.¹⁴⁻¹⁶ Although the monomer-activated method usually leads to less side reactions, it is not the ideal choice when targeting oligomers due to large amounts of concomitantly formed tetraalkylammonium salts after quenching which are hard to separate from the product.^{17,18}

For the development of a simple, solvent-free method to prepare low molecular weight thermoresponsive PGEs using alcoholate initiators, microwave heating represents a promising tool as it has shown to be a fast alternative to conventional heating.^{19,20} During the past decades, microwave-assisted reactions have made their way in virtually all branches of polymer chemistry.²¹⁻²⁵ Compared to conventional heating, often encountered major benefits of microwave-assisted reactions in general are increased yields, higher selectivities, the reduction of side reactions and shortened reaction times, whereas the latter is a result of the rapid and macroscopically uniform heating characteristics present in microwave heating.^{21,22,25-28} Moreover, the up-scaling of microwave-assisted reactions using batch reactors (BR) and continuous flow reactors (CFR)^{29,30} has paved the way to increase the rather poor heating

efficiencies from 10% for small scale syntheses (5 mL) to 30% for large scale syntheses (400 mL).³¹ The CFR setup has also accounted for the limited penetration depth of microwaves, thus, overcoming the major challenge of bringing this technique closer to industrial applicability.^{21,22}

A special field of interest in the microwave-assisted synthesis of well-defined polymers has been controlled ionic ring-opening polymerizations (ROP). Schubert and co-workers first reported on the living cationic ROP of 2-ethyl-2-oxazoline in 2004.³² They investigated reaction rates of a series of 2-alkyl-2-oxazolines and 2-phenyl-2-oxazoline and synthesized polymers with molecular weights up to, or even exceeding, 10 kDa by generally maintaining PDIs below 1.2.³³⁻³⁵ In addition, they prepared statistical-, gradient-³⁶ as well as di-³⁷, tri-³⁸ and tetra-block-copolymers³⁹ and demonstrated the up-scaling of the reactions in BR and CFR.^{40,41} In 2008, Hoogenboom et al. further synthesized thermoresponsive copolymers by copolymerizing 2-ethyl-2-oxazoline and 2-n-propyl-2-oxazoline under microwave-irradiation to obtain copolymers with lower critical solution temperatures (LCSTs) in water ranging from 25 to 100 °C, which was tuned via the molecular weight, comonomer composition and the copolymer concentration.⁴²

Besides the crosslinking of epoxy-resins⁴³ and the step-growth polymerization of epoxide-amine adducts⁴⁴, there have been only a few studies investigating the anionic ROP of epoxides using microwave heating. For example, Trathnigg and co-workers polymerized propylene oxide (PO) using different alcohol starters and catalytic amounts of NaH to obtain amphiphilic polyoxamer-like diblock copolymers.^{45,46} They further synthesized di-, tri- and tetra-block cone-type copolymers using PO, butylene oxide and hexylene oxide as monomers, n-alcohols or poly(ethylene glycol) monomethyl ethers as starters and obtained polymers with molecular weights of up to 2 kDa.⁴⁷ Park and co-workers copolymerized phenyl glycidyl ether (PGE) with CO₂ using various Zn-based metal catalysts containing Co(III), Fe(II), Fe(III) or Ni(II) and obtained degradable poly(ether-carbonate). They synthesized low molecular weight polymers

of up to 2 kDa with PDIs between 1.4 and 2.1 as well as higher molecular weight polymers of 5 to 13 kDa with broader PDIs of 4 to 8.⁴⁸ In the pursuit of an efficient, solvent-free synthetic route to glycerol oligomers, Iaych et al. used the monomer glycerol carbonate, which forms polymerizable glycidol as an intermediate upon microwave irradiation. They obtained mixtures ranging from di- to hexamers with average molecular weights of 300-400 Da.⁴⁹ In another report, Möller and co-workers investigated the microwave-assisted polymerization of ethylene carbonate. They synthesized poly(EO-co-EC) (80:20) copolymers using 3-phenyl-1-propanol or triethylene glycol as initiators and 1,5,7-triazabicyclo[4.4.0]decene as catalyst. Thereby they obtained poly(EC)s with molecular weights of 2.2 to 3.1 kDa and PDIs between 1.6 and 1.8 which were independent of the monomer/initiator ($[M]/[I]$) ratio.⁵⁰ By copolymerizing EC with *tert*-butyl glycidyl ether (TBGE) using CsOH as initiator, they further synthesized carbonate-free poly(EO-co-TBGE) hydroxy telechelic copolymers with molecular weights of 0.7 to 1.7 kDa and PDIs between 1.05 and 1.10 which were also independent of the $[M]/[I]$ ratio due to the subsequent degradation of the carbonate groups.⁵¹ In a recent report, Ahmadi and Ullah used microwave heating to polymerize plant oil derived 1,2-epoxydecane using modified methyl aluminoxane (MMAO-12) and 2,4-pentanedione as catalyst system. After theoretically modelling optimal microwave reaction conditions, they obtained polyethers with molecular weights of up to 2,000 kDa with PDIs of 1.15 within 10 min, which exactly matched the molecular weight characteristics obtained by the conventional heating method.⁵²

In this work, we report the gram scale microwave-assisted synthesis of thermoresponsive OGEs. PGEs have shown to exhibit a phase transition temperature in aqueous solution which is dependent on their molecular weight, copolymer composition and polymer concentration.^{10,17} These polymers have also demonstrated to be suitable materials for functional, thermoresponsive surface coatings which have been applied in cell culture for the non-destructive, temperature-triggered recovery of confluent cell-sheets.¹⁰⁻¹³ Herein, we synthesized homo- and copolymers of GME and EGE using potassium *tert*-butoxide (*t*-BuOK) and

potassium ethoxide (EtOK) as initiators. The polymerizations were carried out in bulk using a multi-mode microwave reactor. The oligomers were characterized by NMR, GPC and MALDI-ToF and their thermoresponsive properties in aqueous solution were investigated by turbidity measurements and compared to the properties of corresponding oligomers/polymers accessible via the conventional oxy-anionic and monomer-activated anionic ROP. In addition, we used a single-mode microwave reactor to monitor the reaction temperature and pressure during the microwave-assisted polymerization and compared reaction kinetics to conventional heating under autoclave conditions. We further synthesized macromonomers by *in situ* acrylation of the oligo(GME-*co*-EGE) copolymers to obtain functional OGEAs which are promising materials for thermoresponsive surface coatings via various grafting-through and grafting-from methods.

EXPERIMENTAL

Materials

All chemicals and solvents were used without further purification unless stated otherwise. GME and EGE from TCI GmbH (Eschborn, Germany) was dried and distilled over CaH_2 and stored over 3 Å molecular sieve. *t*-BuOK (1.0 M in THF) and CaH_2 (93%) were purchased from Acros Organics (Geel, Belgium). EtOK (24 wt.-% in EtOH) and acrylic acid chloride (AAC, 98%) were supplied by Sigma-Aldrich (Steinheim, Germany). Sodium sulfate (Na_2SO_4 , 99%) and 3 Å molecular sieve were purchased from Carl Roth GmbH + Co. KG (Karlsruhe, Germany). Sodium bicarbonate (NaHCO_3 , 99.5%) was supplied by Grüssing GmbH Analytica (Filsum, Germany). Diethyl ether (Et_2O) from VWR Chemicals (Fontenay-sous-Bois, France or Leuven, Belgium) was distilled before use to remove the stabilizer (BHT).

Methods

Polymerizations were carried out in a “Plazmatronika” multi-mode microwave reactor (Warsaw, Poland) with a frequency of 2.45 GHz and a maximum power of 300 W. Monitoring of reaction conditions and kinetic studies were conducted using a single-mode “Initiator+ Robot Eight” microwave synthesizer from Biotage (Uppsala, Sweden), equipped with a noninvasive IR temperature sensor. High precision microwave reaction glass vials ($V = 2\text{-}5$ mL) from Biotage (Uppsala, Sweden) were used as reaction vessels for kinetic studies. Oligomers were centrifuged at 0 °C and 10000 rpm for 20 min using a Rotina 380 R centrifuge from Hettich GmbH & Co.KG (Tuttlingen, Germany). ^1H and ^{13}C NMR spectra were recorded on a Joel ECX at 400 MHz and 100 MHz, respectively, and processed with the software MestReNova (version 7.1.2). Chemical shifts were reported in δ (ppm) and referenced to the respective deuterated solvent peak (CDCl_3). Gel permeation chromatography (GPC) was conducted on an Agilent 1100 Series instrument in tetrahydrofuran (THF) as the eluent at concentrations of 3.5 mg mL^{-1} and a flow rate of 1 mL min^{-1} at 25 °C. Three PLgel mixed-C columns (Agilent,

Waldbronn, Germany) with dimensions of 7.5 x 300 mm and a particle size of 5 μm were used in-line with a refractive index (RI) detector. Calibration was performed with PS standards from PSS (Mainz, Germany) and calculation was performed with PSS Win-GPC software. MALDI-ToF measurements were conducted on an Ultraflex II TOF/TOF from Bruker (Billerica, MA, USA) in the positive ion mode using a linear pathway (LP). The samples were prepared via the dried-droplet method using α -cyano-4-hydroxycinnamic acid as matrix. Briefly, a polymer solution (2 mg mL⁻¹, 100 μL) was mixed with a saturated matrix solution (100 μL) and an acidic acetonitrile solution (20 μL , 33% acetonitrile / 0.1% trifluoroacetic acid in water). A 0.5 μL of the prepared mixture was transferred to a stainless-steel target and allowed to dry under ambient conditions. Spectra were recorded and analyzed using the flexControl (version 3.4) and flexAnalysis (version 3.3) software from Bruker, respectively. Turbidity measurements were performed on a Lambda 950 UV/Vis spectrometer at $\lambda = 500$ nm with a PTP 6 Peltier Temperature Programmer from Perkin Elmer (Waltham, MA, USA). Cloud point temperatures (CPTs) were determined in Milli-Q water at concentrations between 0.1 mg mL⁻¹ and 20 mg mL⁻¹, employing a heating rate of 0.5 $^{\circ}\text{C min}^{-1}$ with a data point recording every 0.2 $^{\circ}\text{C}$. The temperature-dependent transmittance of the aqueous polymer solutions was measured for three up- and down cycles per sample. The CPT was defined as the temperature at the inflection point of the normalized transmittance versus temperature curve.

General Synthetic Procedure

All polymers were synthesized according to the following procedure. A 50 mL Schlenk flask equipped with a magnetic stir bar and a rubber septum was flame-dried under vacuum and flushed with argon consecutively for at least three times. The flask was loaded with the initiator solution (*t*BuOK or EtOK) and followed by the removal of the solvent (THF or EtOH) by distillation. The remaining initiator salt was dried under high vacuum at 60-80 $^{\circ}\text{C}$ for 1-2 h. The Schlenk flask was placed in an ice or water bath (0 $^{\circ}\text{C}$ or 20 $^{\circ}\text{C}$) to dissolve the initiator in

the monomers (GME and/or EGE) for 15-120 min to yield a yellow to orange solution. The flask was placed in the microwave reactor and the solution was heated for at least one irradiation cycle under constant stirring. Each irradiation cycle consisted of three 1 min heating periods at a power of 50% each (150 W), followed by 2 min cooling periods at a power of 0% (0 W).

For the synthesis of OGEs, the reaction mixtures were quenched via the addition of water (Milli-Q, 1 mL) at room temperature and the mixtures were stirred for 1 h. Subsequently, the oligomers were dissolved in Et₂O (10-20 mL), dried over Na₂SO₄ and filtered. After storing the solutions in the fridge overnight, precipitated potassium salts were centrifuged off and the polymer solutions were decanted. The solvent was evaporated, and viscous, slightly yellow oils were obtained.

For the synthesis of OGEAs, the reaction mixtures were cooled to 0 °C in an ice bath and quenched by addition of AAC at 0 °C under stirring for 1 h. After adding Milli-Q water (1 mL) and further stirring at 20 °C for 1 h to hydrolyze excess AAC, the polymers were dissolved in Et₂O (20 mL). Generated salts and acrylic acid were extracted with aqueous, saturated NaHCO₃ for at least three times. The organic phase was collected, and the solvent was evaporated under reduced pressure while protecting the macromonomers from light to prevent polymerization. Slightly viscous, yellow oils were obtained.

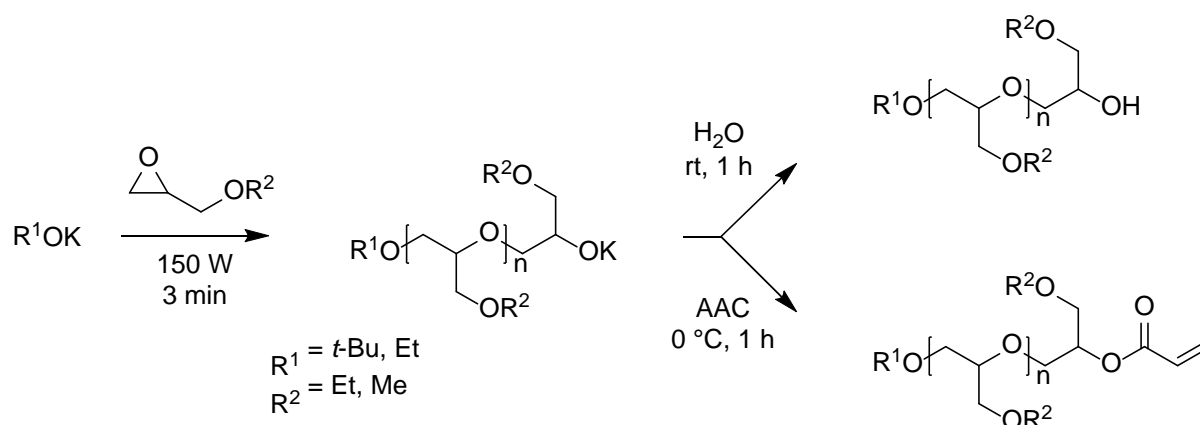
Experimental details and characterization of all synthesized oligomers are given in the Supporting Information (SI).

For kinetic studies, reaction mixtures were prepared as stated above and aliquots of 2.2 mL were transferred into sealed high precision microwave reaction glass vials ($V = 2\text{-}5$ mL), which were heated to 100 °C, subsequently dried under high vacuum at room temperature for at least 1 h and flushed with argon before use. Reaction vials were placed into a single-mode microwave reactor or preheated oil bath and polymerizations were carried out at 40 °C for 15, 30, 60 and 120 min. The oligomers were purified as described above, isolated yields were determined, and the products were characterized by NMR and GPC.

RESULTS AND DISCUSSION

General Approach for the Microwave-Assisted Synthesis of OGEs and OGEAs

Microwave-assisted polymerizations were carried out in bulk at gram scale (2-5 g) using a conventional multi-mode microwave reactor equipped with a magnetic stirrer. Essentially, potassium alcoholate initiators (*t*-BuOK or EtOK) were thoroughly dried in 50 mL Schlenk flasks, flushed with argon, and dissolved in the monomers GME and EGE whilst cooling. The mixtures were subsequently placed into the microwave reactor and irradiated under constant stirring by utilizing at least one heating/cooling cycle. The reactions were then quenched by either addition of water to obtain hydroxy-terminated OGEs or by *in situ* functionalization with AAC to obtain OGEAs (Scheme 1).



SCHEME 1 Microwave-assisted anionic ROP of oligo(glycidyl ether)s (OGEs) and oligo(glycidyl ether) acrylates (OGEAs).

Reactivity, Molecular Weight Control, and Scale-Up of OGE Homopolymers

To assess the reactivity of GME and EGE towards the microwave-assisted anionic ROP, we synthesized homopolymers with targeted molecular weights ($M_{n, \text{theor.}}$) of 1 kDa using *t*-BuOK as initiator, which readily dissolves in both monomers at low temperature (~15 min). Due to the risk of spontaneous polymerization during the dissolution process, the mixtures were cooled to 0 °C using an ice bath to rapidly dissipate the developing heat. Subsequently, the polymerizations were carried out in the microwave reactor applying one heating cycle. If no

distinct increase in viscosity was observed after one heating cycle, an additional heating cycle was applied. As confirmed by NMR spectroscopy and GPC measurements, GME and EGE homopolymers with average molecular weights of about 1.1 kDa and PDIs below 1.2 were obtained in quantitative yield (Table 1, polymers **1-2**). Furthermore, batch sizes could be increased from 2 to 5 g while maintaining polymer characteristics (Table 1, polymers **3-4**). The molecular weights and PDIs of OGEs **1-4** determined by GPC in THF relative to PS standards are in strong agreement with values calculated from MALDI-ToF and ^1H NMR spectra (Table S1). This leads to the conclusion, that PS standards in THF as eluent are an appropriate relative standard for the determination of the molecular weights of PGEs via GPC. In addition, according to Table 1, one heating cycle turned out to be sufficient when targeting OGEs with a molecular weight of 1 kDa.

TABLE 1 Oligo(glycidyl ether)s (OGEs) and oligo(glycidyl ether) acrylates (OGEAs) synthesized by the microwave-assisted anionic ROP of GME and EGE using potassium alcoholate initiators.

OGE / OGEA	batch size [g]	GME: EGE	Initiator	cycles ^a	yield [%]	conv. ^c [%]	$M_{n, theor.}$ [Da]	$M_{n, exp.}$ ^d [Da]	PDI ^d
1	2	1:0	<i>t</i> -BuOK	2	quant.	n.a.	1000	1160	1.16
2	2	0:1	<i>t</i> -BuOK	2	quant.	n.a.	1000	1090	1.15
3	5	1:0	<i>t</i> -BuOK	1	quant.	n.a.	1000	1150	1.18
4	5	0:1	<i>t</i> -BuOK	2	quant.	n.a.	1000	1140	1.16
5	5	1:1	EtOK	1	95	n.a.	1000	870	1.31
6	5	1:3	EtOK	1	98	n.a.	1000	940	1.29
7	5	1:5	EtOK	1	97	n.a.	1000	920	1.30
8	5	1:1	EtOK	1 ^b	95	n.a.	3000	3260	1.14
9	5	1:3	EtOK	3 ^b	93	n.a.	3000	2830	1.17

10	5	1:5	EtOK	2 ^b	95	n.a.	3000	2860	1.16
11	2	1:1	EtOK	1	93	87	1000	870	1.35
12	2	1:3	EtOK	1	89	91	1000	850	1.37
13	2	1:5	EtOK	1	90	72	1000	1110	1.27

^a number of heating/cooling cycles: 3 x (1 min heating + 2 min cooling); ^b modified heating cycle was applied 3 x (2 min heating + 2 min cooling); ^c conversion of end-group functionalization with AAC determined from ¹H NMR spectra and GPC data, n.a.= not applicable; ^d determined from GPC measurements in THF using polystyrene (PS) standards;

Characterization of the homopolymers **3** and **4** by MALDI-ToF mass spectrometry (Figure 1 a-d) revealed molecular weight characteristics in the same range as those determined by GPC measurements (Table S1). MALDI-ToF spectra displaying representative molecular weight distributions including magnifications which reveal all present series of peaks of both oligo(GME) (**3**) and oligo(EGE) (**4**) are displayed in Figure 1 a-b and c-d, respectively.

The main series of peaks in Figure 1 a-d correspond to the K⁺ and the lower intensity Na⁺ ionized oligomers initiated by *t*-BuOK (labeled as X) with repeating units of 88.1 Da (GME) and 102.1 Da (EGE), respectively. In addition, K⁺ and Na⁺ series of hydroxy-telechelic oligomers indicated with the initiator label Y are detectable, but with negligible intensity. These peaks correspond to oligomers initiated by competing residual water impurities. Further, common side reactions occurring during oxy-anionic polymerizations such as chain transfer reactions to the monomer resulting in allyl bond formation, which have been reported previously for the conventional oxy-anionic polymerization of glycidyl ethers⁵ as well as the microwave-assisted polymerization of alkyl oxides^{47,53} (e.g. PO), were neither observed in MALDI-ToF nor in NMR spectra. This might be attributed to the faster reaction kinetics of the microwave-assisted polymerization compared to polymerizations via the conventional oxy-anionic polymerization at elevated temperature as well as the sterically more hindered epoxide monomers GME and EGE, compared to low molecular weight alkyl oxides (e.g. PO).

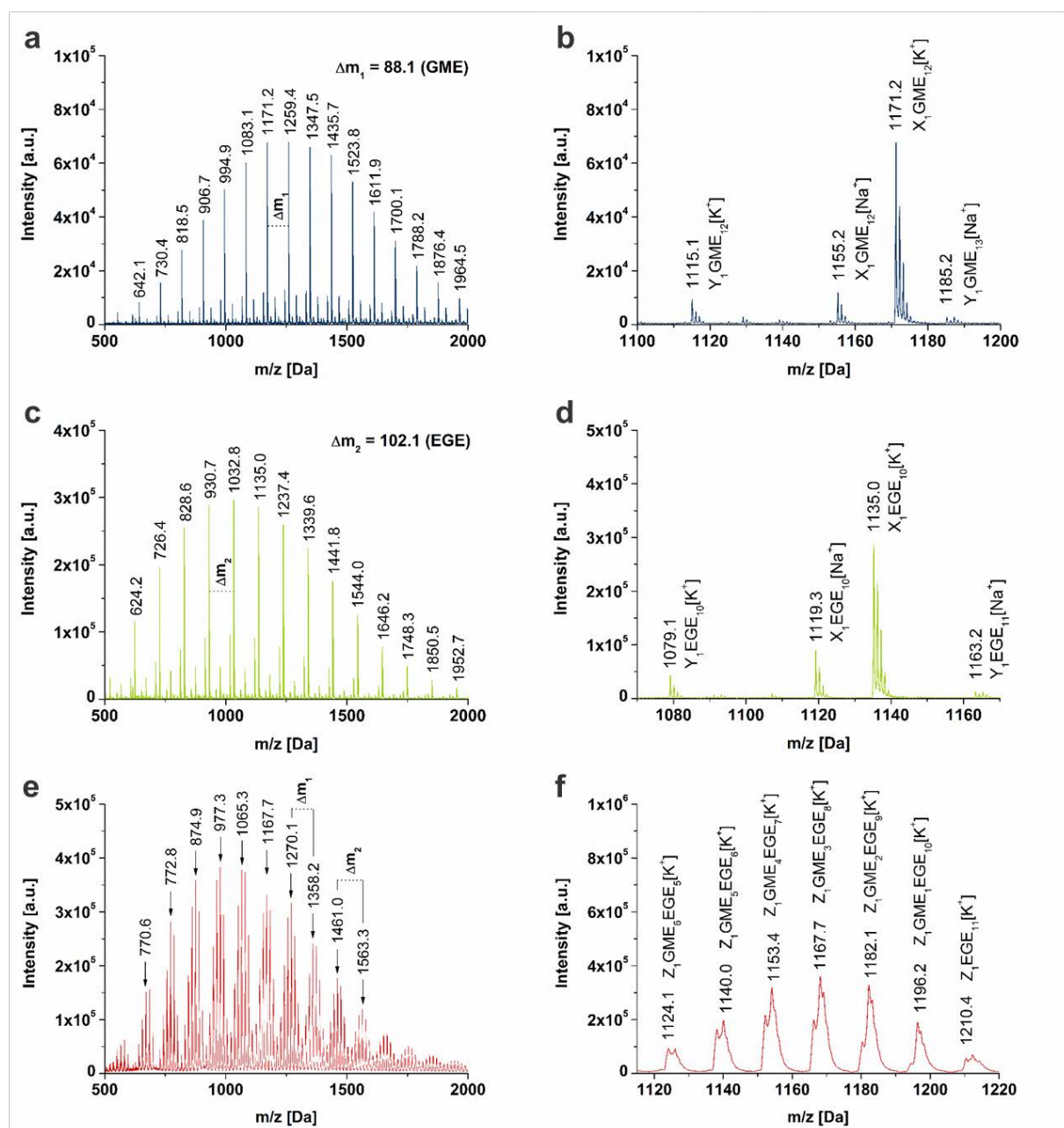


FIGURE 1 Representative MALDI-ToF spectra of GME homopolymer **3** (a-b), EGE homopolymer **4** (c-d) and GME/EGE (1:3) copolymer **6** (e-f). The polymer end-groups X, Y and Z, which represent the initiating species, equal *t*-BuOH, H₂O and EtOH. The lower molecular weight shoulder peaks of the indicated [K⁺] series in graph f correspond to the respective [Na⁺] series.

Synthesis and Molecular Weight Threshold of Thermoresponsive OGE Copolymers

To obtain thermoresponsive OGE copolymers, which have demonstrated to be useful for various biomedical applications, GME and EGE were copolymerized using different monomer ratios ranging from 1:1 to 1:5. Furthermore, EtOK was used as initiator to yield polymers with consistent methyl and ethyl side-groups. It is important to mention at this point that EtOK, which was applied as a solution in EtOH, needs to be dried more thoroughly than *t*-BuOK, which was derived from a solution in THF. It is necessary to fully remove residual EtOH, which can potentially quench and initiate the anionic ROP and hence, lower the molecular weight of the obtained OGEs. Moreover, EtOK is only moderately soluble in bulk GME and EGE mixtures, causing significantly longer dissolution times (~120 min) compared to *t*-BuOK. In addition, cooling of the reaction mixture in a water bath at room temperature was sufficient to dissipate the developing heat and to prevent premature polymerization, which is due to the comparably slow dissolution process of EtOK in the monomer mixture. After microwave heating, copolymers with GME/EGE ratios of 1:1, 1:3 and 1:5 as well as average molecular weights of about 900 Da with PDIs of around 1.3 were obtained (Table 1, polymers **5-7**). Representative ¹H and ¹³C NMR spectra of an OGE (polymer **6**) are shown in Figure S1. Compared to the polymerizations initiated with *t*-BuOK, the molecular weights obtained using EtOK as the initiator are slightly lower, whereas PDIs are higher. This might be caused by residual EtOH in the reaction mixture and an increased likelihood of contamination with traces of water, which can be attributed to the higher hydrophilicity of the EtOK initiator compared to *t*-BuOK and the concomitant longer dissolution periods before polymerization. Characterization of the copolymers via MALDI-ToF confirmed the results obtained from GPC measurements. Representatively, a MALDI-ToF spectrum of polymer **6** with a GME/EGE ratio of 1:3 is displayed in Figure 1 e-f. As illustrated, the differences between peaks can be assigned to both GME and EGE units and the peak series match with copolymers initiated by EtOK. In addition, each set of peaks can be assigned to copolymer species ionized by K⁺ (main peak) and

Na⁺ (shoulder peak) and comprise copolymers with different GME/EGE monomer compositions (Figure 1 f). The average molecular weight of the EtOK initiated OGE copolymers, synthesized in bulk under solvent-free conditions using microwave irradiation, was increased via the adjustment of the [M]/[I] ratio by simply lowering the amount of initiator, while keeping a constant batch size of 5 g. By increasing the heating periods during microwave heating cycles from 1 to 2 min, thermoresponsive copolymers with average molecular weights above 2.8 kDa ($M_{n,theor.} = 3$ kDa) and PDIs below 1.2 were obtained (Table 1, polymers **8-10**). This demonstrates the adjustability of the molecular weight via the [M]/[I] ratio and displays decreasing polymer PDIs with increasing molecular weight as expected for living anionic polymerizations. Attempts to further increase the molecular weight of OGEs to 5 kDa were not successful under the applied reaction conditions and lead to multimodal molecular weight distributions. Representative GPC traces of three copolymers with GME/EGE ratios of 1:3 and M_n of 1, 3 and 5 kDa are shown in Figure S3 in the supplementary information. Whereas OGEs with molecular weights of 1 and 3 kDa show monomodal molecular weight distributions (Figure S3, blue and green curves), the GPC trace of the 5 kDa OGE is more inhomogeneous and comprises both high and low molecular weight shoulders (Figure S3, red curve), which presumably originate from a gel effect. When higher molecular weight OGEs are targeted, the increased viscosity of the reaction mixture results in a decreased chain mobility, which can lead to local overheating and therewith, a rather uncontrolled growth of the polymer chains. As a result, both higher and lower OGE molecular weight fractions are formed, which correspond to the left and right shoulders in the corresponding GPC trace shown in Figure S3 (red curve).

Reaction Kinetics of the Microwave-Assisted vs. the Conventional Oxy-Anionic ROP

To assess the temperature profile during the microwave-assisted polymerization and to estimate the prevailing reaction kinetics, OGEs with a targeted molecular weight of 1 kDa and a GME:EGE ratio of 1:3 were synthesized on a 2 g scale using a single-mode microwave reactor

using EtOK as initiator. As illustrated in Figure S4, when utilizing an irradiation power of 150 W, the reaction temperature peaks at maxima between 140 and 180 °C after each heating period. This suggests the fast progression of the oligomerization under the applied reaction conditions. In addition, the steep increase in temperature during the first heating period ($t \sim 30$ s) as well as the maintained increase in reaction temperature at the beginning of each cooling period indicate the autoacceleration of the polymerization through the exothermic ROP. Due to the high reaction temperatures reached during the microwave-assisted polymerization, reproducible number average molecular weights of $M_n = 960 \pm 50$ ($n = 3$) and average polydispersities of $PDI = 1.28 \pm 0.04$ ($n = 3$) were obtained, which suggests that the reaction is drawn to completion well within one heating/cooling cycle.

To investigate whether the rapid completion of the microwave-assisted polymerization is solely due to the high temperatures reached or whether microwave-specific effects additionally accelerate the reaction, oligo(EGE) homopolymers with a targeted M_n of 2 kDa were synthesized on a 2 g scale in a single-mode microwave reactor as well as under autoclave conditions via conventional heating in an oil bath (PEG 400) using EtOK as initiator. Since autoacceleration was observed at temperatures above 40 °C for both microwave and conventional heating, all reactions were conducted at 40 °C and quenched after 15, 30, 60 and 120 min and immediately cooled down to 0 °C using an ice bath. As illustrated in Figure 2a, the isolated yields of both heating methods approach 95 % indicating that the polymerizations are complete between 60 to 120 min. However, the average yields obtained via the conventional oxy-anionic ROP are about 5-15% lower for analogous reaction times. A similar disparity is evident from M_n values which were determined by GPC and are plotted in Figure 2b. The slightly faster rate of the microwave-assisted reaction might suggest either a microwave-specific acceleration effect or a more efficient heating of the reaction mixture, as compared to the convectional heat transfer via the PEG oil bath. However, as it is displayed in Figure S5, the temperature in the microwave reaction vessel retains itself at 42-43 °C within the first 20-

25 min of the reaction and does not require additional power input. This is presumably caused by the exothermic ROP which self-sustains the energy input. In contrast, heat dissipation from the reaction vessel into the oil bath is likely to be more efficient and might keep the reaction temperature closer to 40 °C, leading to slightly slower reaction kinetics. In conclusion, we have reason to assume that microwave-specific effects are not likely to accelerate the polymerization of glycidyl ether monomers during the oxy-anionic ROP and that the acceleration can be attributed solely to thermal effects. In addition, PDIs slightly decrease as a function of reaction time (Figure 2b), which is typically observed during controlled chain growth reactions, and are well within a range of 1.1-1.3. The normalized GPC traces of the microwave-assisted as well as the conventional oxy-anionic ROP at the different reaction times are compared in Figure S6.

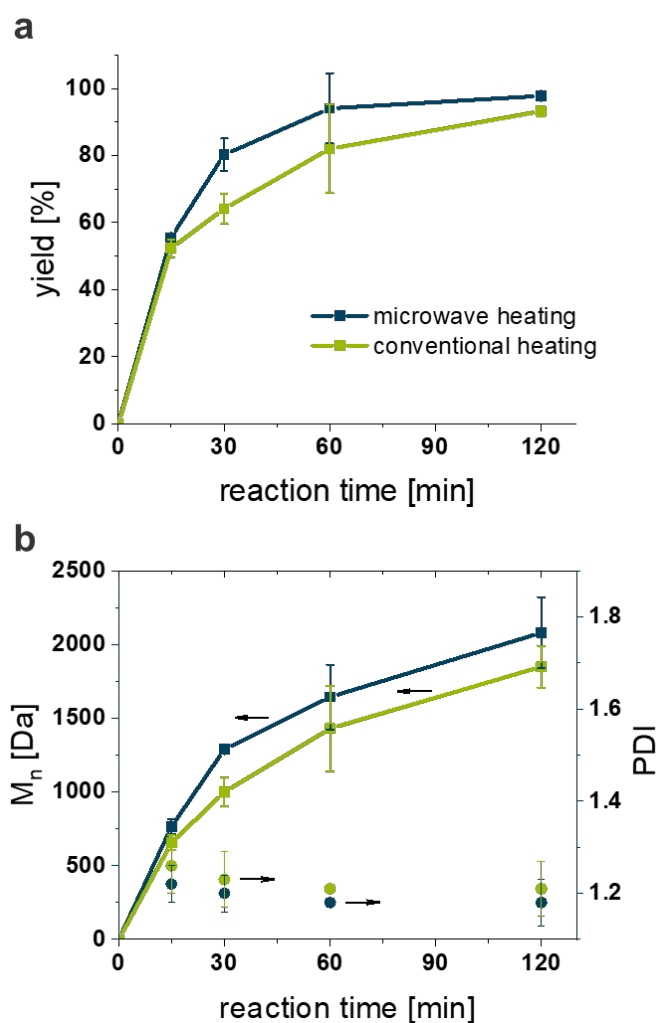


FIGURE 2 Isolated yield (a) and number average molecular weight M_n and PDI (b) determined by GPC in THF against PS standards as a function of reaction time for the microwave-assisted (blue) and conventional (green) oxy-anionic ROP of EGE at 40 °C. ($n = 2$, error bars indicate SD, data points are connected with lines to guide the eye)

Thermoresponsive Properties of OGEs in Aqueous Solution

For comparison of the thermoresponsive properties of the synthesized OGEs with higher molecular weight PGEs, we investigated their thermoresponsive properties in aqueous solution with respect to monomer composition, molecular weight and concentration. The concentration-dependent cloud point temperatures (CPTs) of 1 and 3 kDa oligomers **5-10** determined by UV-VIS transmittance measurements in Milli-Q water are displayed in Figure 3.

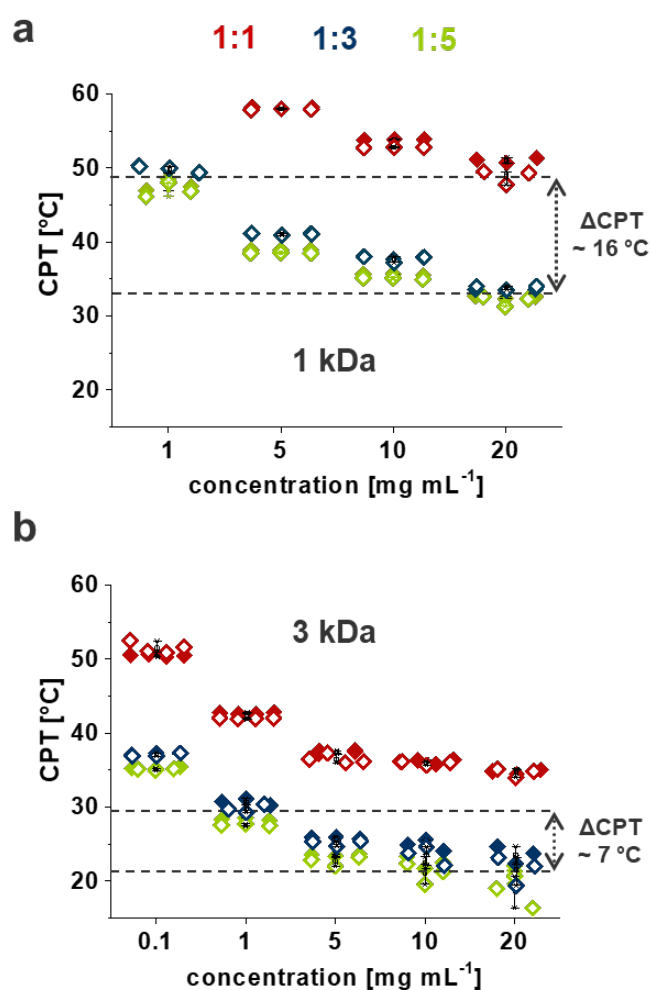


FIGURE 3 Concentration-dependent CPTs determined from turbidity measurements in Milli-Q water at $\lambda = 500$ nm. (a) CPTs of 1 kDa OGEs with GME/EGE ratios of 1:1 (polymer **5**, red diamonds), 1:3 (polymer **6**, blue diamonds), and 1:5 (polymer **7**, green diamonds). (b) CPTs of 3 kDa OGEs with GME/EGE ratios of 1:1 (polymer **8**, red diamonds), 1:3 (polymer **9**, blue diamonds), and 1:5 (polymer **10**, green diamonds). Hollow diamonds represent CPTs obtained from repeated heating cycle curves and color-filled diamonds represent CPTs determined from the respective cooling cycle curves. Black crosses indicate the mean values and whiskers the 90% confidence interval.

CPTs of OGEs are highly concentration-dependent and increase exponentially with decreasing OGE concentration from 20 to 1 or 0.1 mg mL⁻¹. This effect is more pronounced for lower molecular weight 1 kDa OGEs than for the 3 kDa OGEs which is in line with recent reports on higher molecular weight copolymers with a GME/EGE ratio of 1:3 (Figure S7a).¹⁷ Thus, CPTs determined from normalized cooling curves between concentrations of 1 and 20 mg mL⁻¹ span ranges of $\Delta\text{CPT} = 16$ and 15 °C for the 1 kDa polymers **6** (1:3) and **7** (1:5), respectively, whereas they are markedly lower with $\Delta\text{CPT} = 7$ °C for both 3 kDa polymers **9** (1:3) and **10** (1:5) in this concentration range. The observed exponential decrease of the CPT with increasing molecular weight can be attributed to the higher local polymer concentration at higher molecular weight and hence an increased probability for intermolecular, hydrophobically induced aggregation between polymers via chain entanglements.⁵⁴⁻⁵⁷

In agreement with our previous findings, also OGEs synthesized via microwave-assisted heating show a fully reversible phase transition with no significant hysteresis, a linear relationship between the CPT and the GME content within the copolymer (Figure S7b), and a sharpened phase transition with higher molecular weight and concentration (Figure S8). Thus, no difference in thermoresponsive properties was observed for copolymers synthesized via the conventional oxy-anionic or microwave-assisted synthesis.

Synthesis of OGEA Macromonomers via *in situ* Acrylation

Due to their use as surface coating materials for cell culture applications, we directly functionalized OGEs with a polymerizable acrylate end-group to obtain macromonomers which can be used for radical grafting methods on surfaces. We therefore used AAC to quench the microwave-assisted ROP *in situ* and directly obtained OGEAs (Scheme 1). The functionalization was performed at 0 °C in an ice bath by adding AAC to the polymer bulk under stirring. Although the mixing was not ideal due to the rather high viscosity of the polymers at 0 °C, we obtained degrees of end-group functionalization close to 90%, which was calculated from the integrals of the ¹H-NMR spectra considering the determined average molecular weights via GPC. Representative ¹H and ¹³C NMR spectra of an OGE (polymer **12**) are shown in Figure S2. Notably, the synthesized OGEAs with GME/EGE ratios between 1:1 and 1:5 revealed similar molecular weight distributions as their unfunctionalized OGE analogues (Table 1, polymers **11-13**). Preliminary experiments have already shown that the OGEA macromonomers can be covalently grafted onto flat substrates via a photopolymerization and the coated substrates are currently under evaluation.

CONCLUSIONS

A fast ROP of glycidyl ether monomers GME and EGE was performed in bulk at gram scale using a simple and straight-forward microwave-assisted polymerization. We used microwave heating to synthesize OGE homo- and copolymers with different comonomer compositions, well-defined molecular weights of up to 3 kDa and narrow molecular weight distributions. We further found that the rapid microwave-assisted ROP is mainly due to thermal effects and not likely to involve a microwave-specific acceleration. In aqueous solution, the polymers exhibit thermoresponsive behaviour with CPTs dependent on molecular weight, solution concentration and comonomer composition in agreement with previous results from polymers prepared via the conventional oxy-anionic and monomer-activated polymerization. In addition, *in situ*

quenching of OGEs with AAC directly yielded access to end-group-functionalized macromonomers which can be used for, e.g., the coating of surfaces via a grafting-from approach. Perspectively, the microwave-assisted synthesis of OGEAs allows for a convenient scale-up via a batch or continuous flow reaction setup and thus bears potential for industrial application.

ACKNOWLEDGEMENTS

M.W. is grateful to financial support from the Federal Ministry of Education and Research through grant FKZ: 13N13523. The authors thank Dr. Anke Hoppensack for proof reading this manuscript.

REFERENCES

1. C. Mangold, F. Wurm and H. Frey, *Polym. Chem.* **2012**, *3*, 1714.
2. A. Thomas, S. S. Müller and H. Frey, *Biomacromolecules* **2014**, *15*, 1935.
3. A.-L. Brocas, C. Mantzaridis, D. Tunc and S. Carlotti, *Prog. Polym. Sci.* **2013**, *38*, 845.
4. M. Erberich, H. Keul and M. Möller, *Macromolecules* **2007**, *40*, 3070.
5. M. Hans, H. Keul and M. Moeller, *Polymer* **2009**, *50*, 1103.
6. A. Dworak, I. Panchev, B. Trzebicka and W. Walach, *Macromol. Symp.* **2000**, *153*, 233.
7. B. F. Lee, M. J. Kade, J. A. Chute, N. Gupta, L. M. Campos, G. H. Fredrickson, E. J. Kramer, N. A. Lynd and C. J. Hawker, *J. Polym. Sci., Part A: Polym. Chem.* **2011**, *49*, 4498.
8. B. F. Lee, M. Wolffs, K. T. Delaney, J. K. Sprafke, F. A. Leibfarth, C. J. Hawker and N. A. Lynd, *Macromolecules* **2012**, *45*, 3722.
9. S. Aoki, A. Koide, S.-I. Imabayashi and M. Watanabe, *Chem. Lett.* **2002**, 1128.
10. T. Becherer, S. Heinen, Q. Wei, R. Haag and M. Weinhart, *Acta Biomater.* **2015**, *25*, 43.
11. S. Heinen, J. L. Cuéllar-Camacho and M. Weinhart, *Acta Biomater.* **2017**, *59*, 117.
12. S. Heinen, S. Rackow, J. L. Cuellar-Camacho, I. S. Donskyi, W. E. S. Unger and M. Weinhart, *J. Mater. Chem. B* **2018**, *6*, 1489.
13. D. D. Stöbener, M. Uckert, J. L. Cuellar Camacho, A. Hoppensack and M. Weinhart, *ACS Biomater. Sci. Eng.* **2017**, *3*, 2155.
14. M. Gervais, A.-L. Brocas, G. Cendejas, A. Deffieux and S. Carlotti, *Macromolecules* **2010**, *43*, 1778.
15. A. Labbé, S. Carlotti, A. Deffieux and A. Hirao, *Macromol. Symp.* **2007**, *249-250*, 392.
16. J. Meyer, H. Keul and M. Möller, *Macromolecules* **2011**, *44*, 4082.
17. S. Heinen, S. Rackow, A. Schäfer and M. Weinhart, *Macromolecules* **2017**, *50*, 44.
18. J. Herzberger, D. Leibig, J. C. Liermann and H. Frey, *ACS Macro Lett.* **2016**, *5*, 1206.
19. F. Wiesbrock, R. Hoogenboom and U. S. Schubert, *Macromol. Rapid Commun.* **2004**, *25*, 1739.
20. R. Hoogenboom and U. S. Schubert, *Macromol. Rapid Commun.* **2007**, *28*, 368.
21. C. Ebner, T. Bodner, F. Stelzer and F. Wiesbrock, *Macromol. Rapid Commun.* **2011**, *32*, 254.
22. K. Kempe, C. R. Becer and U. S. Schubert, *Macromolecules* **2011**, *44*, 5825.
23. M. Bardts, N. Gonsior and H. Ritter, *Macromol. Chem. Phys.* **2008**, *209*, 25.
24. S. Sinnwell and H. Ritter, *Aust. J. Chem.* **2007**, *60*, 729.

25. A. Sosnik, G. Gotellia and G. A. Abraham, *Prog. Polym. Sci.* **2011**, *36*, 1050.
26. G. B. Dudley, R. Richert and A. E. Stiegman, *Chem. Sci.* **2015**, *6*, 2144.
27. A. de la Hoz, Á. Díaz-Ortiz and A. Moreno, *Chem. Soc. Rev.* **2005**, *34*, 164.
28. J. Jacob, L. H. L. Chia and F. Y. C. Boey, *J. Mater. Sci.* **1995**, *30*, 5321.
29. T. N. Glasnov and C. O. Kappe, *Chem. Eur. J.* **2011**, *17*, 11956.
30. T. N. Glasnov and C. O. Kappe, *Macromol. Rapid Commun.* **2007**, *28*, 395.
31. R. Hoogenboom, T. F. A. Wilms, T. Erdmenger and U. S. Schubert, *Aust. J. Chem.* **2009**, *62*, 236.
32. F. Wiesbrock, R. Hoogenboom, C. H. Abeln and U. S. Schubert, *Macromol. Rapid Commun.* **2004**, *25*, 1895.
33. F. Wiesbrock, R. Hoogenboom, M. A. M. Leenen, M. A. R. Meier, C. H. Abeln and U. S. Schubert, *Macromolecules* **2005**, *38*, 5025.
34. R. Hoogenboom, M. W. M. Fijten, H. M. L. Thijs, B. M. van Lankvelt and U. S. Schubert, *Des. Monomers Polym.* **2005**, *8*, 659.
35. M. Grube, M. N. Leiske, U. S. Schubert and I. Nischang, *Macromolecules* **2018**, *51*, 1905.
36. M. Lobert, R. Hoogenboom, C.-A. Fustin, J.-F. Gohy and U. S. Schubert, *J. Polym. Sci., Part A: Polym. Chem.* **2008**, *46*, 5859.
37. R. Hoogenboom, H. M. L. Thijs, M. W. M. Fijten, B. M. van Lankvelt and U. S. Schubert, *J. Polym. Sci., Part A: Polym. Chem.* **2007**, *45*, 416.
38. R. Hoogenboom, F. Wiesbrock, H. Huang, M. A. M. Leenen, H. M. L. Thijs, S. F. G. M. van Nispen, M. van der Loop, C.-A. Fustin, A. M. Jonas, J.-F. Gohy and U. S. Schubert, *Macromolecules* **2006**, *39*, 4719.
39. R. Hoogenboom, F. Wiesbrock, M. A. M. Leenen, H. M. L. Thijs, H. Huang, C.-A. Fustin, P. Guillet, J.-F. Gohy and U. S. Schubert, *Macromolecules* **2007**, *40*, 2837.
40. R. Hoogenboom, R. M. Paulus, A. Pilotti and U. S. Schubert, *Macromol. Rapid Commun.* **2006**, *27*, 1556.
41. M. Paulus, T. Erdmenger, C. R. Becer, R. Hoogenboom and R. S. Schubert, *Macromol. Rapid Commun.* **2007**, *28*, 484.
42. R. Hoogenboom, H. M. L. Thijs, M. J. H. C. Jochems, B. M. van Lankvelt, M. W. M. Fijtenab and U. S. Schubert, *Chem. Commun.* **2008**, *44*, 5758.
43. J. Canadell, A. Mantecón and V. Cádiz, *Macromol. Chem. Phys.* **2007**, *208*, 2018.
44. J. Theis, H. Ritter and J. E. Klee, *Macromol. Rapid Commun.* **2009**, *30*, 1424.
45. M. I. Malik, B. Trathnigg and C. O. Kappe, *Macromol. Chem. Phys.* **2007**, *208*, 2510.
46. M. I. Malik, B. Trathnigg and C. O. Kappe, *Eur. Polym. J.* **2008**, *44*, 144.
47. M. I. Malik, B. Trathnigg and C. O. Kappe, *Eur. Polym. J.* **2009**, *45*, 899.
48. M. M. Dharman, J.-Y. Ahn, M.-K. Lee, H.-L. Shim, K.-H. Kim, I. Kim and D. W. Park, *Res. Chem. Intermed.* **2008**, *34*, 835.
49. I. Kamal, D. Stéphane, F. Emmanuel, G. Christine, L. Alain and G. Philippe, *J. Appl. Polym. Sci.* **2011**, *120*, 2354.
50. G. Kapiti, H. Keul and M. Möller, *Mater. Today Commun.* **2015**, *5*, 1.
51. G. Kapiti, H. Keul and M. Möller, *Polym. Chem.* **2016**, *7*, 5050.
52. R. Ahmadi and A. Ullah, *RSC Advances* **2017**, *7*, 27946.
53. M. I. Malik, M. Irfan, A. Khan, S. Rahim, R. Abdul-Karim and J. Hashim, *J. Polym. Res.* **2016**, *23*, 258.
54. F. Afroze, E. Nies and H. Berghmans, *J. Mol. Struct.* **2000**, *554*, 55.
55. R. Pamies, K. Zhu, A.-L. Kjøniksen and B. Nyström, *Polym. Bull.* **2009**, *62*, 487.
56. A. Dworak, B. Trzebicka, A. Kowalczyk, C. Tsvetanov and S. Rangelov, *Polimery* **2014**, *59*, 88.
57. S. S. Müller, C. Moers and H. Frey, *Macromolecules* **2014**, *47*, 5492.

**Supporting Information (SI) for the Following Manuscript Submitted to the
Journal of Polymer Science, Part A: Polymer Chemistry**

Fast and Solvent-Free Microwave-Assisted Synthesis of Thermoresponsive Oligo(glycidyl ether)s

Daniel D. Stöbener¹, Dorian Donath¹, Marie Weinhart^{1}*

¹Institute of Chemistry and Biochemistry, Freie Universitaet Berlin, Takustr. 3, D-14195
Berlin, Germany.

*Corresponding author: e-mail marie.weinhart@fu-berlin.de, phone: +49 30 838 75050

KEYWORDS

Oxy-anionic ring-opening polymerization, cloud point temperature, lower critical solution
temperature, thermoresponsive macromonomer

Experimental Details and Characterization of the Synthesized OGE(A)s

Polymer **1** (Homo-GME, end groups: *t*-BuO/OH). *t*-BuOK (2.0 mL, 2.0 mmol), GME (2.0 mL, 22.7 mmol). Yield: 2.10 g (100%). ¹H-NMR (400 MHz; CDCl₃): δ 3.91 (s, 1 H, CHOH); 3.61-3.43 (m, 57 H, polymer backbone); 3.32 (s, 30 H, OCH₃); 1.15 (s, 9 H, OC(CH₃)₃) ppm. ¹³C-NMR (101 MHz; CDCl₃): δ 79.2-78.7 (CH₂CH(CH₂OCH₃)O); 73.8-72.8 (OC(CH₃)₃ + CHCH₂OCH₃); 70.0-69.6 (CH₂CH(CH₂OCH₃)O + CH₂CH(CH₂OCH₃)OH); 61.6 (CH₂OC(CH₃)₃); 59.3 (OCH₃); 27.6 (OC(CH₃)₃) ppm.

Polymer **2** (Homo-EGE, end groups: *t*-BuO/OH). *t*-BuOK (2.0 mL, 2.0 mmol), EGE (2.1 mL, 20.0 mmol). Yield: 2.08 g (100%). ¹H-NMR (400 MHz; CDCl₃): δ 3.91 (s, 1 H, CHOH); 3.63-3.39 (m, 54 H, polymer backbone + OCH₂CH₃); 1.19-1.14 (m, 27 H, OCH₂CH₃ + OC(CH₃)₃) ppm. ¹³C-NMR (101 MHz; CDCl₃): δ 79.2-78.7 (CH₂CH(CH₂OCH₃)O); 72.9-69.6 (OC(CH₃)₃ + CHCH₂OCH₂CH₃ + CH₂CH(CH₂OCH₂CH₃)O + CH₂CH(CH₂OCH₃)OH); 66.9-66.7 (OCH₂CH₃); 61.7 (CH₂OC(CH₃)₃); 27.5 (OC(CH₃)₃); 15.3 (OCH₂CH₃) ppm.

Polymer **3** (Homo-GME, end groups: *t*-BuO/OH). *t*-BuOK (5.0 mL, 5.0 mmol), GME (5.1 mL, 56.7 mmol). Yield: 5.17 g (100%). ¹H-NMR (400 MHz; CDCl₃): δ 3.91 (s, 1 H, CHOH); 3.61-3.43 (m, 53 H, polymer backbone); 3.32 (s, 29 H, OCH₃); 1.15 (s, 9 H, OC(CH₃)₃) ppm. ¹³C-NMR (101 MHz; CDCl₃): δ 79.2-78.7 (CH₂CH(CH₂OCH₃)O); 73.8-72.8 (OC(CH₃)₃ + CHCH₂OCH₃); 70.0-69.6 (CH₂CH(CH₂OCH₃)O + CH₂CH(CH₂OCH₃)OH); 61.6 (CH₂OC(CH₃)₃); 59.3 (OCH₃); 27.6 (OC(CH₃)₃) ppm.

Polymer **4** (Homo-EGE, end groups: *t*-BuO/OH). *t*-BuOK (5.0 mL, 5.0 mmol), EGE (5.3 mL, 49.0 mmol). Yield: 5.20 g (100%). ¹H-NMR (400 MHz; CDCl₃): δ 3.91 (s, 1 H, CHOH); 3.63-3.39 (m, 51 H, polymer backbone + OCH₂CH₃); 1.19-1.14 (m, 25 H, OCH₂CH₃ + OC(CH₃)₃) ppm. ¹³C-NMR (101 MHz; CDCl₃): δ 79.2-78.7 (CH₂CH(CH₂OCH₃)O); 72.9-69.6 (OC(CH₃)₃ + CHCH₂OCH₂CH₃ + CH₂CH(CH₂OCH₂CH₃)O + CH₂CH(CH₂OCH₃)OH); 66.9-66.7 (OCH₂CH₃); 61.7 (CH₂OC(CH₃)₃); 27.5 (OC(CH₃)₃); 15.3 (OCH₂CH₃) ppm.

3 Publications and Manuscripts

Polymer **5** (GME:EGE = 1:1, end groups: EtO/OH). EtOK (2.0 mL, 5.0 mmol), GME (2.4 mL, 26.3 mmol), EGE (2.9 mL, 26.3 mmol). Yield: 4.75 g (95%). $^1\text{H-NMR}$ (400 MHz; CDCl_3): δ 3.91 (s, 1 H, CHOH); 3.76-3.38 (m, 46 H, polymer backbone + OCH_2CH_3); 3.32 (s, 11 H, OCH_3); 1.18-1.14 (m, 12 H, OCH_2CH_3) ppm. $^{13}\text{C-NMR}$ (101 MHz; CDCl_3): δ 78.9-78.6 ($\text{CH}_2\text{CH}(\text{CH}_2\text{OR})\text{O}$); 72.9-72.6 ($\text{CH}(\text{CH}_2\text{OCH}_3)$); 71.7-71.6 ($\text{CH}_2\text{CH}(\text{CH}_2\text{OR})\text{OH}$); 71.0-69.7 ($\text{CH}_2\text{CH}(\text{CH}_2\text{OR})\text{O} + \text{CH}_3\text{CH}_2\text{OCH}_2\text{CH}(\text{CH}_2\text{OR})\text{O} + \text{CH}_2\text{CH}(\text{CH}_2\text{OR})\text{OH}$); 66.9-66.8 (OCH_2CH_3); 59.3 (OCH_3); 15.3 (OCH_2CH_3) ppm.

Polymer **6** (GME:EGE = 1:3, end groups: EtO/OH). EtOK (2.0 mL, 5.0 mmol), GME (1.1 mL, 12.7 mmol), EGE (4.1 mL, 38.0 mmol). Yield: 4.91 g (98%). $^1\text{H-NMR}$ (400 MHz; CDCl_3): δ 3.90 (s, 1 H, CHOH); 3.76-3.42 (m, 58 H, polymer backbone + OCH_2CH_3); 3.32 (s, 7 H, OCH_3); 1.19-1.14 (m, 20 H, OCH_2CH_3) ppm. $^{13}\text{C-NMR}$ (101 MHz; CDCl_3): δ 79.6-78.9 ($\text{CH}_2\text{CH}(\text{CH}_2\text{OR})\text{O}$); 73.0-72.8 ($\text{CH}(\text{CH}_2\text{OCH}_3)$); 71.7-71.6 ($\text{CH}_2\text{CH}(\text{CH}_2\text{OR})\text{OH}$); 71.0-69.6 ($\text{CH}_2\text{CH}(\text{CH}_2\text{OR})\text{O} + \text{CH}_3\text{CH}_2\text{OCH}_2\text{CH}(\text{CH}_2\text{OR})\text{O} + \text{CH}_2\text{CH}(\text{CH}_2\text{OR})\text{OH}$); 66.8 (OCH_2CH_3); 59.3 (OCH_3); 15.3 (OCH_2CH_3) ppm.

Polymer **7** (GME:EGE = 1:5, end groups: EtO/OH). EtOK (2.0 mL, 5.0 mmol), GME (0.8 mL, 8.4 mmol), EGE (4.5 mL, 41.8 mmol). Yield: 4.84 g (97%). $^1\text{H-NMR}$ (400 MHz; CDCl_3): δ 3.90 (s, 1 H, CHOH); 3.75-3.42 (m, 62 H, polymer backbone + OCH_2CH_3); 3.32 (s, 5 H, OCH_3); 1.19-1.14 (m, 23 H, OCH_2CH_3) ppm. $^{13}\text{C-NMR}$ (101 MHz; CDCl_3): δ 79.6-78.9 ($\text{CH}_2\text{CH}(\text{CH}_2\text{OR})\text{O}$); 73.0-72.5 ($\text{CH}(\text{CH}_2\text{OCH}_3)$); 71.7-71.6 ($\text{CH}_2\text{CH}(\text{CH}_2\text{OR})\text{OH}$); 71.0-69.7 ($\text{CH}_2\text{CH}(\text{CH}_2\text{OR})\text{O} + \text{CH}_3\text{CH}_2\text{OCH}_2\text{CH}(\text{CH}_2\text{OR})\text{O} + \text{CH}_2\text{CH}(\text{CH}_2\text{OR})\text{OH}$); 66.8 (OCH_2CH_3); 59.3 (OCH_3); 15.3 (OCH_2CH_3) ppm.

Polymer **8** (GME:EGE = 1:1, end groups: EtO/OH). EtOK (0.7 mL, 1.7 mmol), GME (2.4 mL, 26.3 mmol), EGE (2.9 mL, 26.3 mmol), Yield: 4.77 g (95%). $^1\text{H-NMR}$ (400 MHz; CDCl_3): δ 3.91 (s, 1 H, CHOH); 3.76-3.38 (m, 46 H, polymer backbone + OCH_2CH_3); 3.32 (s, 11 H, OCH_3); 1.18-1.14 (m, 12 H, OCH_2CH_3) ppm. $^{13}\text{C-NMR}$ (101 MHz; CDCl_3): δ 78.9-78.6

(CH₂CH(CH₂OR)O); 72.9-72.6 (CH(CH₂OCH₃); 71.7-71.6 (CH₂CH(CH₂OR)OH); 71.0-69.7 (CH₂CH(CH₂OR)O + CH₃CH₂OCH₂CH(CH₂OR)O + CH₂CH(CH₂OR)OH); 66.9-66.8 (OCH₂CH₃); 59.3 (OCH₃); 15.3 (OCH₂CH₃) ppm.

Polymer **9** (GME:EGE = 1:3, end groups: EtO/OH). EtOK (0.7 mL, 1.7 mmol), GME (1.1 mL, 12.7 mmol), EGE (4.1 mL, 38.0 mmol). Yield: 4.65 g (93%). ¹H-NMR (400 MHz; CDCl₃): δ 3.90 (s, 1 H, CHOH); 3.73-3.42 (m, 110 H, polymer backbone + OCH₂CH₃); 3.33 (s, 13 H, OCH₃); 1.19-1.14 (m, 36 H, OCH₂CH₃) ppm. ¹³C-NMR (101 MHz; CDCl₃): δ 78.9-78.8 (CH₂CH(CH₂OR)O); 72.8 (CH(CH₂OCH₃); 71.7-71.6 (CH₂CH(CH₂OR)OH); 71.0-69.7 (CH₂CH(CH₂OR)O + CH₃CH₂OCH₂CH(CH₂OR)O + CH₂CH(CH₂OR)OH); 66.8 (OCH₂CH₃); 59.3 (OCH₃); 15.3 (OCH₂CH₃) ppm.

Polymer **10** (GME:EGE = 1:5, end groups: EtO/OH). EtOK (0.7 mL, 1.7 mmol), GME (0.8 mL, 8.4 mmol), EGE (4.5 mL, 41.8 mmol). Yield: 4.76 g (95%). ¹H-NMR (400 MHz; CDCl₃): δ 3.90 (s, 1 H, CHOH); 3.73-3.42 (m, 130 H, polymer backbone + OCH₂CH₃); 3.32 (s, 11 H, OCH₃); 1.19-1.14 (m, 46 H, OCH₂CH₃) ppm. ¹³C-NMR (101 MHz; CDCl₃): δ 78.9-78.8 (CH₂CH(CH₂OR)O); 72.8 (CH(CH₂OCH₃); 71.6 (CH₂CH(CH₂OR)OH); 71.0-69.7 (CH₂CH(CH₂OR)O + CH₃CH₂OCH₂CH(CH₂OR)O + CH₂CH(CH₂OR)OH); 66.8 (OCH₂CH₃); 59.3 (OCH₃); 15.3 (OCH₂CH₃) ppm.

Polymer **11** (GME:EGE = 1:1, end groups: EtO/OC(O)CHCH₂). EtOK (0.8 mL, 2.0 mmol), GME (0.9 mL, 10.5 mmol), EGE (1.1 mL, 10.5 mmol), AAC (0.2 mL, 3.0 mmol). Yield: 1.86 g (93%). ¹H-NMR (400 MHz; CDCl₃): δ 6.38 (dd, 1 H, OC(O)CHCH₂); 6.11 (dd, 1 H, OC(O)CHCH₂); 5.79 (dd, 1 H, OC(O)CHCH₂); 5.13 (m, 1 H, CHROC(O)CHCH₂); 3.76-3.38 (m, 46 H, polymer backbone + OCH₂CH₃); 3.32 (s, 11 H, OCH₃); 1.18-1.14 (m, 12 H, OCH₂CH₃) ppm. ¹³C-NMR (101 MHz; CDCl₃): δ 165.7 (OC(O)CHCH₂); 130.9 (OC(O)CHCH₂); 128.7 (OC(O)CHCH₂); 78.9-78.6 (CH₂CH(CH₂OR)O + CH₂CH(CH₂OR)OC(O)CHCH₂); 73.9-73.8 (CH(CH₂OR)OH); 72.9-72.6 (CH(CH₂OCH₃);

3 Publications and Manuscripts

71.7-71.6 ($\underline{\text{C}}\text{H}_2\text{CH}(\text{CH}_2\text{OR})\text{OH}$); 71.0-69.7 ($\underline{\text{C}}\text{H}_2\text{CH}(\text{CH}_2\text{OR})\text{O}$ + $\text{CH}_3\text{CH}_2\text{O}\underline{\text{C}}\text{H}_2\text{CH}(\text{CH}_2\text{OR})\text{O}$ + $\text{CH}_2\underline{\text{C}}\text{H}(\text{CH}_2\text{OR})\text{OH}$); 66.9-66.8 ($\text{O}\underline{\text{C}}\text{H}_2\text{CH}_3$); 59.3 ($\text{O}\underline{\text{C}}\text{H}_3$); 15.3 ($\text{OCH}_2\underline{\text{C}}\text{H}_3$) ppm.

Polymer **12** (GME:EGE = 1:3, end groups: EtO/OC(O)CHCH₂). EtOK (0.8 mL, 2.0 mmol), GME (0.5 mL, 5.3 mmol), EGE (1.7 mL, 15.8 mmol), AAC (0.2 mL, 3.0 mmol). Yield: 1.78 g (89%). ¹H-NMR (400 MHz; CDCl₃): δ 6.40 (dd, 1 H, OC(O)CHCH₂); 6.13 (dd, 1 H, OC(O)CHCH₂); 5.80 (dd, 1 H, OC(O)CHCH₂); 5.15 (m, 1 H, CHROC(O)CHCH₂); 3.76-3.38 (m, 74 H, polymer backbone + OCH₂CH₃); 3.32 (s, 8 H, OCH₃); 1.18-1.14 (m, 26 H, OCH₂CH₃) ppm. ¹³C-NMR (101 MHz; CDCl₃): δ 165.7 (OC(O)CHCH₂); 130.9 (OC(O)CHCH₂); 128.7 (OC(O)CHCH₂); 78.9-78.6 (CH₂CH(CH₂OR)O + CH₂CH(CH₂OR)OC(O)CHCH₂); 73.9-73.8 (CH(CH₂OR)OH); 72.9-72.6 (CH(CH₂OCH₃); 71.7-71.6 (CH₂CH(CH₂OR)OH); 71.0-69.7 (CH₂CH(CH₂OR)O + CH₃CH₂OCH₂CH(CH₂OR)O + CH₂CH(CH₂OR)OH); 66.9-66.8 (OCH₂CH₃); 59.3 (OCH₃); 15.3 (OCH₂CH₃) ppm.

Polymer **13** (GME:EGE = 1:5, end groups: EtO/OC(O)CHCH₂). EtOK (0.8 mL, 2.0 mmol), GME (0.3 mL, 3.5 mmol), EGE (1.8 mL, 17.5 mmol), AAC (0.2 mL, 3.0 mmol). Yield: 1.81 g (90%). ¹H-NMR (400 MHz; CDCl₃): δ 6.40 (dd, 1 H, OC(O)CHCH₂); 6.12 (dd, 1 H, OC(O)CHCH₂); 5.80 (dd, 1 H, OC(O)CHCH₂); 5.15 (m, 1 H, CHROC(O)CHCH₂); 3.76-3.38 (m, 65 H, polymer backbone + OCH₂CH₃); 3.32 (s, 5 H, OCH₃); 1.18-1.14 (m, 24 H, OCH₂CH₃) ppm. ¹³C-NMR (101 MHz; CDCl₃): δ 165.7 (OC(O)CHCH₂); 130.9 (OC(O)CHCH₂); 128.7 (OC(O)CHCH₂); 78.9-78.6 (CH₂CH(CH₂OR)O + CH₂CH(CH₂OR)OC(O)CHCH₂); 73.9-73.8 (CH(CH₂OR)OH); 72.9-72.6 (CH(CH₂OCH₃); 71.7-71.6 (CH₂CH(CH₂OR)OH); 71.0-69.7 (CH₂CH(CH₂OR)O + CH₃CH₂OCH₂CH(CH₂OR)O + CH₂CH(CH₂OR)OH); 66.9-66.8 (OCH₂CH₃); 59.3 (OCH₃); 15.3 (OCH₂CH₃) ppm.

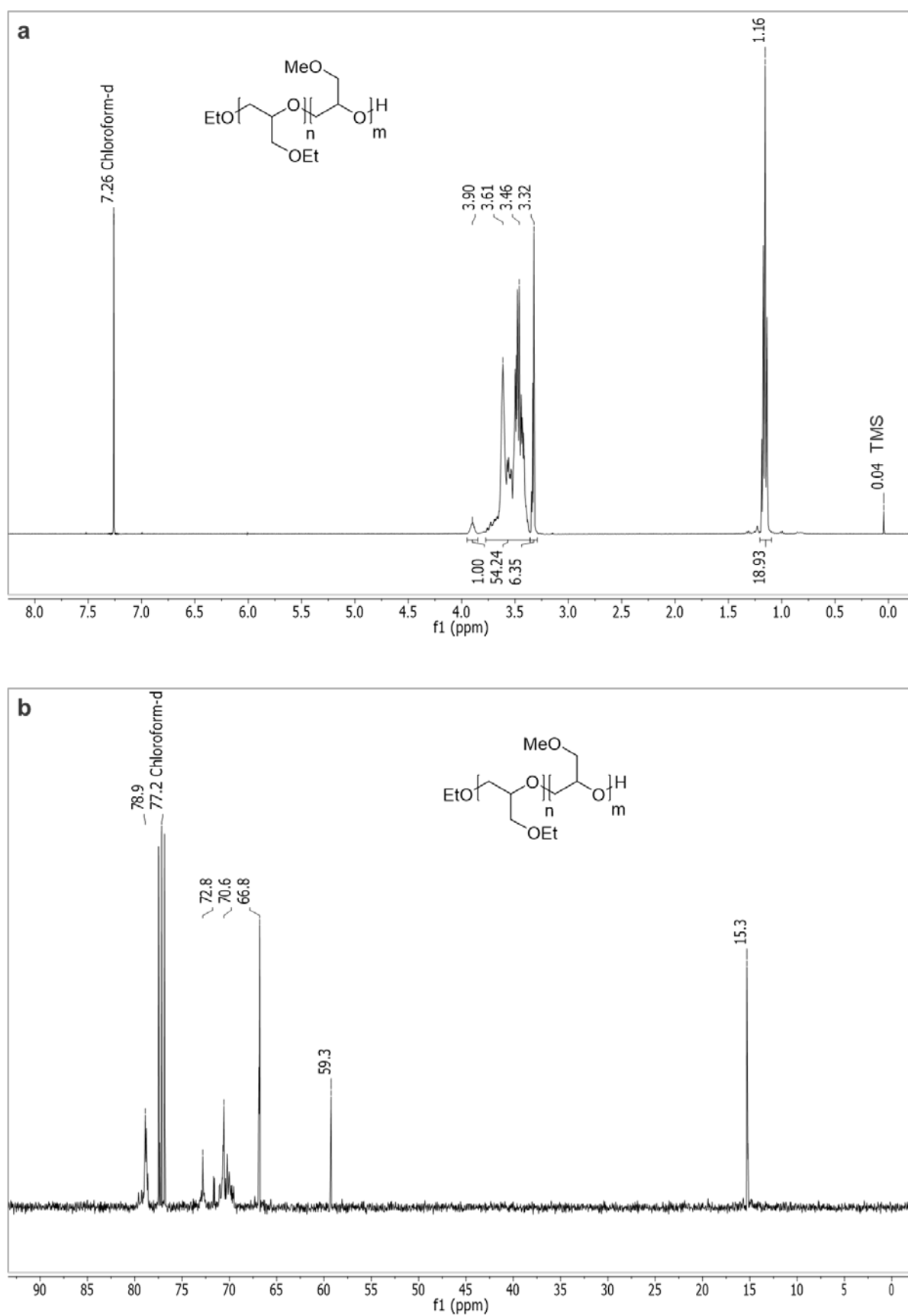
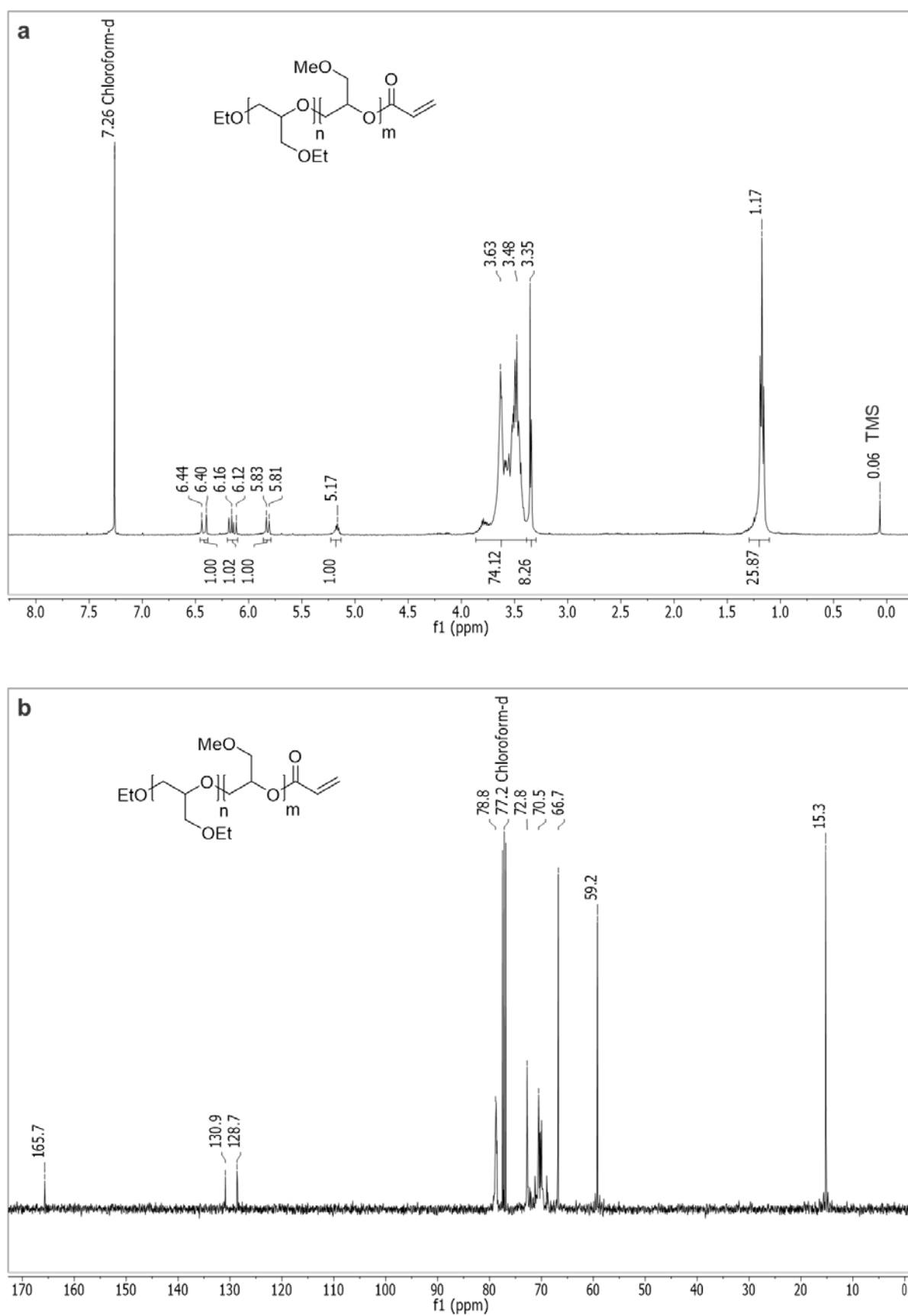


FIGURE S1 Representative ^1H NMR (a) and ^{13}C NMR (b) spectra of an OGE (polymer **6**) recorded in CDCl_3 .



Gel Permeation Chromatography (GPC) of OGEs

Characterization of OGEs via GPC measurements in THF against polystyrene (PS) standards revealed monomodal molecular weight distributions for copolymers with $M_{n, \text{theor.}}$ of 1 kDa (polymer **6**, $M_{n, \text{exp.}} = 940$ Da, PDI = 1.29) and 3 kDa (polymer **9**, $M_{n, \text{exp.}} = 2830$ Da, PDI = 1.17), whereas multimodal distributions were obtained for 5 kDa OGEs (main peak + high molecular weight shoulder: $M_{n, \text{exp.}} = 4730$ Da, PDI = 1.17). The representative GPC traces of OGEs with GME/EGE ratios of 1:3 are displayed in Fig. S3.

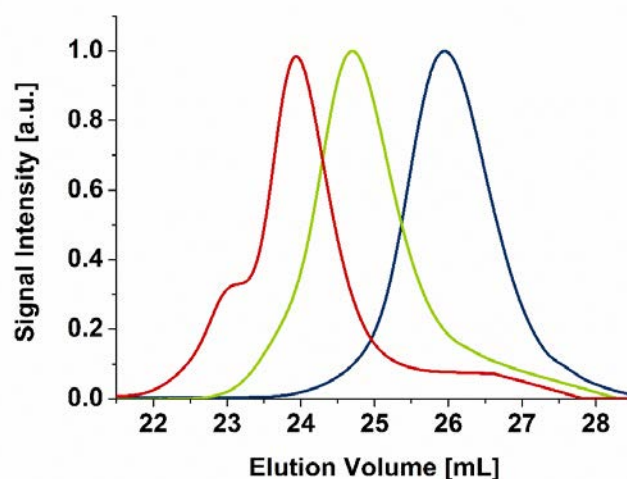


FIGURE S3 Representative GPC traces of OGEs with a GME/EGE ratio of 1:3 and a theoretical molecular weight $M_{n, \text{theor.}}$ of 1 kDa (polymer **6**, blue curve), 3 kDa (polymer **9**, green curve) and 5 kDa (red curve) synthesized by microwave-assisted anionic ROP.

For comparison of the GPC data acquired in THF against PS standards with the results obtained by MALDI-ToF mass spectrometry and ^1H NMR spectroscopy characteristic molecular weight and PDI data for GME and EGE homopolymers are summarized in Table S1.

TABLE S1 Comparison of molecular weight characteristics of OGEs **1-4** determined by GPC in THF relative to PS standards, MALDI-ToF mass spectrometry and ^1H NMR spectroscopy.

OGE	$M_{n, \text{GPC}}$ [Da]	PDI_{GPC}	$M_{n, \text{MALDI}}$ [Da]	$\text{PDI}_{\text{MALDI}}$	$M_{n, \text{NMR}}$ [Da]
1	1160	1.16	1220	1.06	1250
2	1090	1.15	1060	1.08	n.a.
3	1150	1.18	1270	1.07	1260
4	1140	1.16	1080	1.08	n.a.

Since molecular weight characteristics of OGEs determined by GPC in THF are in strong agreement with values determined from MALDI-ToF and ^1H NMR spectra, we conclude that PS standards in THF are an appropriate relative standard for the determination of the molecular weights of poly(glycidyl ethers) (PGEs).

Kinetic Investigation of the Microwave-Assisted Polymerization of OGEs

Temperature and pressure profiles of the microwave-assisted polymerization were recorded on a single-mode “Initiator+ Robot Eight” microwave reactor from Biolin (Uppsala, Sweden). Representative profiles are illustrated in Figure S4. OGEs with a targeted molecular weight of 1 kDa and a GME:EGE ratio of 1:3 were synthesized on a 2 g scale and number average molecular weights of $M_n = 960 \pm 50$ ($n = 3$) as well as average polydispersities of $PDI = 1.28 \pm 0.4$ ($n = 3$) were obtained.

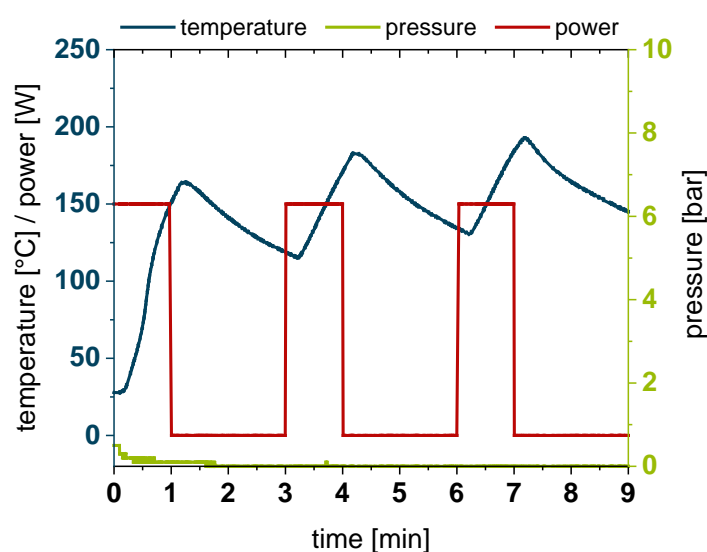


FIGURE S4 Representative temperature and pressure profile during 1 heating/cooling cycle of the microwave-assisted polymerization of an OGE with a targeted molecular weight of 1 kDa and GME:EGE ratio of 1:3. The reaction was performed on a 2 g scale using a single-mode microwave reactor.

For kinetic investigation of the microwave-assisted ROP and comparison with conventional heating, oligo(EGE)s with targeted molecular weights of 2 kDa were synthesized on the 2 g scale at 40 °C and with a maximum power of 40 W. Reactions were quenched after 15, 30, 60 and 120 min and the yield as well as molecular weight characteristics obtained by GPC were compared to the oxy-anionic ROP conducted in an oil bath (PEG 400) at 40 °C. As illustrated in Figure S5, the polymerization self-sustains within the first ~25-30 min due to the exothermic

ROP and the reaction temperature is slightly elevated to 42-43 °C. This exothermic autoacceleration effect is likely to be responsible for the slightly higher yields and molecular weights obtained during the microwave-assisted ROP as compared to the conventional oxy-anionic ROP in an oil bath, since convectonal heat dissipation into the oil bath is supposedly more efficient than in the microwave reactor.

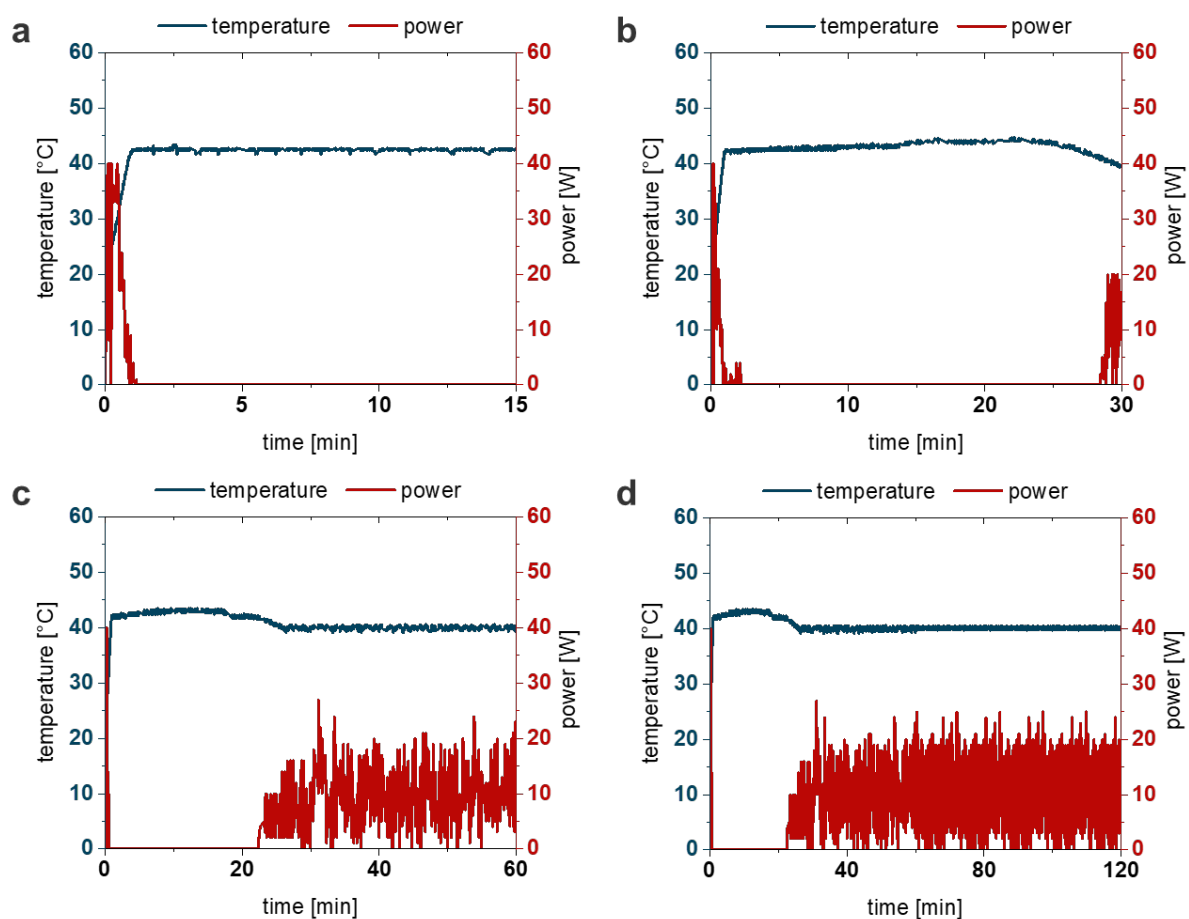


FIGURE S5 Temperature, pressure and power profiles of the microwave-assisted polymerization of oligo(EGE) with a targeted molecular weight of 2 kDa for reaction times of 15 (a), 30 (b), 60 (c) and 120 min (d). The reactions were performed on 2 g scale using a single-mode microwave reactor.

GPC traces of oligo(EGE)s synthesized by microwave as well as conventional heating are illustrated in Figure S6. The shift of the curves towards lower elution volumes visualizes the increase in molecular weight as a function of reaction time.

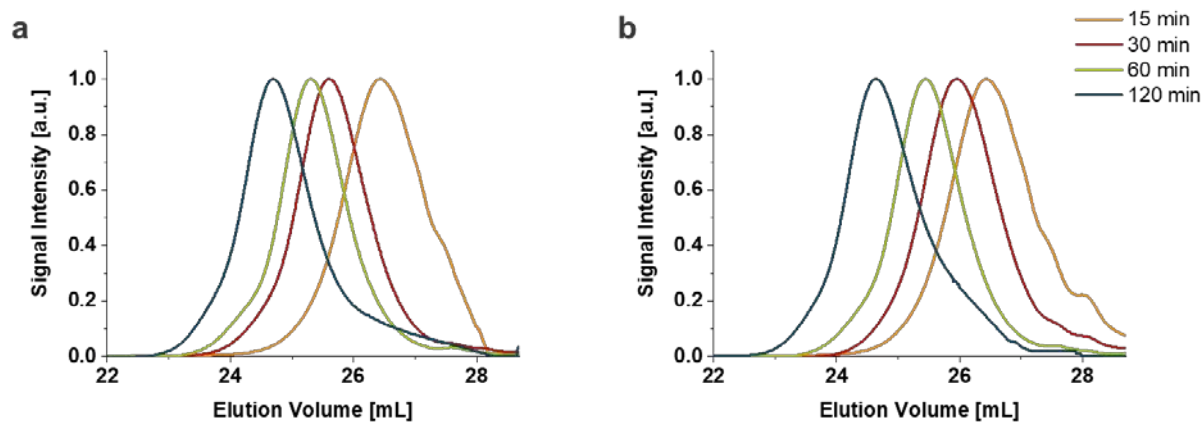


FIGURE S6 Normalized GPC traces as a function of polymerization time for the microwave-assisted (a) and conventional (b) oxy-anionic ROP of oligo(EGE) at 40 °C with a targeted molecular weight of $M_{n, \text{theor.}} = 2$ kDa.

Turbidity Measurements via UV-Vis Transmittance

Cloud point temperatures (CPTs) of PGEs are highly dependent on molecular weight in a range between 1 and 24 kDa and decrease exponentially with increasing molecular weight. Figure S7a displays CPTs of OGEs **5** and **6** together with CPTs of higher molecular weight polymers reported by Heinen *et al.*¹ Further, CPTs of OGEs as a function of GME content can be approximated by a linear relationship. Figure S4b displays CPTs of OGEs **5**, **6** and **7** with molecular weights of 1 kDa and GME contents between 16.7 and 50 mol-% compared to CPTs with 2 kDa OGEs reported by Becherer *et al.*² Via the equation of the given regression curve in Figure S7b the cloud point temperature of a 1 or 2 kDa copolymer with a random comonomer composition can be predicted.

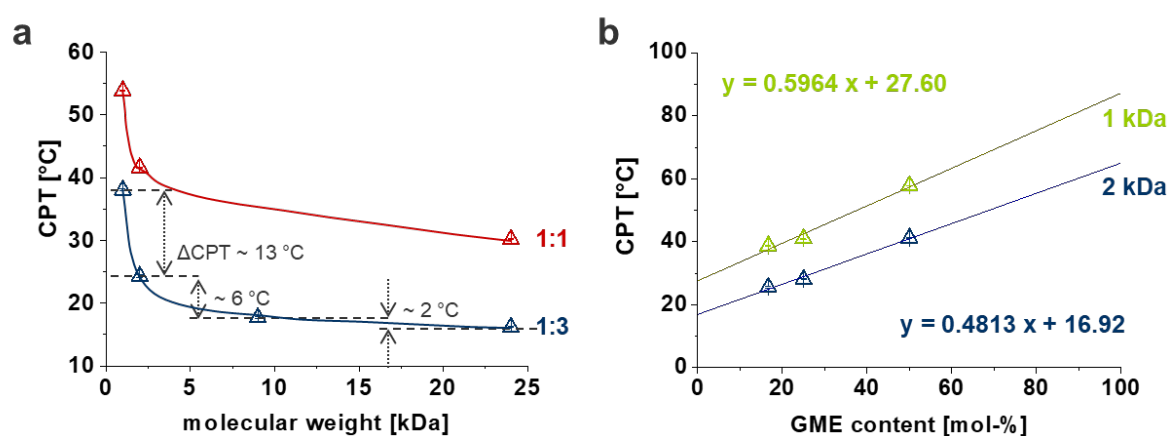


FIGURE S7 (a) Molecular weight-dependent CPTs of PGEs with GME/EGE ratios of 1:1 and 1:3 measured by UV-Vis transmittance in Milli-Q water ($\lambda = 500$ nm) and determined from cooling cycle curves at 10 mg mL^{-1} ($n = 3$, error bars indicate SD). (b) CPTs of OGEs with molecular weights of 1 and 2 kDa as a function of GME content measured by UV-Vis transmittance in Milli-Q water ($\lambda = 500$ nm) and determined from cooling cycle curves at 5 mg mL^{-1} ($n = 3$, error bars indicate SD).

Thermally induced phase transitions of aqueous OGE solutions are less sharp with decreasing molecular weight and concentration. Figure S8 displays representative cooling curves for OGEs

6 and **9** with GME/EGE ratios of 1:3 and molecular weights of 1 and 3 kDa at concentrations of 20-0.1 mg mL⁻¹, respectively.

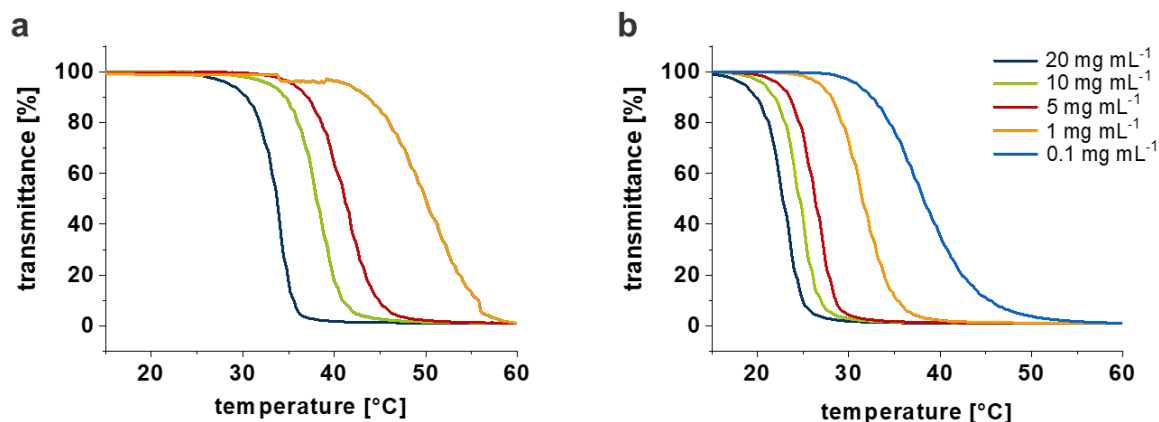


FIGURE S8 Temperature-dependent normalized cooling curves of OGEs **6** (a) and **9** (b) at different concentrations (20-0.1 mg mL⁻¹) accessed by turbidity measurements in Milli-Q water ($\lambda = 500$ nm).

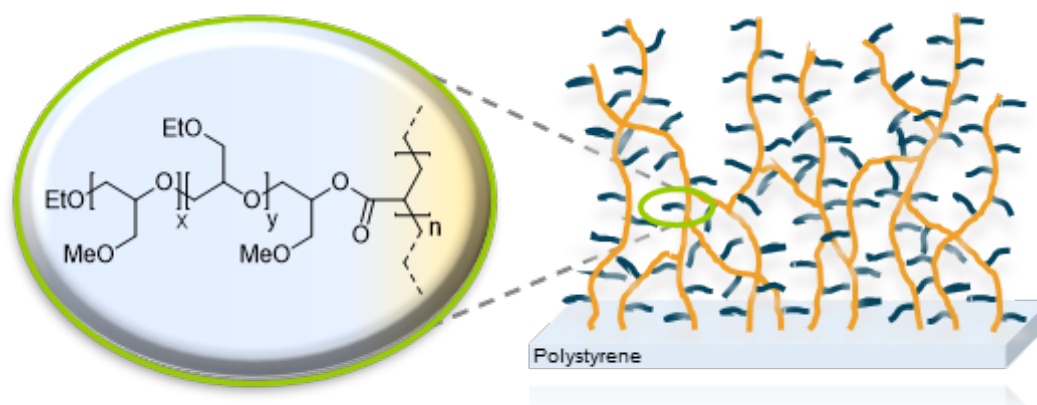
REFERENCES

1. S. Heinen, S. Rackow, A. Schäfer and M. Weinhart, *Macromolecules* **2017**, *50*, 44-53.
2. T. Becherer, S. Heinen, Q. Wei, R. Haag and M. Weinhart, *Acta Biomater.* **2015**, *25*, 43-55.

3.4 Switchable Oligo(glycidyl ether) Acrylate Bottlebrushes “Grafted-from” Polystyrene Surfaces - A Versatile Strategy towards Functional Cell Culture Substrates

Daniel David Stöbener, Johanna Scholz, Uwe Schedler, Marie Weinhart*

The UV-induced “grafting from” of OGEA macromonomers from PS culture substrates under bulk conditions yields porous, thermoresponsive, gel-like bottlebrush coatings. The conditions for photografting as well as the molecular weight of the macromonomers were optimized regarding the fabrication of HDF monolayers. Cell adhesion and cell sheet detachment was correlated with the structure and temperature-dependent hydrophilicity of the coatings.



This chapter was submitted to an appropriate scientific journal and is currently being revised.

"Reprinted with permission from

Daniel David Stöbener, Johanna Scholz, Uwe Schedler, Marie Weinhart,
Biomacromolecules, **2018**, *19* (11), 4207-4218.

Copyright 2018 American Chemical Society."

Switchable Oligo(glycidyl ether) Acrylate Bottlebrushes “Grafted-from” Polystyrene Surfaces - A Versatile Strategy towards Functional Cell Culture Substrates

Daniel David Stöbener[†], Johanna Scholz[†], Uwe Schedler^{†,‡}, Marie Weinhart^{†}*

[†]Institute for Chemistry and Biochemistry, Freie Universitaet Berlin, Takustr. 3, 14195 Berlin, Germany.

[‡]PolyAn GmbH, Rudolf-Baschant-Straße 2, 13086 Berlin, Germany.

*Corresponding author: email marie.weinhart@fu-berlin.de, phone: +49 30 838 75050

ABSTRACT

We introduce a method to functionalize polystyrene (PS) tissue culture substrates with thermoresponsive coatings comprising bottlebrush architectures. Utilizing the UV-induced “grafting from” approach, thermoresponsive oligo(glycidyl ether) acrylate (OGEA) macromonomers were polymerized from PS substrates under bulk conditions. Applying ellipsometry, water contact angle (CA) and atomic force microscopy (AFM) measurements, we found that OGEA coatings exhibit a rough, porous, gel-like structure and exhibit a temperature-dependent phase transition in water through the reversible hydration of OGEA bottlebrush side chains. To assess the utility of the coatings as functional substrates for cell sheet fabrication, human dermal fibroblasts (HDFs) adhesion and detachment was investigated. By adjusting the

bottlebrush properties via coating thickness and structure, we were able to harvest confluent HDF sheets from functionalized PS substrates in a temperature-triggered, controlled manner. As the first report on surface-grafted bottlebrushes comprising thermoresponsive side chains, this study demonstrates the potential of OGEA-based coatings for cell sheet fabrication.

KEYWORDS

Surface-initiated free radical polymerization, bulk photografting, molecular brushes, thermoresponsive macromonomers, switchable surface, cell sheet detachment

INTRODUCTION

The development of “smart” stimuli-responsive coatings has been largely driven by their newly emerging applicability as platforms for bioseparation, diagnostic sensors, drug carriers or functional coatings for tissue culture.¹⁻³ With regards to the latter, thermoresponsive cell culture substrates have been successfully utilized for the temperature-triggered detachment of confluent 2D cell monolayers, which are useful building blocks for 3D tissue engineering or can be used as transplants for regenerative therapy.⁴⁻⁷ Although various strategies have been pursued to functionalize cell culture substrates with thermoresponsive polymer layers, most of the explored approaches rely on brush- or gel-like coating architectures, which can be either “grafted to” or “grafted from” various substrate materials.⁸⁻¹⁰ However, with the objective to extend the accessible property range of thermoresponsive coatings, it is necessary to exploit the entire spectrum of polymer architectures as it is provided by polymer chemistry and macromolecular engineering. A very fitting example for polymer architectures with distinct physical properties are brush-like macromolecules, also commonly referred to as macromolecular brushes or bottlebrushes, which consist of a polymer backbone comprising densely grafted oligo- or polymeric side chains.¹¹⁻¹³ Due to the sterically demanding side chains, bottlebrushes are constrained and usually adopt an entropically unfavorable, extended, rod-like structure in solution.¹⁴⁻¹⁵ As a result, their response to external stimuli, such as solvent,

mechanical triggers or temperature, can lead to unique conformational changes, which strongly deviate from, e.g., linear polymers.^{11, 16} For example, bottlebrushes based on thermoresponsive poly(*N*-isopropyl acrylamide) (PNIPAm) side chains with an estimated molecular weight of ~ 15 kDa grafted from a methacrylate macroinitiator backbone have shown to exhibit a phase transition behaviour in aqueous solution, which is solely characterized by an intramolecular collapse of single PNIPAm bottlebrush chains. As a result, the polymer conformation changes from a rod-like to a coil-like conformation upon increasing the temperature to 32 °C.¹⁷ Further, depending on the molecular weight of the backbone as well as the side chains, bottlebrushes based on poly(2-(dimethylamino)ethyl methacrylate) and poly(*N,N*-dimethylacrylamide) exhibit a highly concentration dependent behaviour, ranging from a temperature-triggered intramolecular collapse at low concentrations all the way to intermolecular aggregation at high concentrations.¹⁸ In another example, thermoresponsive bottlebrushes comprising oligo(ethylene glycol) methacrylate (OEGMA) copolymer side chains exhibited a phase transition temperature tunable via comonomer composition.¹⁹ It was further demonstrated that side chains with a block copolymer structure exhibited two separate phase transitions which lead to the formation of vesicle-like aggregates upon increasing the temperature.¹⁹ Even though several studies have been conducted on bottlebrushes in solution²⁰⁻²², as of yet, there are no reports on surface-tethered coatings based on thermoresponsive macromolecular brush architectures. To improve the performance of PNIPAm-based coatings in terms of cell sheet fabrication, Tang et al. copolymerized *N*-isopropyl acrylamide (NIPAm) with a PNIPAm macromonomer ($M_n = 4.8$ kDa) onto polystyrene (PS) culture substrates using electron beam polymerization.²³ By incorporating comb-like, dangling PNIPAm chains into their coatings, they were able to decrease the detachment time of bovine carotid artery endothelial cell (BAEC) sheets through an accelerated rehydration. However, the maximal incorporated amount of the PNIPAm macromonomer was 5 wt.-%, which is far from the typical side chain density in bottlebrushes.²³ Most of the reported thermoresponsive coatings for cell sheet fabrication are

based on PNIPAm²⁴⁻²⁵, poly[oligo(ethylene glycol) methacrylate]s (POEGMA)s²⁶⁻²⁷ and polyoxazolines²⁸⁻²⁹ and have been prepared by both “grafting from” and “grafting to” methods. Further, thermoresponsive monolayers based on poly(glycidyl ether)s (PGEs) “grafted to” gold model surfaces or applied glass and PS substrates have shown to allow the culture and temperature-triggered, non-destructive detachment of confluent cell sheets.³⁰⁻³³ The facile synthesis of oligo(glycidyl ether) (OGE) macromonomers via oxy-anionic ring-opening polymerization (ROP) and subsequent (meth)acrylation further introduces a pathway for surface functionalization with glycidyl ether-based coatings via “grafting from” approaches.³⁴ In this context, Gunkel et al. grafted glycerol- and glycidyl ether-based bottlebrushes from gold model substrates via surface-initiated atom transfer radical polymerization (SI-ATRP). Utilizing this “grafting from” approach, they obtained protein-resistant coatings with antifouling properties.³⁴ Apart from the just mentioned report, surface-initiated “grafting from” macromonomer methods have been limited to dual-functional antimicrobial/antibiofouling bottlebrush coatings developed by Su, Gao, Zhi et al., who grafted macromonomers based on poly(ethylene glycol) (PEG)-polycation block copolymers from argon plasma-activated poly(dimethyl siloxane) substrates using UV-induced free radical polymerization (FRP).³⁵⁻³⁷ Herein, we applied thermoresponsive oligo(glycidyl ether) acrylate (OGEA) macromonomers which are accessible in one-pot via the convenient oxy-anionic ROP of glycidyl methyl ether (GME) and ethyl glycidyl ether (EGE) under solvent-free conditions as recently reported³⁸ for surface coating. We established an efficient “grafting from” macromonomer approach to yield thermoresponsive OGEA bottlebrushes on PS culture substrates via surface-initiated free radical photografting for further use in cell culture.

EXPERIMENTAL SECTION

A detailed description of all materials applied for synthesis, surface modification and cell culture together with a description of analytical methods and devices used is given in the Supporting Information (SI).

Synthesis of the Oligo(glycidyl ether) Acrylate Macromonomers

Synthesis of thermoresponsive OGEA macromonomers of various molecular weight was performed as reported recently.³⁸ Briefly, glycidyl monomers GME and EGE were polymerized via anionic ROP to yield oligomers of 0.5 and 1kDa with PDIs of 1.2-1.3. Subsequent acrylation yielded the respective OGEA macromonomers. Experimental details and characterization of the synthesized OGEOs are given in the Supporting Information (SI).

Surface Functionalization and Characterization

To characterize the OGEA coatings, PS-coated silicon (Si) wafers were used as model substrates. Si wafers (11 x 11 mm) were rinsed with EtOH and Milli-Q water and dried under a stream of N₂. The samples were spin-coated at 3000 rpm for 60 s applying 50 μ L of a PS solution in toluene (2% (w/w)). Spin-coated samples were dried in vacuo at 400 mbar and 50 °C for 1 h. After washing the surfaces with EtOH and Milli-Q water and drying under a stream of N₂, the thickness and wettability of the PS layers were determined by ellipsometry and static water contact angle (CA) measurements, respectively. To adsorb a thin layer of the photoinitiator benzophenone (BP) onto the substrates, the coated Si wafers were immersed in a dilute BP solution for 20 min to yield an adsorbed BP layer of 1.0 ± 0.3 nm (N = 20) as determined by ellipsometry after careful drying under a stream of N₂.³⁹ For ellipsometric fitting, a Cauchy layer was used, and the refractive index of BP was averaged from literature values and fixed to 1.601.⁴⁰ The precoated samples were spin-coated using 2% (w/w) OGEA solutions in EtOH (30 μ L), protected against light, stored at ambient conditions for 0 or 3 h, and subsequently irradiated by UV light for 15 or 30 min using an irradiance of 25 mW cm⁻² (100%)

to graft the OGEA macromonomers from the PS surface. The coatings were extracted in EtOH for 2 d, washed with Milli-Q water and characterized by ellipsometry, CA, and atomic force microscopy (AFM) measurements. Ellipsometry measurements were conducted in the dry state as well as in Milli-Q water and OGEA layer thicknesses were modeled using the Bruggeman effective medium approximation (EMA).⁴¹ For fitting, the respective refractive indices n of OGEA ($n = 1.450$), air ($n = 1.000$) or water at 20 ($n = 1.334$) and 37 °C ($n = 1.331$) were fixed and air/water volume fractions within the layers were assumed to be 0.5. PS discs ($d = 13$ mm), which were punched out of PS culture dishes for characterization of the OGEA coating properties via AFM measurements as well as PS dishes ($d = 35$ mm) for cell culture experiments were coated as described above for PS-coated Si wafers.

Cell Sheet Fabrication and Viability Assay

Human dermal fibroblasts (HDFs) were isolated as described previously³², cultured in DMEM (4.5 g L⁻¹ glucose) supplemented with 10% FBS in a humidified atmosphere at 37 °C and 5% CO₂. Cells were used in passages 3 to 7 for further experiments.

Cell adhesion and cell sheet detachment experiments were performed on OGEA-coated Falcon[®] PS culture dishes alongside TCPS controls. Sterilization was conducted for 10 min using 70% EtOH and the substrates were washed twice with PBS before cell seeding. HDFs were trypsinized, centrifuged (140 xg, 5 min) and seeded with a density of 1.6×10^5 cells cm⁻² in 2 mL DMEM (1 g L⁻¹ glucose) with 10% FBS per dish ($d = 35$ mm), followed by culture at 37 °C and 5% CO₂ for 24 h. Cells were morphologically analyzed via phase contrast microscopy after 4 and 24 h. In order to trigger cell sheet detachment, confluent cultures were incubated in PBS at 20 °C for 10 min and at 37 °C for 5 min using fresh, pre-warmed PBS. Afterwards, cultures were kept at rt (20 °C) and agitated on an orbital shaker at 50 rpm until the cell sheets detached from the surfaces.

Live/dead staining was performed by adding 50 μM propidium iodide (PI) and 10 μM fluorescein diacetate to the adherent cell cultures and samples were imaged on a Zeiss Observer Z1 microscope in fluorescent mode with appropriate filter sets.

Statistical Evaluation

Graphical illustration of data were performed with OriginPro[®]2018.

RESULTS AND DISCUSSION

Conceptual Rationale, Macromonomer Synthesis and Grafting Approach

We have previously found that thermoresponsive poly(glycidyl ether) (PGE) monolayers adsorbed to applied glass and polystyrene (PS) tissue culture substrates constitute highly cell-compatible coatings, which facilitate the temperature-modulated fabrication of human dermal fibroblast (HDF) sheets.³¹⁻³³ Since PGEs are synthesized under inert, anhydrous conditions via the oxy-anionic ring-opening polymerization (ROP), so far, the immobilization of thermoresponsive PGE coatings onto plastic tissue culture substrates has been restricted to “grafting to” techniques of PGE monolayers (~ 1-3 nm) using functional PGE block copolymers.³²⁻³³ However, our recent report has shown that low molecular weight oligo(glycidyl ether)s (OGEs) based on glycidyl methyl ether (GME) and ethyl glycidyl ether (EGE) exhibit a temperature-dependent phase transition in aqueous solution and can be conveniently end-functionalized into oligo(glycidyl ether) acrylates (OGEAs).³⁸ This class of macromonomers has already been utilized to functionalize gold model substrates via surface-initiated atom-transfer radical polymerization (SI-ATRP) to yield non-responsive, protein resistant bottlebrush coatings.³⁴ On that account, the aim of this work was to develop a method for the UV-induced radical photografting of OGEAs from PS culture dishes to obtain thermoresponsive bottlebrush coatings and to explore their potential as functional tissue culture substrates for the fabrication of cell sheets.

OGEs with targeted molecular weights of 1 kDa and GME:EGE ratios of 1:3 and 1:1 were synthesized via the microwave-assisted oxy-anionic ring-opening polymerization (ROP) according to our previous report using potassium ethoxide (EtOK) as initiator.³⁸ In addition, a shorter OGE with a molecular weight of 0.5 kDa was synthesized using the conventional oxy-anionic ROP. The oligomers were further functionalized by acrylation of the hydroxy end-group to yield well-defined OGEA macromonomers (Table 1).

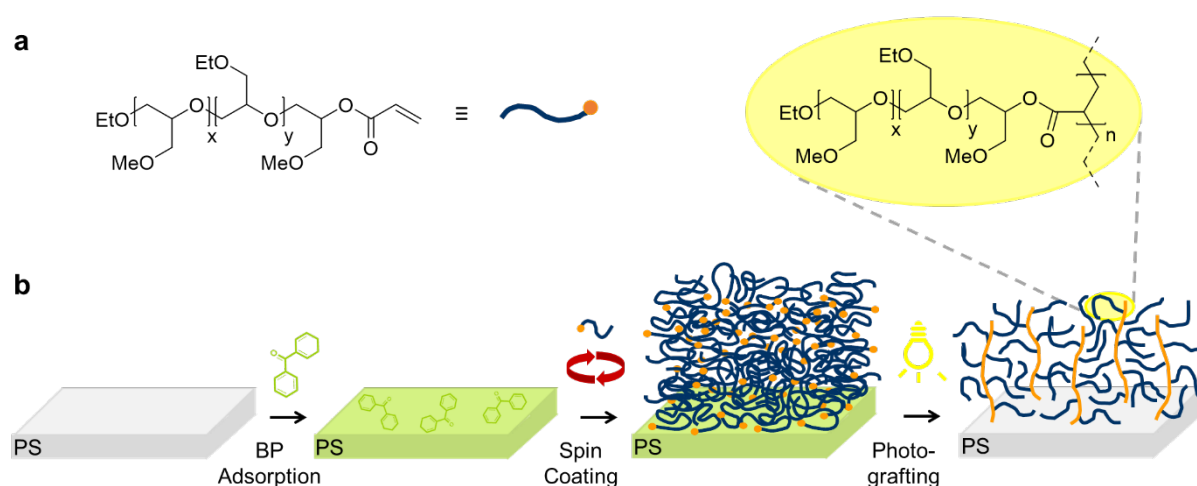
Table 1. Molecular weight characteristics and composition of OGEA_s **1**, **2** and **3**.

OGEA	$M_{n,theor}^a$ [g mol ⁻¹]	$M_{n,NMR}^b$ [g mol ⁻¹]	$M_{n,GPC}^c$ [g mol ⁻¹]	PDI ^c [-]	Y ^d [%]	X ^e [%]	OMe:OEt ratio ^f
1	1000	900	940	1.29	98	95	1 : 3.0
2	1000	880	870	1.31	95	94	1 : 1.1
3	500	490	430	1.23	97	96	1 : 1.2

^a adjusted via monomer/initiator ratio $[M] / [I]$ ($n(\text{GME} + \text{EGE}) / n(\text{EtOK})$); ^b calculated from ¹H NMR spectra of OGE precursors; ^c determined by GPC measurements of OGE precursors in THF as eluent against PS standards; ^d yield of OGE precursors determined by gravimetry; ^e conversion to acrylated OGEA calculated from ¹H NMR spectra; ^f GME/EGE ratio including ethoxy end-group calculated from ¹H NMR spectra.

In order to characterize the coatings via ellipsometry, water contact angle (CA) and atomic force microscopy (AFM) measurements, we spin-coated Si wafers with a foundational PS layer (~ 70-90 nm) to obtain model substrates mimicking conventional PS culture dishes. Since organic solvents are known to decrease the efficiency of photografting from solution due to undesired side reactions⁴²⁻⁴⁴ and since the solubility of OGEA_s in water is limited with respect to temperature and concentration^{38, 45}, we performed photografting from bulk monomer films. The use of free benzophenone (BP) as a photoinitiator for bulk photografting⁴⁶⁻⁴⁷ is well documented and has shown to be an efficient method for the lamination of polymer films⁴⁸⁻⁴⁹ as well as the functionalization of polymer foils.⁵⁰⁻⁵¹ To minimize side reactions with OGEA

macromonomers, which are prone to radical-induced cleavage or crosslinking due to their polyether structure⁵²⁻⁵³, and to initiate the grafting reaction primarily from reactive radicals created on the PS surface, a thin layer of BP (~ 1 nm) was pre-adsorbed onto the PS substrates. This strategy has previously been described for the functionalization of polypropylene membranes via photografting.⁵⁴⁻⁵⁵ Subsequently, OGEAs were spin-coated onto the BP-treated substrates from ethanolic solution (2 wt.-%) to yield bulk macromonomer films. The average thickness and refractive index of the OGEA layers were measured by ellipsometry and determined to be ~ 70 nm and ~ 1.45, respectively, using a Cauchy layer for fitting (Figure S1). After irradiation with UV light ($\lambda = 365$ nm) for 15 min, the thicknesses of the OGEA layers slightly decreased, indicating the compacting of the films through UV-induced radical polymerization (Figure S1). The coatings were subsequently extracted in ethanol for two days in order to remove unreacted monomer and non-immobilized poly(OGEA) to yield stable, covalently attached layers. The generalized chemical structure as well as the procedure applied for the “grafting from” of OGEA bottlebrushes via the UV-induced macromonomer method are illustrated in Scheme 1.



Scheme 1. Structure of the thermoresponsive macromonomer OGEA (a). General procedure for the UV-induced, surfaces-initiated photografting process of OGEA-based thermoresponsive bottlebrushes from PS culture substrates pre-adsorbed with a thin BP layer and general chemical structure of OGEA bottlebrushes (b).

Investigation of OGEA Bottlebrush Coating Structure, Thickness and Wettability via Ellipsometry and Static Water CA Measurements

After extraction of the OGEA layers with ethanol, characterization of the bottlebrush coatings by ellipsometry yielded thicknesses and refractive indices of > 100 nm and ~ 1.1 , respectively. In addition, when fixing the refractive indices of the OGEA coatings to 1.45, fitting of the layer thicknesses resulted in high mean squared errors (> 20) when a Cauchy layer was applied for modelling. Both, unrealistically high layer thicknesses, which exceeded those of the initially spin-coated OGEA films (Figure S1), and insufficiently accurate ellipsometric fits obtained from modeling of OGEA layers by using the Cauchy model, indicated that the obtained bottlebrush coatings exhibit a rough and/or porous structure. Hence, we modeled the layers using the Bruggeman effective medium approximation (EMA), which accounts for inclusions of the surrounding medium (e.g. air or water) with respect to pores and/or surface roughness of the coatings. Adequate ellipsometric fits (mean squared errors ≤ 10) and realistic layer thicknesses were obtained when the refractive index of the bottlebrushes, which were regarded as the continuous medium, was fixed to 1.45 (Figure S1) and the air content, constituting the entrapped medium with a refractive index of 1.0, was set to a volume fraction of 0.5. As illustrated in Figure 1a, the thicknesses of the coatings obtained via the grafting of OGEAs **1** to **3** are all in the range of about 5 - 25 nm with average values around 15 - 20 nm. In addition to the rather large thickness deviations between single samples (Figure 1a), the grafted coatings featured lateral inhomogeneities on the macroscopic scale, which were clearly apparent by visual inspection of the coated Si model substrates. In order to improve the homogeneity of the coatings, bottlebrushes were prepared via an optimized procedure, which included a 3 h resting period of the spin-coated OGEA films before irradiation with UV light. As a result, macroscopically homogeneous coatings with more uniform thicknesses on each independent sample were obtained after ethanol extraction (Figure 1b). In addition, ellipsometric fits with mean squared errors ≤ 5 indicated rather well-defined coating structures. This suggests a more

uniform growth of OGEA bottlebrushes and, as a result, a more regular distribution and size of nanometer-sized air pores within the coatings. A possible explanation for the improved layer homogeneity could be the rearrangement of OGEA macromonomers within the spin-coated films during the 3 h resting period, which might lead to either an assembly or a more even distribution of reactive acrylate groups within the OGEA films. Furthermore, the oxygen content within the OGEA films as well as the diffusion of the BP photoinitiator into the film are further possible factors which might have an impact on the homogeneous grafting of the bottlebrush coatings during irradiation with UV light.

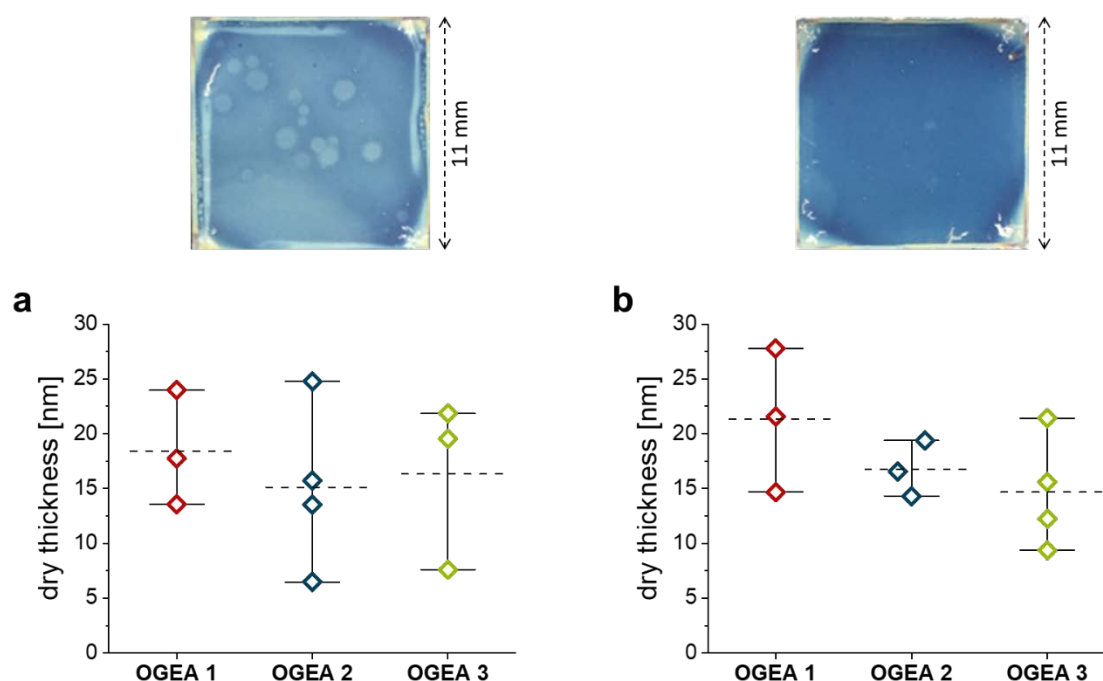


Figure 1. Dry layer thickness of bottlebrush coatings prepared by irradiation of bulk OGEA films with UV light for 15 min directly after spin coating (a) and after a 3 h resting period (b) determined by ellipsometry. Thicknesses are plotted for each replicate together with their mean value (dashed line) and their 90% confidence interval (whiskers). A representative image of the coated PS surface prepared directly after spin coating (a) and after a 3 h resting period (b) is given above the graphs.

Despite the fact that macroscopically uniform coatings were obtained via the optimized grafting procedure, layer thicknesses still deviate significantly between independent samples. This illustrates the sensitivity of the radical “grafting from” process towards environmental factors. Since all experiments were conducted under ambient conditions, quenching of the radical reaction through oxygen is likely to be responsible for the rather large variances in layer thickness. Prolonging the UV irradiation time to 30 min resulted in only moderately increased (5-10 nm) OGEA coating thicknesses (Figure S2) with the applied ellipsometric model.

The wettability of the bottlebrush coatings was investigated by static water CA measurements. As illustrated in Figure 2, coatings which were grafted directly after spin coating of OGEA films displayed fairly hydrophobic properties with CAs up to 85° and around 72° for bottlebrushes comprising side chains with molecular weights of ~ 1 kDa (OGEA 1 and 2) and ~ 0.5 kDa (OGEA 3), respectively (Figure 2a). However, when the optimized grafting procedure was applied, CAs decreased about 10° and the coatings uniformly exhibited more hydrophilic properties (Figure 2b). Since the surface wettability is significantly governed by the homogeneity, roughness and porosity of the coating, the observed differences in contact angles of the OGEA bottlebrushes are in accordance to the results obtained from ellipsometric measurements and justify the assumption of porous/rough bottlebrush coatings.

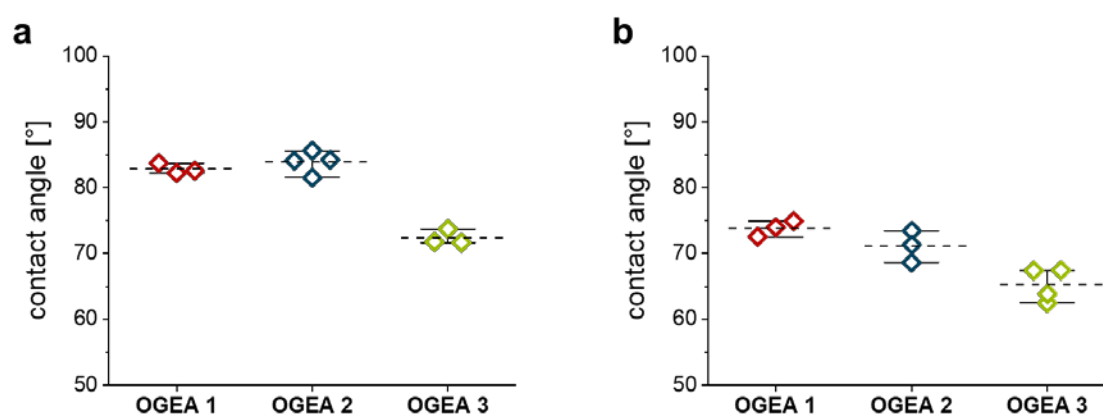


Figure 2. Static water CAs of bottlebrush coatings prepared by irradiation of bulk OGEA films with UV light for 15 min directly after spin coating (a) and after a 3 h resting period (b)

determined by the sessile drop method (2 μL). CAs are plotted for each replicate together with their mean value (dashed line) and their 90% confidence interval (whiskers).

Alternatively, the hydrophobic nature of the coatings could also be caused by the inherent hydrophobicity of the acrylate bottlebrush backbone, as CAs of acrylate-free PGE monolayers have been reported to be in the range of 60-70°. ^{30-33, 56-57} However, the significant drop in contact angle upon changing the coating procedure strongly suggests that the structure and homogeneity of the grafted layers dominates the wettability of the OGEA coatings. This hypothesis is further substantiated by the significantly lower water CAs of bottlebrushes with 0.5 kDa side chains as compared to bottlebrushes with 1.0 kDa side chains, since the acrylate content of OGEA **3** is about 100% higher than for OGEA **1** and **2** (Table 1). In addition, the lower molecular weight of OGEA **3** likely enables a denser grafting of bottlebrush chains, which presumably leads to smaller pores or coatings with decreased roughness after extraction of non-immobilized poly(OGEA) by ethanol. On top of that, bottlebrushes based on OGEA **3** should be much more flexible due to their sterically less demanding side chains, which might enhance the collapse of the porous layers in the dry, non-hydrated state. In contrast, the stiffer bottlebrushes based on OGEA **1** and **2** with longer and more sterically demanding side chains should be much more prone to retain their rough or porous structure under ambient conditions. As illustrated in Figure S3, prolonged irradiation time with UV light did not significantly influence bottlebrush wettability indicating a rather negligible change in the apparent coating structure. This in turn, suggests a low degree of radical-induced side reactions, such as bottlebrush side chain cleavage or intermolecular crosslinking.

Thermoresponsive Properties of OGEA Bottlebrushes in Water

To determine the temperature-dependent swelling of the coatings, bottlebrushes based on OGEA **2** prepared via the optimized grafting procedure were representatively investigated by ellipsometry in water at 20 and 37 °C. Thicknesses were modeled using the Bruggeman EMA

and fitting was performed with fixed refractive indices of 1.45, 1.334 and 1.331 for OGEA in the dry state, in water at 20 °C and 37 °C, respectively. As Figure 3 illustrates, bottlebrushes based on OGEA **2** did not significantly swell when hydrated in water at 20 °C nor exhibit a marked temperature-induced collapse after increasing the temperature to 37 °C. Moreover, ellipsometric fittings yielded mean squared errors ≤ 5 , which further verifies the assumptions made for modeling the thickness in the dry state. The negligible macroscopic swelling of the coatings underpin the porous structure as well as the rather stiff, rod-like conformation of bottlebrushes with side chains of about 1 kDa. However, it has to be noted that the temperature-modulated collapse of OGEA side chains is unlikely to be detected via ellipsometry, especially in case of rough and porous coatings, which are highly diluted by the surrounding medium (e.g. water).

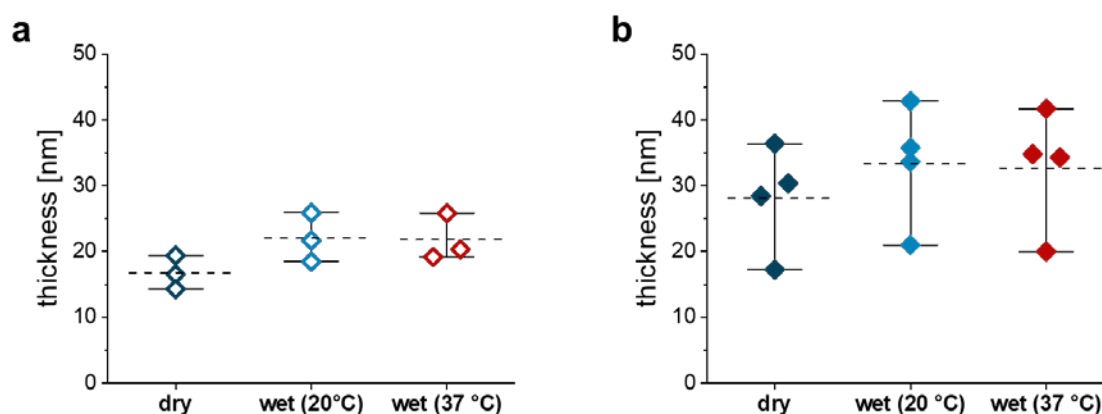


Figure 3. Dry and wet layer thickness at 20 and 37 °C of OGEA **2** bottlebrush coatings irradiated with UV light after a 3 h resting period for 15 min (a) and 30 min (b) determined by ellipsometry. Thicknesses are plotted for each replicate together with their mean value (dashed line) and their 90% confidence interval (whiskers).

In order to detect temperature-induced changes in OGEA side chain hydration, static water CAs were determined at 37 °C using a tempered humidity chamber and compared to CAs measured at 20 °C under ambient conditions. Whereas uncoated PS control substrates did not exhibit any

detectable change in wettability, CAs uniformly displayed a marked increase at 37 °C for bottlebrush coatings based on OGEA 2 and 3 after both grafting under optimized conditions as well as on laterally inhomogeneous coatings which were irradiated immediately after spin coating (Figure 4, Figure S4). This clearly indicates the temperature-modulated dehydration of the bottlebrush side chains upon heating and confirms the thermoresponsive nature of OGEA bottlebrushes via the “switching” from a laterally collapsed, dehydrated state at 37 °C to a more laterally swollen, hydrated state at 20 °C. The more pronounced change in wettability of bottlebrushes with 1 kDa side chains further approves that temperature-modulated CA changes are caused by the reversible de- and rehydration of the OGEA side chains (Figure 4a). Although the change in CAs is partially in the range of error and thus masked by the variance of the radical grafting process, especially for coatings based on OGEA 3 (Figure 4b), differences in CAs were evident on each independent sample. So far, a macroscopic temperature-dependent change in wettability of thermoresponsive PGE-based coatings has not been reported, although changes in the state of hydration of PGE monolayers have been detected by AFM measurements.^{30, 32-33} This further accentuates the rough and/or porous structure of the OGEA bottlebrush coatings, through which the effective OGEA side chain-water interface is increased. Hence, the enlarged surface area is most likely the reason for the enhanced responsiveness, detected via temperature- dependent wettability changes, of the bottlebrush coatings as compared to PGE monolayers.

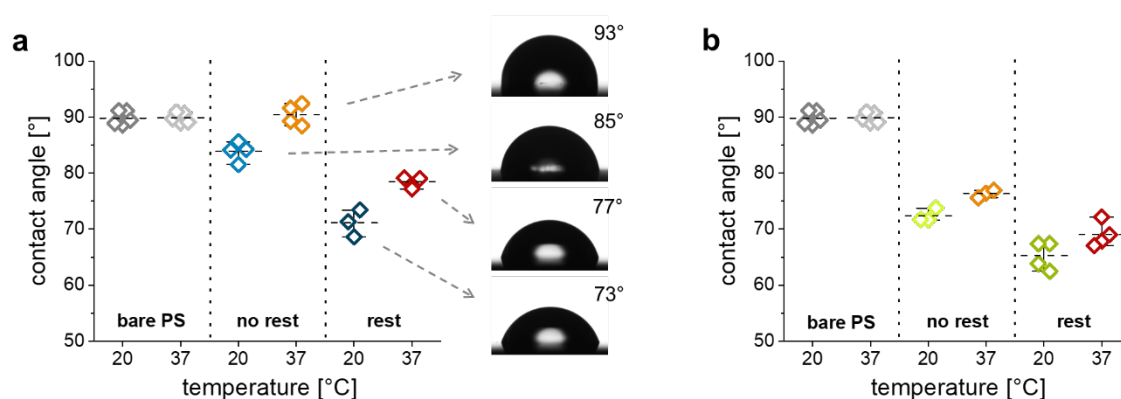


Figure 4. Temperature-dependent static water CAs of OGEA **2** (a) and OGEA **3** (b) irradiated with UV light for 15 min determined by the sessile drop method (2 μ L) using a tempered humidity chamber. Bare PS substrates are shown as controls. CAs are plotted for each replicate together with their mean value (dashed line) and their 90% confidence interval (whiskers).

Investigation of Coating Morphology and Properties of OGEA Bottlebrushes by AFM

The morphology of OGEA **2** and **3** bottlebrush coatings prepared by the optimized grafting procedure was investigated by AFM in Milli-Q water at 20 and 37 °C in order to further deduce the coating structure via surface roughness as well as to determine temperature-dependent morphological changes. The latter would indicate a phase transition of the coatings induced by the bottlebrush side chains. Morphological images of coatings prepared on Si model substrates using irradiation times of 15 min are displayed on a 5 μ m scale in Figure 5. Both, OGEA **2**- (Figure 5a-f) and **3**-based (Figure 5g-l) bottlebrush coatings exhibit a rough, “hairy” to particulate-like structure at 20 and 37 °C. This is also apparent from 2 μ m images illustrated in Figure S5 and illustrates the characteristic rod-like structure of the grafted bottlebrushes. Verduzco and co-workers observed a similar surface morphology of films prepared by spin-casting mixed bottlebrush copolymers comprising PS and PEG side chains on indium tin oxide (ITO) substrates.⁵⁸ Although the particulate-like peaks are most likely composed of multiple bottlebrush chains, the finer topology of OGEA **3**-based coatings clearly reflects the smaller diameter of bottlebrushes with 0.5 kDa side chains. In comparison, the apparent diameters of the particulate-like structures illustrated in Figure 5 and S5 are much larger (~ 30-70 nm) than the theoretically estimated width of single bottlebrushes, which are approximately 1.5 and 3 nm considering the contour length of 0.5 and 1.0 kDa OGE side chains, respectively.^{30, 56} For comparison, the morphology and surface roughness profile of a flat PS-coated Si wafer is shown in Figure S6. As we have shown in one of our recent reports³², the typical roughness of a PS

films spin-coated onto Si substrates is significantly lower ($R_q \sim 0.42$ nm) than the roughness of photografted OGEA bottlebrush coatings (Table S1).

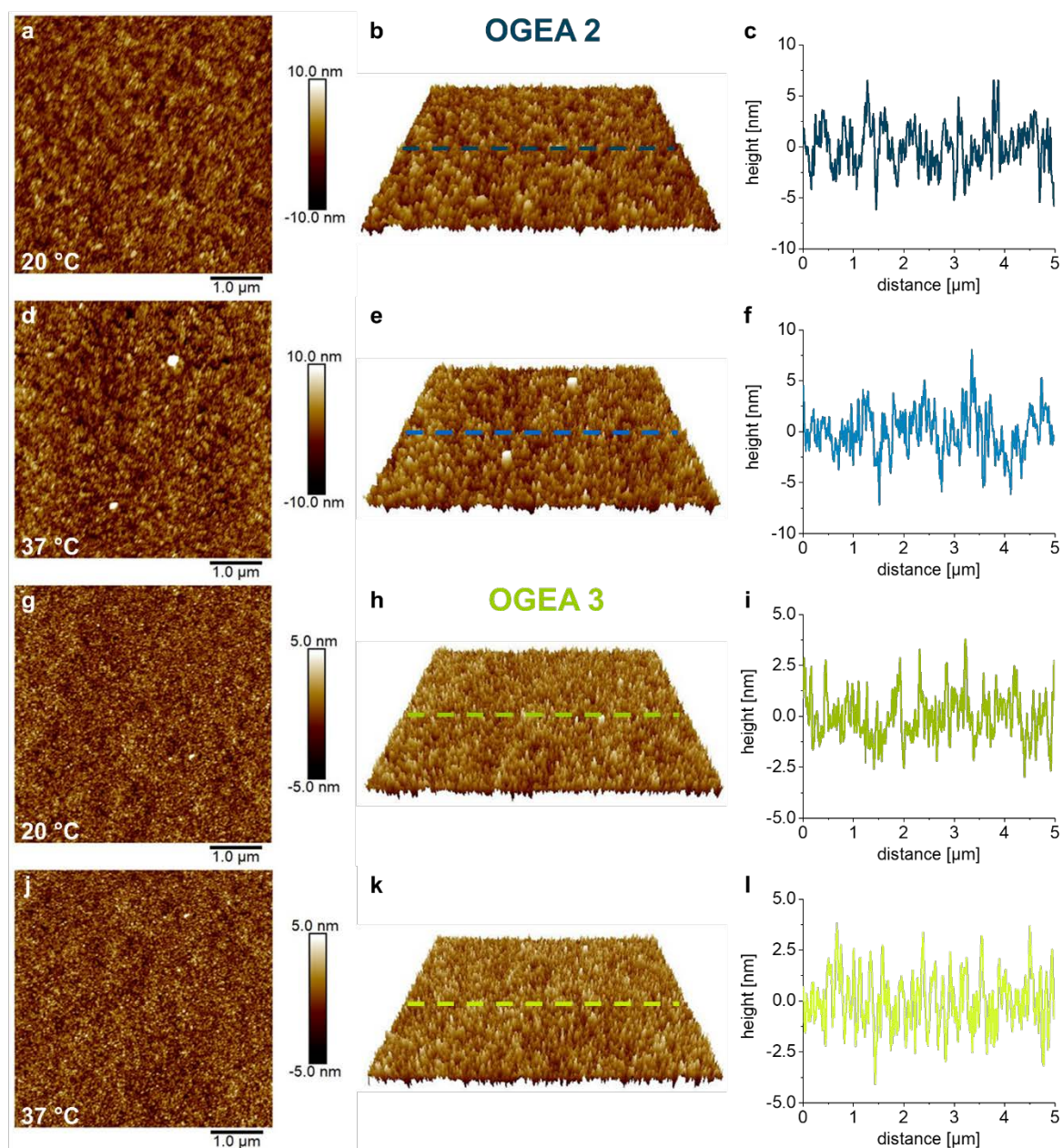


Figure 5. 2D and 3D surface topography and cross section profiles of 5 μm images of OGEA 2 coatings at 20 °C (a, b, c) and 37 °C (d, e, f) as well as OGEA 3 coatings at 20 °C (g, h, i) and 37 °C (j, k, l) on PS-coated Si wafers prepared via 15 min UV-irradiation and measured in Milli-Q water by AFM in quantitative nanomechanical mapping (QNM) mode.

In addition, the markedly higher roughness of OGEA **2**-based coatings suggests the more rigid and porous structure of bottlebrush coatings with 1 kDa side chains which is in accordance with the interpretation of our results obtained from ellipsometry and CA measurements (Figure 1-2, Figure S2-3). The average roughness parameters summarized in Table S1 confirm the significant differences between OGEA **2**- and **3**-based coatings with average mean squared roughness R_q values of 2-3 and ~ 1 nm, respectively. While roughness values slightly increase for coatings prepared from OGEA **2** upon prolonged irradiation time (30 min), the roughness slightly decreases for OGEA **3**-based coatings. This indicates further growth of bottlebrush chains upon irradiation for 30 min and hints the tighter structure and more flexible nature of bottlebrushes with 0.5 kDa side chains. As illustrated in Figure 5 and S5 and summarized in Table S1, a change in temperature from 20 to 37 °C does not result in an altered roughness and, hence, does not indicate a macroscopic, vertical swelling or collapse of the coatings upon temperature variation. This agrees with the results of the ellipsometric swelling measurements of OGEA **2** coatings presented in Figure 3 and indicates the generally rather rigid and gel-like structure of the prepared bottlebrush coatings. AFM measurements on analogously prepared coatings on regular, applied PS culture dishes further support this conclusion. As illustrated in Figure 6, the structure of the bare PS substrates, which comprise a inhomogeneous, scratch-like roughness on the nanometer-scale (Figure 6a, d), is considerably altered after coating with a thermoresponsive bottlebrush layer. Although the initial roughness is not leveled and shows a marked increase upon coating, the characteristic morphology of the PS dishes is evidently lost (Figure 6b, e). In addition, images c and f in Figure 6, suggest that longer grafting times (30 min) lead to a denser, less rough bottlebrush coating, which is in accordance with the slightly decreasing roughness of OGEA **3** coatings determined on Si model substrates (Table S1). Moreover, the characteristic particulate-like, “hairy” bottlebrush structure, which was evident from AFM images recorded on Si substrates (Figure 5, Figure S5), apparently translates onto

PS culture substrates (Figure 6e, f). These results further prove the viability of the surface-initiated photografting of OGEA bottlebrushes from applied PS culture substrates.

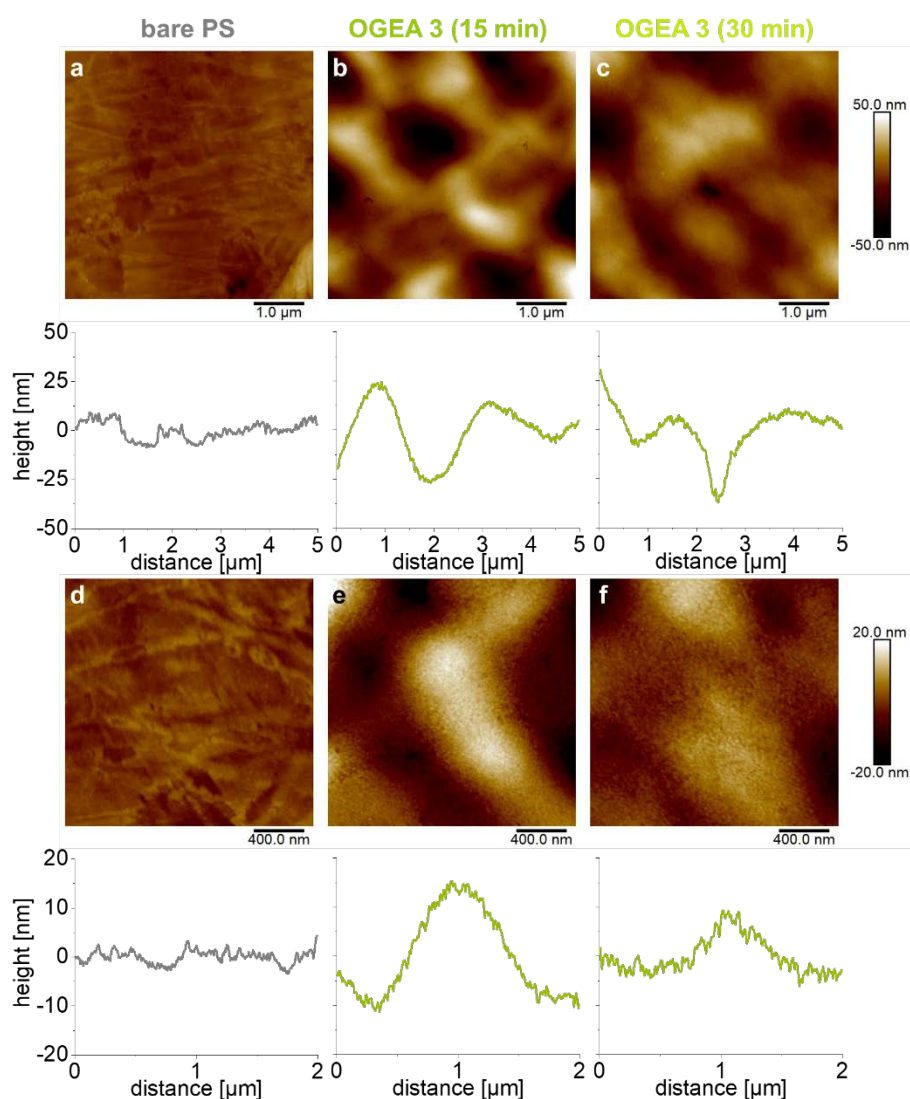


Figure 6. 2D surface topography of bare PS culture dishes (a, d) and PS culture dishes photografted with OGEA 3 coatings for 15 min (b, e) and 30 min (c, f) on a 5 μm (a, b, c) and 2 μm (d, e, f) scale measured in Milli-Q water at 20 $^{\circ}\text{C}$ by AFM in QNM mode.

In addition to morphological changes, the material properties of the PS culture surfaces grafted with OGEA 3 layers markedly differ from those of bare PS substrates. Figures S6-S8 compare the deformation, the Young's modulus (DMT modulus) and the adhesion measured by AFM via QNM in Milli-Q water at 20 and 37 $^{\circ}\text{C}$. Although surface deformation is not significantly different from bare PS (Figure S7d, h), topological changes in the deformation images (Figure

S7a, b, c, e, f, g) clearly resemble the particulate-like bottlebrush structure of OGEA **3** coatings. The rather small deformation ($\sim 1\text{-}2$ nm) of the coatings further indicates the stiffness of the bottlebrushes. In contrast, the Young's modulus, which was calculated using the DMT (Derjaguin-Muller-Toporov) model, substantially decreased with increasing bottlebrush thickness from $\sim 60\text{-}80$ MPa for bare PS down to ~ 5 MPa for OGEA **3** coatings grafted for 30 min (Figure S8). This clearly indicates the presence of a flexible, gel-like layer, which softens upon prolonged photografting and further suggests that the bottlebrush coatings exhibit a gradient-like profile with a more gel-like structure in proximity to the PS substrate and a more bottlebrush-like structure on the top of the coating. Compared to literature values, which suggest Young's moduli of bare PS in the range of ~ 1 GPa⁵⁹⁻⁶⁰, the rather low values we obtained from our measurements ($\sim 60\text{-}80$ MPa) presumably originate from the low indentation force applied (500 pN). In addition, the applied DMT model uses the force retraction curve to extract the Young's modulus and is therefore highly sensitive towards adhesive interactions between the AFM tip and the surface, which might also contribute to the underestimated Young's moduli of bare PS. Furthermore, adhesion forces between the AFM tip and the bottlebrush coatings are slightly shifted towards lower values as compared to bare PS substrates (Figure S9). In agreement with the measured contact angles, this illustrates the slightly more hydrophilic and hydrated nature of the OEGA coatings compared to PS, which results in a lesser degree of hydrophobic interactions between the polymer chains and the AFM tip as we reported previously for ultrathin PGE coatings on PS.³² Although the material properties of OGEA coatings slightly vary with temperature (Figure S7-S9), significant changes in deformation, Young's modulus and adhesion could not be detected between 20 and 37 °C. This further indicates, that the OGEA side chains are mainly responsible for the temperature-dependent phase transition of the coatings and that the macroscopic changes in bottlebrush structure only occur to a negligible extent, as it was shown by ellipsometry and CA measurement (Figure 3, Figure 4).

Performance of OGEA Bottlebrush for Cell Sheet Fabrication

Human dermal fibroblasts (HDFs) were cultured on thermoresponsive OGEA bottlebrushes to assess whether they support cell growth and constitute suitable substrates for the temperature-triggered fabrication of confluent cell sheets. To compare cell adhesion to our previously developed PGE monolayers, HDFs were seeded on OGEA coatings with a density of 1.6×10^5 cells cm^{-2} . As illustrated in Figure S10a and b, initial cell adhesion after 4 h was poor on bottlebrush coatings based on OGEA **1** and **2** prepared via the non-optimized grafting method, as compared to tissue culture polystyrene (TCPS) control substrates (Figure 7c). Due to the relatively high seeding densities, cells recovered within 24 h of culture and formed adherent confluent monolayers. However, the formed HDF sheets detached spontaneously during culture in the incubator at 37 °C (N = 4). Interestingly, fibroblasts showed indistinguishable behavior on both coatings prepared from OGEA **1** with a more hydrophobic (GME:EGE 1:3) and OGEA **2** with a more hydrophilic comonomer ratio (GME:EGE 1:1). This illustrates that cellular behaviour is mainly governed by the porous structure of the bottlebrush coatings rather than the comonomer ratio of the side chains. Hence, both, weak initial cell adhesion and premature detachment of HDFs can be explained by the relatively hydrophobic nature of the coatings, which is introduced by porosity and surface roughness. As illustrated in Figure 2a and 4a, water CAs of OGEA **1** and **2** bottlebrushes prepared via photografting immediately after spin coating are above 80° at 20 °C and even approach values of ~ 90° under standard cell culture conditions at 37 °C. These values are in the range of untreated, bare PS, which is well known for its rather cell-repellant properties. We assume that the poor cell adhesion is caused by the retarded adsorption of cell adhesion-mediating proteins from cell culture medium to the surface due to the porous and side chain collapsed structure of the bottlebrush layers. Consequently, the protein-mediated attachment of HDFs is retarded. Upon applying the optimized grafting procedure to fabricate OGEA **2** coatings (1 kDa side chains), initial cell adhesion drastically improved (Figure S10c) due to the more hydrophilic nature of

the bottlebrushes (Figure 2 and 4). However, confluent HDF sheets still partially detached uncontrolled during incubation at 37 °C (3 out of 4 samples). In contrast, OGEA **3** coatings (0.5 kDa side chains) with a similar hydrophilicity prepared by the non-optimized method allowed for the controlled detachment of HDF sheets (N = 2) upon reducing the temperature to 20 °C (Figure S10d). This indicates, that although both coatings exhibit a similar wettability, structural differences between bottlebrush coatings with 1 and 0.5 kDa side chains crucially influence cell behaviour. As illustrated in Figure 7, HDF sheets could be reproducibly fabricated on OGEA **3**-based bottlebrush coatings prepared via the optimized grafting method utilizing irradiation times of 15 (Figure 7a) and 30 min (Figure 7b). Both substrates displayed cell-adhesive properties similar to those of TCPS controls (Figure 7c). OGEA **3** bottlebrushes grafted for 15 and 30 min possess CAs of about 65°, which is in the range of TCPS as well as in good agreement with PGE-based monolayer coatings.^{30-33, 56-57} Evidently, grafted OGEA **3** bottlebrush layers successfully facilitate the controlled detachment of confluent HDF sheets within 37.0 ± 8.4 (N = 6) and 46.8 ± 16.8 min (N = 6), respectively, upon cooling from standard cell culture conditions (37 °C) to 20 °C. HDF detachment times are in a similar realm as reported for PGE brushes on glass and PS culture substrates,^{31, 33} which on first glance contradicts the enhanced swelling properties observed for PNIPAm gels which had 5% of a PNIPAm macromonomer incorporated to obtain comb-like gels.²³ However, the detected insignificant changes in HDF detachment times from OGEA bottlebrush substrates and PGE monolayers are reasonable, as the rather rigid bottlebrush coatings do not further trigger cell sheet detachment by significant macroscopic, vertical swelling. Hence, the main driving force for the detachment of HDF sheets from OGEA layers seems to be the temperature-induced change in side chain hydration, which is in accordance to the proposed mechanism of HDF sheet detachment from PGE monolayers.³¹⁻³³ Similar detachment times were observed from Dworak and co-workers, who harvested confluent HDF monolayers from POEGMA brushes immobilized on glass culture substrates within ~ 30 min by lowering the temperature to

17.5 °C.²⁶⁻²⁷ Prolonged UV-irradiation times in the fabrication of the coatings did not yield an improved cell response.

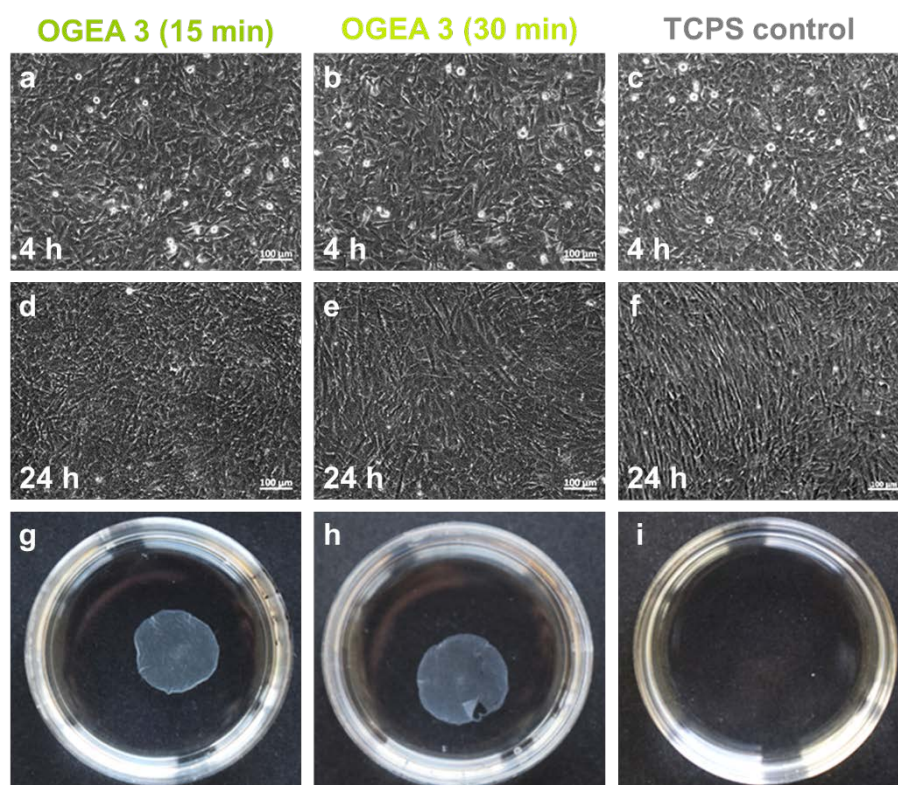


Figure 7. Representative phase contrast images of HDFs 4 h (a, b, c) and 24 h (d, e, f) after seeding and macroscopic photographs of the culture dishes after temperature reduction to 20 °C (g, h, i) on OGEA 3 coatings prepared via 15 and 30 min UV-irradiation and TCPS controls. Only OGEA 3-coated dishes released HDF sheets when triggered thermally.

In addition, live-dead assays showed that HDF stayed viable on OGEA 3 bottlebrush coatings, similar to HDFs cultured on standard TCPS substrates (Figure S11). These results clearly demonstrate the utility of OGEA-based bottlebrush coatings as a thermoresponsive platform for cell sheet fabrication.

CONCLUSION

We applied the „grafting from” macromonomer approach to functionalize PS culture substrates with thermoresponsive OGEA bottlebrush coatings via surface-initiated photografting under bulk conditions. As the first report utilizing this technique, we obtained rigid, porous, gel-like coatings with structure- and temperature-dependent wetting properties, which we adjusted via the grafting procedure, irradiation time and the molecular weight of OGEA macromonomers. Culture experiments with HDFs showed that adhesion of cells to the substrates at 37 °C can be tuned via the coating structure and that confluent HDF sheets can be harvested from the bottlebrush substrates at 20 °C via the temperature-induced rehydration of thermoresponsive OGEA side chains. Due to the broad spectrum of attainable properties, the coatings developed in this work constitute excellent prospects for cell sheet fabrication and as “smart” substrates for various tissue culture and biomedical applications. The versatility of the presented photografting process with respect to the copolymerization of OGEA macromonomers of different molecular weights and comonomer compositions potentially allows the manufacture of thermoresponsive coatings with finely tuned properties. In summary, the presented coating strategy does not only constitute an efficient and scalable process for the manufacture of PGE-based thermoresponsive coatings, but further embodies a method to extend the attainable coating properties in terms of introducing novel layer architectures. In the future, this might not only offer an extended applicability of PGE-based coatings for the fabrication of new types of cell sheets, but also enable an in-depth investigation of the underlying mechanism of cell sheet detachment, especially regarding the roles of temperature-induced macroscopic swelling versus changes in coating hydration on the nanoscale.

ASSOCIATED CONTENT

Supporting Information. Detailed description of materials and methods used, synthesis and characterization of OGEAs, detailed characterization of OGEA bottlebrushes via ellipsometry

and water CA measurements, bottlebrush coating morphology and material properties investigated by AFM, cell adhesion and detachment studies and viability assay.

ACKNOWLEDGEMENTS

M.W. is grateful to financial support from the Federal Ministry of Education and Research through grant FKZ: 13N13523. The authors thank Dr. Anke Hoppensack for proof reading this manuscript.

REFERENCES

- (1) Aguilar, M. R.; San Román, J., *Smart Polymers and Their Applications*. Woodhead Publishing: Kidlington, UK, 2014.
- (2) Wei, M.; Gao, Y.; Li, X.; Serpe, M. J. Stimuli-Responsive Polymers and Their Applications. *Polym. Chem.* **2017**, *8*, 127-143.
- (3) Stuart, M. A. C.; Huck, W. T. S.; Genzer, J.; Müller, M.; Ober, C.; Stamm, M.; Sukhorukov, G. B.; Szleifer, I.; Tsukruk, V. V.; Urban, M.; Winnik, F.; Zauscher, S.; Luzinov, I.; Minko, S. Emerging Applications of Stimuli-Responsive Polymer Materials. *Nat. Mater.* **2010**, *9*, 101.
- (4) Nagase, K.; Yamato, M.; Kanazawa, H.; Okano, T. Poly(*N*-Isopropylacrylamide)-based Thermoresponsive Surfaces Provide New Types of Biomedical Applications. *Biomaterials* **2018**, *153*, 27-48.
- (5) Tang, Z.; Okano, T. Recent Development of Temperature-Responsive Surfaces and Their Application for Cell Sheet Engineering. *Regener. Biomater.* **2014**, *1*, 91-102.
- (6) Matsuura, K.; Utoh, R.; Nagase, K.; Okano, T. Cell Sheet Approach for Tissue Engineering and Regenerative Medicine. *J. Controlled Release* **2014**, *190*, 228-239.
- (7) Elloumi-Hannachi, I.; Yamato, M.; Okano, T. Cell Sheet Engineering: A Unique Nanotechnology for Scaffold-Free Tissue Reconstruction with Clinical Applications in Regenerative Medicine. *J. Intern. Med.* **2010**, *267*, 54-70.
- (8) Nash, M. E.; Healy, D.; Carroll, W. M.; Elvira, C.; Rochev, Y. A. Cell and Cell Sheet Recovery from pNIPAm Coatings; Motivation and History to Present Day Approaches. *J. Mater. Chem.* **2012**, *22*, 19376-19389.
- (9) Kobayashi, J.; Okano, T. Thermoresponsive Thin Hydrogel-Grafted Surfaces for Biomedical Applications. *React. Funct. Polym.* **2013**, *73*, 939-944.
- (10) Tang, Z.; Akiyama, Y.; Okano, T. Recent Development of Temperature-Responsive Cell Culture Surface using Poly(*N*-Isopropylacrylamide). *J. Polym. Sci., Part B: Polym. Phys.* **2014**, *52*, 917-926.
- (11) Sheiko, S. S.; Sumerlin, B. S.; Matyjaszewski, K. Cylindrical Molecular Brushes: Synthesis, Characterization, and Properties. *Prog. Polym. Sci.* **2008**, *33*, 759-785.
- (12) Feng, C.; Li, Y.; Yang, D.; Hu, J.; Zhang, X.; Huang, X. Well-Defined Graft Copolymers: From Controlled Synthesis to Multipurpose Applications. *Chem. Soc. Rev.* **2011**, *40*, 1282-1295.
- (13) Verduzco, R.; Li, X.; Pesek, S. L.; Stein, G. E. Structure, Function, Self-Assembly, and Applications of Bottlebrush Copolymers. *Chem. Soc. Rev.* **2015**, *44*, 2405-2420.
- (14) Zhang, B.; Fischer, K.; Schmidt, M. Cylindrical Polypeptide Brushes. *Macromol. Chem. Phys.* **2005**, *206*, 157-162.

- (15) Chen, Y. Shaped Hairy Polymer Nanoobjects. *Macromolecules* **2012**, *45*, 2619-2631.
- (16) Lee, H.-i.; Pietrasik, J.; Sheiko, S. S.; Matyjaszewski, K. Stimuli-Responsive Molecular Brushes. *Prog. Polym. Sci.* **2010**, *35*, 24-44.
- (17) Li, C.; Gunari, N.; Fischer, K.; Janshoff, A.; Schmidt, M. New Perspectives for the Design of Molecular Actuators: Thermally Induced Collapse of Single Macromolecules from Cylindrical Brushes to Spheres. *Angew. Chem., Int. Ed.* **2004**, *43*, 1101-1104.
- (18) Pietrasik, J.; Sumerlin, B. S.; Lee, R. Y.; Matyjaszewski, K. Solution Behavior of Temperature-Responsive Molecular Brushes Prepared by ATRP. *Macromol. Chem. Phys.* **2007**, *208*, 30-36.
- (19) Yamamoto, S.-i.; Pietrasik, J.; Matyjaszewski, K. ATRP Synthesis of Thermally Responsive Molecular Brushes from Oligo(ethylene oxide) Methacrylates. *Macromolecules* **2007**, *40*, 9348-9353.
- (20) Li, X.; ShamsiJazeyi, H.; Pesek, S. L.; Agrawal, A.; Hammouda, B.; Verduzco, R. Thermoresponsive PNIPAAm Bottlebrush Polymers with Tailored Side-Chain Length and End-Group Structure. *Soft Matter* **2014**, *10*, 2008-2015.
- (21) Henn, D. M.; Fu, W.; Mei, S.; Li, C. Y.; Zhao, B. Temperature-Induced Shape Changing of Thermosensitive Binary Heterografted Linear Molecular Brushes between Extended Wormlike and Stable Globular Conformations. *Macromolecules* **2017**, *50*, 1645-1656.
- (22) Wang, S.; Liu, C.; Zhou, H.; Gao, C.; Zhang, W. An Efficient Route to Synthesize Thermoresponsive Molecular Bottlebrushes of Poly[O-Aminobenzyl Alcohol-Graft-Poly(N-Isopropylacrylamide)]. *Polym. Chem.* **2017**, *8*, 1932-1942.
- (23) Tang, Z.; Akiyama, Y.; Yamato, M.; Okano, T. Comb-Type Grafted Poly(N-Isopropylacrylamide) Gel Modified Surfaces for Rapid Detachment of Cell Sheet. *Biomaterials* **2010**, *31*, 7435-7443.
- (24) Mizutani, A.; Kikuchi, A.; Yamato, M.; Kanazawa, H.; Okano, T. Preparation of Thermoresponsive Polymer Brush Surfaces and their Interaction with Cells. *Biomaterials* **2008**, *29*, 2073-2081.
- (25) Fukumori, K.; Akiyama, Y.; Yamato, M.; Okano, T. A Facile Method for Preparing Temperature-Responsive Cell Culture Surfaces by using a Thioxanthone Photoinitiator immobilized on a Polystyrene Surface. *ChemNanoMat* **2016**, *2*, 454-460.
- (26) Dworak, A.; Utrata-Wesołek, A.; Szweda, D.; Kowalczyk, A.; Trzebicka, B.; Anioł, J.; Sieroń, A. L.; Klama-Baryła, A.; Kawecki, M. Poly[Tri(Ethylene Glycol) Ethyl Ether Methacrylate]-Coated Surfaces for Controlled Fibroblasts Culturing. *ACS Appl. Mater. Interfaces* **2013**, *5*, 2197-2207.
- (27) Kawecki, M.; Kraut, M.; Klama-Baryła, A.; Łabuś, W.; Kitala, D.; Nowak, M.; Glik, J.; Sieroń, A. L.; Utrata-Wesołek, A.; Trzebicka, B.; Dworak, A.; Szweda, D. Transfer of Fibroblast Sheets Cultured on Thermoresponsive Dishes with Membranes. *J. Mater. Sci.: Mater. Med.* **2016**, *27*, 111.
- (28) Dworak, A.; Utrata-Wesołek, A.; Oleszko, N.; Wałach, W.; Trzebicka, B.; Anioł, J.; Sieroń, A. L.; Klama-Baryła, A.; Kawecki, M. Poly(2-Substituted-2-Oxazoline) Surfaces for Dermal Fibroblasts Adhesion and Detachment. *J. Mater. Sci.: Mater. Med.* **2014**, *25*, 1149-1163.
- (29) Oleszko, N.; Wałach, W.; Utrata-Wesołek, A.; Kowalczyk, A.; Trzebicka, B.; Klama-Baryła, A.; Hoff-Lenczewska, D.; Kawecki, M.; Lesiak, M.; Sieroń, A. L.; Dworak, A. Controlling the Crystallinity of Thermoresponsive Poly(2-Oxazoline)-based Nanolayers to Cell Adhesion and Detachment. *Biomacromolecules* **2015**, *16*, 2805-2813.
- (30) Heinen, S.; Cuéllar-Camacho, J. L.; Weinhart, M. Thermoresponsive Poly(glycidyl ether) Brushes on Gold: Surface Engineering Parameters and Their Implication for Cell Sheet Fabrication. *Acta Biomater.* **2017**, *59*, 117-128.

- (31) Heinen, S.; Rackow, S.; Cuellar-Camacho, J. L.; Donskyi, I. S.; Unger, W. E. S.; Weinhart, M. Transfer of Functional Thermoresponsive Poly(glycidyl ether) Coatings for Cell Sheet Fabrication from Gold to Glass Surfaces. *J. Mater. Chem. B* **2018**, *6*, 1489-1500.
- (32) Stöbener, D. D.; Uckert, M.; Cuellar Camacho, J. L.; Hoppensack, A.; Weinhart, M. Ultrathin Poly(glycidyl ether) Coatings on Polystyrene for Temperature-Triggered Human Dermal Fibroblast Sheet Fabrication. *ACS Biomater. Sci. Eng.* **2017**, *3*, 2155-2165.
- (33) Stöbener, D. D.; Hoppensack, A.; Scholz, J.; Weinhart, M. Cell Sheet Fabrication from Self-Assembled Thermoresponsive Poly(glycidyl ether) Brushes – Approaching Vascular Tissue Engineering. **2018**, *submitted*.
- (34) Gunkel, G.; Weinhart, M.; Becherer, T.; Haag, R.; Huck, W. T. S. Effect of Polymer Brush Architecture on Antibiofouling Properties. *Biomacromolecules* **2011**, *12*, 4169-4172.
- (35) Su, Y.; Zhi, Z.; Gao, Q.; Xie, M.; Yu, M.; Lei, B.; Li, P.; Ma, P. X. Autoclaving-Derived Surface Coating with in Vitro and in Vivo Antimicrobial and Antibiofilm Efficacies. *Adv. Healthcare Mater.* **2017**, *6*, 1601173.
- (36) Gao, Q.; Yu, M.; Su, Y.; Xie, M.; Zhao, X.; Li, P.; Ma, P. X. Rationally Designed Dual Functional Block Copolymers for Bottlebrush-Like Coatings: In Vitro and in Vivo Antimicrobial, Antibiofilm, and Antifouling Properties. *Acta Biomater.* **2017**, *51*, 112-124.
- (37) Zhi, Z.; Su, Y.; Xi, Y.; Tian, L.; Xu, M.; Wang, Q.; Padidan, S.; Li, P.; Huang, W. Dual-Functional Polyethylene Glycol-b-Polyhexanide Surface Coating with in vitro and in vivo Antimicrobial and Antifouling Activities. *ACS Appl. Mater. Interfaces* **2017**, *9*, 10383-10397.
- (38) Stöbener, D. D.; Donath, D.; Weinhart, M. Fast and Solvent-Free Microwave-Assisted Synthesis of Thermoresponsive Oligo(glycidyl ether)s. **2018**, *submitted*.
- (39) Matuschewski, H.; Schedler, U. Method for Production of Plastic Article with Hydrophobic Graft Coating. WO 2014108278 A1, Jul 17, 2014.
- (40) Smith, P. A. S.; Most, E. E. Quaternary Hydrazones and Their Rearrangement. *J. Org. Chem.* **1957**, *22*, 358-362.
- (41) Aspnes, D. E.; Theeten, J. B.; Hottier, F. Investigation of Effective-Medium Models of Microscopic Surface Roughness by Spectroscopic Ellipsometry. *Phys. Rev. B* **1979**, *20*, 3292-3302.
- (42) Allmér, K.; Hult, A.; Rånby, B. Surface Modification of Polymers. II. Grafting with Glycidyl Acrylates and the Reactions of the Grafted Surfaces with Amines. *J. Polym. Sci., Part A: Polym. Chem.* **1989**, *27*, 1641-1652.
- (43) Li, G.; He, G.; Zheng, Y.; Wang, X.; Wang, H. Surface Photografting Initiated by Benzophenone in Water and Mixed Solvents Containing Water and Ethanol. *J. Appl. Polym. Sci.* **2012**, *123*, 1951-1959.
- (44) Deng, J.-P.; Yang, W.-T.; Rånby, B. Surface Photograft Polymerization of Vinyl Acetate on Low Density Polyethylene Film. Effects of Solvent. *Polym. J.* **2000**, *32*, 834.
- (45) Labbé, A.; Carlotti, S.; Deffieux, A.; Hirao, A. Controlled Polymerization of Glycidyl Methyl Ether Initiated by Onium Salt/Triisobutylaluminum and Investigation of the Polymer LCST. *Macromol. Symp.* **2007**, *249-250*, 392-397.
- (46) Yang, W.; Rånby, B. Bulk Surface Photografting Process and Its Applications. I. Reactions and Kinetics. *J. Appl. Polym. Sci.* **1996**, *62*, 533-543.
- (47) Yang, W.; Rånby, B. Bulk Surface Photografting Process and Its Applications. II. Principal Factors Affecting Surface Photografting. *J. Appl. Polym. Sci.* **1996**, *62*, 545-555.
- (48) Yang, W. T.; Rånby, B. Bulk Surface Photografting Process and Its Application. III. Photolamination of Polymer Films. *J. Appl. Polym. Sci.* **1997**, *63*, 1723-1732.
- (49) Wang, H.; Brown, H. R. Lamination of High-Density Polyethylene by Bulk Photografting and the Mechanism of Adhesion. *J. Appl. Polym. Sci.* **2005**, *97*, 1097-1106.
- (50) Han, J.; Wang, X.; Wang, H. Superhydrophobic Surface Fabricated by Bulk Photografting of Acrylic Acid onto High-Density Polyethylene. *J. Colloid Interface Sci.* **2008**, *326*, 360-365.

- (51) Castell, P.; Wouters, M.; With, G. d.; Fischer, H.; Huijs, F. Surface Modification of Poly(propylene) by Photoinitiators: Improvement of Adhesion and Wettability. *J. Appl. Polym. Sci.* **2004**, *92*, 2341-2350.
- (52) Utrata-Wesołek, A.; Trzcińska, R.; Galbas, K.; Trzebicka, B.; Dworak, A. Photodegradation of Polyglycidol in Aqueous Solutions Exposed to UV Irradiation. *Polym. Degrad. Stab.* **2011**, *96*, 907-918.
- (53) Utrata-Wesołek, A.; Żymełka-Miara, I.; Kowalczyk, A.; Trzebicka, B.; Dworak, A. Photocrosslinking of Polyglycidol and Its Derivative: Route to Thermoresponsive Hydrogels. *Photochem. Photobiol.* **2018**, *94*, 52-60.
- (54) Piletsky, S. A.; Matuschewski, H.; Schedler, U.; Wilpert, A.; Piletska, E. V.; Thiele, T. A.; Ulbricht, M. Surface Functionalization of Porous Polypropylene Membranes with Molecularly Imprinted Polymers by Photograft Copolymerization in Water. *Macromolecules* **2000**, *33*, 3092-3098.
- (55) Yu, H.-Y.; Xu, Z.-K.; Lei, H.; Hu, M.-X.; Yang, Q. Photoinduced Graft Polymerization of Acrylamide on Polypropylene Microporous Membranes for the Improvement of Antifouling Characteristics in a Submerged Membrane-Bioreactor. *Sep. Purif. Technol.* **2007**, *53*, 119-125.
- (56) Heinen, S.; Weinhart, M. Poly(glycidyl ether)-based Monolayers on Gold Surfaces: Control of Grafting Density and Chain Conformation by Grafting Procedure, Surface Anchor, and Molecular Weight. *Langmuir* **2017**, *33*, 2076-2086.
- (57) Becherer, T.; Heinen, S.; Wei, Q.; Haag, R.; Weinhart, M. In-Depth Analysis of Switchable Glycerol Based Polymeric Coatings for Cell Sheet Engineering. *Acta Biomater.* **2015**, *25*, 43-55.
- (58) Li, X.; Prukop, S. L.; Biswal, S. L.; Verduzco, R. Surface Properties of Bottlebrush Polymer Thin Films. *Macromolecules* **2012**, *45*, 7118-7127.
- (59) Du, B.; Tsui, O. K. C.; Zhang, Q.; He, T. Study of Elastic Modulus and Yield Strength of Polymer Thin Films Using Atomic Force Microscopy. *Langmuir* **2001**, *17*, 3286-3291.
- (60) Ghorbal, A.; Brahim, A. B. Evaluation of Nanotribological Behavior of Amorphous Polystyrene: The Macromolecular Weight Effect. *Polym. Test.* **2013**, *32*, 1174-1180.

Supporting Information (SI) for the following manuscript

Switchable Oligo(glycidyl ether) Acrylate
Bottlebrushes “Grafted-from” Polystyrene Surfaces
- A Versatile Strategy towards Functional Cell
Culture Substrates

Daniel David Stöbener[†], Johanna Scholz[†], Uwe Schedler^{†,‡}, Marie Weinhart^{†}*

[†]Institute for Chemistry and Biochemistry, Freie Universität Berlin, Takustr. 3, D-14195
Berlin, Germany.

[‡]PolyAn GmbH, Rudolf-Baschant-Straße 2, 13086 Berlin, Germany.

*Corresponding author: e-mail: marie.weinhart@fu-berlin.de, phone: +49 30 838 75050

Keywords

Surface-initiated free radical polymerization, bulk photografting, molecular brushes,
thermoreponsive macromonomers, switchable surface, cell sheet detachment

Materials

Materials for synthesis and surface modification. All chemicals and solvents were supplied by Sigma Aldrich (Steinheim, Germany) and used without further purification unless otherwise stated. GME and EGE were supplied by TCI GmbH (Eschborn, Germany), dried and distilled over CaH_2 and stored over 3 Å molecular sieve. CaH_2 (93%) and benzophenone (BP, 99%) were purchased from Acros Organics (Geel, Belgium). EtOK (24 wt.-% in EtOH), triethylamine (TEA, $\geq 99.5\%$) and acrylic acid chloride (AAC, 98%) were acquired from Sigma-Aldrich (Steinheim, Germany). Sodium sulfate (Na_2SO_4 , 99%) and 3 Å molecular sieve were purchased from Carl Roth GmbH + Co. KG (Karlsruhe, Germany). Sodium bicarbonate (NaHCO_3 , 99.5%) was supplied by Grüssing GmbH Analytica (Filsum, Germany). THF was predried via the solvent system MB SPS-800 from M. Braun GmbH (Garching, Germany), refluxed with elemental sodium and a pinch of benzophenone and subsequently distilled on 3 Å molecular sieve before use. Diethyl ether (Et_2O) was purchased from VWR Chemicals (Fontenay-sous-Bois, France or Leuven, Belgium) and distilled before use to remove BHT stabilizer. Ethanol was distilled under reduced pressure before use to remove impurities. Silicon (Si) wafers cut in to pieces (11 x 11 mm) were supplied by Silchem GmbH (Freiberg, Germany) and washed with ethanol and dried under a stream of N_2 .

Materials for cell culture. Falcon[®] PS culture dishes (d = 35 mm) were purchased from Th. Geyer GmbH & Co. KG (Berlin, Germany) and tissue culture PS (d = 35 mm) were supplied by VWR International (Leuven, Belgium). Dulbecco's modified Eagle medium (DMEM 4.5 g/L glucose #31966-021 and DMEM 1 g/L glucose #21885108), dispase II (#17105-041), Penicillin-Streptomycin (#15140122), and trypsin/EDTA solution (#15400054) were purchased from Thermo Fisher Scientific (Darmstadt, Germany). Accutase[®] solution (#A6964), propidium iodide (#P4170) and fluorescein diacetate (#F7378) were supplied by Sigma Aldrich (Steinheim, Germany). Fetal bovine serum was purchased from PAN-Biotech GmbH (#P30-3306, Aidenbach, Germany) and from Biochrom (#S 0615, Berlin, Germany). Collagenase

NB4 (#17454) was supplied by Serva GmbH (Halle, Germany). All further expendable cell culture materials were purchased from Sarstedt (Nümbrecht, Germany).

Methods

Polymer Synthesis and Characterization. Polymerizations were carried out in a “Plazmatronika” multi-mode microwave reactor (Warsaw, Poland) with a frequency of 2.45 GHz and a maximum power of 300 W. Oligomers were centrifuged at 0 °C and 10000 rpm for 20 min using a Rotina 380 R centrifuge from Hettich GmbH & Co.KG (Tuttlingen, Germany). ¹H and ¹³C NMR spectra were recorded on a Joel ECX at 400 MHz and 100 MHz, respectively, and processed with the software MestReNova (version 7.1.2). Chemical shifts were reported in δ (ppm) and referenced to the respective deuterated solvent peak (CDCl₃). Gel permeation chromatography (GPC) was conducted in tetrahydrofuran (THF) as eluent at a concentration of 3.5 mg mL⁻¹ and a flow rate of 1 mL min⁻¹ at 25 °C using an Agilent 1100 Series instrument. Three 7.5 x 300 mm PLgel (PSS, Mainz, Germany, particle size: 5 μ m) mixed-C columns (Agilent, Waldbronn, Germany) were used in-line. Calibration was performed with PS standards from PSS (Mainz, Germany), a refractive index (RI) detector was used and calculations were performed with PSS Win-GPC software.

Surface Modification and Characterization. A WS-650-23 spin coater from Laurell Technologies Corporation (North Wales, PA, USA) was used for spin coating. PS solutions were prepared using PS from Falcon[®] culture dishes ($M_n=132$ g mol⁻¹, PDI=1.9) supplied by Th. Geyer GmbH & Co. KG (Berlin, Germany). Static water contact angles (CAs) were measured using the sessile drop method using an OCA contact angle system from DataPhysics Instruments GmbH (Filderstadt, Germany). CAs were determined before and after surface functionalization and fitted with the software SCA202 (version 3.12.11). For fitting, the Young-Laplace model was applied on a drop of Milli-Q water (2 μ L) which was placed onto the respective surface. Temperature-dependent CA measurements were performed in a tempered

humidity chamber. Samples were equilibrated for at least 30 min at 37 °C and a drop of Milli-Q water (2 μ L) was dispensed and immediately deposited on the samples. To test for homogeneity and reproducibility, on each sample, CAs on at least three different spots and at least four independent substrates ($n = 4$) were measured. To determine the dry layer thickness of the coatings, spectroscopic ellipsometry was applied at an incident angle of 70° using a SENpro spectroscopic ellipsometer from SENTECH Instruments GmbH (Berlin, Germany). The thickness of the SiO₂ layer and of the spin-coated PS layer were determined separately and respective average values of at least three different spots on the surface were taken and their average values were fixed for the subsequent modeling of the adsorbed BP and spin coated OGEA layers. The thickness of the adsorbed BP intermediate layer was measured and a Cauchy layer with a fixed refractive index of 1.601 averaged from literature values was used for fitting.¹ OGEA layer thicknesses were modeled using the Bruggeman effective medium approximation (EMA)² and fitted assuming mixtures of OGEA bottlebrushes with air or water. For photografting, samples with spin coated OGEA layers were irradiated with UV light using a UV-KUB 2 from KLOÉ (Montpellier, France) with a wavelength of 365 nm and an irradiance of 25 mW cm⁻² (100%) for 15-30 min. AFM measurements were performed on an AFM Nanoscope MultiMode 8 equipped with a fluid cell and a thermal application (TA) controller from Bruker (Billerica, MA, USA). The morphology and material properties of the PGE-3.0 coatings was measured in PeakForce QNM (Quantitative NanoMechanics) mode. Coated Si wafers were mounted on the AFM head, degassed Milli-Q water was inserted into the liquid cell and the TA controller was set to the desired temperature (37 or 20 °C) and equilibrated for at least 10 min prior to each measurement. To obtain high resolution images with reduced sample damage, SNL-10 cantilevers from Bruker (Billerica, MA, USA) with a nominal spring constant of 0.3 N m⁻¹ and a tip radius of 2-12 nm were used, and images were recorded with a loading peak force of 500 pN, 512 points per line and scan rates of 1.0 Hz. Obtained images were analyzed with the Nanoscope analysis software (version 1.4) and processed using 1st order

flattening. Roughness and depth analysis tools were used to obtain the surface parameters. Microscopic images of HDFs were taken on a Zeiss Observer Z1 from Carl Zeiss Microscopy GmbH (Jena, Germany). The software Zen 2 Version 2.0.0.0 from Carl Zeiss Microscopy GmbH (Jena, Germany) was used for evaluation. A Nikon D3100 from Nikon GmbH (Düsseldorf, Germany) was used to take macroscopic photographs of the culture substrates.

Synthesis of the Oligo(glycidyl ether)s

Oligo(glycidyl ether)s (OGE)s were synthesized in bulk via oxy-anionic ROP using microwave- or conventional heating according to the following procedure. A 50 mL Schlenk flask equipped with a magnetic stir bar and a rubber septum was flame-dried and flushed with argon at least three times. The flask was loaded with the EtOK initiator solution and the solvent EtOH was removed by distillation. The remaining initiator salt was dried under high vacuum at 80 °C for 2 h and kept under an inert argon atmosphere. The Schlenk flask was cooled down to 20 °C using a water bath and the monomers GME and EGE were added to dissolve the initiator. For the synthesis of OGEs with a targeted molecular weight of 1 kDa, homogeneous solutions were obtained after 2 h. Subsequently, the flask was placed in a multi-mode microwave reactor and the solution was heated under constant stirring utilizing three irradiation cycles. Each irradiation cycle consisted of three 1 min heating periods at a power of 50% each (150 W), which were followed by 2 min cooling periods at a power of 0% (0 W). In case OGEs with a molecular weight of 500 Da were targeted, the monomer/initiator mixture was stirred for 2 h at 20 °C, slowly heated up to 50 °C within a period of 1 h until the suspension turned into a homogeneous solution, and stirred overnight (20 h) at 50 °C. The reaction mixtures were cooled to rt., quenched with Milli-Q water (1 mL) and stirred for 30 min. The products were dissolved in Et₂O (10-20 mL), dried over anhydrous Na₂SO₄ and filtered. After storing the solutions in the fridge overnight, potassium salts were centrifuged off and the polymer solutions were decanted. The solvent was evaporated, and viscous, slightly yellow oils were obtained.

OGE **1** (1 kDa, GME:EGE = 1:3, end groups: EtO/OH). EtOK (2.0 mL, 5.0 mmol), GME (1.1 mL, 12.7 mmol), EGE (4.1 mL, 38.0 mmol). Yield: 4.91 g (98%). $^1\text{H-NMR}$ (400 MHz; CDCl_3): δ 3.91 (s, 1 H, CH_2OH); 3.76-3.38 (m, 46 H, polymer backbone + OCH_2CH_3); 3.32 (s, 11 H, OCH_3); 1.18-1.14 (m, 12 H, OCH_2CH_3) ppm. $^{13}\text{C-NMR}$ (101 MHz; CDCl_3): δ 78.9-78.6 ($\text{CH}_2\text{CH}(\text{CH}_2\text{OR})\text{O}$); 72.9-72.6 ($\text{CH}(\text{CH}_2\text{OCH}_3)$); 71.7-71.6 ($\text{CH}_2\text{CH}(\text{CH}_2\text{OR})\text{OH}$); 71.0-69.7 ($\text{CH}_2\text{CH}(\text{CH}_2\text{OR})\text{O} + \text{CH}_3\text{CH}_2\text{OCH}_2\text{CH}(\text{CH}_2\text{OR})\text{O} + \text{CH}_2\text{CH}(\text{CH}_2\text{OR})\text{OH}$); 66.9-66.8 (OCH_2CH_3); 59.3 (OCH_3); 15.3 (OCH_2CH_3) ppm.

OGE **2** (1 kDa, GME:EGE = 1:1, end groups: EtO/OH). EtOK (2.0 mL, 5.0 mmol), GME (2.4 mL, 26.3 mmol), EGE (2.9 mL, 26.3 mmol). Yield: 4.75 g (95%). $^1\text{H-NMR}$ (400 MHz; CDCl_3): δ 3.90 (s, 1 H, CH_2OH); 3.76-3.42 (m, 58 H, polymer backbone + OCH_2CH_3); 3.32 (s, 7 H, OCH_3); 1.19-1.14 (m, 20 H, OCH_2CH_3) ppm. $^{13}\text{C-NMR}$ (101 MHz; CDCl_3): δ 79.6-78.9 ($\text{CH}_2\text{CH}(\text{CH}_2\text{OR})\text{O}$); 73.0-72.8 ($\text{CH}(\text{CH}_2\text{OCH}_3)$); 71.7-71.6 ($\text{CH}_2\text{CH}(\text{CH}_2\text{OR})\text{OH}$); 71.0-69.6 ($\text{CH}_2\text{CH}(\text{CH}_2\text{OR})\text{O} + \text{CH}_3\text{CH}_2\text{OCH}_2\text{CH}(\text{CH}_2\text{OR})\text{O} + \text{CH}_2\text{CH}(\text{CH}_2\text{OR})\text{OH}$); 66.8 (OCH_2CH_3); 59.3 (OCH_3); 15.3 (OCH_2CH_3) ppm.

OGE **3** (0.5 kDa, GME:EGE = 1:1, end groups: EtO/OH). EtOK (2.0 mL, 5.0 mmol), GME (2.4 mL, 26.3 mmol), EGE (2.9 mL, 26.3 mmol). Yield: 4.84 g (97%). $^1\text{H-NMR}$ (400 MHz; CDCl_3): δ 3.90 (s, 1 H, CH_2OH); 3.75-3.42 (m, 62 H, polymer backbone + OCH_2CH_3); 3.32 (s, 5 H, OCH_3); 1.19-1.14 (m, 23 H, OCH_2CH_3) ppm. $^{13}\text{C-NMR}$ (101 MHz; CDCl_3): δ 79.6-78.9 ($\text{CH}_2\text{CH}(\text{CH}_2\text{OR})\text{O}$); 73.0-72.5 ($\text{CH}(\text{CH}_2\text{OCH}_3)$); 71.7-71.6 ($\text{CH}_2\text{CH}(\text{CH}_2\text{OR})\text{OH}$); 71.0-69.7 ($\text{CH}_2\text{CH}(\text{CH}_2\text{OR})\text{O} + \text{CH}_3\text{CH}_2\text{OCH}_2\text{CH}(\text{CH}_2\text{OR})\text{O} + \text{CH}_2\text{CH}(\text{CH}_2\text{OR})\text{OH}$); 66.8 (OCH_2CH_3); 59.3 (OCH_3); 15.3 (OCH_2CH_3) ppm.

Synthesis of Oligo(glycidyl ether) Acrylates

OGEs were dried in a Schlenk flask at 70 °C under high vacuum for 2 h. The oligomers were dissolved in dry THF, TEA was added, and the reaction mixtures were cooled to 0 °C using an ice bath. AAC was added dropwise, the flasks were wrapped in aluminum foil and the reaction

mixtures were stirred overnight (20 h) while warming to rt. (20 °C). After adding Milli-Q water (1 mL) and stirring at rt for 30 min to hydrolyze excess AAC, the products were dissolved in Et₂O (20 mL) and salts as well as the excess of the formed acrylic acid were extracted with aqueous, saturated NaHCO₃ at least three times. The organic phase was collected, dried over anhydrous Na₂SO₄, filtered, and the solvent was evaporated under reduced pressure while protecting the macromonomers from light to prevent premature polymerization. Slightly viscous, yellow oils were obtained.

OGEA **1** (1 kDa, GME:EGE = 1:3, end groups: EtO/OC(O)CHCH₂). OGE **1** (3 g, 3 mmol), AAC (0.37 mL, 4.5 mmol), TEA (0.64 mL, 4.5 mmol), THF (10 mL). Yield: 87%. Conversion: 95%. ¹H-NMR (400 MHz; CDCl₃): δ 6.38 (dd, 1 H, OC(O)CHCH₂); 6.11 (dd, 1 H, OC(O)CHCH₂); 5.79 (dd, 1 H, OC(O)CHCH₂); 5.13 (m, 1 H, CHROC(O)CHCH₂); 3.76-3.38 (m, 46 H, polymer backbone + OCH₂CH₃); 3.32 (s, 11 H, OCH₃); 1.18-1.14 (m, 12 H, OCH₂CH₃) ppm. ¹³C-NMR (101 MHz; CDCl₃): δ 165.7 (OC(O)CHCH₂); 130.9 (OC(O)CHCH₂); 128.7 (OC(O)CHCH₂); 78.9-78.6 (CH₂CH(CH₂OR)O) + CH₂CH(CH₂OR)OC(O)CHCH₂); 73.9-73.8 (CH(CH₂OR)OH); 72.9-72.6 (CH(CH₂OCH₃); 71.7-71.6 (CH₂CH(CH₂OR)OH); 71.0-69.7 (CH₂CH(CH₂OR)O) + CH₃CH₂OCH₂CH(CH₂OR)O + CH₂CH(CH₂OR)OH); 66.9-66.8 (OCH₂CH₃); 59.3 (OCH₃); 15.3 (OCH₂CH₃) ppm.

OGEA **2** (1 kDa, GME:EGE = 1:1, end groups: EtO/OC(O)CHCH₂). OGE **2** (3 g, 3 mmol), AAC (0.37 mL, 4.5 mmol), TEA (0.64 mL, 4.5 mmol), THF (10 mL). Yield: 82%. Conversion: 94%. ¹H-NMR (400 MHz; CDCl₃): δ 6.40 (dd, 1 H, OC(O)CHCH₂); 6.13 (dd, 1 H, OC(O)CHCH₂); 5.80 (dd, 1 H, OC(O)CHCH₂); 5.15 (m, 1 H, CHROC(O)CHCH₂); 3.76-3.38 (m, 74 H, polymer backbone + OCH₂CH₃); 3.32 (s, 8 H, OCH₃); 1.18-1.14 (m, 26 H, OCH₂CH₃) ppm. ¹³C-NMR (101 MHz; CDCl₃): δ 165.7 (OC(O)CHCH₂); 130.9 (OC(O)CHCH₂); 128.7 (OC(O)CHCH₂); 78.9-78.6 (CH₂CH(CH₂OR)O + CH₂CH(CH₂OR)OC(O)CHCH₂); 73.9-73.8

(CH(CH₂OR)OH); 72.9-72.6 (CH(CH₂OCH₃); 71.7-71.6 (CH₂CH(CH₂OR)OH); 71.0-69.7 (CH₂CH(CH₂OR)O + CH₃CH₂OCH₂CH(CH₂OR)O + CH₂CH(CH₂OR)OH); 66.9-66.8 (OCH₂CH₃); 59.3 (OCH₃); 15.3 (OCH₂CH₃) ppm.

OGEA **3** (0.5 kDa, GME:EGE = 1:1, end groups: EtO/OC(O)CHCH₂). OGE **3** (4 g, 8 mmol), AAC (1.0 mL, 12.1 mmol), TEA (1.67 mL, 12.1 mmol), THF (10 mL). Yield: 80%. Conversion: 96%. ¹H-NMR (400 MHz; CDCl₃): δ 6.38 (dd, 1 H, OC(O)CHCH₂); 6.11 (dd, 1 H, OC(O)CHCH₂); 5.79 (dd, 1 H, OC(O)CHCH₂); 5.13 (m, 1 H, CHROC(O)CHCH₂); 3.76-3.38 (m, 46 H, polymer backbone + OCH₂CH₃); 3.32 (s, 11 H, OCH₃); 1.18-1.14 (m, 12 H, OCH₂CH₃) ppm. ¹³C-NMR (101 MHz; CDCl₃): δ 165.7 (OC(O)CHCH₂); 130.9 (OC(O)CHCH₂); 128.7 (OC(O)CHCH₂); 78.9-78.6 (CH₂CH(CH₂OR)O + CH₂CH(CH₂OR)OC(O)CHCH₂); 73.9-73.8 (CH(CH₂OR)OH); 72.9-72.6 (CH(CH₂OCH₃); 71.7-71.6 (CH₂CH(CH₂OR)OH); 71.0-69.7 (CH₂CH(CH₂OR)O + CH₃CH₂OCH₂CH(CH₂OR)O + CH₂CH(CH₂OR)OH); 66.9-66.8 (OCH₂CH₃); 59.3 (OCH₃); 15.3 (OCH₂CH₃) ppm.

Characterization of OGEA Bottlebrushes via Ellipsometry and Water CA Measurements

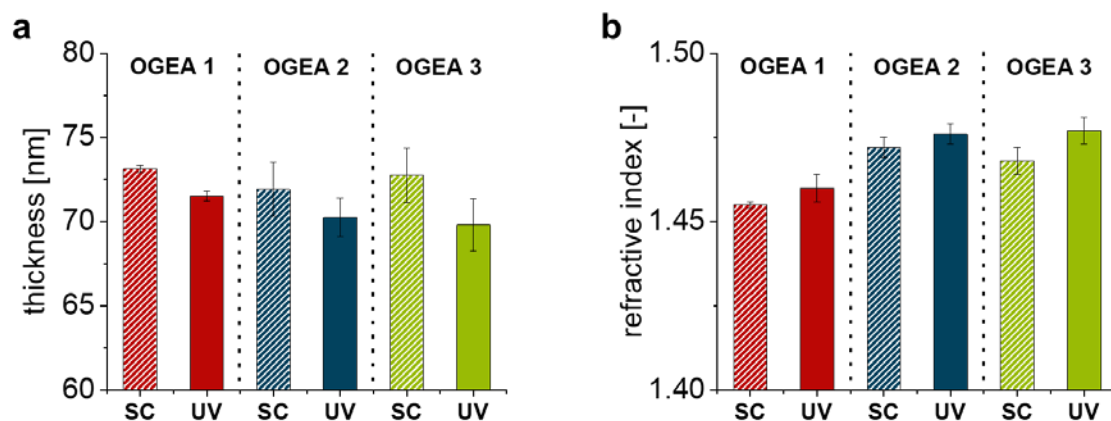


Figure S1. Layer thickness (a) and refractive index (b) of OGEA films after spin coating (SC) and after irradiation with UV light for 15 min determined by ellipsometry (N = 3, error bars indicate SEM).

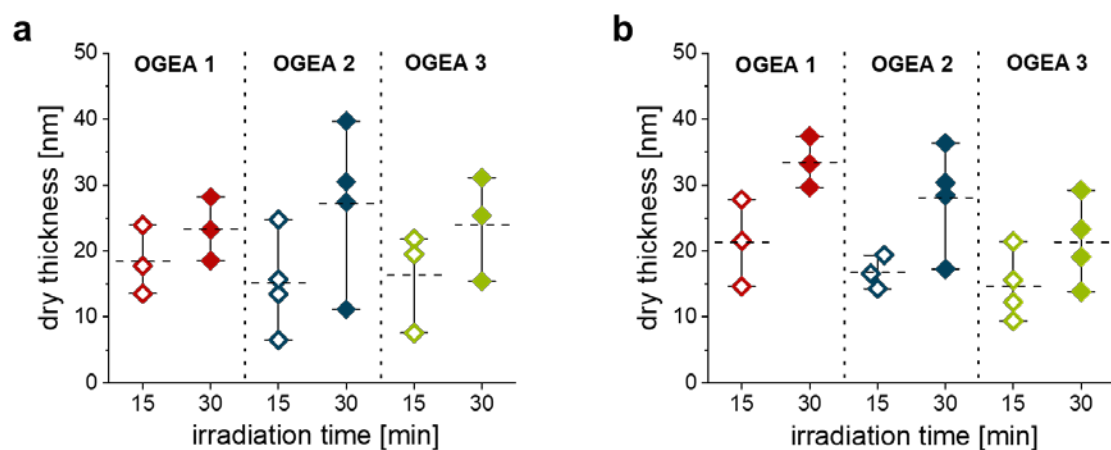


Figure S2. Dry layer thickness of bottlebrush coatings prepared by irradiation of bulk OGEA films with UV light for 15 and 30 min directly after spin coating (a) and after a 3 h resting period (b) determined by ellipsometry. Thicknesses are plotted for each replicate together with their mean value (dashed line) and their 90% confidence interval (whiskers).

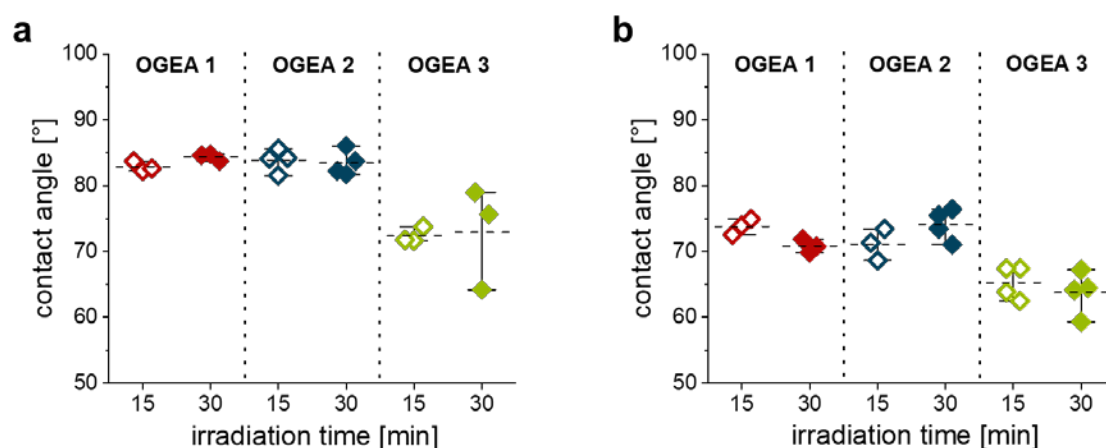


Figure S3. Static water CAs of bottlebrush coatings prepared by irradiation of bulk OGEA films with UV light for 15 and 30 min directly after spin coating (a) and after a 3 h resting period (b) determined by the sessile drop method (2 μ L). CAs are plotted for each replicate together with their mean value (dashed line) and their 90% confidence interval (whiskers).

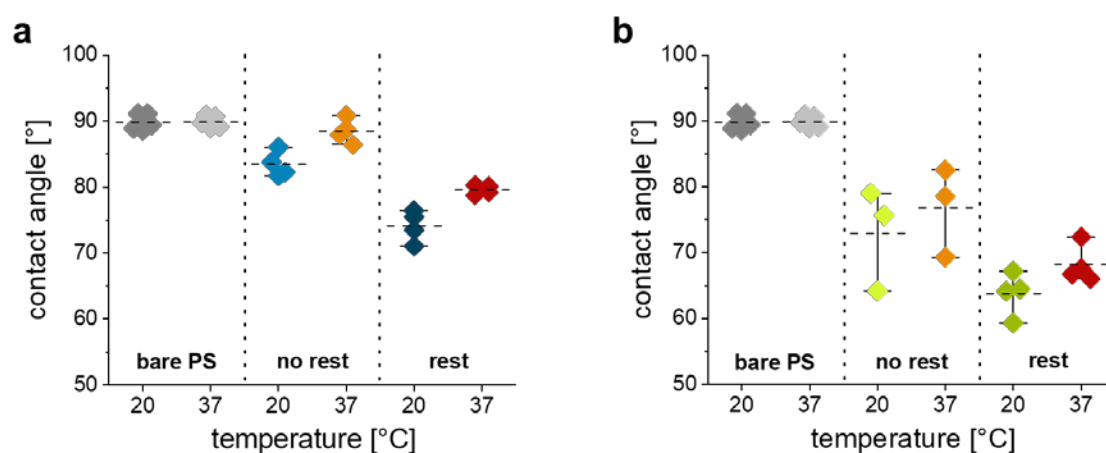


Figure S4. Temperature-dependent static water CAs of OGEA 2 (a) and OGEA 3 (b) irradiated with UV light for 30 min determined by the sessile drop method (2 μ L) using a tempered humidity chamber. Bare PS substrates are shown as controls. CAs are plotted for each replicate together with their mean value (dashed line) and their 90% confidence interval (whiskers).

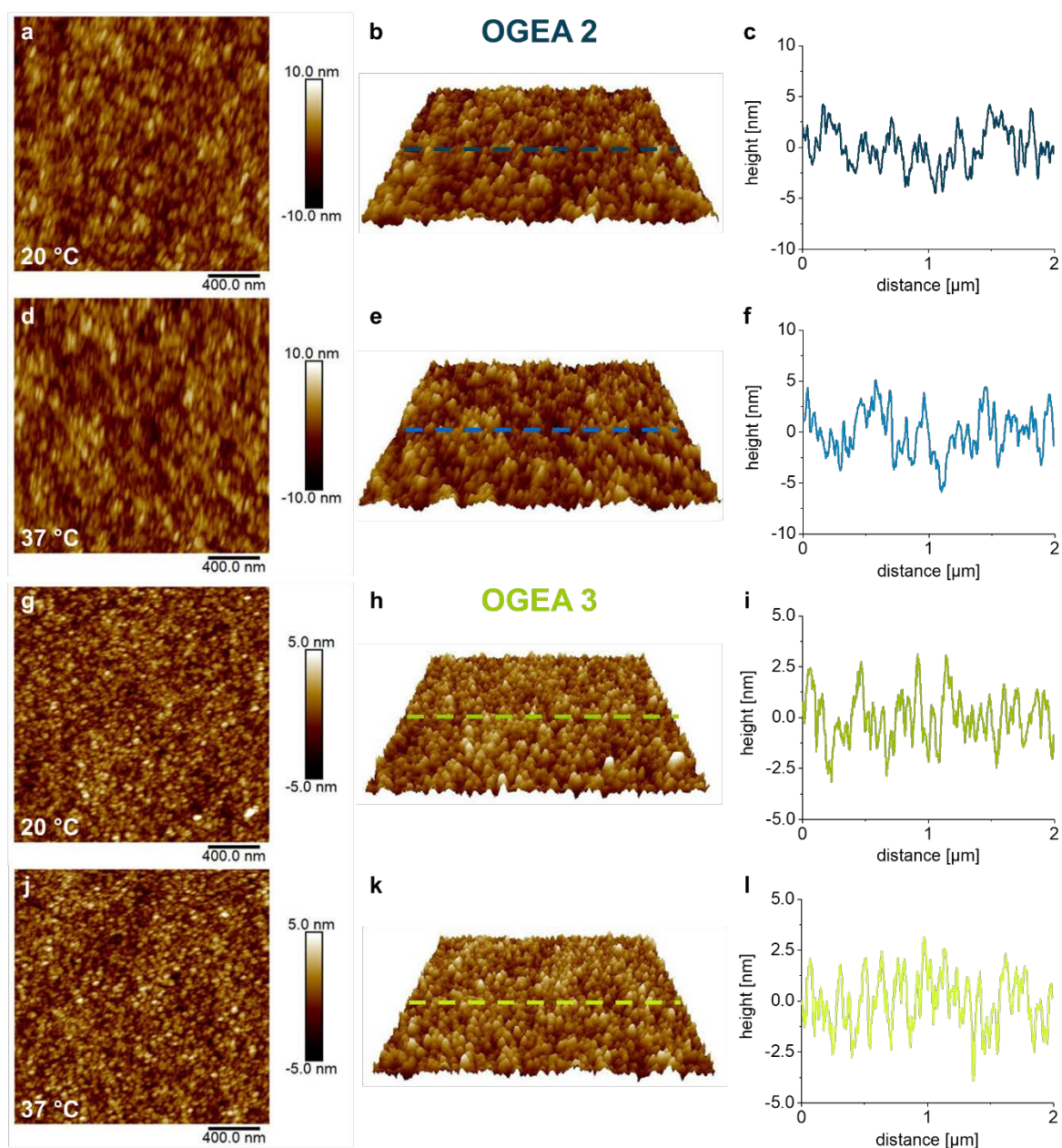
Bottlebrush Coating Morphology and Material Properties by AFM in QNM Mode

Figure S5. 2D and 3D surface topography and cross section profiles of 2 μm images of OGEA 2 coatings at 20 °C (a, b, c) and 37 °C (d, e, f) as well as OGEA 3 coatings at 20 °C (g, h, i) and 37 °C (j, k, l) on PS-coated Si wafers prepared via 15 min UV-irradiation and measured in Milli-Q water by AFM in QNM mode.

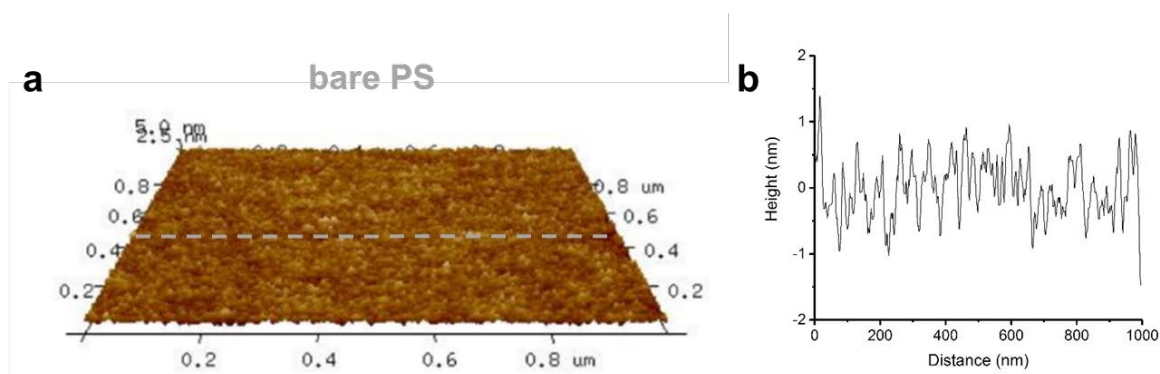


Figure S6. 3D surface topography (a) and cross section profile (b) of a 1 μm images of bare PS spin-coated on a Si wafer measured in Milli-Q water at 20 $^{\circ}\text{C}$ using AFM in QNM mode.

Table S1. Main roughness parameters obtained from 5 and 2 μm QNM images measured by AFM. Values for the root-mean squared roughness R_q , mean roughness R_a , and maximal roughness R_{max} (peak to valley vertical variation) in Milli-Q water at 20 and 37 $^{\circ}\text{C}$ for OGEA **2** and **3** coatings grafted for 15 and 30 min ($N = 3$).

OGEA	t [min]	T [$^{\circ}\text{C}$]	$R_q \pm \text{SD}$ [nm]	$R_a \pm \text{SD}$ [nm]	$R_{\text{max}} \pm \text{SD}$ [nm]
2	15	20	2.12 ± 0.09	1.68 ± 0.06	13.28 ± 1.12
		37	2.30 ± 0.25	1.80 ± 0.14	26.67 ± 1.48
	30	20	2.86 ± 0.46	2.23 ± 0.39	31.65 ± 9.24
		37	2.94 ± 0.38	2.34 ± 0.31	22.78 ± 11.16
3	15	20	1.27 ± 0.07	1.01 ± 0.05	24.06 ± 9.72
		37	1.25 ± 0.05	0.99 ± 0.03	16.34 ± 7.07
	30	20	1.09 ± 0.01	0.87 ± 0.01	12.00 ± 2.17
		37	1.12 ± 0.02	0.89 ± 0.02	9.43 ± 1.46

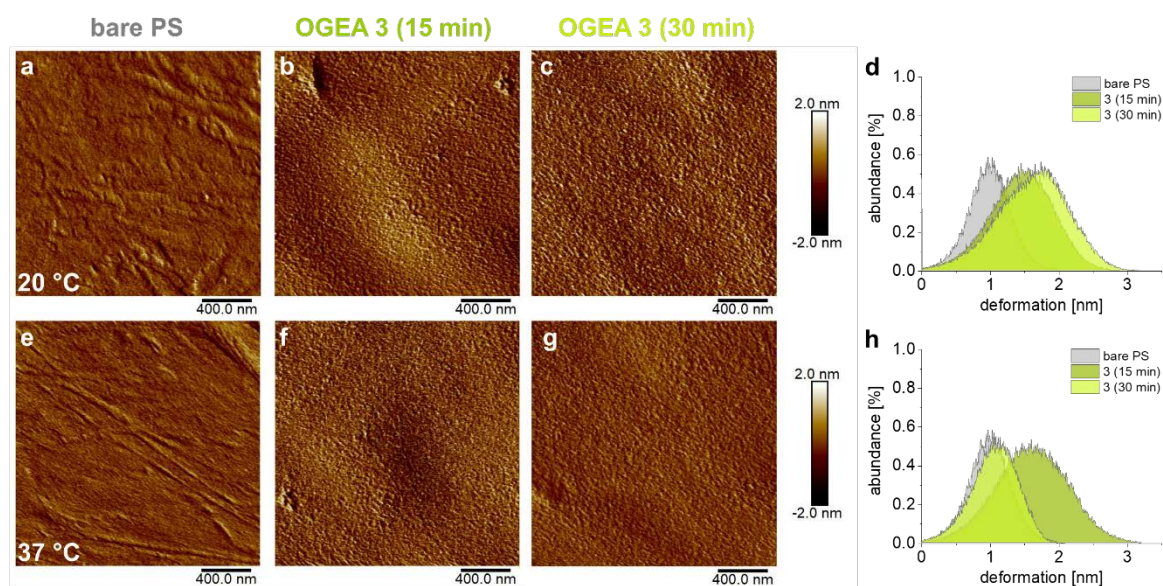


Figure S7. Representative deformation images (2 μm) of a bare PS culture dish (a, e) in comparison to PS culture dishes photografted with OGEA 3 for 15 min (b, f) and 30 min (c, g) measured in Milli-Q water at 20 (a, b, c) and 37 °C (e, f, g) by AFM in QNM mode and associated comparative depth histograms (d, h).

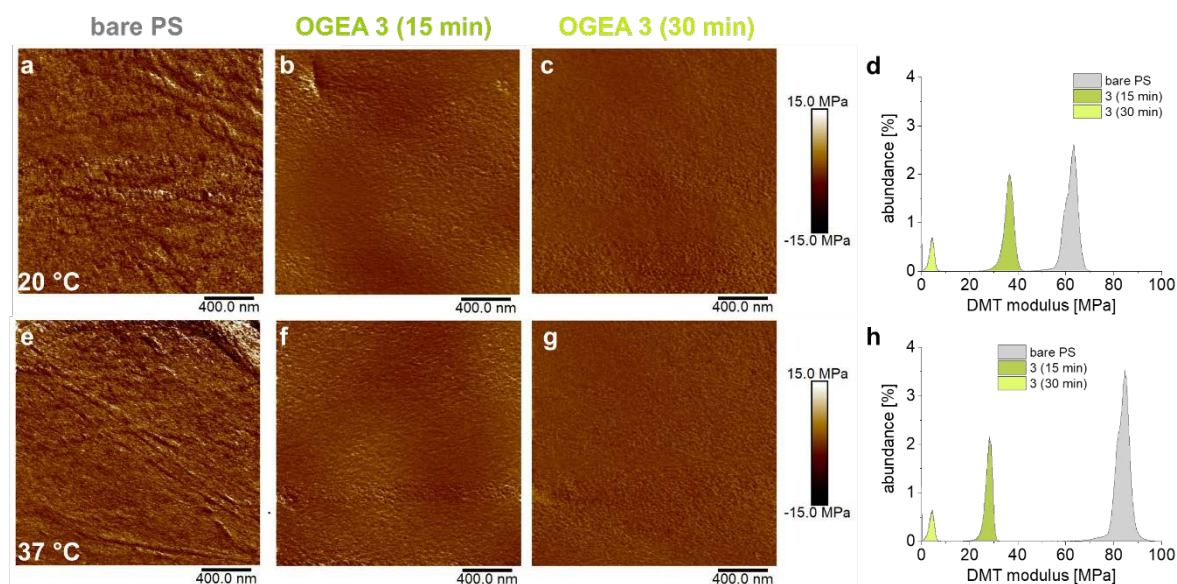


Figure S8. Representative images (2 μm) of the Young's modulus (DMT modulus) of a bare PS culture dish (a, e) in comparison to PS culture dishes photografted with OGEA 3 for 15 min (b, f) and 30 min (c, g) measured in Milli-Q water at 20 (a, b, c) and 37 °C (e, f, g) by AFM in QNM mode and associated comparative depth histograms (d, h).

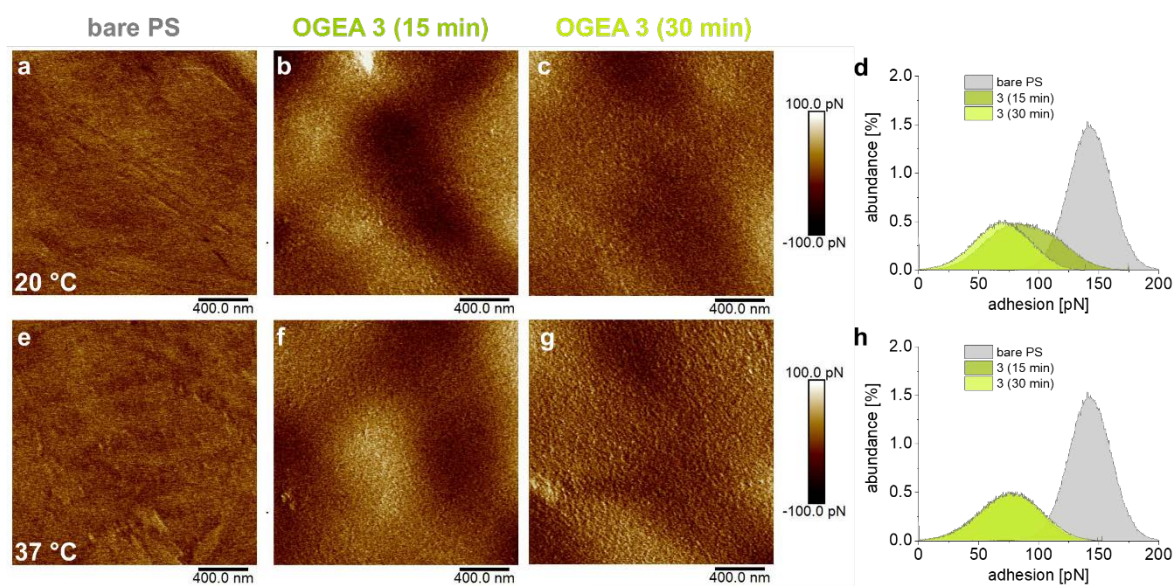


Figure S9. Representative adhesion images (2 μm) of a bare PS culture dish (a, e) in comparison to PS culture dishes photografted with OGEA **3** for 15 min (b, f) and 30 min (c, g) measured in Milli-Q water at 20 (a, b, c) and 37 °C (e, f, g) by AFM in QNM mode and associated comparative depth histograms (d, h).

Cell Adhesion and Detachment Studies and Viability Assays

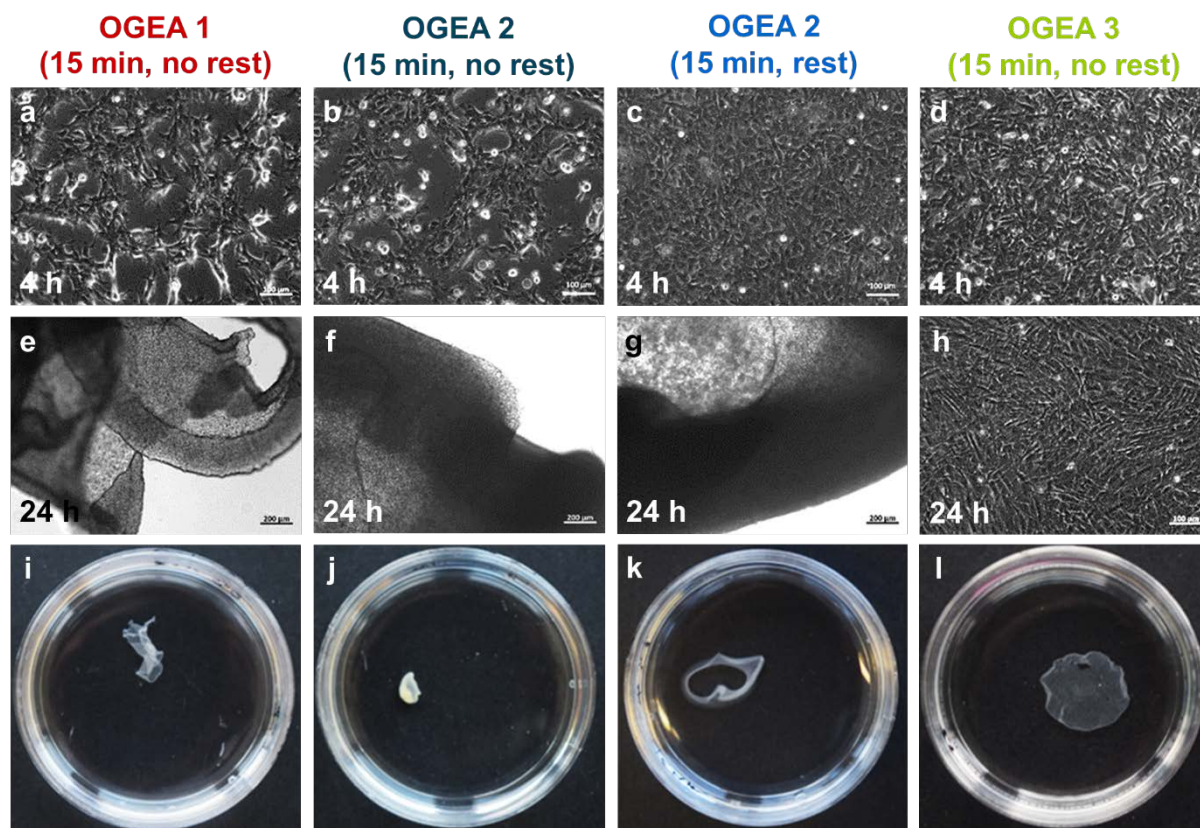


Figure S10. Representative phase contrast images of HDFs 4 h (a, b, c, d) and 24 h (e, f, g, h) after seeding and macroscopic photographs of the culture dishes after temperature reduction to 20 °C (i, j, k, l) on OGEA 1, 2 and 3.

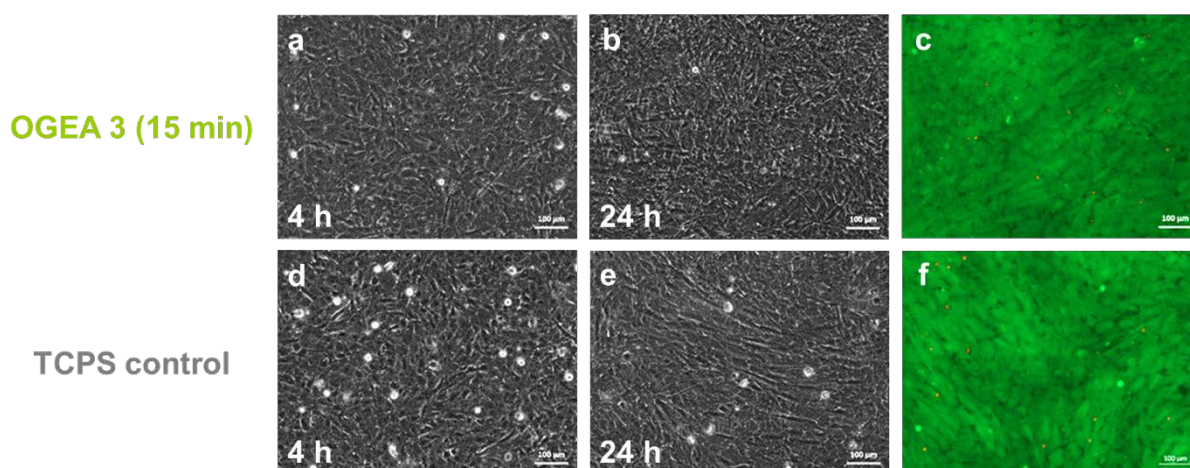


Figure S11. Representative phase contrast images of HDFs 4 and 16 h after seeding on OGEA 3 coatings (a, b) prepared via the optimized grafting protocol with 15 min UV-irradiation and

TCPS controls (d, e) and respective images of live/dead staining (c, f) with fluorescein diacetate (green) and propidium iodide (red).

REFERENCES

- (1) Smith, P. A. S.; Most, E. E. Quaternary Hydrazones and Their Rearrangement. *J. Org. Chem.* **1957**, *22*, 358-362.
- (2) Aspnes, D. E.; Theeten, J. B.; Hottier, F. Investigation of Effective-Medium Models of Microscopic Surface Roughness by Spectroscopic Ellipsometry. *Phys. Rev. B* **1979**, *20*, 3292-3302.

4 Summary and Conclusions

In this work, thermoresponsive glycidyl ether-based coatings on applied PS tissue culture substrates were developed and utilized for the temperature-triggered fabrication of cell sheets. With the objective to establish efficient, scalable and transferable coating procedures, both “grafting to” and “grafting from” approaches were pursued in order to covalently immobilize thermoresponsive PGE and OGEA coatings based on the two monomers GME and EGE onto common PS tissue culture substrates. In both approaches, UV-induced photografting was utilized and BP was either used as a PGE-bound immobilizing agent for C, H-insertion (“grafting to”) or as a photoinitiator for the surface-initiated free radical polymerization of OGEAs (“grafting from”).

In the first part of the work in hand, functionalization of PS culture substrates with PGE monolayers via the “grafting to” approach was pursued. In order to obtain thermoresponsive PGEs with a reactive anchor for covalent immobilization on PS, a photo-reactive BP epoxide monomer was synthesized. Using the monomer-activated anionic ROP, block copolymers with a random, high molecular weight thermoresponsive block comprising GME and EGE and a short, hydrophobic BP block were synthesized via sequential monomer addition. In the following, the PGE block copolymers were adsorbed onto PS substrates from dilute ethanolic solution to form stable, ultrathin, sub-nanometer (0.7 ± 0.1 nm) layers, which exhibit a pancake-like structure. QCM-D experiments indicated that the physical adsorption of PGEs was not only driven by the hydrophobic BP anchor block, but also by an inherent affinity of PGE towards the PS substrates. The adsorbed layers were subsequently immobilized on the substrates via their BP anchor block by UV-induced C, H-insertion and their ultrathin, pancake-like conformation was confirmed by ellipsometry measurements, a significant change in water CA from the bare PS to the PGE-coated PS substrates, as well as by AFM force-distance measurements, which showed a significant reduction in the adhesion force between the AFM tip and the substrates after applying the PGE coatings. Although protein adsorption from serum-containing cell culture medium monitored by QCM-D measurements only showed moderate increase in the amount of adsorbed proteins on PGE coatings, as compared to bare PS surfaces, and the protein adsorption was significantly lower than on hydrophilic TCPS substrates, cell adhesion studies revealed, that HDF proliferation was comparable on both, PGE coatings and standard TCPS culture substrates. In addition, HDFs could be reproducibly cultured and detached as confluent monolayers from PGE-coated PS culture substrates, whereas they did not proliferate to confluency on bare PS and did not detach in a temperature-triggered manner from

TCPS nor PGE-coated TCPS substrates. In summary, these results strongly indicate, that the adhesion of HDFs on PS substrates is mediated by the ultrathin PGE coatings. In addition, the detachment of confluent HDF sheets is based on a cooperative effect comprising the temperature-triggered, partial rehydration of PGE chains and the inherent cell repellent nature of the hydrophobic PS substrate, which presumably lowers cell adhesion strength and helps to facilitate reproducible cell sheet detachment. As the first report on functional, thermoresponsive coatings in the sub-nanometer range, the utilization of ultrathin PGE coatings as culture substrates for cell sheet fabrication reveals the importance of the nature of the substrate material, its interaction with the thermoresponsive polymer coating and its influence on cell adhesion and detachment. Furthermore, the reliable detachment of HDF sheets from ultrathin PGE coatings demonstrates, that only small changes in surface hydration upon temperature reduction can be sufficient to render the substrates cell repellent. From both, the materials science as well as the tissue engineering point of view, the study of ultrathin PGE coatings constitutes a valuable contribution for an improved understanding of the structure-property relationship and the formulation of generalized design guidelines for thermoresponsive coatings on applied tissue culture substrates. In addition, the material-efficient coating process via adsorption from dilute ethanolic solution and rapid UV curing represents a scalable and substrate geometry-independent method for the manufacture of various substrate types and is therefore potentially suitable for the large-scale production of functional cell culture substrates.

To extend the range of applicability of PGE monolayers “grafted to” PS substrates with regards to more demanding cell lines, an adsorption protocol for the directed self-assembly of PGE block copolymers was established. To this effect, the phase transition and aggregation behaviour PGE block copolymers comprising a hydrophobic BP anchor block in aqueous solution was investigated. Temperature-dependent UV-Vis turbidimetry and DLS measurements revealed, that the BP-driven aggregation of PGE block copolymers could be minimized under dilute conditions and at temperatures well below the CPT of PGE. Under these conditions, water constitutes a selective solvent from which the block copolymers self-assemble onto PS substrates via the selective physical adsorption of the hydrophobic BP anchor block. In this manner, PGE monolayers with a brush-like conformation were obtained and subsequently immobilized by irradiation with UV light to yield stable, covalently attached coatings. AFM measurements revealed that the brushes undergo a reversible rehydration in water, when the temperature is decreased from standard cell culture conditions (37 °C) to room temperature (20 °C). In addition, theoretical estimation of the grafting density via the packing parameter ($2R_f l^{-1}$) showed that the PGE brushes are well within the brush regime and in a

similar realm as self-assembled PGE monolayers on gold as well as PGE block copolymers adsorbed to glass substrates. In contrast to gold and glass surfaces, which are non-adhesive towards thermoresponsive PGE chains, the inherent adhesive nature of PGE towards PS, which was confirmed by QCM-D measurements, indicated a temperature-modulated pancake-to-brush transition of the PGE monolayers, as compared to the mushroom-to-brush transition which was observed for PGE brushes on gold and glass. Compared to ultrathin PGE coatings, PGE brushes showed improved proliferation of endothelial cells (HUVECs). Hence, the brush coatings were tested for the culture and detachment of three different cell sheet types, namely HDFs, HAoSMCs and HUVECs, which are the main constituents in vascular tissue, in order to provide a thermoresponsive platform for the fabrication of artificial blood vessels. The detachment of HDF, HAoSMC and HUVEC sheets with viabilities comparable to cells cultured on standard TCPS substrates was facilitated by the PGE brush coatings. However, cell culture studies evidently displayed the paramount importance of the applied culture conditions, particularly the cell seeding density, the chosen culture time as well as the degree of supplementation of the used culture medium, on the successful and temporally controlled detachment of the respective cell monolayers. This illustrates the importance of both, cell culture conditions and thermoresponsive coating properties for the successful fabrication of cell sheets. In conclusion, glycidyl ether-based monolayers have shown to be a potent thermoresponsive platform for the detachment of different types of cell sheets from application relevant PS culture substrates. The general design parameters for PEG brushes, which were established on gold model surfaces and transferred to applied glass substrates, were successfully applied to self-assembled PGE brush coatings on hydrophobic PS surfaces. Further, this study has shown that a significant role can be ascribed to the nature of the substrate material with regards to the VPTT of the thermoresponsive coating as well as regarding cell adhesion and detachment. In addition, cell sheet detachment from PGE brushes was reliably triggered via the partial rehydration of PGE chains at 20 °C. As one of the first reports on self-assembled thermoresponsive brush coatings on an applied tissue culture material, the results presented in this work constitute a valuable contribution to the field of thermoresponsive surfaces for tissue culture applications and are relevant to a broader scientific community.

In the second part of this work, a fast and solvent-free synthetic pathway to OGEA macromonomers, which are suitable for surface-initiated radical photografting, was developed utilizing microwave heating. The microwave-assisted oxy-anionic ROP proved to be a convenient and viable method for the synthesis of OGEs under bulk conditions, which was found to be due to the rapid and uniform heating during microwave irradiation. In fact, a

comparison of the reaction rate to conventional heating, which was performed as a control experiment under autoclave conditions, revealed that the fast reaction rates can be solely attributed to the high temperatures reached within the microwave reactor. Further, the thermoresponsive properties of the OGEs in aqueous solution matched those of OGEs synthesized via the conventional polymerization method and even extended the previously established property profile of thermoresponsive PGEs. The results presented in this work clearly indicated an exponential increase in PGE CPTs in aqueous solution with decreasing molecular weight. This is due to the lower local concentration in solutions containing low molecular weight OGEs, which delays the dehydration and consequent aggregation of polymer chains upon increasing the temperature. In addition, *in situ* acrylation of OGEs was established as a method to obtain OGEAs in a one-pot procedure, which constitutes a practical synthetic pathway to directly obtain reactive macromonomers. Besides being a valuable contribution to the polymer science community, the microwave-assisted polymerization of OGEAs bears potential for technical scale-up, e.g., by utilizing a continuous reaction setup, and therefore introduces a possible pathway for large-scale industrial implementation.

Based on the synthesized OGEAs, a photografting process was developed to functionalize PS culture substrates with thermoresponsive bottlebrush coatings via a “grafting from” approach. The “grafting from” of OGEA macromonomers was successfully established under bulk conditions using macromonomer films which were spin-coated onto PS substrates comprising pre-adsorbed layers of the photoinitiator BP. Thermoresponsive coatings with porous, rather rigid, gel-like bottlebrush structures were obtained, as it was confirmed by ellipsometry, water CA and AFM measurements. Depending on the molecular weight and comonomer composition of the OGEA macromonomers as well as on the chosen grafting conditions, the porous structure and, hence, the wetting properties of the coatings could be adjusted ranging from moderately hydrophobic and therefore cell adhesive to hydrophobic and therefore rather cell repellent at both ambient temperature (20 °C) and under standard cell culture conditions (37 °C). Further, temperature-dependent CA and ellipsometry measurements indicated the reversible, temperature-modulated rehydration of OGE bottlebrush side chains within the coatings. Using HDFs as an eligible model cell line, confluent cell sheets were harvested from OGEA bottlebrushes in a controlled manner after optimizing the coating structure and grafting conditions. Most interestingly, HDF sheet detachment was found to be triggered by the temperature-modulated rehydration of the bottlebrush side chains, since the macroscopic collapse and swelling of the gel-like coatings upon temperature variation was not observed. In contrast, significantly increased water CAs at 37 °C indicated the dehydration of OGEA

bottlebrush side chains on the nanometer-scale. Such a macroscopic, temperature-dependent change in wettability has not been observed for PGE monolayer coatings. This proves that thermoresponsive coatings based on PGEs undergo a temperature-dependent change in hydration, which is amplified by introducing surface roughness and porosity into the coatings, as it is the case for the presented OGEA-based bottlebrushes. As the first report of surface-tethered, thermoresponsive bottlebrushes on an applied tissue culture material, the coatings developed in this work have high potential to expand the attainable properties of thermoresponsive, glycidyl ether-based substrates. This is mainly owed to their constrained conformation comprising densely grafted OGE side chains, which are a unique feature of bottlebrushes in general, and may further allow access to coatings with specific mechanical properties. Due to the myriad of alterable parameters embodied within the developed grafting process, such as the monomer composition and molecular weight, the potential use of various co-monomers, the monomer deposition method as well as the irradiation procedure, OGEA coatings are promising prospects for an expanded range of application of glycidyl ether-based coatings, especially for the fabrication of various types of cell sheets, e.g., particularly regarding the detachment of highly adhesive cells.

The results of this work demonstrate that PGE-based coatings can be fabricated on applied PS culture substrates by convenient, material-efficient and substrate geometry-independent coating methods. As compared to other techniques, such as the rather expensive EBP or synthetically sophisticated CRP, utilization of simple photochemistry based on BP is energy-efficient and constitutes a versatile approach, which offers high transferability. The presented studies further illustrate the accessibility of PGE coatings with different architectures and properties, which makes them excellent prospects as functional substrates for the detachment of a myriad of different cell sheets with further use in tissue engineering.

In addition, the hydrophobic PS culture substrates were found to have a profound effect on the adhesion and detachment of HDFs from ultrathin PGE monolayers as well as on the structure, conformation and thermal response of PGE brushes. Most interestingly, temperature-dependent physical characterization of the fabricated coatings indicated that cell sheet detachment is induced by slight changes in polymer hydration on the molecular level, since macroscopic changes in wettability could only be attested for the developed bottlebrush coatings and was neither observed for ultrathin PGE monolayers nor PGE brushes. As it is often reported in literature, the successful fabrication of cell sheets, e.g., from PNIPAm coatings, is usually explained by distinct temperature-dependent changes in coating hydrophilicity and/or a macroscopic swelling, which triggers cell sheet detachment mechanically. However, the

findings of this work indicate that macroscopic changes in wettability and/or swelling of thermoresponsive coatings is not always necessary to successfully fabricate cell sheets. Hence, the presented studies entail valuable results for the formulation of a generalized cell detachment mechanism and therefore strongly encourage in-depth investigations on the roles of the thermoresponsive coatings, the culture substrate and the used cell types in cell sheet detachment. With respect to thermoresponsive PGE-based coatings, there is reason to assume that the degree of polymer hydration may be substantially different from PNIPAm-based coatings, both, below and above the VPTT. In this regard, the comparative characterization of PGEs and PNIPAm in solution and on surfaces by complementary methods, such as NMR, DSC, QCM-D and ellipsometry, might elucidate differing observations with respect to cell sheet fabrication.

5 Outlook

Preliminary experiments have already shown, that brush coatings based on self-assembled PGE block copolymer monolayers can be adsorbed and immobilized on other culture substrate materials, in particular on PET, PC and NC. Since these materials are not only available as 2D bulk substrates but are also commonly manufactured as membranes, an investigation on the effect of substrate porosity on cell adhesion and sheet detachment constitutes a worthwhile subject to be studied in a future work. This is not only due to the supposedly enhanced rehydration of the thermoresponsive coatings through the porous substrates, but also due to the flexibility of the membrane materials, which has already shown to be convenient for cell sheet transplantation or transfer to complex, artificial 3D tissue constructs and scaffolds. In addition, the different chemical properties as well as the different hydrophilicities of the available substrate materials might introduce the possibility for an in-depth study regarding the influence of the substrate material on the VPTT of PGE coatings, which would further contribute to a better understanding of surface-tethered, self-assembled thermoresponsive monolayers. In this regard, in-depth studies on the degree of polymer and coating hydration at 20 and 37 °C by complementary methods, such as by NMR spectroscopy and DSC of PGE solutions as well as, e.g., QCM-D measurements of PGE coatings, might help to provide a more detailed, generalized cell sheet detachment mechanism.

In addition to the coating structures presented and discussed in this work, the statistical copolymerization of epoxide monomers comprising photo-reactive BP moieties via the monomer-activated oxy-anionic ROP offers a route for the fabrication of thermoresponsive hydrogels. It was already shown that PGE-based hydrogel coatings can be immobilized and crosslinked on PS substrates and that hydrogel thickness can be adjusted using the spin coating technique. Preliminary experiments have shown that such hydrogels can be used to detach HDF sheets, however, further fine-tuning of the temperature-induced swelling/deswelling of the PGE hydrogels via their thickness, comonomer composition as well as their degree of crosslinking by simultaneous retention of cell-adhesive properties at 37 °C are still necessary in order to obtain thermoresponsive substrates with reliable properties.

Perspectively, the OGEA bottlebrush coatings developed in this work have a high potential to be successfully transferred to various substrate materials, such as PET, PC, PVDF or NC, which are commonly used in tissue engineering, as well as for biomedical applications in general. Due to their unique physical properties and porous structure, thermoresponsive bottlebrushes are not only excellent prospects in the field of cell sheet fabrication and as a foundation for cell sheet-

based 3D tissue engineering, but also constitute worthwhile systems regarding their investigated for applications such as biosensing or bioseparation. The convenient accessibility of OGEA macromonomers via the potentially scalable, one-pot, microwave-assisted synthesis further underpins their utility as functional materials for surface functionalization, and possibly also as macromonomers for the synthesis of thermoresponsive molecular devices. To this end, the synthesis of OGEA bottlebrushes via a CRP method and the investigation of their thermoresponsive properties in aqueous solution might elucidate their potential regarding further applications.

6 Kurzzusammenfassung / Short Summary

6.1 Kurzzusammenfassung

Im Rahmen der vorliegenden Arbeit wurden thermoresponsive Beschichtungen auf Basis von Polyglycidylethern (PGE) für angewandte Polystyrol (PS) Zellkultursubstrate entwickelt. Zur Funktionalisierung von PS mittels „Pfropfung“ wurden hierfür thermoresponsive Blockcopolymere synthetisiert. Durch die sequenzielle, monomer-aktivierte, oxy-anionische ringöffnende Polymerisation wurden Blockcopolymere mit einem langen, thermoresponsiven Block, sowie einem kurzen, hydrophoben Benzophenon (BP) Ankerblock hergestellt. Diese bilden auf PS nach Adsorption und anschließender Immobilisierung des BP Ankerblocks durch Bestrahlung mit UV Licht ultradünne Schichten aus, welche die Adhäsion humaner dermaler Fibroblasten (HDFs) vermitteln. Durch Absenken der Temperatur lassen sich konfluente HDF Monolagen ernten, wobei das Ablösen der Zellschichten auf der partiellen Rehydratisierung der PGE Schicht sowie den zellabweisenden Eigenschaften des PS Untergrunds beruht. In der Folge wurden selbstassemblierte Monolagen auf Basis von PGE Blockcopolymeren unter selektiven Löslichkeitsbedingungen hergestellt und durch UV Bestrahlung kovalent auf PS Substraten verankert. Die so erhaltenen Polymerbürsten unterlaufen bei Temperaturenniedrigung einen „Pfannkuchen-zu-Bürsten“ Übergang und eignen sich zur temperaturgesteuerten Herstellung von Zellmonolagen bestehend aus HDFs, humanen glatten Muskelzellen und humanen Endothelzellen, welche die Grundbausteine zur Herstellung von künstlichen Blutgefäßen darstellen. Um PS Substrate mittels „Pfropfpolymerisation“ zu funktionalisieren, wurde die lösungsmittelfreie, Mikrowellen-unterstützte Synthese von wohldefinierten Oligoglycidylethern (OGEs) entwickelt. Diese weisen molekulargewichts- und konzentrationsabhängige thermoresponsive Eigenschaften in wässriger Lösung auf. Kurze Reaktionszeiten konnten ausschließlich den hohen erreichten Temperaturen während des Mikrowellen Prozesses zugeschrieben werden. Des Weiteren wurden OGE Acrylat Makromonomere durch Quenchen der ringöffnenden Polymerisation *in situ* synthetisiert. PS Substrate konnten in der Folge durch oberflächeninduzierte Photopolymerisation von OGE Acrylaten funktionalisiert werden. Die hierdurch erhaltenen molekularen Flaschenbürsten weisen eine poröse, steife und gelartige Struktur auf und eignen sich aufgrund der Rehydratisierung von thermoresponsiven OGE Seitenketten zum Ablösen konfluenter HDF Monolagen. Zusammenfassend wurden in der vorliegenden Arbeit einfache Methoden zur Funktionalisierung angewandter PS Zellkultursubstrate mit thermoresponsiven PGE Beschichtungen etabliert. Diese weisen ein hohes Potential als funktionelle Substrate zur Herstellung konfluenter Zellmonolagen auf.

6.2 Short Summary

Within this work, thermoresponsive coatings based on poly(glycidyl ether)s (PGEs) were developed for applied polystyrene (PS) tissue culture substrates. Following the “grafting to” approach, block copolymers comprising a random, high molecular weight, thermoresponsive block and a short, hydrophobic benzophenone (BP) block were synthesized via the sequential, monomer-activated, oxy-anionic ring-opening polymerization (ROP). Ultrathin layers in the sub-nanometer range were immobilized on PS by physical adsorption and UV-induced C, H-insertion of PGE block copolymers via their photo-reactive BP anchor block. The coatings mediated the adhesion of human dermal fibroblasts (HDFs) and allowed the temperature-triggered detachment of confluent cell sheets. HDF sheet detachment was found to be induced by the cooperative effects between the partial rehydration of the PGE chains and the cell repellent PS substrate background. In order to improve the performance of PGE monolayers, block copolymers were subsequently self-assembled on PS substrates from dilute aqueous solution under selective solvent conditions. UV immobilization yielded thermoresponsive polymer brushes, which undergo a “pancake-to-brush” transition upon temperature reduction. The improved structure and thermal response of the brush-like PGE coatings as well as the optimization of cell culture parameters facilitated the fabrication of confluent HDF, human aortic smooth muscle cell (HAoSMC) and human umbilical vein endothelial cell (HUVEC) sheets, which constitute the main building blocks of blood vessels. To functionalize PS culture substrates via the “grafting from” approach, a solvent-free, microwave-assisted synthesis of well-defined oligo(glycidyl ether)s (OGEs) was developed. Fast reaction rates could be solely attributed to the high reaction temperatures reached during microwave heating and the obtained oligomers exhibited highly molecular weight- and concentration-dependent CPTs in water. Further, end-functional oligo(glycidyl ether) acrylate (OGEA) macromonomers were synthesized by *in situ* quenching of the oxy-anionic ROP. Subsequently, a photopolymerization process was developed to graft OGEA macromonomers from PS culture substrates. Surface-initiated photografting from bulk macromonomer films yielded porous, rigid, gel-like OGEA coatings with unique bottlebrush properties. Bottlebrushes with optimized structure proved to be functional coatings for the fabrication of HDF sheets. The controlled detachment of cell sheets was found to be triggered by the rehydration of OGEA bottlebrush side chains rather than a macroscopic swelling of the gel-like coatings upon temperature reduction. In summary, this work introduces facile methods for the functionalization of applied PS tissue culture surfaces with thermoresponsive, PGE-based coatings and demonstrates their high potential as functional substrates for cell sheet fabrication.

7 References

- (1) Stuart, M. A. C.; Huck, W. T. S.; Genzer, J.; Müller, M.; Ober, C.; Stamm, M.; Sukhorukov, G. B.; Szleifer, I.; Tsukruk, V. V.; Urban, M.; Winnik, F.; Zauscher, S.; Luzinov, I.; Minko, S. Emerging Applications of Stimuli-Responsive Polymer Materials. *Nat. Mater.* **2010**, *9*, 101.
- (2) Cabane, E.; Zhang, X.; Langowska, K.; Palivan, C. G.; Meier, W. Stimuli-Responsive Polymers and Their Applications in Nanomedicine. *Biointerphases* **2012**, *7*, 9.
- (3) Pasparakis, G.; Vamvakaki, M. Multiresponsive Polymers: Nano-Sized Assemblies, Stimuli-Sensitive Gels and Smart Surfaces. *Polym. Chem.* **2011**, *2*, 1234-1248.
- (4) Gil, E. S.; Hudson, S. M. Stimuli-Responsive Polymers and Their Bioconjugates. *Prog. Polym. Sci.* **2004**, *29*, 1173-1222.
- (5) Wei, M.; Gao, Y.; Li, X.; Serpe, M. J. Stimuli-Responsive Polymers and Their Applications. *Polym. Chem.* **2017**, *8*, 127-143.
- (6) de la Rosa, V. R.; Woisel, P.; Hoogenboom, R. Supramolecular Control over Thermoresponsive Polymers. *Mater. Today* **2016**, *19*, 44-55.
- (7) Culver, H. R.; Clegg, J. R.; Peppas, N. A. Analyte-Responsive Hydrogels: Intelligent Materials for Biosensing and Drug Delivery. *Acc. Chem. Res.* **2017**, *50*, 170-178.
- (8) Bergueiro, J.; Calderón, M. Thermoresponsive Nanodevices in Biomedical Applications. *Macromol. Biosci.* **2015**, *15*, 183-199.
- (9) Alexander, A.; Ajazuddin; Khan, J.; Saraf, S.; Saraf, S. Polyethylene Glycol (PEG)–Poly(N-Isopropylacrylamide) (PNIPAAm) Based Thermosensitive Injectable Hydrogels for Biomedical Applications. *Eur. J. Pharm. Biopharm.* **2014**, *88*, 575-585.
- (10) Knipe, J. M.; Peppas, N. A. Multi-Responsive Hydrogels for Drug Delivery and Tissue Engineering Applications. *Regener. Biomater.* **2014**, *1*, 57-65.
- (11) Ward, M. A.; Georgiou, T. K. Thermoresponsive Polymers for Biomedical Applications. *Polymers* **2011**, *3*, 1215.
- (12) Cole, M. A.; Voelcker, N. H.; Thissen, H.; Griesser, H. J. Stimuli-Responsive Interfaces and Systems for the Control of Protein–Surface and Cell–Surface Interactions. *Biomaterials* **2009**, *30*, 1827-1850.
- (13) Wischerhoff, E.; Badi, N.; Laschewsky, A.; Lutz, J.-F., Smart Polymer Surfaces: Concepts and Applications in Biosciences. In *Bioactive Surfaces*, Börner, H. G.; Lutz, J.-F., Eds. Springer Berlin Heidelberg: Berlin, Heidelberg, 2011; pp 1-33.

- (14) Wischerhoff, E.; Badi, N.; Lutz, J.-F.; Laschewsky, A. Smart Bioactive Surfaces. *Soft Matter* **2010**, *6*, 705-713.
- (15) Dhowre, H. S.; Rajput, S.; Russell, N. A.; Zelzer, M. Responsive Cell–Material Interfaces. *Nanomedicine* **2015**, *10*, 849-871.
- (16) Nagase, K.; Okano, T.; Ohshima, H., Bioseparation Using Thermoresponsive Polymers. In *Encyclopedia of Biocolloid and Biointerface Science 2v Set*, John Wiley & Sons, Inc.: 2016; pp 220-230.
- (17) Nagase, K.; Okano, T. Thermoresponsive-Polymer-Based Materials for Temperature-Modulated Bioanalysis and Bioseparations. *J. Mater. Chem. B* **2016**, *4*, 6381-6397.
- (18) Aseyev, V.; Tenhu, H.; Winnik, F. M., Non-Ionic Thermoresponsive Polymers in Water. In *Self Organized Nanostructures of Amphiphilic Block Copolymers II*, Müller, A. H. E.; Borisov, O., Eds. Springer Berlin Heidelberg: Berlin, Heidelberg, 2011; pp 29-89.
- (19) Zhang, Q.; Weber, C.; Schubert, U. S.; Hoogenboom, R. Thermoresponsive Polymers with Lower Critical Solution Temperature: From Fundamental Aspects and Measuring Techniques to Recommended Turbidimetry Conditions. *Mater. Horiz.* **2017**, *4*, 109-116.
- (20) Weber, C.; Hoogenboom, R.; Schubert, U. S. Temperature Responsive Bio-Compatible Polymers Based on Poly(Ethylene Oxide) and Poly(2-Oxazoline)s. *Prog. Polym. Sci.* **2012**, *37*, 686-714.
- (21) Niskanen, J.; Tenhu, H. How to Manipulate the Upper Critical Solution Temperature (UCST)? *Polym. Chem.* **2017**, *8*, 220-232.
- (22) Osváth, Z.; Iván, B. The Dependence of the Cloud Point, Clearing Point, and Hysteresis of Poly(N-Isopropylacrylamide) on Experimental Conditions: The Need for Standardization of Thermoresponsive Transition Determinations. *Macromol. Chem. Phys.* **2017**, *218*, 1600470.
- (23) Schild, H. G. Poly(N-Isopropylacrylamide): Experiment, Theory and Application. *Prog. Polym. Sci.* **1992**, *17*, 163-249.
- (24) Lutz, J.-F.; Weichenhan, K.; Akdemir, Ö.; Hoth, A. About the Phase Transitions in Aqueous Solutions of Thermoresponsive Copolymers and Hydrogels Based on 2-(2-Methoxyethoxy)Ethyl Methacrylate and Oligo(Ethylene Glycol) Methacrylate. *Macromolecules* **2007**, *40*, 2503-2508.
- (25) Li, C.; Ma, Y.; Tian, Z. Thermal Switching of Thermoresponsive Polymer Aqueous Solutions. *ACS Macro Lett.* **2017**, 53-58.
- (26) Serin, G.; Nguyen, H. H.; Marty, J.-D.; Micheau, J.-C.; Gernigon, V.; Mingotaud, A.-F.; Bajon, D.; Soulet, T.; Massenot, S.; Coudret, C. Terahertz Time-Domain Spectroscopy of Thermoresponsive Polymers in Aqueous Solution. *J. Phys. Chem. B* **2016**, *120*, 9778-9787.

- (27) Sun, S.-t.; Wu, P.-y. Spectral Insights into Microdynamics of Thermoresponsive Polymers from the Perspective of Two-Dimensional Correlation Spectroscopy. *Chin. J. Polym. Sci.* **2017**, *35*, 700-712.
- (28) Termühlen, F.; Kuckling, D.; Schönhoff, M. Isothermal Titration Calorimetry to Probe the Coil-to-Globule Transition of Thermoresponsive Polymers. *J. Phys. Chem. B* **2017**, *121*, 8611-8618.
- (29) Avraham, H.; Martin, K.; M., W. F. Poly(N-Isopropylacrylamide) Phase Diagrams: Fifty Years of Research. *Angew. Chem., Int. Ed.* **2015**, *54*, 15342-15367.
- (30) Kooij, E. S.; Sui, X.; Hempenius, M. A.; Zandvliet, H. J. W.; Vancso, G. J. Probing the Thermal Collapse of Poly(N-Isopropylacrylamide) Grafts by Quantitative in Situ Ellipsometry. *J. Phys. Chem. B* **2012**, *116*, 9261-9268.
- (31) Schmaljohann, D.; Beyerlein, D.; Nitschke, M.; Werner, C. Thermo-Reversible Swelling of Thin Hydrogel Films Immobilized by Low-Pressure Plasma. *Langmuir* **2004**, *20*, 10107-10114.
- (32) Schmaljohann, D.; Nitschke, M.; Schulze, R.; Eing, A.; Werner, C.; Eichhorn, K.-J. In Situ Study of the Thermoresponsive Behavior of Micropatterned Hydrogel Films by Imaging Ellipsometry. *Langmuir* **2005**, *21*, 2317-2322.
- (33) Schmaljohann, D.; Oswald, J.; Jørgensen, B.; Nitschke, M.; Beyerlein, D.; Werner, C. Thermo-Responsive PNIPAAm-g-PEG Films for Controlled Cell Detachment. *Biomacromolecules* **2003**, *4*, 1733-1739.
- (34) Takei, Y. G.; Aoki, T.; Sanui, K.; Ogata, N.; Sakurai, Y.; Okano, T. Dynamic Contact Angle Measurement of Temperature-Responsive Surface Properties for Poly(N-Isopropylacrylamide) Grafted Surfaces. *Macromolecules* **1994**, *27*, 6163-6166.
- (35) Buller, J.; Laschewsky, A.; Wischerhoff, E. Photoreactive Oligoethylene Glycol Polymers - Versatile Compounds for Surface Modification by Thin Hydrogel Films. *Soft Matter* **2013**, *9*, 929-937.
- (36) Plunkett, K. N.; Zhu, X.; Moore, J. S.; Leckband, D. E. PNIPAM Chain Collapse Depends on the Molecular Weight and Grafting Density. *Langmuir* **2006**, *22*, 4259-4266.
- (37) Laloyaux, X.; Mathy, B.; Nysten, B.; Jonas, A. M. Surface and Bulk Collapse Transitions of Thermoresponsive Polymer Brushes. *Langmuir* **2010**, *26*, 838-847.
- (38) Zhuang, P.; Dirani, A.; Glinel, K.; Jonas, A. M. Temperature Dependence of the Surface and Volume Hydrophilicity of Hydrophilic Polymer Brushes. *Langmuir* **2016**, *32*, 3433-3444.

- (39) Gambinossi, F.; Sefcik, L. S.; Wischerhoff, E.; Laschewsky, A.; Ferri, J. K. Engineering Adhesion to Thermoresponsive Substrates: Effect of Polymer Composition on Liquid–Liquid–Solid Wetting. *ACS Appl. Mater. Interfaces* **2015**, *7*, 2518-2528.
- (40) Kaufmann, M.; Jia, Y.; Renner, L.; Gupta, S.; Kuckling, D.; Werner, C.; Pompe, T. Tuneable Swelling of Thermo- and PH-Responsive Copolymer Films. *Soft Matter* **2010**, *6*, 937-944.
- (41) Kobayashi, J.; Arisaka, Y.; Yui, N.; Akiyama, Y.; Yamato, M.; Okano, T. Effect of Temperature Changes on Serum Protein Adsorption on Thermoresponsive Cell-Culture Surfaces Monitored by a Quartz Crystal Microbalance with Dissipation. *Int. J. Mol. Sci.* **2018**, *19*, 1516.
- (42) Kessel, S.; Schmidt, S.; Müller, R.; Wischerhoff, E.; Laschewsky, A.; Lutz, J.-F.; Uhlig, K.; Lankenau, A.; Duschl, C.; Fery, A. Thermoresponsive PEG-Based Polymer Layers: Surface Characterization with AFM Force Measurements. *Langmuir* **2010**, *26*, 3462-3467.
- (43) Willet, N.; Gabriel, S.; Jerome, C.; Du Prez, F. E.; Duwez, A.-S. Collapsing and Reswelling Kinetics of Thermoresponsive Polymers on Surfaces: A Matter of Confinement and Constraints. *Soft Matter* **2014**, *10*, 7256-7261.
- (44) Akiyama, Y.; Kushida, A.; Yamato, M.; Kikuchi, A.; Okano, T. Surface Characterization of Poly(N-Isopropylacrylamide) Grafted Tissue Culture Polystyrene by Electron Beam Irradiation, Using Atomic Force Microscopy, and X-Ray Photoelectron Spectroscopy. *J. Nanosci. Nanotechnol.* **2007**, *7*, 796-802.
- (45) Cheng, X.; Canavan, H. E.; Stein, M. J.; Hull, J. R.; Kweskin, S. J.; Wagner, M. S.; Somorjai, G. A.; Castner, D. G.; Ratner, B. D. Surface Chemical and Mechanical Properties of Plasma-Polymerized N-Isopropylacrylamide. *Langmuir* **2005**, *21*, 7833-7841.
- (46) Chung, J. E.; Yokoyama, M.; Yamato, M.; Aoyagi, T.; Sakurai, Y.; Okano, T. Thermo-Responsive Drug Delivery from Polymeric Micelles Constructed Using Block Copolymers of Poly(N-Isopropylacrylamide) and Poly(Butylmethacrylate). *J. Controlled Release* **1999**, *62*, 115-127.
- (47) Kurisawa, M.; Yokoyama, M.; Okano, T. Gene Expression Control by Temperature with Thermo-Responsive Polymeric Gene Carriers. *J. Controlled Release* **2000**, *69*, 127-137.
- (48) Akimoto, J.; Nakayama, M.; Okano, T. Temperature-Responsive Polymeric Micelles for Optimizing Drug Targeting to Solid Tumors. *J. Controlled Release* **2014**, *193*, 2-8.
- (49) Mori, T.; Maeda, M. Temperature-Responsive Formation of Colloidal Nanoparticles from Poly(N-Isopropylacrylamide) Grafted with Single-Stranded DNA. *Langmuir* **2004**, *20*, 313-319.

- (50) Lai, J. J.; Hoffman, J. M.; Ebara, M.; Hoffman, A. S.; Estournès, C.; Wattiaux, A.; Stayton, P. S. Dual Magnetic-/Temperature-Responsive Nanoparticles for Microfluidic Separations and Assays. *Langmuir* **2007**, *23*, 7385-7391.
- (51) Nagase, K.; Kobayashi, J.; Okano, T. Temperature-Responsive Intelligent Interfaces for Biomolecular Separation and Cell Sheet Engineering. *J. R. Soc., Interface* **2009**, *6*, S293-S309.
- (52) Nagase, K.; Sakurada, Y.; Onizuka, S.; Iwata, T.; Yamato, M.; Takeda, N.; Okano, T. Thermoresponsive Polymer-Modified Microfibers for Cell Separations. *Acta Biomater.* **2017**, *53*, 81-92.
- (53) Yamada, N.; Okano, T.; Sakai, H.; Karikusa, F.; Sawasaki, Y.; Sakurai, Y. Thermo-Responsive Polymeric Surfaces; Control of Attachment and Detachment of Cultured Cells. *Macromol. Chem., Rapid Commun.* **1990**, *11*, 571-576.
- (54) Okano, T.; Yamada, N.; Okuhara, M.; Sakai, H.; Sakurai, Y. Mechanism of Cell Detachment from Temperature-Modulated, Hydrophilic-Hydrophobic Polymer Surfaces. *Biomaterials* **1995**, *16*, 297-303.
- (55) Nagase, K.; Yamato, M.; Kanazawa, H.; Okano, T. Poly(N-Isopropylacrylamide)-Based Thermoresponsive Surfaces Provide New Types of Biomedical Applications. *Biomaterials* **2018**, *153*, 27-48.
- (56) Nash, M. E.; Healy, D.; Carroll, W. M.; Elvira, C.; Rochev, Y. A. Cell and Cell Sheet Recovery from Pnepam Coatings; Motivation and History to Present Day Approaches. *J. Mater. Chem.* **2012**, *22*, 19376-19389.
- (57) Kobayashi, J.; Okano, T. Thermoresponsive Thin Hydrogel-Grafted Surfaces for Biomedical Applications. *React. Funct. Polym.* **2013**, *73*, 939-944.
- (58) Tang, Z.; Okano, T. Recent Development of Temperature-Responsive Surfaces and Their Application for Cell Sheet Engineering. *Regener. Biomater.* **2014**, *1*, 91-102.
- (59) Tang, Z.; Akiyama, Y.; Okano, T. Recent Development of Temperature-Responsive Cell Culture Surface Using Poly(N-Isopropylacrylamide). *J. Polym. Sci., Part B: Polym. Phys.* **2014**, *52*, 917-926.
- (60) Takahashi, H.; Okano, T. Cell Sheet-Based Tissue Engineering for Organizing Anisotropic Tissue Constructs Produced Using Microfabricated Thermoresponsive Substrates. *Adv. Healthcare Mater.* **2015**, *4*, 2388-2407.
- (61) Yamato, M.; Okano, T. Cell Sheet Engineering. *Mater. Today* **2004**, *7*, 42-47.
- (62) Matsuda, N.; Shimizu, T.; Yamato, M.; Okano, T. Tissue Engineering Based on Cell Sheet Technology. *Adv. Mater.* **2007**, *19*, 3089-3099.

- (63) Elloumi-Hannachi, I.; Yamato, M.; Okano, T. Cell Sheet Engineering: A Unique Nanotechnology for Scaffold-Free Tissue Reconstruction with Clinical Applications in Regenerative Medicine. *J. Intern. Med.* **2010**, *267*, 54-70.
- (64) Kobayashi, J.; Okano, T. Fabrication of a Thermoresponsive Cell Culture Dish: A Key Technology for Cell Sheet Tissue Engineering. *Sci. Technol. Adv. Mater.* **2010**, *11*, 014111.
- (65) Haraguchi, Y.; Shimizu, T.; Yamato, M.; Okano, T. Scaffold-Free Tissue Engineering Using Cell Sheet Technology. *RSC Adv.* **2012**, *2*, 2184-2190.
- (66) Umemoto, T.; Yamato, M.; Nishida, K.; Okano, T. Regenerative Medicine of Cornea by Cell Sheet Engineering Using Temperature-Responsive Culture Surfaces. *Chin. Sci. Bull.* **2013**, *58*, 4349-4356.
- (67) Owaki, T.; Shimizu, T.; Yamato, M.; Okano, T. Cell Sheet Engineering for Regenerative Medicine: Current Challenges and Strategies. *Biotechnol. J.* **2014**, *9*, 904-914.
- (68) Matsuura, K.; Utoh, R.; Nagase, K.; Okano, T. Cell Sheet Approach for Tissue Engineering and Regenerative Medicine. *J. Controlled Release* **2014**, *190*, 228-239.
- (69) Neo, P. Y.; Teh, T. K. H.; Tay, A. S. R.; Asuncion, M. C. T.; Png, S. N.; Toh, S. L.; Goh, J. C.-H. Stem Cell-Derived Cell-Sheets for Connective Tissue Engineering. *Connect. Tissue Res.* **2016**, *57*, 428-442.
- (70) Nishida, K.; Yamato, M.; Hayashida, Y.; Watanabe, K.; Yamamoto, K.; Adachi, E.; Nagai, S.; Kikuchi, A.; Maeda, N.; Watanabe, H.; Okano, T.; Tano, Y. Corneal Reconstruction with Tissue-Engineered Cell Sheets Composed of Autologous Oral Mucosal Epithelium. *N. Engl. J. Med.* **2004**, *351*, 1187-1196.
- (71) Ohki, T.; Yamato, M.; Ota, M.; Takagi, R.; Murakami, D.; Kondo, M.; Sasaki, R.; Namiki, H.; Okano, T.; Yamamoto, M. Prevention of Esophageal Stricture after Endoscopic Submucosal Dissection Using Tissue-Engineered Cell Sheets. *Gastroenterology* **2012**, *143*, 582-588.e582.
- (72) Kuramoto, G.; Takagi, S.; Ishitani, K.; Shimizu, T.; Okano, T.; Matsui, H. Preventive Effect of Oral Mucosal Epithelial Cell Sheets on Intrauterine Adhesions. *Hum. Reprod.* **2015**, *30*, 406-416.
- (73) Yokoyama, T.; Ohashi, K.; Kuge, H.; Kanehiro, H.; Iwata, H.; Yamato, M.; Nakajima, Y. In Vivo Engineering of Metabolically Active Hepatic Tissues in a Neovascularized Subcutaneous Cavity. *Am. J. Transplant.* **2006**, *6*, 50-59.
- (74) Iwata, T.; Yamato, M.; Tsuchioka, H.; Takagi, R.; Mukobata, S.; Washio, K.; Okano, T.; Ishikawa, I. Periodontal Regeneration with Multi-Layered Periodontal Ligament-Derived Cell Sheets in a Canine Model. *Biomaterials* **2009**, *30*, 2716-2723.

- (75) Yamamoto, K.; Yamato, M.; Morino, T.; Sugiyama, H.; Takagi, R.; Yaguchi, Y.; Okano, T.; Kojima, H. Middle Ear Mucosal Regeneration by Tissue-Engineered Cell Sheet Transplantation. *NPJ Regen. Med.* **2017**, *2*, 6.
- (76) Ebihara, G.; Sato, M.; Yamato, M.; Mitani, G.; Kutsuna, T.; Nagai, T.; Ito, S.; Ukai, T.; Kobayashi, M.; Kokubo, M.; Okano, T.; Mochida, J. Cartilage Repair in Transplanted Scaffold-Free Chondrocyte Sheets Using a Minipig Model. *Biomaterials* **2012**, *33*, 3846-3851.
- (77) Masato, S.; Masayuki, Y.; Kosuke, H.; Teruo, O.; Joji, M. Articular Cartilage Regeneration Using Cell Sheet Technology. *Anat. Rec.* **2014**, *297*, 36-43.
- (78) Kanzaki, M.; Yamato, M.; Yang, J.; Sekine, H.; Kohno, C.; Takagi, R.; Hatakeyama, H.; Isaka, T.; Okano, T.; Onuki, T. Dynamic Sealing of Lung Air Leaks by the Transplantation of Tissue Engineered Cell Sheets. *Biomaterials* **2007**, *28*, 4294-4302.
- (79) Sawa, Y.; Miyagawa, S.; Sakaguchi, T.; Fujita, T.; Matsuyama, A.; Saito, A.; Shimizu, T.; Okano, T. Tissue Engineered Myoblast Sheets Improved Cardiac Function Sufficiently to Discontinue Lvas in a Patient with DCM: Report of a Case. *Surg. Today* **2012**, *42*, 181-184.
- (80) Teichmann, J.; Gramm, S., *Electron Beam Immobilization of Functionalized Poly(Vinyl Methyl Ether) Thin Films on Polymer Surfaces – Towards Stimuli Responsive Coatings for Biomedical Purposes*. 2011; Vol. 5, p 970.
- (81) Teichmann, J.; Nitschke, M.; Pette, D.; Valtink, M.; Gramm, S.; Härtel, F. V.; Noll, T.; Funk, R. H. W.; Engelmann, K.; Werner, C. Thermo-Responsive Cell Culture Carriers Based on Poly(Vinyl Methyl Ether)—the Effect of Biomolecular Ligands to Balance Cell Adhesion and Stimulated Detachment. *Sci. Technol. Adv. Mater.* **2015**, *16*, 045003 (045013pp).
- (82) Teichmann, J.; Valtink, M.; Gramm, S.; Nitschke, M.; Werner, C.; Funk, R. H.; Engelmann, K. Human Corneal Endothelial Cell Sheets for Transplantation: Thermo-Responsive Cell Culture Carriers to Meet Cell-Specific Requirements. *Acta Biomater.* **2013**, *9*, 5031-5039.
- (83) Lee, B.; Jiao, A.; Yu, S.; You, J. B.; Kim, D.-H.; Im, S. G. Initiated Chemical Vapor Deposition of Thermoresponsive Poly(N-Vinylcaprolactam) Thin Films for Cell Sheet Engineering. *Acta Biomater.* **2013**, *9*, 7691-7698.
- (84) Cortez-Lemus, N. A.; Licea-Claverie, A. Poly(N-Vinylcaprolactam), a Comprehensive Review on a Thermoresponsive Polymer Becoming Popular. *Prog. Polym. Sci.* **2016**, *53*, 1-51.
- (85) Lutz, J.-F.; Akdemir, Ö.; Hoth, A. Point by Point Comparison of Two Thermosensitive Polymers Exhibiting a Similar LCST: Is the Age of Poly(NIPAM) Over? *J. Am. Chem. Soc.* **2006**, *128*, 13046-13047.

- (86) Lutz, J.-F.; Hoth, A. Preparation of Ideal Peg Analogues with a Tunable Thermosensitivity by Controlled Radical Copolymerization of 2-(2-Methoxyethoxy)Ethyl Methacrylate and Oligo(Ethylene Glycol) Methacrylate. *Macromolecules* **2006**, *39*, 893-896.
- (87) Buller, J.; Laschewsky, A.; Lutz, J.-F.; Wischerhoff, E. Tuning the Lower Critical Solution Temperature of Thermoresponsive Polymers by Biospecific Recognition. *Polym. Chem.* **2011**, *2*, 1486-1489.
- (88) Jonas, A. M.; Glinel, K.; Oren, R.; Nysten, B.; Huck, W. T. S. Thermo-Responsive Polymer Brushes with Tunable Collapse Temperatures in the Physiological Range. *Macromolecules* **2007**, *40*, 4403-4405.
- (89) Uhlig, K.; Boerner, H.; Wischerhoff, E.; Lutz, J.-F.; Jaeger, M.; Laschewsky, A.; Duschl, C. On the Interaction of Adherent Cells with Thermoresponsive Polymer Coatings. *Polymers* **2014**, *6*, 1164.
- (90) Uhlig, K.; Boysen, B.; Lankenau, A.; Jaeger, M.; Wischerhoff, E.; Lutz, J.-F.; Laschewsky, A.; Duschl, C. On the Influence of the Architecture of Poly(Ethylene Glycol)-Based Thermoresponsive Polymers on Cell Adhesion. *Biomicrofluidics* **2012**, *6*, 24129.
- (91) Uhlig, K.; Wischerhoff, E.; Lutz, J.-F.; Laschewsky, A.; Jaeger, M. S.; Lankenau, A.; Duschl, C. Monitoring Cell Detachment on PEG-Based Thermoresponsive Surfaces Using TIRF Microscopy. *Soft Matter* **2010**, *6*, 4262-4267.
- (92) Wischerhoff, E.; Uhlig, K.; Lankenau, A.; Börner, H. G.; Laschewsky, A.; Duschl, C.; Lutz, J.-F. Controlled Cell Adhesion on PEG-Based Switchable Surfaces. *Angew. Chem., Int. Ed.* **2008**, *47*, 5666-5668.
- (93) Vancoillie, G.; Frank, D.; Hoogenboom, R. Thermoresponsive Poly(Oligo Ethylene Glycol Acrylates). *Prog. Polym. Sci.* **2014**, *39*, 1074-1095.
- (94) Badi, N. Non-Linear PEG-Based Thermoresponsive Polymer Systems. *Prog. Polym. Sci.* **2017**, *66*, 54-79.
- (95) Dworak, A.; Utrata-Wesołek, A.; Szweda, D.; Kowalczyk, A.; Trzebicka, B.; Anioł, J.; Sieroń, A. L.; Klama-Baryła, A.; Kawecki, M. Poly[Tri(Ethylene Glycol) Ethyl Ether Methacrylate]-Coated Surfaces for Controlled Fibroblasts Culturing. *ACS Appl. Mater. Interfaces* **2013**, *5*, 2197-2207.
- (96) Kawecki, M.; Kraut, M.; Klama-Baryła, A.; Łabuś, W.; Kitala, D.; Nowak, M.; Glik, J.; Sieroń, A. L.; Utrata-Wesołek, A.; Trzebicka, B.; Dworak, A.; Szweda, D. Transfer of Fibroblast Sheets Cultured on Thermoresponsive Dishes with Membranes. *J. Mater. Sci.: Mater. Med.* **2016**, *27*, 111.

- (97) Aoi, K.; Suzuki, H.; Okada, M. Architectural Control of Sugar-Containing Polymers by Living Polymerization: Ring-Opening Polymerization of 2-Oxazolines Initiated with Carbohydrate Derivatives. *Macromolecules* **1992**, *25*, 7073-7075.
- (98) Dworak, A.; Trzebicka, B.; Kowalczyk, A.; Tsvetanov, C.; Rangelov, S. Polyoxazolines - Mechanism of Synthesis and Solution Properties. *Polymery* **2014**, *59*, 88-94.
- (99) Wiesbrock, F.; Hoogenboom, R.; Abeln, C. H.; Schubert, U. S. Single-Mode Microwave Ovens as New Reaction Devices: Accelerating the Living Polymerization of 2-Ethyl-2-Oxazoline. *Macromol. Rapid Commun.* **2004**, *25*, 1895-1899.
- (100) Agnieszka, K.; Juraj, K.; Kornelia, B.; Barbara, T.; Andrzej, D. Star Poly(2-Ethyl-2-Oxazoline)s—Synthesis and Thermosensitivity. *Polymer International* **2011**, *60*, 1001-1009.
- (101) Hoogenboom, R.; Thijs, H. M. L.; Fijten, M. W. M.; van Lankvelt, B. M.; Schubert, U. S. One-Pot Synthesis of 2-Phenyl-2-Oxazoline-Containing Quasi-Diblock Copoly(2-Oxazoline)s under Microwave Irradiation. *J. Polym. Sci., Part A: Polym. Chem.* **2007**, *45*, 416-422.
- (102) Hoogenboom, R.; Wiesbrock, F.; Huang, H.; Leenen, M. A. M.; Thijs, H. M. L.; van Nispen, S. F. G. M.; van der Loop, M.; Fustin, C.-A.; Jonas, A. M.; Gohy, J.-F.; Schubert, U. S. Microwave-Assisted Cationic Ring-Opening Polymerization of 2-Oxazolines: A Powerful Method for the Synthesis of Amphiphilic Triblock Copolymers. *Macromolecules* **2006**, *39*, 4719-4725.
- (103) Hoogenboom, R.; Wiesbrock, F.; Leenen, M. A. M.; Thijs, H. M. L.; Huang, H.; Fustin, C.-A.; Guillet, P.; Gohy, J.-F.; Schubert, U. S. Synthesis and Aqueous Micellization of Amphiphilic Tetrablock Ter- and Quarterpoly(2-Oxazoline)s. *Macromolecules* **2007**, *40*, 2837-2843.
- (104) Wiesbrock, F.; Hoogenboom, R.; Leenen, M. A. M.; Meier, M. A. R.; Abeln, C. H.; Schubert, U. S. Investigation of the Living Cationic Ring-Opening Polymerization of 2-Methyl-, 2-Ethyl-, 2-Nonyl-, and 2-Phenyl-2-Oxazoline in a Single-Mode Microwave Reactor. *Macromolecules* **2005**, *38*, 5025-5034.
- (105) Hoogenboom, R.; Fijten, M. W. M.; Thijs, H. M. L.; van Lankvelt, B. M.; Schubert, U. S. Microwave-Assisted Synthesis and Properties of a Series of Poly(2-Alkyl-2-Oxazoline)s. *Des. Monomers Polym.* **2005**, *8*, 659-671.
- (106) Ning, Z.; Tilo, P.; Ihsan, A.; Robert, L.; Carsten, W.; Rainer, J. Tailored Poly(2-Oxazoline) Polymer Brushes to Control Protein Adsorption and Cell Adhesion. *Macromol. Biosci.* **2012**, *12*, 926-936.

- (107) Grube, M.; Leiske, M. N.; Schubert, U. S.; Nischang, I. POx as an Alternative to PEG? A Hydrodynamic and Light Scattering Study. *Macromolecules* **2018**, *51*, 1905-1916.
- (108) Hoogenboom, R.; Thijs, H. M. L.; Jochems, M. J. H. C.; van Lankvelt, B. M.; Fijtenab, M. W. M.; Schubert, U. S. Tuning the LCST of Poly(2-Oxazoline)s by Varying Composition and Molecular Weight: Alternatives to Poly(N-Isopropylacrylamide)? *Chem. Commun.* **2008**, *44*, 5758-5760.
- (109) Oleszko, N.; Utrata-Wesołek, A.; Wałach, W.; Libera, M.; Hercog, A.; Szeluga, U.; Domański, M.; Trzebicka, B.; Dworak, A. Crystallization of Poly(2-Isopropyl-2-Oxazoline) in Organic Solutions. *Macromolecules* **2015**, *48*, 1852-1859.
- (110) Oleszko-Torbus, N.; Wałach, W.; Utrata-Wesołek, A.; Dworak, A. Control of the Crystalline Properties of 2-Isopropyl-2-Oxazoline Copolymers in Condensed State and in Solution Depending on the Composition. *Macromolecules* **2017**, *50*, 7636-7645.
- (111) Dworak, A.; Utrata-Wesołek, A.; Oleszko, N.; Wałach, W.; Trzebicka, B.; Anioł, J.; Sieroń, A. L.; Klama-Baryła, A.; Kawecki, M. Poly(2-Substituted-2-Oxazoline) Surfaces for Dermal Fibroblasts Adhesion and Detachment. *J. Mater. Sci.: Mater. Med.* **2014**, *25*, 1149-1163.
- (112) Oleszko, N.; Wałach, W.; Utrata-Wesołek, A.; Kowalczyk, A.; Trzebicka, B.; Klama-Baryła, A.; Hoff-Lenczewska, D.; Kawecki, M.; Lesiak, M.; Sieroń, A. L.; Dworak, A. Controlling the Crystallinity of Thermoresponsive Poly(2-Oxazoline)-Based Nanolayers to Cell Adhesion and Detachment. *Biomacromolecules* **2015**, *16*, 2805-2813.
- (113) Thomas, A.; Müller, S. S.; Frey, H. Beyond Poly(Ethylene Glycol): Linear Polyglycerol as a Multifunctional Polyether for Biomedical and Pharmaceutical Applications. *Biomacromolecules* **2014**, *15*, 1935-1954.
- (114) Herzberger, J.; Niederer, K.; Pohlitz, H.; Seiwert, J.; Worm, M.; Wurm, F. R.; Frey, H. Polymerization of Ethylene Oxide, Propylene Oxide, and Other Alkylene Oxides: Synthesis, Novel Polymer Architectures, and Bioconjugation. *Chem. Rev.* **2016**, *116*, 2170-2243.
- (115) Gerecke, C.; Edlich, A.; Giulbudagian, M.; Schumacher, F.; Zhang, N.; Said, A.; Yealland, G.; Lohan, S. B.; Neumann, F.; Meinke, M. C.; Ma, N.; Calderón, M.; Hedtrich, S.; Schäfer-Korting, M.; Kleuser, B. Biocompatibility and Characterization of Polyglycerol-Based Thermoresponsive Nanogels Designed as Novel Drug-Delivery Systems and Their Intracellular Localization in Keratinocytes. *Nanotoxicology* **2017**, *11*, 267-277.
- (116) Aoki, S.; Koide, A.; Imabayashi, S.-I.; Watanabe, M. Novel Thermosensitive Polyethers Prepared by Anionic Ring-Opening Polymerization of Glycidyl Ether Derivatives. *Chem. Lett.* **2002**, 1128-1129.

- (117) Ogura, M.; Tokuda, H.; Imabayashi, S.-i.; Watanabe, M. Preparation and Solution Behavior of a Thermoresponsive Diblock Copolymer of Poly(Ethyl Glycidyl Ether) and Poly(Ethylene Oxide). *Langmuir* **2007**, *23*, 9429-9434.
- (118) Chen, Z.; FitzGerald, P. A.; Kobayashi, Y.; Ueno, K.; Watanabe, M.; Warr, G. G.; Atkin, R. Micelle Structure of Novel Diblock Polyethers in Water and Two Protic Ionic Liquids (EAN and PAN). *Macromolecules* **2015**, *48*, 1843-1851.
- (119) Yumi, K.; Yuzo, K.; Takahiro, K.; Kazuhide, U.; Hisashi, K.; Masayoshi, W. Self-Assembly of Polyether Diblock Copolymers in Water and Ionic Liquids. *Macromol. Rapid Commun.* **2016**, *37*, 1207-1211.
- (120) Tsuda, R.; Kodama, K.; Ueki, T.; Kokubo, H.; Imabayashi, S.-i.; Watanabe, M. LCST-Type Liquid-Liquid Phase Separation Behaviour of Poly(Ethylene Oxide) Derivatives in an Ionic Liquid. *Chem. Commun.* **2008**, 4939-4941.
- (121) Inoue, S.; Kakikawa, H.; Nakadan, N.; Imabayashi, S.-i.; Watanabe, M. Thermal Response of Poly(Ethoxyethyl Glycidyl Ether) Grafted on Gold Surfaces Probed on the Basis of Temperature-Dependent Water Wettability. *Langmuir* **2009**, *25*, 2837-2841.
- (122) Labbé, A.; Carlotti, S.; Deffieux, A.; Hirao, A. Controlled Polymerization of Glycidyl Methyl Ether Initiated by Onium Salt/Triisobutylaluminum and Investigation of the Polymer LCST. *Macromol. Symp.* **2007**, *249-250*, 392-397.
- (123) Labbé, A.; Brocas, A.-L.; Ibarboure, E.; Ishizone, T.; Hirao, A.; Deffieux, A.; Carlotti, S. Selective Ring-Opening Polymerization of Glycidyl Methacrylate: Toward the Synthesis of Cross-Linked (Co)Polyethers with Thermoresponsive Properties. *Macromolecules* **2011**, *44*, 6356-6364.
- (124) Reinicke, S.; Schmelz, J.; Lapp, A.; Karg, M.; Hellweg, T.; Schmalz, H. Smart Hydrogels Based on Double Responsive Triblock Terpolymers. *Soft Matter* **2009**, *5*, 2648-2657.
- (125) Karg, M.; Reinicke, S.; Lapp, A.; Hellweg, T.; Schmalz, H. Temperature-Dependent Gelation Behaviour of Double Responsive P2VP-b-PEO-b-P(GME-co-EGE) Triblock Terpolymers: A SANS Study. *Macromol. Symp.* **2011**, *306-307*, 77-88.
- (126) Weinhart, M.; Becherer, T.; Haag, R. Switchable, Biocompatible Surfaces Based on Glycerol Copolymers. *Chem. Commun.* **2011**, *47*, 1553-1555.
- (127) Becherer, T.; Heinen, S.; Wei, Q.; Haag, R.; Weinhart, M. In-Depth Analysis of Switchable Glycerol Based Polymeric Coatings for Cell Sheet Engineering. *Acta Biomater.* **2015**, *25*, 43-55.

- (128) Heinen, S.; Rackow, S.; Schäfer, A.; Weinhart, M. A Perfect Match: Fast and Truly Random Copolymerization of Glycidyl Ether Monomers to Thermoresponsive Copolymers. *Macromolecules* **2017**, *50*, 44-53.
- (129) Heinen, S.; Cuéllar-Camacho, J. L.; Weinhart, M. Thermoresponsive Poly(Glycidyl Ether) Brushes on Gold: Surface Engineering Parameters and Their Implication for Cell Sheet Fabrication. *Acta Biomater.* **2017**, *59*, 117-128.
- (130) Heinen, S.; Weinhart, M. Poly(Glycidyl Ether)-Based Monolayers on Gold Surfaces: Control of Grafting Density and Chain Conformation by Grafting Procedure, Surface Anchor, and Molecular Weight. *Langmuir* **2017**, *33*, 2076-2086.
- (131) Heinen, S.; Rackow, S.; Cuellar-Camacho, J. L.; Donskyi, I. S.; Unger, W. E. S.; Weinhart, M. Transfer of Functional Thermoresponsive Poly(Glycidyl Ether) Coatings for Cell Sheet Fabrication from Gold to Glass Surfaces. *J. Mater. Chem. B* **2018**, *6*, 1489-1500.
- (132) Utrata-Wesołek, A.; Oleszko, N.; Trzebicka, B.; Anioł, J.; Zagdańska, M.; Lesiak, M.; Sieroń, A.; Dworak, A. Modified Polyglycidol Based Nanolayers of Switchable Philicity and Their Interactions with Skin Cells. *Eur. Polym. J.* **2013**, *49*, 106-117.
- (133) Isono, T.; Miyachi, K.; Satoh, Y.; Sato, S.-i.; Kakuchi, T.; Satoh, T. Design and Synthesis of Thermoresponsive Aliphatic Polyethers with a Tunable Phase Transition Temperature. *Polym. Chem.* **2017**, *8*, 5698-5707.
- (134) Brocas, A.-L.; Mantzaridis, C.; Tunc, D.; Carlotti, S. Polyether Synthesis: From Activated or Metal-Free Anionic Ring-Opening Polymerization of Epoxides to Functionalization. *Prog. Polym. Sci.* **2013**, *38*, 845-873.
- (135) Mangold, C.; Wurm, F.; Frey, H. Functional PEG-Based Polymers with Reactive Groups Via Anionic ROP of Tailor-Made Epoxides. *Polym. Chem.* **2012**, *3*, 1714-1721.
- (136) Haamann, D.; Keul, H.; Klee, D.; Möller, M. Functionalization of Linear and Star-Shaped Polyglycidols with Vinyl Sulfonate Groups and Their Reaction with Different Amines and Alcohols. *Macromolecules* **2010**, *43*, 6295-6301.
- (137) Lee, B. F.; Kade, M. J.; Chute, J. A.; Gupta, N.; Campos, L. M.; Fredrickson, G. H.; Kramer, E. J.; Lynd, N. A.; Hawker, C. J. Poly(Allyl Glycidyl Ether) - A Versatile and Functional Polyether Platform. *J. Polym. Sci., Part A: Polym. Chem.* **2011**, *49*, 4498-4504.
- (138) Erberich, M.; Keul, H.; Möller, M. Polyglycidols with Two Orthogonal Protective Groups: Preparation, Selective Deprotection, and Functionalization. *Macromolecules* **2007**, *40*, 3070-3079.

- (139) Libera, M.; Trzebicka, B.; Kowalczyk, A.; Wałach, W.; Dworak, A. Synthesis and Thermoresponsive Properties of Four Arm, Amphiphilic Poly(Tert-Butyl-Glycidylether)-Block-Polyglycidol Stars. *Polymer* **2011**, *52*, 250-257.
- (140) Hans, M.; Keul, H.; Moeller, M. Chain Transfer Reactions Limit the Molecular Weight of Polyglycidol Prepared Via Alkali Metal Based Initiating Systems. *Polymer* **2009**, *50*, 1103-1108.
- (141) Anne-Laure, B.; Gabriel, C.; Sylvain, C.; Alain, D.; Stephane, C. Controlled Synthesis of Polyepichlorohydrin with Pendant Cyclic Carbonate Functions for Isocyanate-Free Polyurethane Networks. *J. Polym. Sci., Part A: Polym. Chem.* **2011**, *49*, 2677-2684.
- (142) Gervais, M.; Brocas, A.-L.; Cendejas, G.; Deffieux, A.; Carlotti, S. Synthesis of Linear High Molar Mass Glycidol-Based Polymers by Monomer-Activated Anionic Polymerization. *Macromolecules* **2010**, *43*, 1778-1784.
- (143) Gervais, M.; Labbé, A.; Carlotti, S.; Deffieux, A. Direct Synthesis of α -Azido, Ω -Hydroxypolyethers by Monomer-Activated Anionic Polymerization. *Macromolecules* **2009**, *42*, 2395-2400.
- (144) Matthieu, G.; Anne-Laure, B.; Gabriel, C.; Alain, D.; Stephane, C. Linear High Molar Mass Polyglycidol and Its Direct α -Azido Functionalization. *Macromol. Symp.* **2011**, *308*, 101-111.
- (145) Herzberger, J.; Frey, H. Epicyanohydrin: Polymerization by Monomer Activation Gives Access to Nitrile-, Amino-, and Carboxyl-Functional Poly(Ethylene Glycol). *Macromolecules* **2015**, *48*, 8144-8153.
- (146) Meyer, J.; Keul, H.; Möller, M. Poly(Glycidyl Amine) and Copolymers with Glycidol and Glycidyl Amine Repeating Units: Synthesis and Characterization. *Macromolecules* **2011**, *44*, 4082-4091.
- (147) da Silva, R. M. P.; Mano, J. F.; Reis, R. L. Smart Thermoresponsive Coatings and Surfaces for Tissue Engineering: Switching Cell-Material Boundaries. *Trends Biotechnol.* **2007**, *25*, 577-583.
- (148) Brun-Graeppi, A. K. A. S.; Richard, C.; Bessodes, M.; Scherman, D.; Merten, O.-W. Thermoresponsive Surfaces for Cell Culture and Enzyme-Free Cell Detachment. *Prog. Polym. Sci.* **2010**, *35*, 1311-1324.
- (149) Tekin, H.; Sanchez, J. G.; Tsinman, T.; Langer, R.; Khademhosseini, A. Thermoresponsive Platforms for Tissue Engineering and Regenerative Medicine. *AIChE Journal* **2011**, *57*, 3249-3258.

- (150) Reed, J. A.; Love, S. A.; Lucero, A. E.; Haynes, C. L.; Canavan, H. E. Effect of Polymer Deposition Method on Thermoresponsive Polymer Films and Resulting Cellular Behavior. *Langmuir* **2012**, *28*, 2281-2287.
- (151) Canavan, H. E.; Cheng, X.; Graham, D. J.; Ratner, B. D.; Castner, D. G. Cell Sheet Detachment Affects the Extracellular Matrix: A Surface Science Study Comparing Thermal Liftoff, Enzymatic, and Mechanical Methods. *J. Biomed. Mater. Res., Part A* **2005**, *75A*, 1-13.
- (152) Canavan, H. E.; Cheng, X.; Graham, D. J.; Ratner, B. D.; Castner, D. G. Surface Characterization of the Extracellular Matrix Remaining after Cell Detachment from a Thermoresponsive Polymer. *Langmuir* **2005**, *21*, 1949-1955.
- (153) Canavan, H. E.; Graham, D. J.; Cheng, X.; Ratner, B. D.; Castner, D. G. Comparison of Native Extracellular Matrix with Adsorbed Protein Films Using Secondary Ion Mass Spectrometry. *Langmuir* **2007**, *23*, 50-56.
- (154) Halperin, A.; Kröger, M. Theoretical Considerations on Mechanisms of Harvesting Cells Cultured on Thermoresponsive Polymer Brushes. *Biomaterials* **2012**, *33*, 4975-4987.
- (155) Lee, J. H.; Khang, G.; Lee, J. W.; Lee, H. B. Interaction of Different Types of Cells on Polymer Surfaces with Wettability Gradient. *J. Colloid Interface Sci.* **1998**, *205*, 323-330.
- (156) Michael, C. C.; Ryan, G. T.; Nathan, D. G. Protein-Surface Interactions on Stimuli-Responsive Polymeric Biomaterials. *Biomed. Mater.* **2016**, *11*, 022002.
- (157) Akiyama, Y.; Kikuchi, A.; Yamato, M.; Okano, T. Ultrathin Poly(N-Isopropylacrylamide) Grafted Layer on Polystyrene Surfaces for Cell Adhesion/Detachment Control. *Langmuir* **2004**, *20*, 5506-5511.
- (158) Fukumori, K.; Akiyama, Y.; Yamato, M.; Kobayashi, J.; Sakai, K.; Okano, T. Temperature-Responsive Glass Coverslips with an Ultrathin Poly(N-Isopropylacrylamide) Layer. *Acta Biomater.* **2009**, *5*, 470-476.
- (159) Fukumori, K.; Akiyama, Y.; Kumashiro, Y.; Kobayashi, J.; Yamato, M.; Sakai, K.; Okano, T. Characterization of Ultra-Thin Temperature-Responsive Polymer Layer and Its Polymer Thickness Dependency on Cell Attachment/Detachment Properties. *Macromol. Biosci.* **2010**, *10*, 1117-1129.
- (160) Yamato, M.; Okuhara, M.; Karikusa, F.; Kikuchi, A.; Sakurai, Y.; Okano, T. Signal Transduction and Cytoskeletal Reorganization Are Required for Cell Detachment from Cell Culture Surfaces Grafted with a Temperature-Responsive Polymer. *J. Biomed. Mater. Res.* **1999**, *44*, 44-52.

- (161) Yamato, M.; Konno, C.; Kushida, A.; Hirose, M.; Mika, U.; Kikuchi, A.; Okano, T. Release of Adsorbed Fibronectin from Temperature-Responsive Culture Surfaces Requires Cellular Activity. *Biomaterials* **2000**, *21*, 981-986.
- (162) Okano, T.; Yamada, N.; Sakai, H.; Sakurai, Y. A Novel Recovery System for Cultured Cells Using Plasma-Treated Polystyrene Dishes Grafted with Poly(N-Isopropylacrylamide). *J. Biomed. Mater. Res.* **1993**, *27*, 1243-1251.
- (163) Fukumori, K.; Akiyama, Y.; Kumashiro, Y.; Kobayashi, J.; Yamato, M.; Sakai, K.; Okano, T. Characterization of Ultra-Thin Temperature-Responsive Polymer Layer and Its Polymer Thickness Dependency on Cell Attachment/Detachment Properties. *Macromol. Biosci.* **2010**, *10*, 1117-1129.
- (164) Nash, M. E.; Carroll, W. M.; Foley, P. J.; Maguire, G.; Connell, C. O.; Gorelov, A. V.; Beloshapkin, S.; Rochev, Y. A. Ultra-Thin Spin Coated Crosslinkable Hydrogels for Use in Cell Sheet Recovery-Synthesis, Characterisation to Application. *Soft Matter* **2012**, *8*, 3889-3899.
- (165) von Recum, H. A.; Kim, S. W.; Kikuchi, A.; Okuhara, M.; Sakurai, Y.; Okano, T. Novel Thermally Reversible Hydrogel as Detachable Cell Culture Substrate. *J. Biomed. Mater. Res.* **1998**, *40*, 631-639.
- (166) von Recum, H.; Kikuchi, A.; Okuhara, M.; Sakurai, Y.; Okano, T.; Kim, S. Retinal Pigmented Epithelium Culture on Thermally Responsive Polymer Porous Substrates. *J. Biomater. Sci., Polym. Ed.* **1998**, *9*, 1241-1253.
- (167) Pan, Y. V.; Wesley, R. A.; Luginbuhl, R.; Denton, D. D.; Ratner, B. D. Plasma Polymerized N-Isopropylacrylamide: Synthesis and Characterization of a Smart Thermally Responsive Coating. *Biomacromolecules* **2001**, *2*, 32-36.
- (168) Rollason, G.; Davies, J. E.; Sefton, M. V. Preliminary Report on Cell Culture on a Thermally Reversible Copolymer. *Biomaterials* **1993**, *14*, 153-155.
- (169) Kobayashi, J.; Yamato, M.; Okano, T. On-Off Affinity Binding Modulation on Thermoresponsive Polymer-Grafted Surfaces for Capture and Release of Proteins and Cells. *J. Biomater. Sci., Polym. Ed.* **2017**, *28*, 939-957.
- (170) Gilcreest, V. P.; Carroll, W. M.; Rochev, Y. A.; Blute, I.; Dawson, K. A.; Gorelov, A. V. Thermoresponsive Poly(N-Isopropylacrylamide) Copolymers: Contact Angles and Surface Energies of Polymer Films. *Langmuir* **2004**, *20*, 10138-10145.
- (171) Moran, M. T.; Carroll, W. M.; Gorelov, A.; Rochev, Y. Intact Endothelial Cell Sheet Harvesting from Thermoresponsive Surfaces Coated with Cell Adhesion Promoters. *J. R. Soc., Interface* **2007**, *4*, 1151-1157.

- (172) Nash, M. E.; Carroll, W. M.; Nikoloskya, N.; Yang, R.; Connell, C. O.; Gorelov, A. V.; Dockery, P.; Liptrot, C.; Lyng, F. M.; Garcia, A.; Rochev, Y. A. Straightforward, One-Step Fabrication of Ultrathin Thermoresponsive Films from Commercially Available PNIPAM for Cell Culture and Recovery. *ACS Appl. Mater. Interfaces* **2011**, *3*, 1980-1990.
- (173) Nash, M. E.; Carroll, W. M.; Velasco, D.; Gomez, J.; Gorelov, A. V.; Elezov, D.; Gallardo, A.; Rochev, Y. A.; Elvira, C. Synthesis and Characterization of a Novel Thermoresponsive Copolymer Series and Their Application in Cell and Cell Sheet Regeneration. *J. Biomater. Sci., Polym. Ed.* **2013**, *24*, 253-268.
- (174) Nash, M. E.; Fan, X.; Carroll, W. M.; Gorelov, A. V.; Barry, F. P.; Shaw, G.; Rochev, Y. A. Thermoresponsive Substrates Used for the Expansion of Human Mesenchymal Stem Cells and the Preservation of Immunophenotype. *Stem Cell Rev. Rep.* **2013**, *9*, 148-157.
- (175) Dzhoyashvili, N. A.; Thompson, K.; Gorelov, A. V.; Rochev, Y. A. Film Thickness Determines Cell Growth and Cell Sheet Detachment from Spin-Coated Poly(N-Isopropylacrylamide) Substrates. *ACS Appl. Mater. Interfaces* **2016**, *8*, 27564-27572.
- (176) Selezneva, I. I.; Gorelov, A. V.; Rochev, Y. A. Use of Thermosensitive Polymer Material on the Basis of N-Isopropylacrylamide and N-Tert-Butylacrylamide Copolymer in Cell Technologies. *Bull. Exp. Biol. Med.* **2006**, *142*, 538-541.
- (177) Maeda, T.; Kanda, T.; Yonekura, Y.; Yamamoto, K.; Aoyagi, T. Hydroxylated Poly(N-Isopropylacrylamide) as Functional Thermoresponsive Materials. *Biomacromolecules* **2006**, *7*, 545-549.
- (178) Kaneko, Y.; Nakamura, S.; Sakai, K.; Kikuchi, A.; Aoyagi, T.; Sakurai, Y.; Okano, T. Deswelling Mechanism for Comb-Type Grafted Poly(N-Isopropylacrylamide) Hydrogels with Rapid Temperature Responses. *Polym. Gels Networks* **1998**, *6*, 333-345.
- (179) Kaneko, Y.; Nakamura, S.; Sakai, K.; Aoyagi, T.; Kikuchi, A.; Sakurai, Y.; Okano, T. Rapid Deswelling Response of Poly(N-Isopropylacrylamide) Hydrogels by the Formation of Water Release Channels Using Poly(Ethylene Oxide) Graft Chains. *Macromolecules* **1998**, *31*, 6099-6105.
- (180) Murakami, D.; Yamato, M.; Nishida, K.; Ohki, T.; Takagi, R.; Yang, J.; Namiki, H.; Okano, T. The Effect of Micropores in the Surface of Temperature-Responsive Culture Inserts on the Fabrication of Transplantable Canine Oral Mucosal Epithelial Cell Sheets. *Biomaterials* **2006**, *27*, 5518-5523.
- (181) Kim, S. J.; Kim, W. I.; Yamato, M.; Okano, T.; Kikuchi, A.; Kwon, O. H. Successive Grafting of PHEMA and PIPAAm onto Cell Culture Surface Enables Rapid Cell Sheet Recovery. *Tissue Eng. Regener. Med.* **2013**, *10*, 139-145.

- (182) Feil, H.; Bae, Y. H.; Feijen, J.; Kim, S. W. Mutual Influence of Ph and Temperature on the Swelling of Ionizable and Thermosensitive Hydrogels. *Macromolecules* **1992**, *25*, 5528-5530.
- (183) Feil, H.; Bae, Y. H.; Feijen, J.; Kim, S. W. Effect of Comonomer Hydrophilicity and Ionization on the Lower Critical Solution Temperature of N-Isopropylacrylamide Copolymers. *Macromolecules* **1993**, *26*, 2496-2500.
- (184) Aoyagi, T.; Ebara, M.; Sakai, K.; Sakurai, Y.; Okano, T. Novel Bifunctional Polymer with Reactivity and Temperature Sensitivity. *J. Biomater. Sci., Polym. Ed.* **2000**, *11*, 101-110.
- (185) Ebara, M.; Aoyagi, T.; Sakai, K.; Okano, T. Introducing Reactive Carboxyl Side Chains Retains Phase Transition Temperature Sensitivity in N-Isopropylacrylamide Copolymer Gels. *Macromolecules* **2000**, *33*, 8312-8316.
- (186) Akiyama, Y.; Kikuchi, A.; Yamato, M.; Okano, T. Accelerated Cell-Sheet Recovery from a Surface Successively Grafted with Polyacrylamide and Poly(N-Isopropylacrylamide). *Acta Biomater.* **2014**, *10*, 3398-3408.
- (187) Ebara, M.; Yamato, M.; Nagai, S.; Aoyagi, T.; Kikuchi, A.; Sakai, K.; Okano, T. Incorporation of New Carboxylate Functionalized Co-Monomers to Temperature-Responsive Polymer-Grafted Cell Culture Surfaces. *Surf. Sci.* **2004**, *570*, 134-141.
- (188) Ebara, M.; Yamato, M.; Hirose, M.; Aoyagi, T.; Kikuchi, A.; Sakai, K.; Okano, T. Copolymerization of 2-Carboxyisopropylacrylamide with N-Isopropylacrylamide Accelerates Cell Detachment from Grafted Surfaces by Reducing Temperature. *Biomacromolecules* **2003**, *4*, 344-349.
- (189) Kwon, O. H.; Kikuchi, A.; Yamato, M.; Sakurai, Y.; Okano, T. Rapid Cell Sheet Detachment from Poly(N-Isopropylacrylamide)-Grafted Porous Cell Culture Membranes. *J. Biomed. Mater. Res.* **2000**, *50*, 82-89.
- (190) Kwon, O. H.; Kikuchi, A.; Yamato, M.; Okano, T. Accelerated Cell Sheet Recovery by Co-Grafting of PEG with PIPAAM onto Porous Cell Culture Membranes. *Biomaterials* **2003**, *24*, 1223-1232.
- (191) Tsuda, Y.; Kikuchi, A.; Yamato, M.; Nakao, A.; Sakurai, Y.; Umezu, M.; Okano, T. The Use of Patterned Dual Thermoresponsive Surfaces for the Collective Recovery as Co-Cultured Cell Sheets. *Biomaterials* **2005**, *26*, 1885-1893.
- (192) Yukiko, T.; Akihiko, K.; Masayuki, Y.; Yasuhisa, S.; Mitsuo, U.; Teruo, O. Control of Cell Adhesion and Detachment Using Temperature and Thermoresponsive Copolymer Grafted Culture Surfaces. *J. Biomed. Mater. Res., Part A* **2004**, *69A*, 70-78.

- (193) Ebara, M.; Yamato, M.; Aoyagi, T.; Kikuchi, A.; Sakai, K.; Okano, T. Temperature-Responsive Cell Culture Surfaces Enable “On–Off” Affinity Control between Cell Integrins and RGDS Ligands. *Biomacromolecules* **2004**, *5*, 505-510.
- (194) Ebara, M.; Yamato, M.; Aoyagi, T.; Kikuchi, A.; Sakai, K.; Okano, T. Temperature-Responsive Cell Culture Surfaces Enable “On–Off” Affinity Control between Cell Integrins and Rgdsligands. *Biomacromolecules* **2004**, *10*, 505-510.
- (195) Nishi, M.; Kobayashi, J.; Pechmann, S.; Yamato, M.; Akiyama, Y.; Kikuchi, A.; Uchida, K.; Textor, M.; Yajima, H.; Okano, T. The Use of Biotin–Avidin Binding to Facilitate Biomodification of Thermoresponsive Culture Surfaces. *Biomaterials* **2007**, *28*, 5471-5476.
- (196) Ebara, M.; Yamato, M.; Aoyagi, T.; Kikuchi, A.; Sakai, K.; Okano, T. The Effect of Extensible PEG Tethers on Shielding between Grafted Thermo-Responsive Polymer Chains and Integrin–RGD Binding. *Biomaterials* **2008**, *29*, 3650-3655.
- (197) Ebara, M.; Yamato, M.; Aoyagi, T.; Kikuchi, A.; Sakai, K.; Okano, T. A Novel Approach to Observing Synergy Effects of Phsrn on Integrin–RGD Binding Using Intelligent Surfaces. *Adv. Mater.* **2008**, *20*, 3034-3038.
- (198) Hatakeyama, H.; Kikuchi, A.; Yamato, M.; Okano, T. Influence of Insulin Immobilization to Thermoresponsive Culture Surfaces on Cell Proliferation and Thermally Induced Cell Detachment. *Biomaterials* **2005**, *26*, 5167-5176.
- (199) Hatakeyama, H.; Kikuchi, A.; Yamato, M.; Okano, T. Bio-Functionalized Thermoresponsive Interfaces Facilitating Cell Adhesion and Proliferation. *Biomaterials* **2006**, *27*, 5069-5078.
- (200) Hatakeyama, H.; Kikuchi, A.; Yamato, M.; Okano, T. Patterned Biofunctional Designs of Thermoresponsive Surfaces for Spatiotemporally Controlled Cell Adhesion, Growth, and Thermally Induced Detachment. *Biomaterials* **2007**, *28*, 3632-3643.
- (201) Arisaka, Y.; Kobayashi, J.; Yamato, M.; Akiyama, Y.; Okano, T. Switching of Cell Growth/Detachment on Heparin-Functionalized Thermoresponsive Surface for Rapid Cell Sheet Fabrication and Manipulation. *Biomaterials* **2013**, *34*, 4214-4222.
- (202) Kobayashi, J.; Hayashi, M.; Ohno, T.; Nishi, M.; Arisaka, Y.; Matsubara, Y.; Kakidachi, H.; Akiyama, Y.; Yamato, M.; Horii, A.; Okano, T. Surface Design of Antibody-Immobilized Thermoresponsive Cell Culture Dishes for Recovering Intact Cells by Low-Temperature Treatment. *J. Biomed. Mater. Res., Part A* **2014**, *102*, 3883-3893.
- (203) Mizutani, A.; Kikuchi, A.; Yamato, M.; Kanazawa, H.; Okano, T. Preparation of Thermoresponsive Polymer Brush Surfaces and Their Interaction with Cells. *Biomaterials* **2008**, *29*, 2073-2081.

- (204) Li, L.; Zhu, Y.; Li, B.; Gao, C. Fabrication of Thermoresponsive Polymer Gradients for Study of Cell Adhesion and Detachment. *Langmuir* **2008**, *24*, 13632-13639.
- (205) Kenichi, N.; Minami, W.; Akihiko, K.; Masayuki, Y.; Teruo, O. Thermo-Responsive Polymer Brushes as Intelligent Biointerfaces: Preparation Via ATRP and Characterization. *Macromol. Biosci.* **2011**, *11*, 400-409.
- (206) Takahashi, H.; Nakayama, M.; Yamato, M.; Okano, T. Controlled Chain Length and Graft Density of Thermoresponsive Polymer Brushes for Optimizing Cell Sheet Harvest. *Biomacromolecules* **2010**, *11*, 1991-1999.
- (207) Xu, F. J.; Zhong, S. P.; Yung, L. Y. L.; Kang, E. T.; Neoh, K. G. Surface-Active and Stimuli-Responsive Polymer-Si(100) Hybrids from Surface-Initiated Atom Transfer Radical Polymerization for Control of Cell Adhesion. *Biomacromolecules* **2004**, *5*, 2392-2403.
- (208) Matsuzaka, N.; Takahashi, H.; Nakayama, M.; Kikuchi, A.; Okano, T. Effect of the Hydrophobic Basal Layer of Thermoresponsive Block Co-Polymer Brushes on Thermally-Induced Cell Sheet Harvest. *J. Biomater. Sci., Polym. Ed.* **2012**, *23*, 1301-1314.
- (209) Takahashi, H.; Matsuzaka, N.; Nakayama, M.; Kikuchi, A.; Yamato, M.; Okano, T. Terminally Functionalized Thermoresponsive Polymer Brushes for Simultaneously Promoting Cell Adhesion and Cell Sheet Harvest. *Biomacromolecules* **2012**, *13*, 253-260.
- (210) Anderson, C. R.; Gambinossi, F.; DiLillo, K. M.; Laschewsky, A.; Wischerhoff, E.; Ferri, J. K.; Sefcik, L. S. Tuning Reversible Cell Adhesion to Methacrylate-Based Thermoresponsive Polymers: Effects of Composition on Substrate Hydrophobicity and Cellular Responses. *J. Biomed. Mater. Res., Part A* **2017**, *105*, 2416-2428.
- (211) Sefcik, L. S.; Kaminski, A.; Ling, K.; Laschewsky, A.; Lutz, J.-F.; Wischerhoff, E. Effects of PEG-Based Thermoresponsive Polymer Brushes on Fibroblast Spreading and Gene Expression. *Cell. Mol. Bioeng.* **2013**, *6*, 287-298.
- (212) Dormán, G.; Nakamura, H.; Pulsipher, A.; Prestwich, G. D. The Life of Pi Star: Exploring the Exciting and Forbidden Worlds of the Benzophenone Photophore. *Chem. Rev.* **2016**, *116*, 15284-15398.
- (213) Dormán, G.; Prestwich, G. D. Benzophenone Photophores in Biochemistry. *Biochemistry* **1994**, *33*, 5661-5673.
- (214) Turro, N. J.; Ramamurthy, V.; Scaiano, J. C., *Principles of Molecular Photochemistry: An Introduction*. University Science Books: Herndon, VA, 2009.
- (215) Klán, P.; Wirz, J., *Photochemistry of Organic Compounds: From Concepts to Practice*. John Wiley & Sons: Chichester, U.K., 2009.

- (216) Dormán, G.; Prestwich, G. D. Using Photolabile Ligands in Drug Discovery and Development. *Trends Biotechnol.* **2000**, *18*, 64-77.
- (217) Schönberg, A.; Mustafa, A. Reactions of Non-Enolizable Ketones in Sunlight. *Chem. Rev.* **1947**, *40*, 181-200.
- (218) Spighi, G.; Gaveau, M.-A.; Mestdagh, J.-M.; Poisson, L.; Soep, B. Gas Phase Dynamics of Triplet Formation in Benzophenone. *Phys. Chem. Chem. Phys.* **2014**, *16*, 9610-9618.
- (219) Aloïse, S.; Ruckebusch, C.; Blanchet, L.; Réhault, J.; Buntinx, G.; Huvenne, J.-P. The Benzophenone S1(N,Π*) → T1(N,Π*) States Intersystem Crossing Reinvestigated by Ultrafast Absorption Spectroscopy and Multivariate Curve Resolution. *J. Phys. Chem. A* **2008**, *112*, 224-231.
- (220) Yabumoto, S.; Sato, S.; Hamaguchi, H.-o. Vibrational and Electronic Infrared Absorption Spectra of Benzophenone in the Lowest Excited Triplet State. *Chem. Phys. Lett.* **2005**, *416*, 100-103.
- (221) Sergentu, D.-C.; Maurice, R.; Havenith, R. W. A.; Broer, R.; Roca-Sanjuan, D. Computational Determination of the Dominant Triplet Population Mechanism in Photoexcited Benzophenone. *Phys. Chem. Chem. Phys.* **2014**, *16*, 25393-25403.
- (222) Marazzi, M.; Mai, S.; Roca-Sanjuán, D.; Delcey, M. G.; Lindh, R.; González, L.; Monari, A. Benzophenone Ultrafast Triplet Population: Revisiting the Kinetic Model by Surface-Hopping Dynamics. *J. Phys. Chem. Lett.* **2016**, *7*, 622-626.
- (223) Zhang, Z. P.; Rong, M. Z.; Zhang, M. Q. Mechanically Robust, Self-Healable, and Highly Stretchable “Living” Crosslinked Polyurethane Based on a Reversible C-C Bond. *Adv. Funct. Mater.* **2018**, *28*, 1706050.
- (224) Mita, I.; Takagi, T.; Horie, K.; Shindo, Y. Photosensitized Degradation of Polystyrene by Benzophenone in Benzene Solution. *Macromolecules* **1984**, *17*, 2256-2260.
- (225) Millan, M. D.; Locklin, J.; Fulghum, T.; Baba, A.; Advincula, R. C. Polymer Thin Film Photodegradation and Photochemical Crosslinking: FT-IR Imaging, Evanescent Waveguide Spectroscopy, and QCM Investigations. *Polymer* **2005**, *46*, 5556-5568.
- (226) Carbone, N. D.; Ene, M.; Lancaster, J. R.; Koberstein, J. T. Kinetics and Mechanisms of Radical-Based Branching/Cross-Linking Reactions in Preformed Polymers Induced by Benzophenone and Bis-Benzophenone Photoinitiators. *Macromolecules* **2013**, *46*, 5434-5444.
- (227) Utrata-Wesołek, A.; Żymełka-Miara, I.; Kowalczyk, A.; Trzebicka, B.; Dworak, A. Photocrosslinking of Polyglycidol and Its Derivative: Route to Thermoresponsive Hydrogels. *Photochem. Photobiol.* **2018**, *94*, 52-60.

- (228) Utrata-Wesołek, A.; Trzcińska, R.; Galbas, K.; Trzebicka, B.; Dworak, A. Photodegradation of Polyglycidol in Aqueous Solutions Exposed to UV Irradiation. *Polym. Degrad. Stab.* **2011**, *96*, 907-918.
- (229) Cheng, X.; Wang, Y.; Hanein, Y.; Böhringer, K. F.; Ratner, B. D. Novel Cell Patterning Using Microheater-Controlled Thermoresponsive Plasma Films. *J. Biomed. Mater. Res., Part A* **2004**, *70A*, 159-168.
- (230) Kumar, P. R. A.; Sreenivasan, K.; Kumary, T. V. Alternate Method for Grafting Thermoresponsive Polymer for Transferring in Vitro Cell Sheet Structures. *J. Appl. Polym. Sci.* **2007**, *105*, 2245-2251.
- (231) Wang, H. Y.; Kobayashi, T.; Fujii, N. Surface Molecular Imprinting on Photosensitive Dithiocarbamoyl Polyacrylonitrile Membranes Using Photograft Polymerization. *J. Chem. Tech. Biotech.* **1997**, *70*, 355-362.
- (232) Lee, H. J.; Matsuda, T. Surface Photograft Polymerization on Segmented Polyurethane Using the Iniferter Technique. *J. Biomed. Mater. Res.* **1999**, *47*, 564-567.
- (233) Heise, C.; Schedler, U.; Wettmarshausen, S.; Friedrich, J. F. Plasma-Brominated Cyclo-Olefin Polymer Slides: Suitable Macroinitiators for Activator Regenerated by Electron Transfer/Atom Radical Transfer Polymerization. *J. Appl. Polym. Sci.* **2014**, *131*.
- (234) Anderson, C. R.; Abecunas, C.; Warrenner, M.; Laschewsky, A.; Wischerhoff, E. Effects of Methacrylate-Based Thermoresponsive Polymer Brush Composition on Fibroblast Adhesion and Morphology. *Cell. Mol. Bioeng.* **2017**, *10*, 75-88.
- (235) Morra, M.; Cassinelli, C., Thermal Recovery of Cells Cultured on Poly(N-Isopropylacrylamide) Surface-Grafted Polystyrene Dishes. In *Surface Modification of Polymeric Biomaterials*, Ratner, B. D.; Castner, D. G., Eds. Springer US: Boston, MA, 1997; pp 175-181.
- (236) Matsuda, K.; Yamada, K.; Ebihara, T.; Izumi, T.; Hirata, M. Thermo-Responsive Properties of Poly(Tetrafluoroethylene) Surfaces Photografted with Hydrophilic Monomers around Ordinary Temperatures. *J. Photopolym. Sci. Technol.* **1999**, *12*, 21-26.
- (237) Yang, B.; Yang, W. Thermo-Sensitive Switching Membranes Regulated by Pore-Covering Polymer Brushes. *J. Membr. Sci.* **2003**, *218*, 247-255.
- (238) Curti, P. S.; Moura, M. R. d.; Veiga, W.; Radovanovic, E.; Rubira, A. F.; Muniz, E. C. Characterization of PNIPAAm Photografted on PET and PS Surfaces. *Appl. Surf. Sci.* **2005**, *245*, 223-233.

- (239) Wu, G.; Li, Y.; Han, M.; Liu, X. Novel Thermo-Sensitive Membranes Prepared by Rapid Bulk Photo-Grafting Polymerization of N,N-Diethylacrylamide onto the Microfiltration Membranes Nylon. *J. Membr. Sci.* **2006**, *283*, 13-20.
- (240) Biazar, E.; Khorasani, M.; Daliri, M. Cell Sheet Engineering: Solvent Effect on Nanometric Grafting of Poly-N-Isopropylacrylamide onto Polystyrene Substrate under Ultraviolet Radiation. *Int. J. Nanomedicine* **2011**, *6*, 295-302.
- (241) Ma, D.; Chen, H.; Shi, D.; Li, Z.; Wang, J. Preparation and Characterization of Thermo-Responsive PDMS Surfaces Grafted with Poly(N-Isopropylacrylamide) by Benzophenone-Initiated Photopolymerization. *J. Colloid Interface Sci.* **2009**, *332*, 85-90.
- (242) Lin, J. B.; Isenberg, B. C.; Shen, Y.; Schorsch, K.; Sazonova, O. V.; Wong, J. Y. Thermo-Responsive Poly(N-Isopropylacrylamide) Grafted onto Microtextured Poly(Dimethylsiloxane) for Aligned Cell Sheet Engineering. *Colloids Surf., B* **2012**, *99*, 108-115.
- (243) Backman, D. E.; LeSavage, B. L.; Shah, S. B.; Wong, J. Y. A Robust Method to Generate Mechanically Anisotropic Vascular Smooth Muscle Cell Sheets for Vascular Tissue Engineering. *Macromol. Biosci.* **2017**, *17*, 1600434.
- (244) Noh, I.; Goodman, S. L.; Hubbell, J. A. Chemical Modification and Photograft Polymerization Upon Expanded Poly(Tetrafluoroethylene). *J. Biomater. Sci., Polym. Ed.* **1998**, *9*, 407-426.
- (245) Rånby, B.; Guo, F. Z. "Surface-Photografting": New Applications to Synthetic Fibers. *Polym. Adv. Technol.* **1994**, *5*, 829-836.
- (246) Piletsky, S. A.; Matuschewski, H.; Schedler, U.; Wilpert, A.; Piletska, E. V.; Thiele, T. A.; Ulbricht, M. Surface Functionalization of Porous Polypropylene Membranes with Molecularly Imprinted Polymers by Photograft Copolymerization in Water. *Macromolecules* **2000**, *33*, 3092-3098.
- (247) Ziani-Cherif, H.; Abe, Y.; Imachi, K.; Matsuda, T. Visible-Light-Induced Surface Graft Polymerization Via Camphorquinone Impregnation Technique. *J. Biomed. Mater. Res.* **2002**, *59*, 386-389.
- (248) Sergeeva, T. A.; Matuschewski, H.; Piletsky, S. A.; Bendig, J.; Schedler, U.; Ulbricht, M. Molecularly Imprinted Polymer Membranes for Substance-Selective Solid-Phase Extraction from Water by Surface Photo-Grafting Polymerization. *J. Chromatogr. A* **2001**, *907*, 89-99.
- (249) Patrito, N.; McCague, C.; Chiang, S.; Norton, P. R.; Petersen, N. O. Photolithographically Patterned Surface Modification of Poly(Dimethylsiloxane) Via UV-Initiated Graft Polymerization of Acrylates. *Langmuir* **2006**, *22*, 3453-3455.

- (250) Yu, H.-Y.; Xu, Z.-K.; Lei, H.; Hu, M.-X.; Yang, Q. Photoinduced Graft Polymerization of Acrylamide on Polypropylene Microporous Membranes for the Improvement of Antifouling Characteristics in a Submerged Membrane-Bioreactor. *Sep. Purif. Technol.* **2007**, *53*, 119-125.
- (251) Li, G.; He, G.; Zheng, Y.; Wang, X.; Wang, H. Surface Photografting Initiated by Benzophenone in Water and Mixed Solvents Containing Water and Ethanol. *J. Appl. Polym. Sci.* **2012**, *123*, 1951-1959.
- (252) Allmér, K.; Hult, A.; Rånby, B. Surface Modification of Polymers. II. Grafting with Glycidyl Acrylates and the Reactions of the Grafted Surfaces with Amines. *J. Polym. Sci., Part A: Polym. Chem.* **1989**, *27*, 1641-1652.
- (253) Rånby, B. 'Surface Photografting' onto Polymers - a New Method for Adhesion Control. *J. Adhes. Sci. Technol.* **1995**, *9*, 599-613.
- (254) Stragliotto, M. F.; Strumia, M. C.; Gomez, C. G.; Romero, M. R. Optimization of UV-Induced Graft Polymerization of Acrylic Acid on Polypropylene Films Using Cds as Light Sensor. *Ind. Eng. Chem. Res.* **2018**, *57*, 1188-1196.
- (255) Deng, J.-P.; Yang, W.-T.; Rånby, B. Surface Photograft Polymerization of Vinyl Acetate on Low Density Polyethylene Film. Effects of Solvent. *Polym. J.* **2000**, *32*, 834.
- (256) Li, J. Y.; Sun, Y. M.; Zeng, H.; Xue, W. X.; Xiao, Y.; Yu, Q. Preparation of Photoluminescence Films Containing Rare Earth Complexes by UV Photograft Polymerization. *J. Appl. Polym. Sci.* **2003**, *89*, 662-667.
- (257) Yang, P.; Deng, J.; Yang, W. Surface Photografting Polymerization of Methyl Methacrylate in N,N-Dimethylformamide on Low Density Polyethylene Film. *Macromol. Chem. Phys.* **2004**, *205*, 1096-1102.
- (258) Allmér, K.; Hult, A.; Rånby, B. Surface Modification of Polymers. I. Vapour Phase Photografting with Acrylic Acid. *J. Polym. Sci., Part A: Polym. Chem.* **1988**, *26*, 2099-2111.
- (259) Ulbricht, M.; Oechel, A.; Lehmann, C.; Tomaschewski, G.; Hicke, H. G. Gas-Phase Photoinduced Graft Polymerization of Acrylic Acid onto Polyacrylonitrile Ultrafiltration Membranes. *J. Appl. Polym. Sci.* **1995**, *55*, 1707-1723.
- (260) Castell, P.; Wouters, M.; With, G. d.; Fischer, H.; Huijs, F. Surface Modification of Poly(Propylene) by Photoinitiators: Improvement of Adhesion and Wettability. *J. Appl. Polym. Sci.* **2004**, *92*, 2341-2350.
- (261) Wang, H.; Brown, H. R. Lamination of High-Density Polyethylene by Bulk Photografting and the Mechanism of Adhesion. *J. Appl. Polym. Sci.* **2005**, *97*, 1097-1106.

- (262) Han, J.; Wang, X.; Wang, H. Superhydrophobic Surface Fabricated by Bulk Photografting of Acrylic Acid onto High-Density Polyethylene. *J. Colloid Interface Sci.* **2008**, *326*, 360-365.
- (263) Zhang, Z. Q.; Li, H.; Lv, X. Y.; Liu, H. Z.; Theng, L. X. MMA-Grafted PE Separators of Lithium-Ion Battery Prepared by UV-Radiated Grafting. *Adv. Mater. Res.* **2012**, *463-464*, 1378-1381.
- (264) Rånby, B. Surface Modification and Lamination of Polymers by Photografting. *Int. J. Adhes. Adhes.* **1999**, *19*, 337-343.
- (265) Rånby, B.; Yang, W. T.; Tretinnikov, O. Surface Photografting of Polymer Fibers, Films and Sheets. *Nucl. Instrum. Methods Phys. Res., Sect. B* **1999**, *151*, 301-305.
- (266) Sheng, W.; Li, B.; Wang, X.; Dai, B.; Yu, B.; Jia, X.; Zhou, F. Brushing up from "Anywhere" under Sunlight: A Universal Surface-Initiated Polymerization from Polydopamine-Coated Surfaces. *Chem. Sci.* **2015**, *6*, 2068-2073.
- (267) Daniel, H.; Lisa, Z.; Muhammad, I.; Tao, Z.; Maximilian, S.; Michael, S.; Claudia, T.; Karsten, H.; Rainer, J.; Ihsan, A. Mussel-Inspired Polymer Carpets: Direct Photografting of Polymer Brushes on Polydopamine Nanosheets for Controlled Cell Adhesion. *Adv. Mater.* **2016**, *28*, 1489-1494.
- (268) Fukumori, K.; Akiyama, Y.; Yamato, M.; Okano, T. A Facile Method for Preparing Temperature-Responsive Cell Culture Surfaces by Using a Thioxanthone Photoinitiator Immobilized on a Polystyrene Surface. *ChemNanoMat* **2016**, *2*, 454-460.
- (269) Yang, W. T.; Rånby, B. Bulk Surface Photografting Process and Its Application. III. Photolamination of Polymer Films. *J. Appl. Polym. Sci.* **1997**, *63*, 1723-1732.
- (270) Yang, W.; Rånby, B. Bulk Surface Photografting Process and Its Applications. I. Reactions and Kinetics. *J. Appl. Polym. Sci.* **1996**, *62*, 533-543.
- (271) Yang, W.; Rånby, B. Bulk Surface Photografting Process and Its Applications. II. Principal Factors Affecting Surface Photografting. *J. Appl. Polym. Sci.* **1996**, *62*, 545-555.
- (272) Gunkel, G.; Weinhart, M.; Becherer, T.; Haag, R.; Huck, W. T. S. Effect of Polymer Brush Architecture on Antibiofouling Properties. *Biomacromolecules* **2011**, *12*, 4169-4172.
- (273) Sheiko, S. S.; Sumerlin, B. S.; Matyjaszewski, K. Cylindrical Molecular Brushes: Synthesis, Characterization, and Properties. *Prog. Polym. Sci.* **2008**, *33*, 759-785.
- (274) Zhang, M.; Müller, A. H. E. Cylindrical Polymer Brushes. *J. Polym. Sci., Part A: Polym. Chem.* **2005**, *43*, 3461-3481.
- (275) Sumerlin, B. S.; Matyjaszewski, K., Molecular Brushes – Densely Grafted Copolymers. In *Macromolecular Engineering*, Matyjaszewski, K.; Gnanou, Y.; Leibler, L., Eds. 2007.

- (276) Verduzco, R.; Li, X.; Pesek, S. L.; Stein, G. E. Structure, Function, Self-Assembly, and Applications of Bottlebrush Copolymers. *Chem. Soc. Rev.* **2015**, *44*, 2405-2420.
- (277) Feng, C.; Li, Y.; Yang, D.; Hu, J.; Zhang, X.; Huang, X. Well-Defined Graft Copolymers: From Controlled Synthesis to Multipurpose Applications. *Chem. Soc. Rev.* **2011**, *40*, 1282-1295.
- (278) Lee, H.-i.; Pietrasik, J.; Sheiko, S. S.; Matyjaszewski, K. Stimuli-Responsive Molecular Brushes. *Prog. Polym. Sci.* **2010**, *35*, 24-44.
- (279) Chen, Y. Shaped Hairy Polymer Nanoobjects. *Macromolecules* **2012**, *45*, 2619-2631.
- (280) Li, C.; Gunari, N.; Fischer, K.; Janshoff, A.; Schmidt, M. New Perspectives for the Design of Molecular Actuators: Thermally Induced Collapse of Single Macromolecules from Cylindrical Brushes to Spheres. *Angew. Chem., Int. Ed.* **2004**, *43*, 1101-1104.
- (281) Pietrasik, J.; Sumerlin, B. S.; Lee, R. Y.; Matyjaszewski, K. Solution Behavior of Temperature-Responsive Molecular Brushes Prepared by ATRP. *Macromol. Chem. Phys.* **2007**, *208*, 30-36.
- (282) Yamamoto, S.-i.; Pietrasik, J.; Matyjaszewski, K. ATRP Synthesis of Thermally Responsive Molecular Brushes from Oligo(Ethylene Oxide) Methacrylates. *Macromolecules* **2007**, *40*, 9348-9353.
- (283) Li, X.; ShamsiJazeyi, H.; Pesek, S. L.; Agrawal, A.; Hammouda, B.; Verduzco, R. Thermoresponsive PNIPAAm Bottlebrush Polymers with Tailored Side-Chain Length and End-Group Structure. *Soft Matter* **2014**, *10*, 2008-2015.
- (284) Telford, A. M.; Meagher, L.; Glattauer, V.; Gengenbach, T. R.; Easton, C. D.; Neto, C. Micropatterning of Polymer Brushes: Grafting from Dewetting Polymer Films for Biological Applications. *Biomacromolecules* **2012**, *13*, 2989-2996.
- (285) Ma, H.; Hyun, J.; Stiller, P.; Chilkoti, A. "Non-Fouling" Oligo(Ethylene Glycol)-Functionalized Polymer Brushes Synthesized by Surface-Initiated Atom Transfer Radical Polymerization. *Adv. Mater.* **2004**, *16*, 338-341.
- (286) Kizhakkedathu, J. N.; Janzen, J.; Le, Y.; Kainthan, R. K.; Brooks, D. E. Poly(Oligo(Ethylene Glycol)Acrylamide) Brushes by Surface Initiated Polymerization: Effect of Macromonomer Chain Length on Brush Growth and Protein Adsorption from Blood Plasma. *Langmuir* **2009**, *25*, 3794-3801.
- (287) Chang, Y.; Shih, Y.-J.; Ko, C.-Y.; Jhong, J.-F.; Liu, Y.-L.; Wei, T.-C. Hemocompatibility of Poly(Vinylidene Fluoride) Membrane Grafted with Network-Like and Brush-Like Antifouling Layer Controlled Via Plasma-Induced Surface Pegylation. *Langmuir* **2011**, *27*, 5445-5455.

- (288) Peter, D.; Karl, F.; Manfred, S.; S., S. S.; Martin, M. Zylindrische Molekulare Bürsten. *Angew. Chem.* **1997**, *109*, 2894-2897.
- (289) Ramin, D.; Norbert, H.; Karl, F.; Manfred, S. Amphipolar Core-Shell Cylindrical Brushes. *Macromol. Rapid Commun.* **1999**, *20*, 444-449.
- (290) Djalali, R.; Li, S.-Y.; Schmidt, M. Amphipolar Core-Shell Cylindrical Brushes as Templates for the Formation of Gold Clusters and Nanowires. *Macromolecules* **2002**, *35*, 4282-4288.
- (291) Andreas, M.; François, R. Synthesis of Well-Defined Macromonomers and Comb Copolymers from Polymers Made by Atom Transfer Radical Polymerization. *J. Polym. Sci., Part A: Polym. Chem.* **2003**, *41*, 3425-3439.
- (292) Zhang, B.; Fischer, K.; Schmidt, M. Cylindrical Polypeptide Brushes. *Macromol. Chem. Phys.* **2005**, *206*, 157-162.
- (293) Aleksandra, M.; Sebastian, M.; Barbara, T.; Dirk, K.; Wojciech, W.; Hans-Juergen, A.; Andrzej, D. Polyether Core-Shell Cylinder-Polymerization of Polyglycidol Macromonomers. *Macromol. Chem. Phys.* **2005**, *206*, 2018-2026.
- (294) Gao, Q.; Yu, M.; Su, Y.; Xie, M.; Zhao, X.; Li, P.; Ma, P. X. Rationally Designed Dual Functional Block Copolymers for Bottlebrush-Like Coatings: In Vitro and in Vivo Antimicrobial, Antibiofilm, and Antifouling Properties. *Acta Biomater.* **2017**, *51*, 112-124.
- (295) Zhi, Z.; Su, Y.; Xi, Y.; Tian, L.; Xu, M.; Wang, Q.; Padidan, S.; Li, P.; Huang, W. Dual-Functional Polyethylene Glycol-b-Polyhexanide Surface Coating with in Vitro and in Vivo Antimicrobial and Antifouling Activities. *ACS Appl. Mater. Interfaces* **2017**, *9*, 10383-10397.
- (296) Su, Y.; Zhi, Z.; Gao, Q.; Xie, M.; Yu, M.; Lei, B.; Li, P.; Ma, P. X. Autoclaving-Derived Surface Coating with in Vitro and in Vivo Antimicrobial and Antibiofilm Efficacies. *Adv. Healthcare Mater.* **2017**, *6*, 1601173.
- (297) Healy, D.; Nash, M.; Gorleov, A.; Thompson, K.; Dockery, P.; Rochev, Y. An Investigation of Cell Growth and Detachment from Thermoresponsive Physically Crosslinked Networks. *Colloids Surf., B* **2017**, *159*, 159-165.
- (298) Healy, D.; Nash, M. E.; Gorelov, A.; Thompson, K.; Dockery, P.; Belochapkin, S.; Madden, J.; Rochev, Y. A. Nanometer-Scale Physically Adsorbed Thermoresponsive Films for Cell Culture. *Int. J. Polym. Mater. Po.* **2017**, *66*, 221-234.
- (299) Healy, D.; Nash, M. E.; Gorelov, A.; Thompson, K.; Dockery, P.; Beloshapkin, S.; Rochev, Y. Fabrication and Application of Photocrosslinked, Nanometer-Scale, Physically Adsorbed Films for Tissue Culture Regeneration. *Macromol. Biosci.* **2017**, *17*, 1600175.

- (300) Schmidt, S.; Zeiser, M.; Hellweg, T.; Duschl, C.; Fery, A.; Möhwald, H. Adhesion and Mechanical Properties of PNIPAM Microgel Films and Their Potential Use as Switchable Cell Culture Substrates. *Adv. Funct. Mater.* **2010**, *20*, 3235-3243.
- (301) Liao, T.; Moussallem, M. D.; Kim, J.; Schlenoff, J. B.; Ma, T. N-Isopropylacrylamide-Based Thermoresponsive Polyelectrolyte Multilayer Films for Human Mesenchymal Stem Cell Expansion. *Biotechnol. Prog.* **2010**, *26*, 1705-1713.
- (302) Aubouy, M. Organization of Polymers at Interfaces. *Phys. Rev. E* **1997**, *56*, 3370-3377.
- (303) Marques, C.; Joanny, J. F.; Leibler, L. Adsorption of Block Copolymers in Selective Solvents. *Macromolecules* **1988**, *21*, 1051-1059.
- (304) Dan, N.; Tirrell, M. Self-Assembly of Block Copolymers with a Strongly Charged and a Hydrophobic Block in a Selective, Polar Solvent. Micelles and Adsorbed Layers. *Macromolecules* **1993**, *26*, 4310-4315.
- (305) Wittmer, J.; Joanny, J. F. Charged Diblock Copolymers at Interfaces. *Macromolecules* **1993**, *26*, 2691-2697.
- (306) Abraham, T.; Giasson, S.; Gohy, J. F.; Jérôme, R.; Müller, B.; Stamm, M. Adsorption Kinetics of a Hydrophobic-Hydrophilic Diblock Polyelectrolyte at the Solid-Aqueous Solution Interface: A Slow Birth and Fast Growth Process. *Macromolecules* **2000**, *33*, 6051-6059.
- (307) Sikka, M.; Schneider, J.; Tirrell, M.; Amiel, C. Adsorption of Hydrophilic-Hydrophobic Block Copolymers on Silica from Aqueous Solutions. *Macromol. Symp.* **1995**, *98*, 1147-1147.
- (308) Marques, C. M.; Joanny, J. F. Block Copolymer Adsorption in a Nonselective Solvent. *Macromolecules* **1989**, *22*, 1454-1458.
- (309) Motschmann, H.; Stamm, M.; Toprakcioglu, C. Adsorption Kinetics of Block Copolymers from a Good Solvent: A Two-Stage Process. *Macromolecules* **1991**, *24*, 3681-3688.
- (310) Dorgan, J. R.; Stamm, M.; Toprakcioglu, C.; Jerome, R.; Fetters, L. J. End-Attaching Copolymer Adsorption: Kinetics and Effects of Chain Architecture. *Macromolecules* **1993**, *26*, 5321-5330.
- (311) Pagac, E. S.; Prieve, D. C.; Solomentsev, Y.; Tilton, R. D. A Comparison of Polystyrene-Poly(Ethylene Oxide) Diblock Copolymer and Poly(Ethylene Oxide) Homopolymer Adsorption from Aqueous Solutions. *Langmuir* **1997**, *13*, 2993-3001.
- (312) de Vos, W. M.; de Keizer, A.; Kleijn, J. M.; Cohen Stuart, M. A. The Production of PEO Polymer Brushes Via Langmuir-Blodgett and Langmuir-Schaeffer Methods: Incomplete Transfer and Its Consequences. *Langmuir* **2009**, *25*, 4490-4497.

- (313) Loh, X. J.; Cheong, W. C. D.; Li, J.; Ito, Y. Novel Poly(N-Isopropylacrylamide)-Poly[(R)-3-Hydroxybutyrate]-Poly(N-Isopropylacrylamide) Triblock Copolymer Surface as a Culture Substrate for Human Mesenchymal Stem Cells. *Soft Matter* **2009**, *5*, 2937-2946.
- (314) Loh, X. J.; Gong, J.; Sakuragi, M.; Kitajima, T.; Liu, M.; Li, J.; Ito, Y. Surface Coating with a Thermoresponsive Copolymer for the Culture and Non-Enzymatic Recovery of Mouse Embryonic Stem Cells. *Macromol. Biosci.* **2009**, *9*, 1069-1079.
- (315) Nakayama, M.; Yamada, N.; Kumashiro, Y.; Kanazawa, H.; Yamato, M.; Okano, T. Thermoresponsive Poly(N-Isopropylacrylamide)-Based Block Copolymer Coating for Optimizing Cell Sheet Fabrication. *Macromol. Biosci.* **2012**, *12*, 751-760.
- (316) Sakuma, M.; Kumashiro, Y.; Nakayama, M.; Tanaka, N.; Umemura, K.; Yamato, M.; Okano, T. Control of Cell Adhesion and Detachment on Langmuir-Schaefer Surface Composed of Dodecyl-Terminated Thermo-Responsive Polymers. *J. Biomater. Sci. Polym. Ed.* **2014**, *25*, 431-443.
- (317) Sakuma, M.; Kumashiro, Y.; Nakayama, M.; Tanaka, N.; Umemura, K.; Yamato, M.; Okano, T. Thermoresponsive Nanostructured Surfaces Generated by the Langmuir-Schaefer Method Are Suitable for Cell Sheet Fabrication. *Biomacromolecules* **2014**, *15*, 4160-4167.
- (318) Sudo, Y.; Sakai, H.; Nabae, Y.; Hayakawa, T.; Kakimoto, M.-a. Preparation of Hyperbranched Polystyrene-g-Poly(N-Isopropylacrylamide) Copolymers and Its Application to Novel Thermo-Responsive Cell Culture Dishes. *Polymer* **2015**, *70*, 307-314.
- (319) Sudo, Y.; Sakai, H.; Nabae, Y.; Hayakawa, T.; Kakimoto, M.-a. Role of Hyperbranched Polystyrene on Thermo-Responsive Cell Culture Dishes Prepared by Hyperbranched Polystyrene-g-Poly(N-Isopropylacrylamide). *Polymer* **2016**, *100*, 77-85.
- (320) Sudo, Y.; Kawai, R.; Sakai, H.; Kikuchi, R.; Nabae, Y.; Hayakawa, T.; Kakimoto, M.-a. Star-Shaped Thermoresponsive Polymers with Various Functional Groups for Cell Sheet Engineering. *Langmuir* **2018**, *34*, 653-662.

8 Patent Applications, Publications and Conference Contributions

Patent Applications

1) Marie Weinhart, Daniel Stöbener, A thermoresponsive polymer and its use in a cell culture support, EPO, 2016, FU182EP.

Peer Reviewed Publications

2) Stöbener, D. D.; Scholz, J.; Schedler, U.; Weinhart, M. Oligo(glycidyl ether) Acrylate Bottlebrushes “Grafted-from” Polystyrene Surfaces – A Versatile Strategy towards Functional Cell Culture Substrates, *under revision*, **2018**.

3) Stöbener, D. D.; Hoppensack, A.; Scholz, J.; Weinhart, M. Endothelial, Smooth Muscle and Fibroblast Cell Sheet Fabrication from Self-assembled Thermoresponsive Poly(glycidyl ether) Brushes, *under revision*, **2018**.

4) Stöbener, D. D.; Donath, D.; Weinhart, M. Fast and Solvent-Free Microwave-Assisted Synthesis of Thermoresponsive Oligo(glycidyl ether)s, *J. Polym. Sci.: Part A, Polym. Chem.*, *accepted*, **2018**.

5) Stöbener, D. D.; Uckert, M.; Cuellar-Camacho, J. L.; Hoppensack, A.; Weinhart, M. Ultrathin Poly(glycidyl ether) Coatings on Polystyrene for Temperature-Triggered Human Dermal Fibroblast Sheet Fabrication, *ACS Biomater. Sci. Eng.*, **2017**, 3 (9), 2155-2165.

6) Stöbener, D. D.; Paulus, F.; Welle, A.; Wöll, C.; Haag, R. Dynamic Protein Adsorption onto Dendritic Polyglycerol Sulfate Self-Assembled Monolayers, *under revision*, **2018**.

7) Nguyen, R.; Galy, N.; Singh, A. K.; Paulus, F.; Stöbener, D.; Schlesener, C.; Sharma, S. K.; Haag, R.; Len, C. A Simple and Efficient Process for Large Scale Glycerol Oligomerization by Microwave Irradiation, *Catalysts*, **2017**, 7 (4), 123.

8) Zhong, Y.; Dimde, M.; Stöbener, D.; Meng, F.; Deng, C.; Zhong, Z.; Haag, R. Micelles with Sheddable Dendritic Polyglycerol Sulfate Shells Show Extraordinary Tumor Targetability and Chemotherapy in Vivo, *ACS Appl. Mater. Interfaces*, **2016**, 8 (41), 27530-27538.

Poster Presentations

9) Stöbener, D.; Hoppensack, A.; Uckert, M.; Cuellar-Camacho, J. L.; Weinhart, M. Thermoresponsive Poly(Glycidyl Ether) Coatings for Cell Sheet Fabrication, Makromolekulares Kolloquium, Freiburg, Germany, **2017**.

10) Stöbener, D.; Heinen, S.; Becherer, T.; Qiang, W.; Haag, R.; Weinhart, M. Linear Polyglycerol Derivatives with Adjustable LCST and Good Biocompatibility, 27th European Conference on Biomaterials, Kraków, Poland, **2015**.

11) Stöbener, D.; Weinhart, M.; Becherer, T.; Ziem, B.; Dimde, M.; Paulus, F.; Steinhilber, D.; Haag, R. Glycerol Based Polymers for Protein and Cell Resistant Surfaces, Makromolekulares Kolloquium, Freiburg, Germany, **2014**.

9 Curriculum Vitae

For reasons of data protection, the curriculum vitae is not published in the electronic version.